AD-A114 375 NEW MEXICO ENGINEERING RESEARCH INST ALBUQUERQUE F/G 13/13
REINFORCED CONCRETE BEAMS UNDER COMBINED AXIAL AND LATERAL LOAD--ETC(U)
JAN 82 G E LANE F29601-76-C-0015
UNCLASSIFIED NMERI-SSR-71 AFWL-TR-81-99 NL

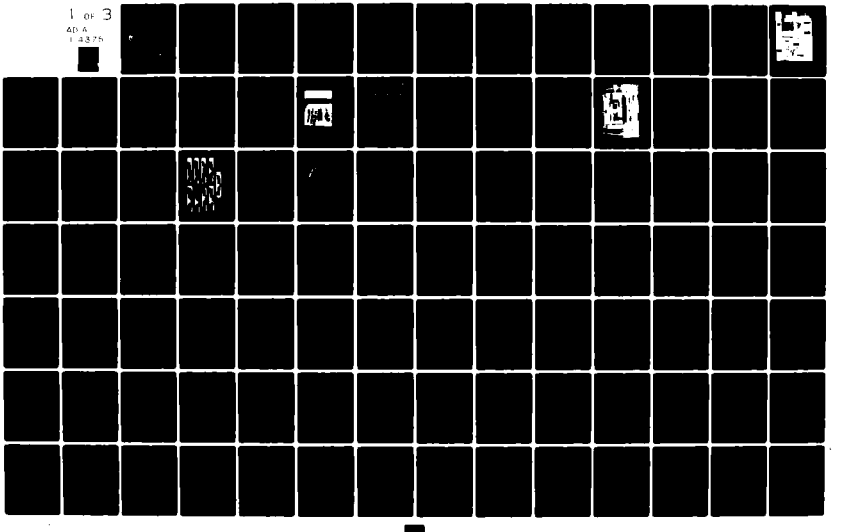

AFWL-TR-
81-99

REINFORCED CONCRETE BEAMS UNDER COMBINED AXIAL AND LATERAL LOADING

Golden E. Lane, Jr.

New Mexico Engineering Research Institute
University of New Mexico
Albuquerque, NM 87131

January 1982

Final Report

AIR FORCE WEAPONS LABORATORY
Air Force Systems Command
Kirtland Air Force Base, NM 87117

This final report was prepared by the New Mexico Engineering Research Institute, Albuquerque, New Mexico, under Contract F29601-76-C-0015, Job Order 672A0824 with the Air Force Weapons Laboratory, Kirtland Air Force Base, New Mexico. Mr. Douglas R. Seemann (NTES) was the Laboratory Project Officer-in-Charge.

The Public Affairs Office has reviewed this report, and it is releasable to the National Technical Information Service, where it will be available to the general public, including foreign nationals.

If your address has changed, if you wish to be removed from our mailing list, or if your organization no longer employs the addressee, please notify AFWL/NTES, Kirtland AFB, NM 87117 to help us maintain a current mailing list.

This technical report has been reviewed and is approved for publication.

Douglas R. Seemann

DOUGLAS R. SEEMANN
Project Officer

FOR THE COMMANDER

James H. Lee Jr.

JAMES H. LEE, JR.
Lt Colonel, USAF
Chief, Technology Applications Br

Maynard A. Plamondon

MAYNARD A. PLAMONDON
Chief, Civil Engrg Rsch Division

DO NOT RETURN COPIES OF THIS REPORT UNLESS CONTRACTUAL OBLIGATIONS OR NOTICE ON A SPECIFIC DOCUMENT REQUIRES THAT IT BE RETURNED.

UNCLASSIFIED

SECURITY CLASSIFICATION OF THIS PAGE *(When Data Entered)*

REPORT DOCUMENTATION PAGE	READ INSTRUCTIONS BEFORE COMPLETING FORM
1. REPORT NUMBER: AFWL-TR-81-99	2. GOVT ACCESSION NO.: AD-A114 375
	3. RECIPIENT'S CATALOG NUMBER:
4. TITLE *(and Subtitle)*: REINFORCED CONCRETE BEAMS UNDER COMBINED AXIAL AND LATERAL LOADING	5. TYPE OF REPORT & PERIOD COVERED: Final Report
	6. PERFORMING ORG. REPORT NUMBER: NMERI-SSR-71
7. AUTHOR(s): Golden E. Lane, Jr.	8. CONTRACT OR GRANT NUMBER(s): F29601-76-C-0015
9. PERFORMING ORGANIZATION NAME AND ADDRESS: New Mexico Engineering Research Institute, University of New Mexico, Albuquerque, NM 87131	10. PROGRAM ELEMENT, PROJECT, TASK AREA & WORK UNIT NUMBERS: 64312F/672A0824
11. CONTROLLING OFFICE NAME AND ADDRESS: Air Force Weapons Laboratory (NTES), Kirtland Air Force Base, NM 87117	12. REPORT DATE: January 1982
	13. NUMBER OF PAGES: 230
14. MONITORING AGENCY NAME & ADDRESS *(if different from Controlling Office)*	15. SECURITY CLASS. *(of this report)*: Unclassified
	15a. DECLASSIFICATION DOWNGRADING SCHEDULE

16. DISTRIBUTION STATEMENT *(of this Report)*

Approved for public release; distribution unlimited.

17. DISTRIBUTION STATEMENT *(of the abstract entered in Block 20, if different from Report)*

18. SUPPLEMENTARY NOTES

Appendixes B and C include work performed by the University of Colorado at Boulder and San Diego State University.

19. KEY WORDS *(Continue on reverse side if necessary and identify by block number)*

Reinforced Concrete
Axial Load
Shear Failure
Flexural Load
Displacement Control
Combined Loading
Reinforced Concrete Beams

20. ABSTRACT *(Continue on reverse side if necessary and identify by block number)*

Nine hinge-supported reinforced concrete beams were tested under displacement control with a proportional axial and symmetrical two-point lateral loading system. The nine beams were divided into three test series of three beams each. The beams in Series 1 contained shear reinforcement and were loaded monotonically to failure. Those in Series 2 contained no shear reinforcement and were loaded similarly to the first series. The Series 3 beams were shear reinforced and were loaded to failure under cyclic loading. Each beam had a

DD FORM 1 JAN 73 1473 EDITION OF 1 NOV 65 IS OBSOLETE

UNCLASSIFIED

SECURITY CLASSIFICATION OF THIS PAGE *(When Data Entered)*

20. ABSTRACT (Continued)

3.82-m span, a 229- by 381-mm cross section, and an effective depth of 317 mm. Reinforcement consisted of three No. 6 bars in tension and two No. 2 bars in compression. Shear reinforcement consisted of No. 2 stirrups at a spacing of 152 mm. Measurements consisted of steel and concrete strain, axial and lateral loads, pressure, displacement, and rotation. The Series 1 and 3 beams failed in flexural tension, and the Series 2 beams failed in shear compression. Also reported are the results of two companion plain concrete testing programs: (1) multiaxial testing of cubes, and (2) displacement-controlled cylinder tests.

CONTENTS

ILLUSTRATIONS

TABLES

I. INTRODUCTION

BACKGROUND

Although a significant amount of research has been directed toward the understanding of the behavior of reinforced concrete structures, there are some areas in which knowledge is incomplete. One such area is the mathematical modeling of the response of reinforced concrete structures under a wide variety of load conditions and ranges. Predicting the response of reinforced concrete structures loaded beyond the elastic range to collapse is an example of a case that cannot be adequately modeled. Specific areas that are not well understood include bond behavior between reinforcing steel and concrete, total multiaxial behavior of concrete, and strain rate effects on the behavior of concrete.

OBJECTIVE

This investigation was undertaken in an attempt to add to the basic understanding of the behavior of reinforced concrete members loaded to collapse. The specific objective of this research was to provide an elementary but well-defined data base of the material properties and the response of reinforced concrete beams subjected to combined flexural, axial, and shear forces. The resulting data are to be used in the development and verification of reinforced concrete behavioral models.

SCOPE

The experimental investigation consisted of three main areas of testing: static testing of reinforced concrete beams, multiaxial testing of plain concrete cubes, and displacement-controlled uniaxial tests on concrete cylinders.

The central area was the testing of nine reinforced concrete beams by the New Mexico Engineering Research Institute (NMERI). Nine hinge-supported reinforced concrete beams were tested under displacement control with a proportional axial and symmetrical two-point loading system. The nine beams were divided into three test series of three beams each. The beams in Series 1 contained shear reinforcement and were loaded monotonically to failure. Those in Series 2 contained no shear reinforcement and were loaded similarly to the first series. The Series 3 beams were shear reinforced and were loaded to

failure under cyclic loading. Data from these tests are presented in Appendix A.

Investigation of the other two areas was conducted by two universities under contract to NMERI. Multiaxial testing of 102-mm plain concrete cubes was performed at the University of Colorado. These cubes were cast from the concrete used for the beam fabrication. The results of this testing are reported in Appendix B. Displacement-controlled uniaxial compression tests were performed on 152-mm by 304-mm standard cylinders cast with the beams. This work was performed at San Diego State University. The results are reported in Appendix C.

PREVIOUS COMBINED-LOAD BEAM TESTS

The beam testing program reported herein was an extension of a previous investigation conducted at the Eric H. Wang Civil Engineering Research Facility (CERF) in 1975 (Ref. 1). The geometry and material properties were the same in the two programs except for the absence of shear reinforcement in the present Series 2 beams.

In the previous investigation, 17 simply supported reinforced concrete beams were tested to collapse under combined flexural, axial, and shear forces. The beams were loaded laterally through a symmetrical two-point loading system and axially through the plastic centroid. Loads were applied by a single hydraulic system designed to provide a constant ratio between axial and lateral loads for the duration of the test. The two test parameters were axial-to-lateral-load ratio and shear-span-to-beam-depth ratio. Electrical measurements of beam behavior included steel strain on the longitudinal rebar, concrete strain, vertical deflections along the length of the beam, end rotations, and lateral and axial loads. In addition, a photoelastic coating sheet was bonded to one side of the beams and overlaid with a sheet of Polaroid film. The experimental results from the beam tests were compared with data calculated with an analytical behavioral model developed as part of this effort. The general beam behavior calculated from the analytical model agreed well with the measured results, especially in the region up to maximum load.

---

1. Lane, Golden E., Jr., *Behavior of Reinforced Concrete Beams Under Combined Axial and Lateral Loading*, AFWL-TR-76-130, Air Force Weapons Laboratory, Kirtland Air Force Base, New Mexico, May 1977.

II. BEAM TESTING PROGRAM

The beam testing program consisted of statically testing to collapse nine rectangular reinforced concrete beams. Four sets of three beams each were cast for the test program. One set, however, was used in shakedown tests of the loading apparatus. Table 1 presents the test matrix.

TABLE 1. TEST MATRIX

Concrete batch	Casting date	Beam test series no.	Load type	Remarks
1	6/20/80	1	Monotonic to failure	Contained shear reinforcement
2	6/26/80	Shakedown	Used for checking out testing apparatus	Two with and one without shear reinforcement
3	7/03/80	2	Monotonic to failure	Contained no shear reinforcement
4	7/09/80	3	Cyclic to failure	Contained shear reinforcement

The duration of the tests varied from 2 to 5 min. All beams had the same span length, cross section, hinged end supports, and point of load application. However, the Series 2 beams contained no shear reinforcement. The two test parameters considered were shear reinforcement and type of loading, i.e., monotonic or cyclic. Figure 1 shows the general loading scheme for the beams. The axial-to-lateral-load ratio, P/F, remained constant at approximately 3.2 for the duration of each test.

GEOMETRY

Figure 2 shows the beam specimen geometry. The beam span was 3.82 m from center to center of the pivoted shafts at the beam ends. Included in the length are the end reaction devices shown in Figures 2 and 3. Except for the lack of shear reinforcement in the Series 2 beams, the cross-sectional properties and geometry were the same for all specimens. The beams were 381 mm in

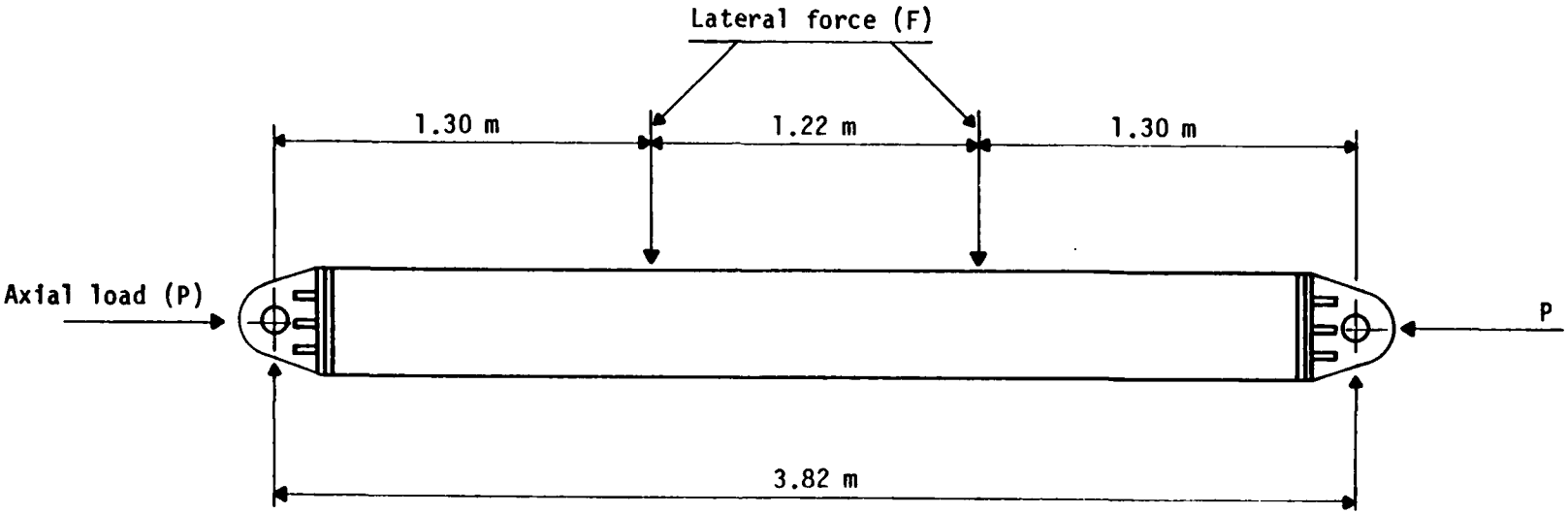

Figure 1. General loading configuration.

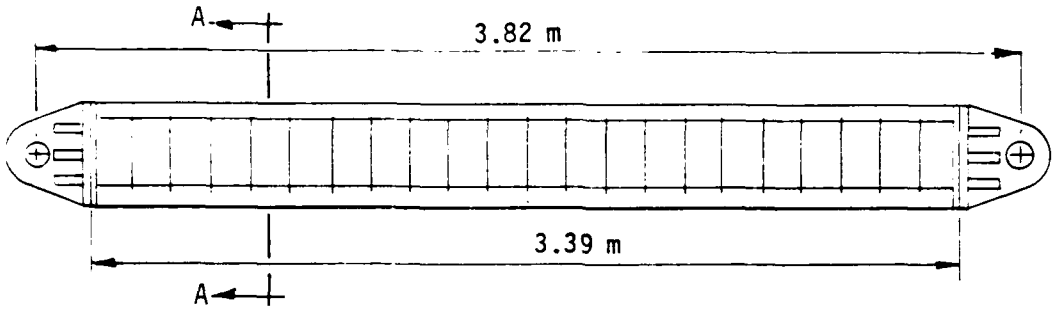

a. Elevation.

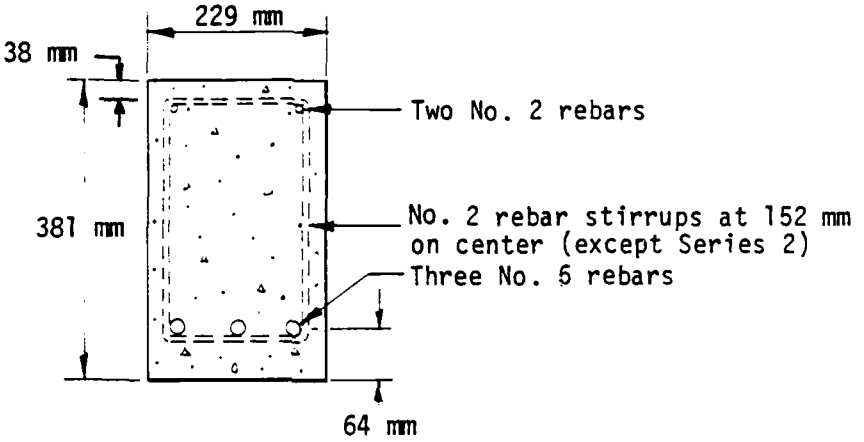

b. Section A-A.

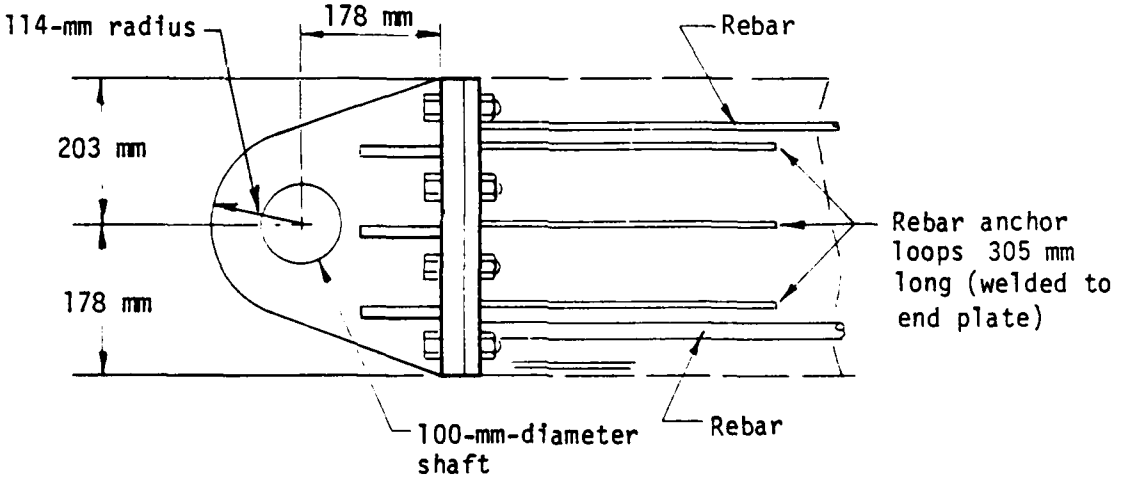

c. End detail.

Figure 2. Beam geometry.

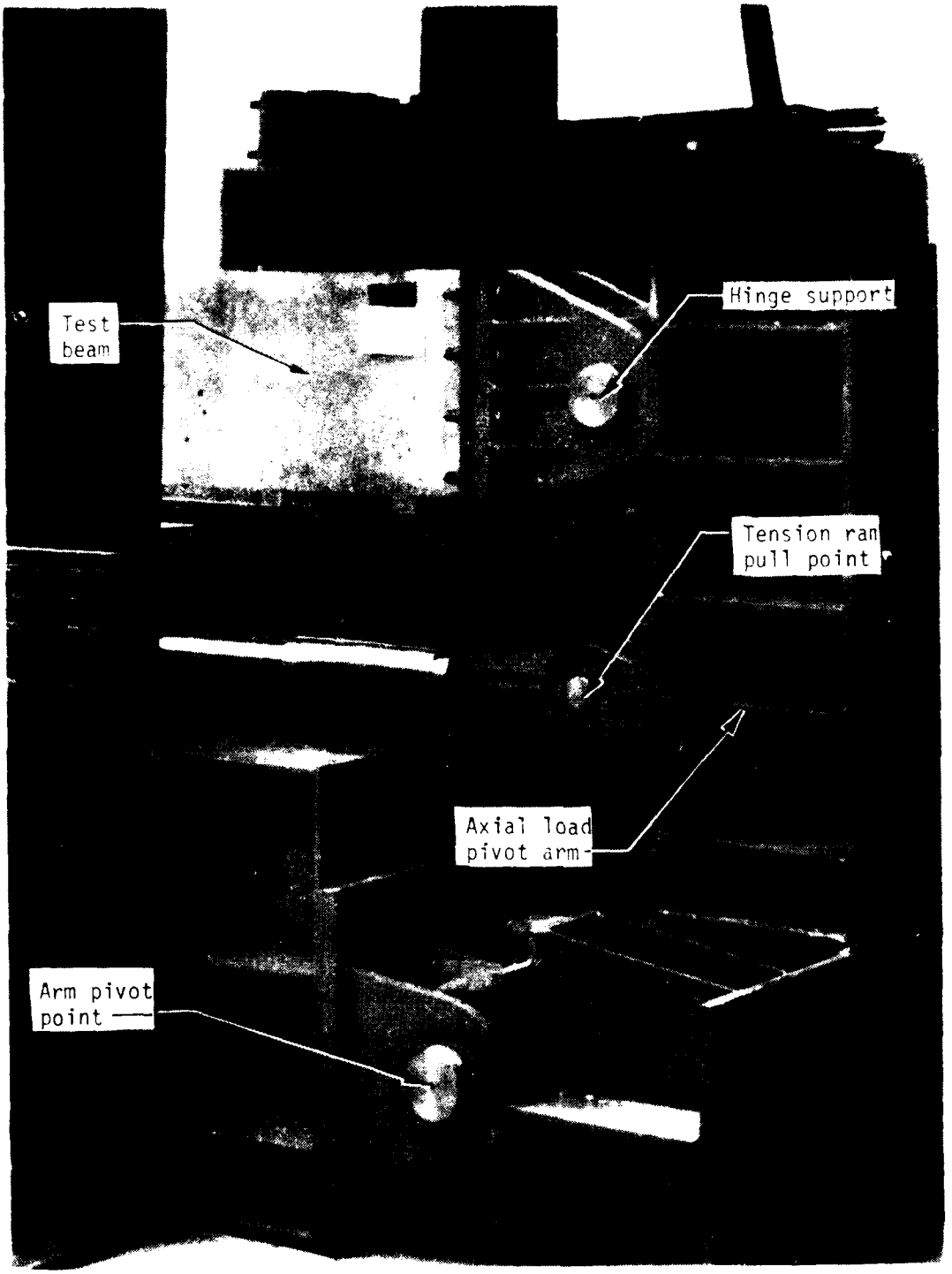

Figure 3. Axial load system.

overall depth and 229 mm wide, with a depth from the compressive face of the concrete to the centroid of the tensile steel of 317 mm. Tensile reinforcement consisted of three No. 6 reinforcing bars (rebar). The beams were considered to be singly reinforced in spite of the two No. 2 bars at the top of the beams. These two bars were included to assist in beam fabrication and to provide a means of making strain measurements in the compression zone.

To facilitate axial load application, the concrete portion of the beams was terminated at end bearing plates to which the end reaction devices were bolted. The longitudinal reinforcement was welded to the end bearing plates to assure adequate anchorage for the bars and to assure development of the full flexure and shear capacities of the beams. Additional reinforcement was also welded to the end plates to provide a mechanism for shear transfer between the concrete and the end supports. Figure 2 shows the detail of the end bearing plates.

REINFORCING STEEL

The principal longitudinal reinforcement, which consisted of three No. 6 bars, had a measured yield strength of 427 MPa and conformed to American Society for Testing and Materials (ASTM) specification A15-60. All of the steel was produced from the same heat to insure consistency among the beam specimens. A typical stress-strain curve is shown in Figure 4.

The stirrups and compression reinforcement were intermediate-grade steel conforming to ASTM specification A15 with a measured yield strength of 359 MPa. Although not covered by ASTM specification A305, the No. 2 bars had deformations similar to those of the No. 6 bars. Figure 5 shows a typical stress-strain curve for the No. 2 bars.

CONCRETE

The concrete used in the beams and in the other test specimens had a nominal compressive strength of 35 MPa and was produced with Type I/II portland cement and a maximum-size aggregate of 10 mm. The coarse aggregate was a crushed material of uniform gradation. The fine aggregate was a washed sand conforming to ASTM specification C-33 and had less than 2 percent by weight

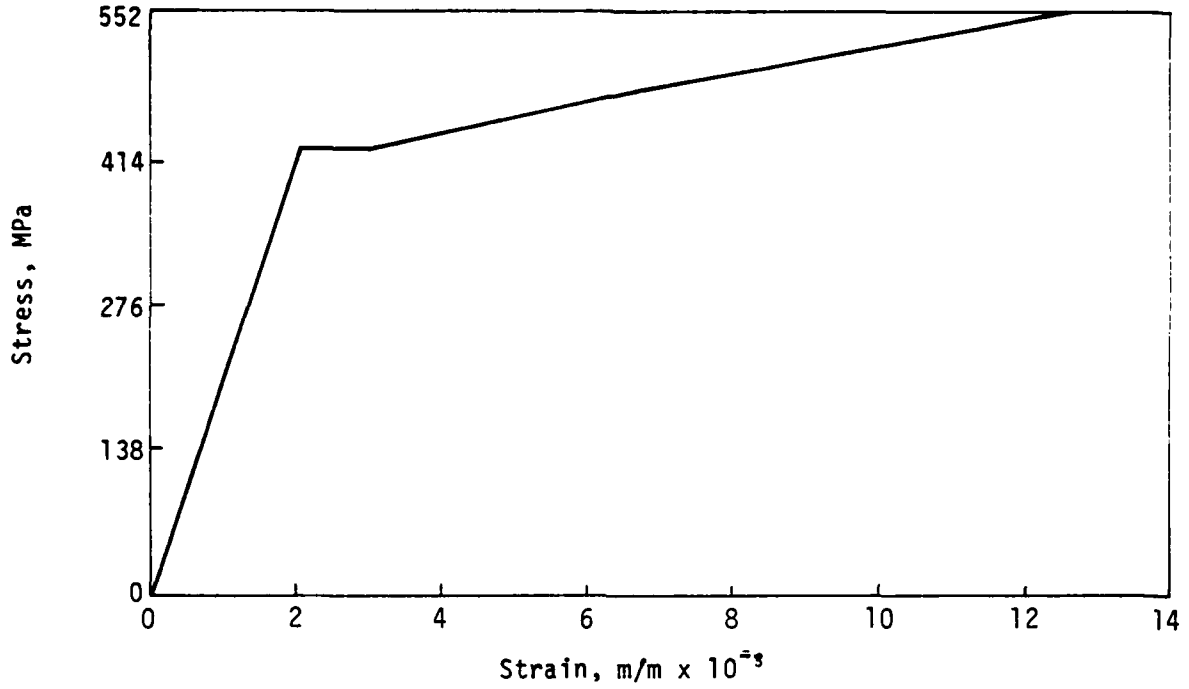

Figure 4. Stress-strain curve, No. 6 bars.

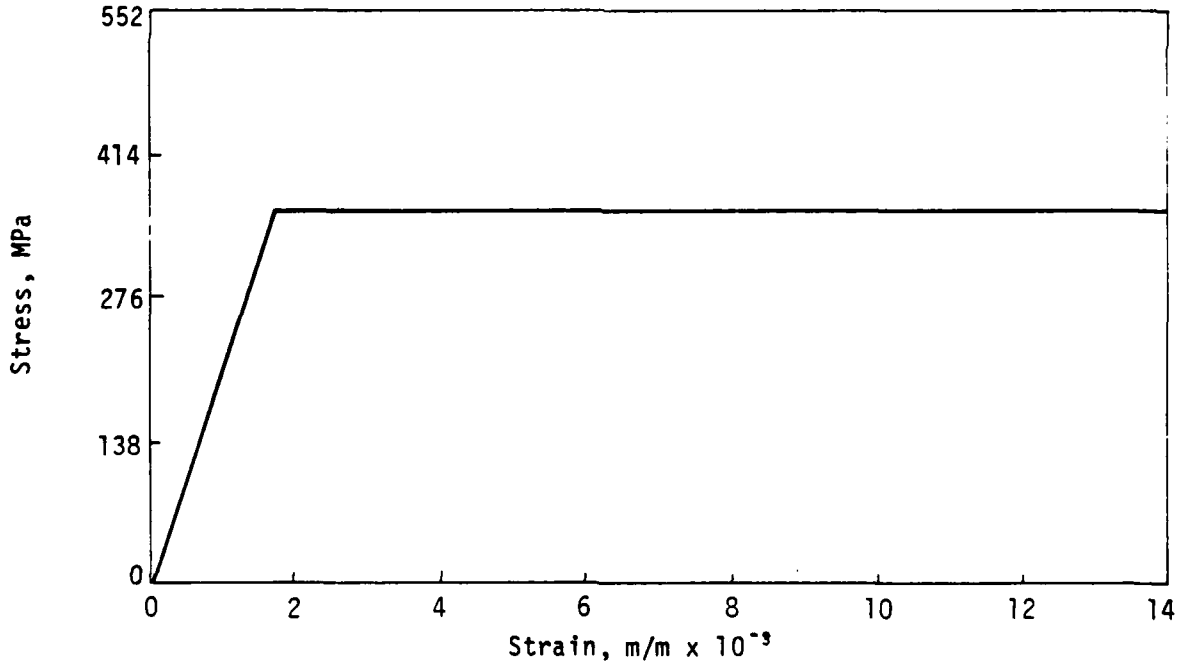

Figure 5. Stress-strain curve, No. 2 bars.

passing the No. 200 sieve. The fineness modulus of the sand varied from 2.6 to 3.1. The concrete mix is shown below.

Cement	289 kg
Fine aggregate	739 kg
Coarse aggregate (10 mm crushed)	576 kg
Water	175 kg
Admixture	
Master Builders Pozzolith 300 N	59 ml

The concrete was mixed in a Daffin mobile concrete mixer which produces the concrete by a continuous mixing process. The beams and auxillary specimens were cast in four batches. Each batch consisted of three beams, twenty 152-mm by 305-mm cylinders, twenty-four 102-mm cubes, and nine pullout specimens. The beam concrete was compacted with an electric vibrator probe. The other specimens were compacted by rodding. All specimens were cured under polyethylene plastic sheets. Results of tests on the concrete control cylinders are presented in Table 2.

INSTRUMENTATION

Instrumentation for all of the beams was generally similar. The main exception was the absence of stirrup strains for the Series 2 beams. Measurements made included vertical deflection along the beam, vertical and horizontal deflections at the support shafts, steel and concrete strain at various locations, rotation at the beam ends, and lateral and horizontal loads.

Displacement--Figure 6 shows the layout of the measurement stations and the location of displacement measurements. Vertical deflection measurements were made at seven locations along the beam (stations 0, 2, 3, 4, 5, 6, and 8). The measurements were made with Celsco linear potentiometers connected to the back of the beams at middepth. The same type of potentiometers were used to measure the horizontal movement of the end supports. Figure 7 shows the potentiometer attached to a beam.

Strain--Strain measurement locations are shown in Figure 8. Steel strain in the longitudinal tensile reinforcement was measured at stations 2 through 6. The measurements were made on the middle reinforcing bar. Strain measurements on the two compression steel bars were also taken at stations 2 through

TABLE 2. BEAM TEST CONCRETE STRENGTH DATA

Batch	Test no.	Test date	Age at testing, days	Cylinder[a] test, MPa	Beam[b] test, MPa	Split cylinder test, MPa
1						
Series 1						
Cast 6/20/80	1-1	10/16/80	118	37.4	3.59	---
7 day - 26.3 MPa	1-2	10/17/80	119	38.2	3.50	---
14 day - 32.0 MPa	1-3	10/21/80	123	38.9	3.76	---
28 day - 34.6 MPa						
SDSU[c] - 34.0 MPa						
2						
Shakedown	1	9/23/80	89	36.3	---	---
Cast 6/26/80	2	10/07/80	103	37.9	3.21	5.62
7 day - 27.6 MPa	3	11/06/80	138	31.9	5.32	3.93
14 day - 29.0 MPa						
28 day - 34.7 MPa						
SDSU - 36.1 MPa						
3						
Series 2	2-1	10/24/80	113	33.0	4.59	---
Cast 7/03/80	2-2	10/28/80	117	40.3	4.60	4.38
7 day - 24.1 MPa	2-3	10/31/80	120	31.0	5.31	3.66
14 day - 29.9 MPa						
28 day - 33.5 MPa						
SDSU - 36.9 MPa						
4						
Series 3	3-1	11/10/80	124	29.9	4.70	3.96
Cast 7/09/80	3-2	11/18/80	132	40.6	5.04	4.65
7 day - 27.3 MPa	3-3	11/20/80	134	41.2	4.79	3.75
14 day - ---						
28 day - 34.1 MPa						
SDSU - 34.7 MPa						

[a]152- by 305-mm cylinder; average of three cylinders.

[b]152- by 152- by 533-mm beam; modulus of rupture.

[c]Tests at San Diego State University; average of six cylinders.

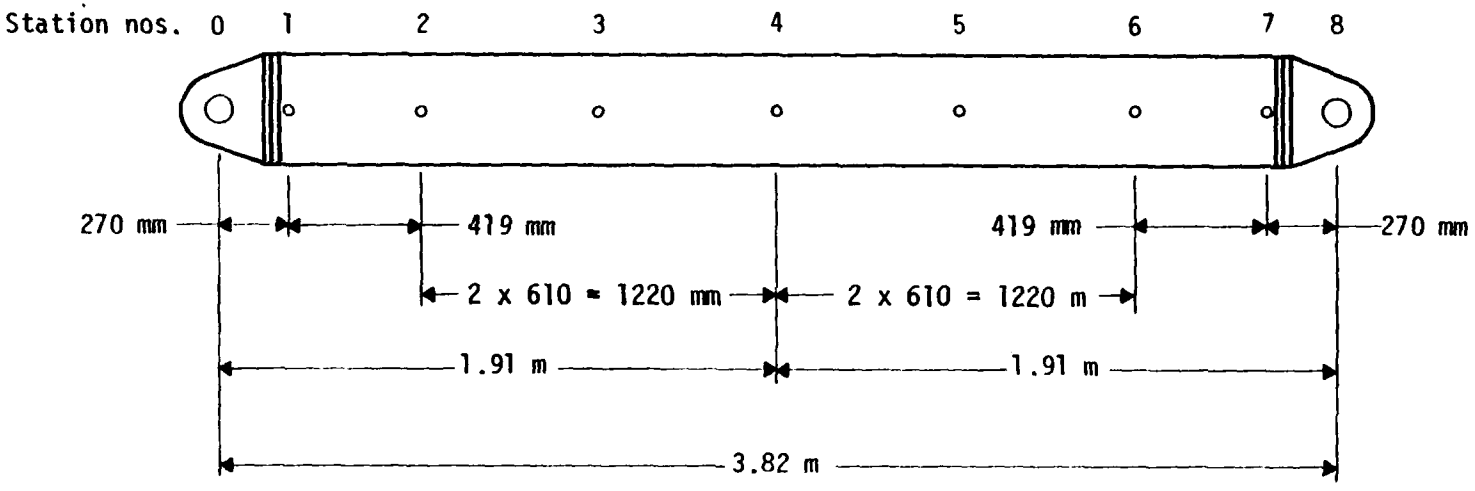

Measurements:
Stations 0 and 8, horizontal and vertical displacement.
Stations 1 and 7, rotation only.
Stations 2 through 6, vertical deflection.
Stations 2 through 6, strain (See Fig. 8).

Figure 6. Measurement station layout.

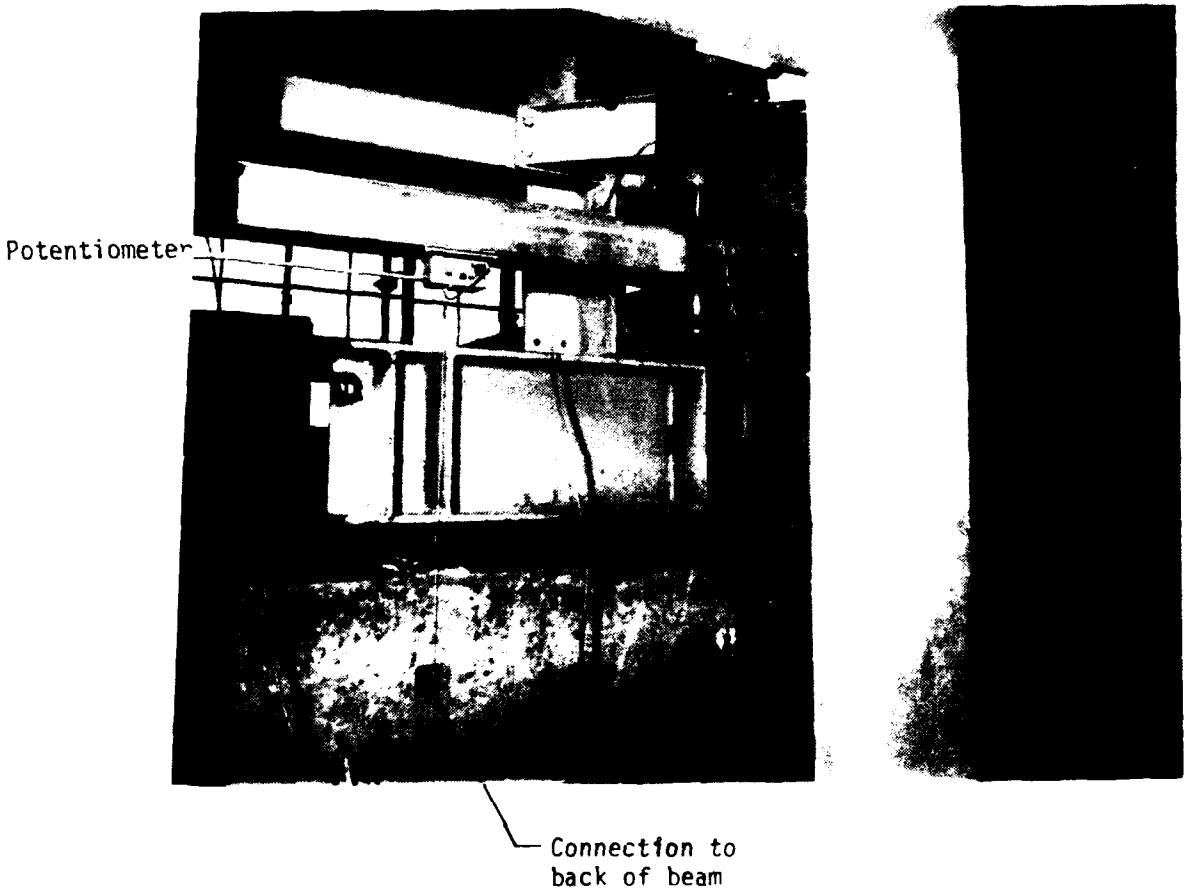

Figure 7. Potentiometer attachment.

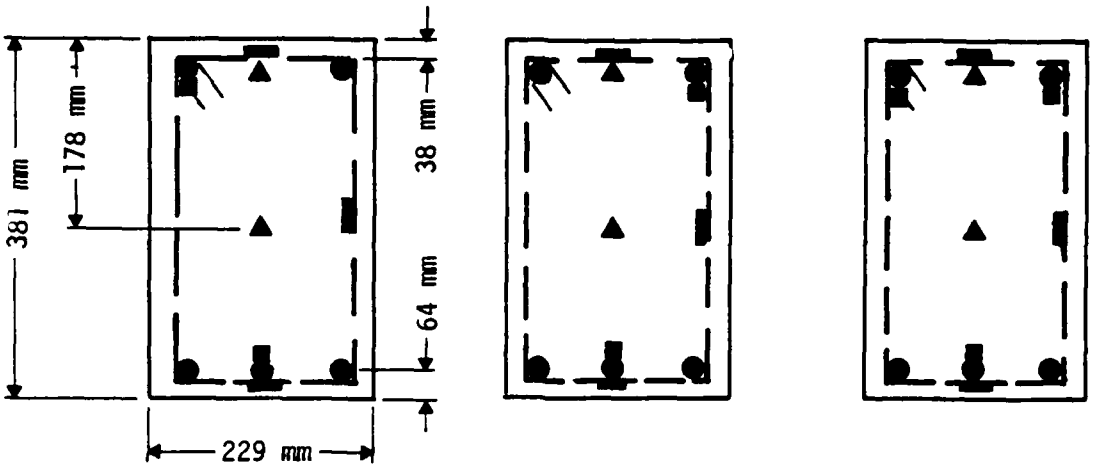

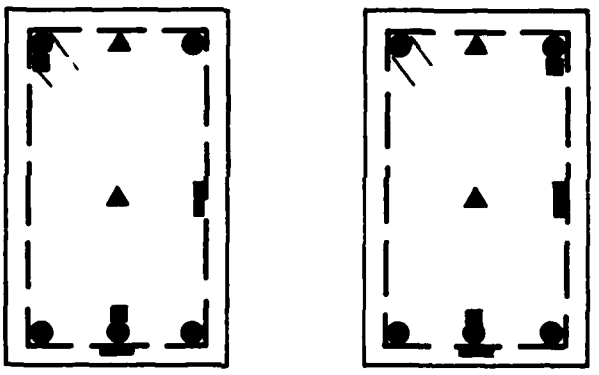

Legend

■ Longitudinal steel strain

▬ Vertical or transverse steel strain

▲ Embedded concrete strain

Figure 8. Strain measurement locations.

6. At station 4, the beam centerline, a strain gage was mounted on each bar. At the remaining stations, the measurements were taken on alternate sides of the beam. Vertical and transverse steel strains were taken on stirrups. For Series 1 and 3, vertical strains were measured on opposite sides of the beams at stations 2 through 6, and transverse strains were made alternately at the top and bottom of the beams at stations 2 through 6. For Series 2, which had no shear reinforcement in the shear span, vertical and transverse strains were made at stations 3, 4, and 5. Measurements were made with 350-Ω, epoxy-backed, foil strain gages which had a 13-mm gage length and a gage factor of 2.125.

Concrete strains were measured near the top and at the middle of the beams at stations 2 through 6. These strains were measured with epoxy-encapsulated, 120-Ω, embedded strain gages with a 30-mm gage length and a gage factor of 2.10.

Rotation--Rotation measurements were made at both ends of the beams with gages specially fabricated by NMERI. The rotation gages consisted of a pendulum suspended from the paddle portion of a DX-type velocity gage. The rotation of the pendulum relative to the gage body was measured by the variable inductance transducer of the velocity gage.

Load--Load measurements were made at the vertical ram providing the lateral load and at the two horizontal rams providing the axial load. These measurements were made with load cells fabricated and calibrated by NMERI. In-line hydraulic pressure was also monitored.

DATA ACQUISITION

The data were recorded, stored, and plotted on a Hewlett-Packard model 3052 data acquisition system. The voltage output from the system's digital multimeter was recorded on a floppy disk. The sampling rate was approximately two samples per second for every channel. The same system was used to reduce and plot the data.

TEST APPARATUS

Figure 9 shows a schematic drawing of the load application system. The loading device used in this investigation was the same test frame used in the

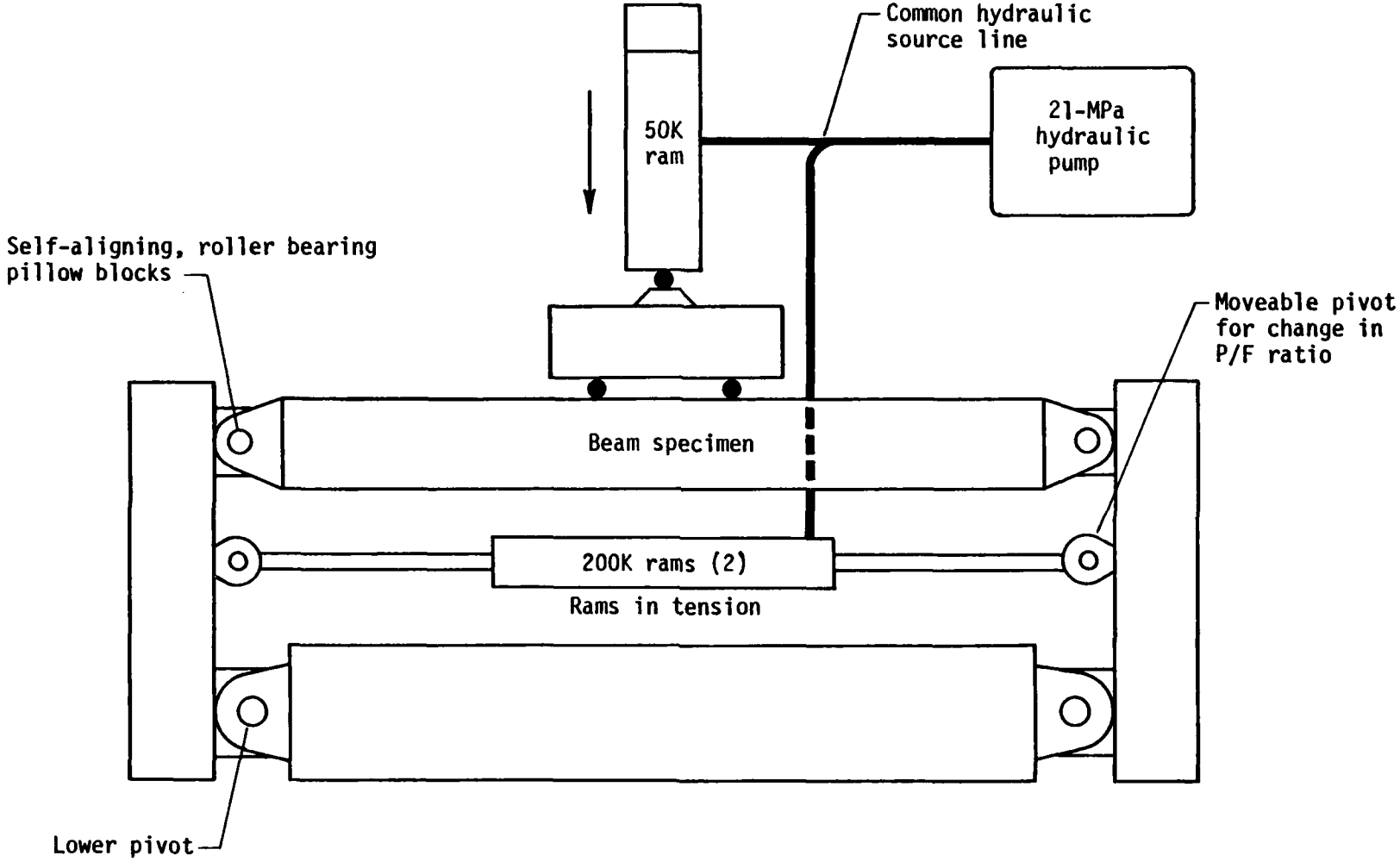

Figure 9. Schematic of beam loading system.

previous beam testing program reported in Reference 1. It was also the same frame used by Crist (Ref. 2) in a reinforced concrete deep beam study. The frame was modified to accommodate axial load application. Figure 10 shows the modified test frame which consisted of an upper portion that provided reaction for the lateral load and a lower portion that provided the axial load and support system. The two portions were tied together by five vertical structural T-sections.

Lateral load was applied by a 377-kN-capacity hydraulic ram with a 300-mm stroke. Axial load was applied by two 890-kN-capacity double-acting rams with 600-mm strokes, mounted in a horizontal position. A single hydraulic system was used to activate the rams to insure a constant P/F ratio throughout each test. The hydraulic system had a capacity of 21 MPa.

The total lateral load was divided into a two-point load by a steel distribution beam which imparted force to the beams through 64-mm-diameter rollers and 102- by 229- by 19-mm steel bearing plates. One end of the distribution beam was free to translate and rotate while the other end was only free to rotate. The bearing plates were seated to the beams with a thin layer of high-strength gypsum compound. The length of the shear span was established by the position of the lateral loads.

Axial load was applied to the beams with the two horizontal rams in tension; this resulted in compression on the beam because of the pivoting of the vertical reaction arms (Figs. 3 and 9). The P/F ratio was defined by the pull-point position of the rams on the reaction arms. To adjust the P/F ratio, the connection point of the tension rams to the pivot arm could be changed. The hinged condition at the ends of the beams was insured by transmitting the axial load through self-aligning, roller-bearing pillow blocks and 102-mm-diameter steel shafts. The axial force was applied through the plastic centroid of the beam cross section. The plastic centroid of a section, as defined by the 1977 ACI Building Code (Ref. 3), is the centroid of resistance to load

---

2. Crist, R. A., *Shear Behavior of Deep Reinforced Concrete Beams, Vol. II: Static Tests*, AFWL-TR-67-61, Air Force Weapons Laboratory, Kirtland Air Force Base, New Mexico, October 1967.

3. *Building Code Requirements for Reinforced Concrete, ACI (318-77)*, American Concrete Institute, Detroit, Michigan, 1977.

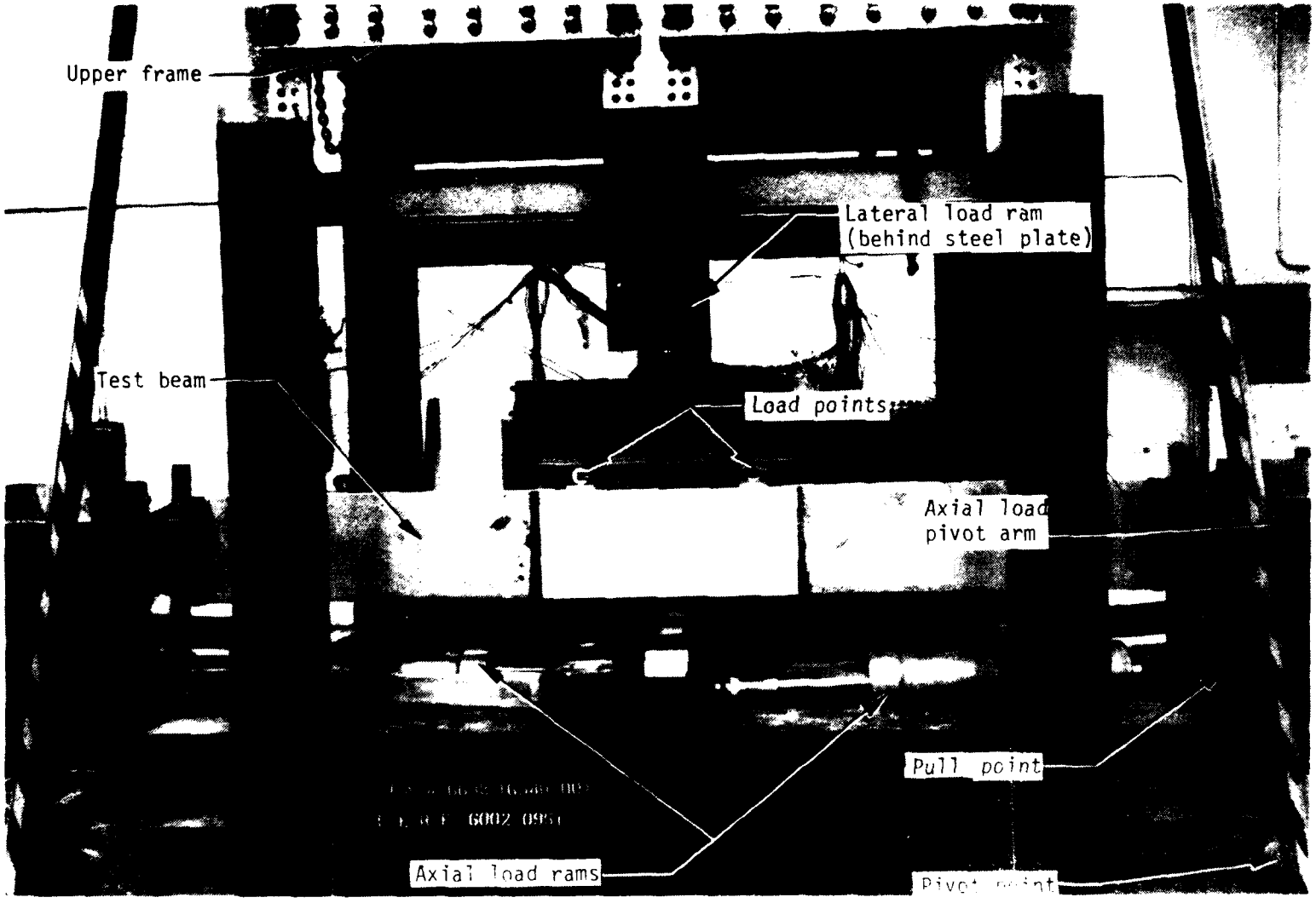

Figure 10. Test frame.

computed under the assumption that the concrete is uniformly stressed to failure (f'_c) and the reinforcing steel is uniformly stressed to yield strength (f'_y).

To insure that the forces measured in the horizontal rams during the tests could be accurately converted to axial forces in the test beams, a series of calibration tests was conducted prior to actual beam testing. The calibration tests consisted of loading a dummy beam axially while measuring the forces in the hydraulic rams with force links and the axial load in the beam with a load cell. Under the assumption that all joints in the mechanical linkage between the horizontal rams and the dummy beam were frictionless, the calculated axial load in the beam was compared to the load indicated by the load cell. The agreement between calculated and measured forces in the dummy beam was within 10 percent; however, the corrections derived from the calibration tests were used to determine axial loads in the beams during the actual tests.

The displacement control feature of the tests was accomplished with a Datatrak programmer system. This entailed etching the desired deflection-time history onto a special metallic paper. The paper was then placed on a drum that rotated at a rate selected to produce the desired test duration. As the drum rotated, a servomotor moved a sensor on the paper, keeping it in contact with the upper surface of the etched program. The servomotor also positioned the wiper of a set of point potentiometers which provided an electrical analog signal proportional to desired beam displacement as a function of time. A linear potentiometer was used to monitor actual beam deflection. The difference between the actual and the desired potentiometer voltages formed an error signal. A current proportional to this error signal was supplied to a Moog servovalve which increased or decreased the pressure on the beam's hydraulic cylinders as needed to make the error signal zero. The control parameters for the monotonic tests, Series 1 and 2, were a 152-mm maximum centerline deflection at approximately 300 s. The displacement-time functions for all three series are shown in Figure 11. The five control points where the deflection was to drop off--13, 23, 32, 51, and 102 mm--were selected on the basis of the load-deflection behavior of the Series 1 beams. The points were selected to provide unload cycles midway in the linear region, near yield, in the flat portion of the curve, just into strain-softening, and late into strain-softening.

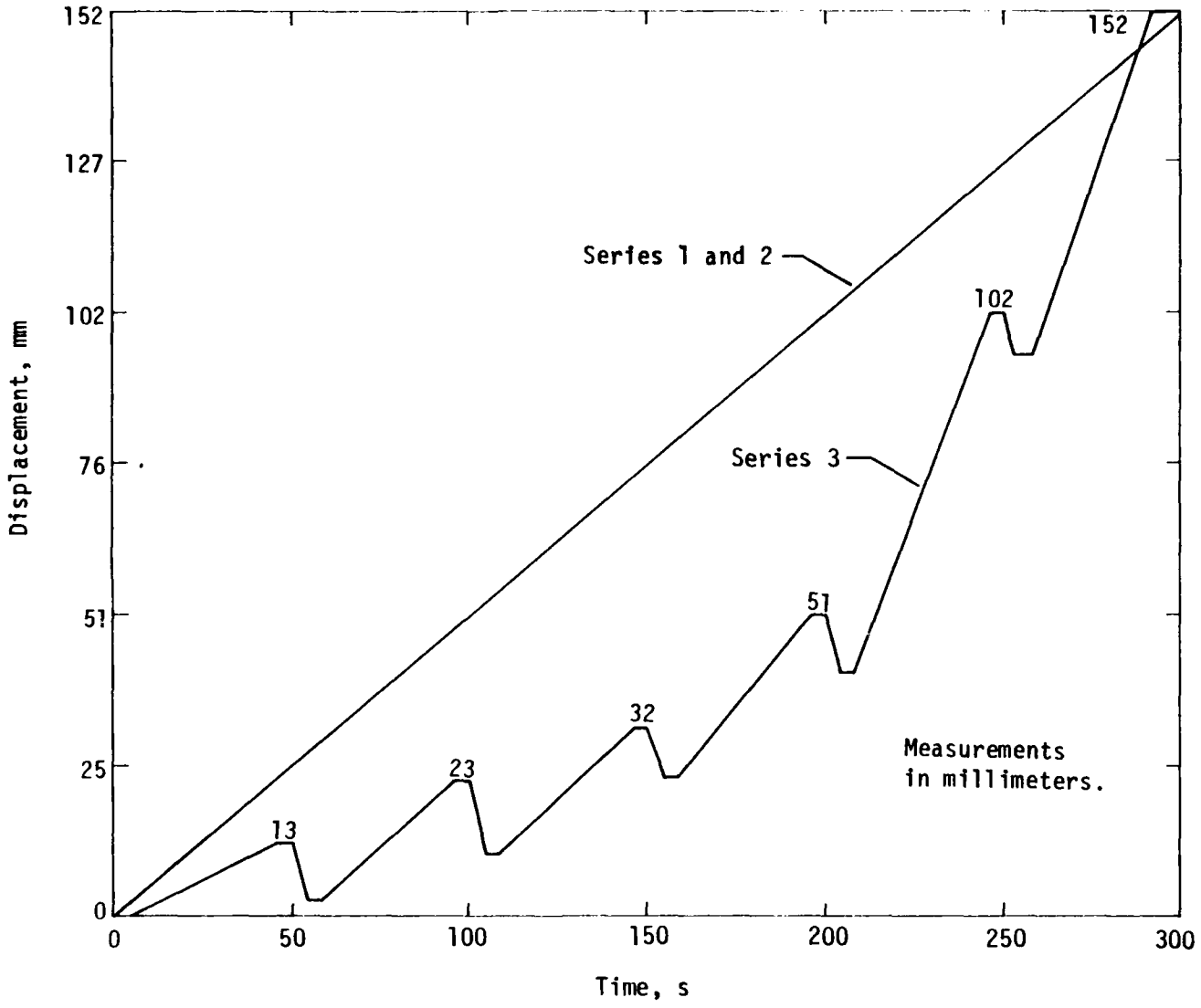

Figure 11. Displacement-time histories.

III. BEAM TESTING RESULTS

Table 3 presents a summary of the test results. The P/F ratios presented in Table 3 were calculated from measured loads, which is the reason for the variation in a parameter that should be constant.

Data from the beam tests are presented in Appendix A. For Series 1 and 2, where possible, data traces for symmetric locations were plotted on the same graph. Because of the cyclic loading in Series 3, representative plots of the symmetric measurement locations are presented.

TABLE 3. SUMMARY OF TEST DATA

Beam test designation	Test date	Concrete strength, MPa	Concrete age at testing, days	Maximum lateral load, kN	P/F ratio	Failure mode
1-1	10/16/80	37.4	118	235.7	3.24	Flexural tension
1-2	10/17/80	38.2	119	224.0	3.32	Flexural tension
1-3	10/21/80	38.9	123	222.5	3.40	Flexural tension
2-1	10/24/80	33.0	113	217.3	3.39	Shear compression
2-2	10/28/80	40.3	117	205.8	3.26	Shear compression
2-3	10/31/80	31.0	120	218.5	3.38	Shear compression
3-1	11/10/80	29.9	124	237.8	3.28	Flexural tension
3-2	11/18/80	40.6	132	231.0	3.04	Flexural tension
3-3	11/20/80	41.2	134	228.5	3.11	Flexural tension

GENERAL BEHAVIOR

The general response of the beams can be illustrated by their load-centerline deflection curves. Figure 12 shows the idealized load-deflection curve for the beams. The initial behavior is linear to about 10 percent of the maximum load. The concrete then cracks, and the curve is again fairly linear at a reduced stiffness. When the tension reinforcement begins to yield, the curve becomes very nonlinear and flattens out. When the concrete in the compression zone begins to crush and spall, the beam resistance decreases with increasing deflection. For beams failing in shear, the behavior is the same up to the maximum shear resistance of the beam. The shear failure then results in sudden collapse of the beam. The cyclically loaded beams have the same

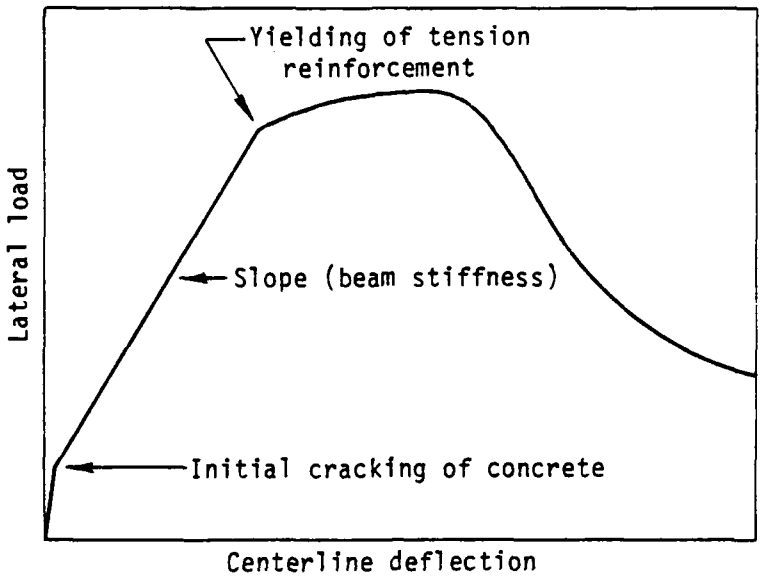

Figure 12. Idealized load-centerline deflection curve.

general behavior as the monotonically loaded beams except for the addition of the unloading and reloading hysteretic loops. The loops also progressively exhibit a stiffness reduction.

SERIES 1 BEAMS

The Series 1 beams were monotonically loaded to failure under a two-point lateral load and a proportional axial load. The Series 1 tests were conducted to determine the correlation between beams tested under load control and those tested under deflection control. Figure 13 presents the load-deflection curves for the three Series 1 beams along with the curve for beams 4-3-1 and 4-3-2 of the load control study (Ref. 1). The calculated curve is also included.

All of the beams exhibited the same behavior through the yielding of the tensile reinforcement and out to the maximum load capacity. The strain softening portions of the deflection control beams are similar, falling between the curves for the load control beams.

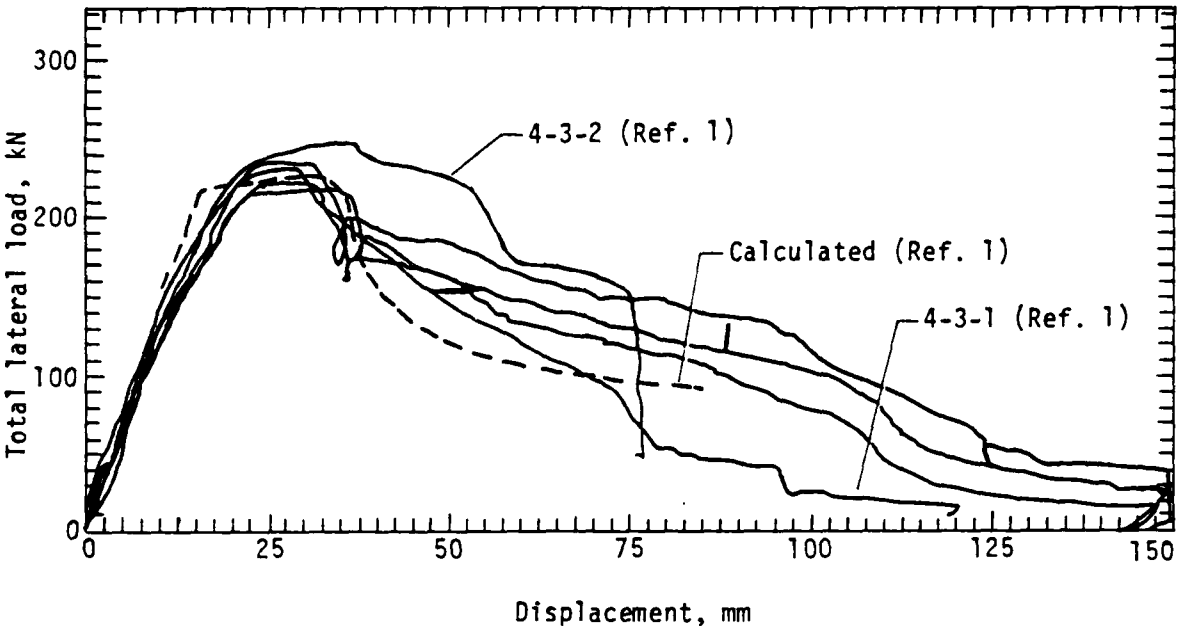

Figure 13. Load-centerline deflection, Series 1.

Also compared are the reinforcing steel strain data at the centerline of beam 4-3-1 (Ref. 1) and beam 1-1. Figures 14 and 15 present the tensile and compression strain plots, respectively. From the data presented, it appears there was little difference in the behaviors of the load controlled and the deflection controlled beams.

The mode of failure of the Series 1 beams was flexural tension; i.e., the tension reinforcement began yielding prior to crushing of the concrete. Because of the deflection control, the beams did not suddenly collapse, allowing measurement of the flexural resistance up to the maximum deflection of 150 mm. Because the load duration of the tests was relatively short, the concrete cracks were not marked at various load intervals, but were all marked and photographed at the conclusion of each test. Figure 16 shows the final crack patterns of all beams.

SERIES 2 BEAMS

These beams contained no web reinforcement in the shear span. The calculated maximum total lateral load for shear failure, based on the ACI code, was 180 kN. The calculated maximum lateral load for the flexural resistance was 225 kN. Figure 17 presents the load-deflection curves for the Series 2 beams.

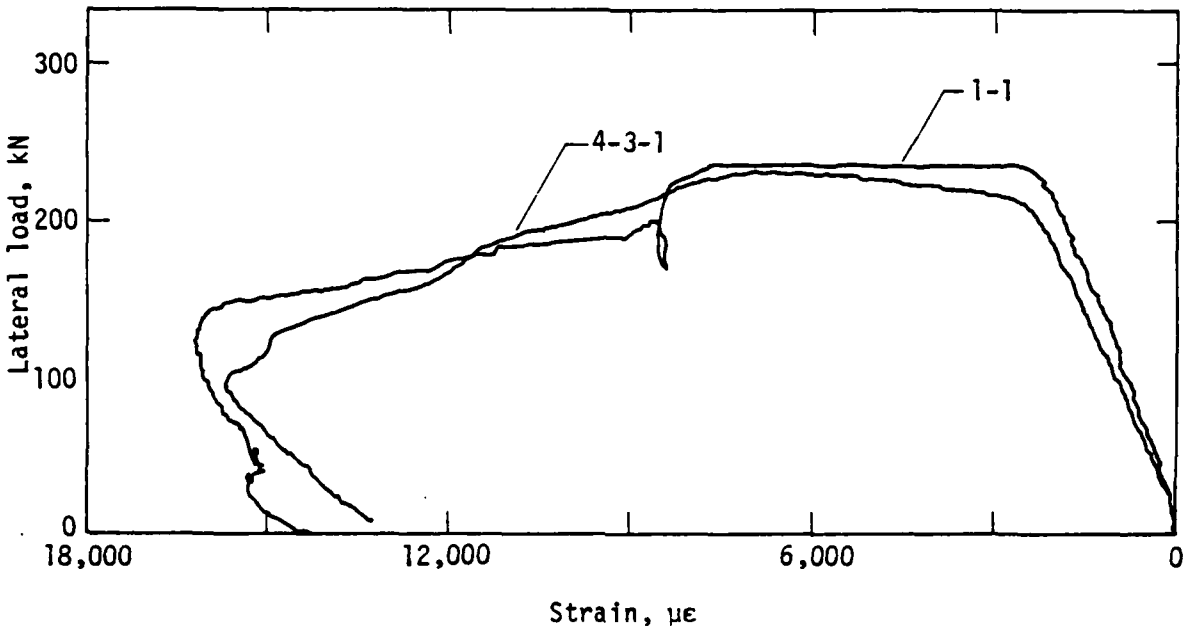

Figure 14. Centerline tensile steel strain.

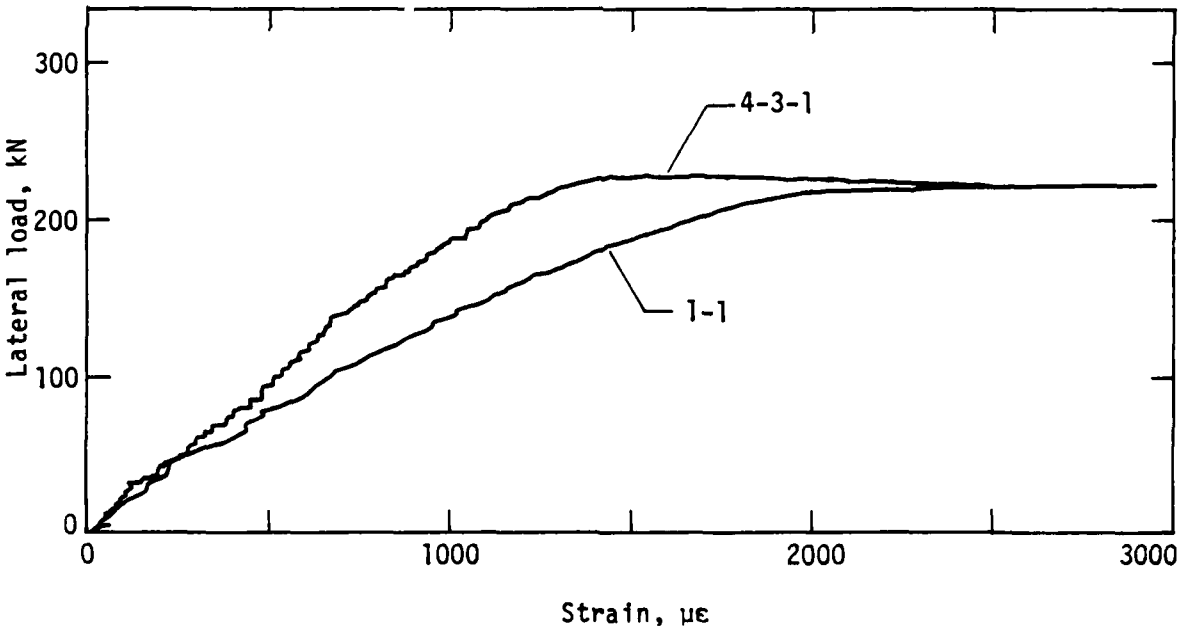

Figure 15. Centerline compression steel strain.

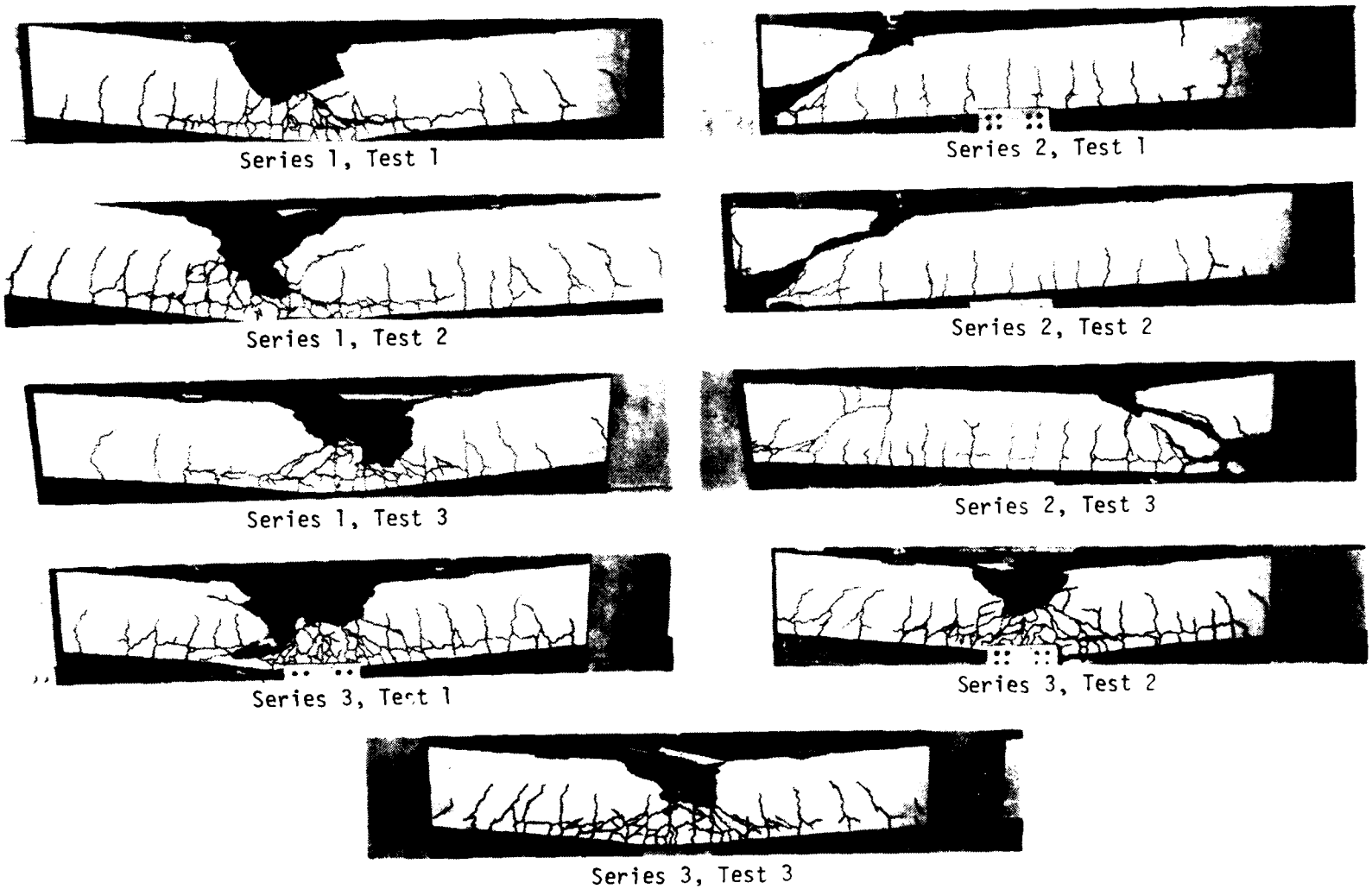

Figure 16. Final crack patterns for beams tested.

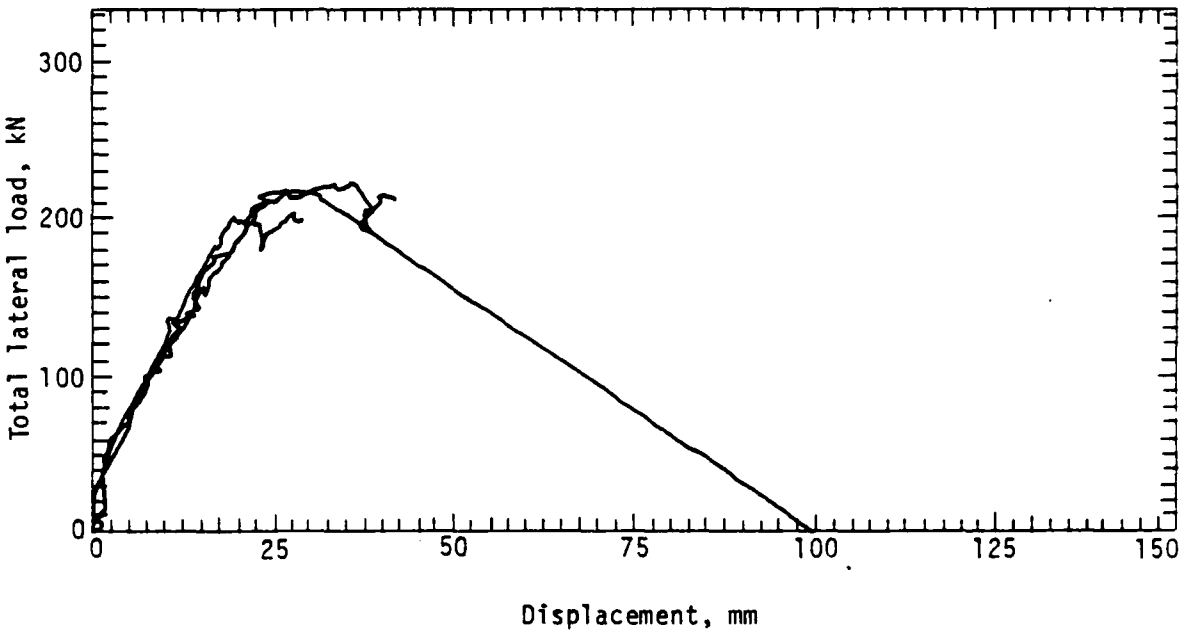

Figure 17. Load-centerline deflection, Series 2.

The general load-deflection behavior of the beams was the same as the Series 1 beams up to yield of the tensile reinforcement. After the tensile reinforcement began to yield, the shear crack became more apparent and widened. When the crack extended into the compression zone, the beams collapsed. The deflection control system was not sensitive enough to stop the beam from collapsing. The failure loads were only slightly less than the maximum beam resistance.

SERIES 3 BEAMS

The Series 3 beams were constructed in the same way as the Series 1 beams. However, they were loaded under five load-unload cycles. The programmed deflection-time history is shown in Figure 11. The history was intended to provide unload cycles at about midway in the linear range, near yield of the tensile reinforcement, in the flat portion of the curve, just into the strain-softening region, and late in the strain-softening region. The envelope of the load-deflection history generally coincides with the load-deflection curves for the Series 1 beams. The load-deflection curves for the beams are shown in Figure 18. Two significant aspects of the behavior are the hysteretic loops and the stiffness degradation at increasing deflection.

Figure 19 presents load-centerline plots of one beam test from each series.

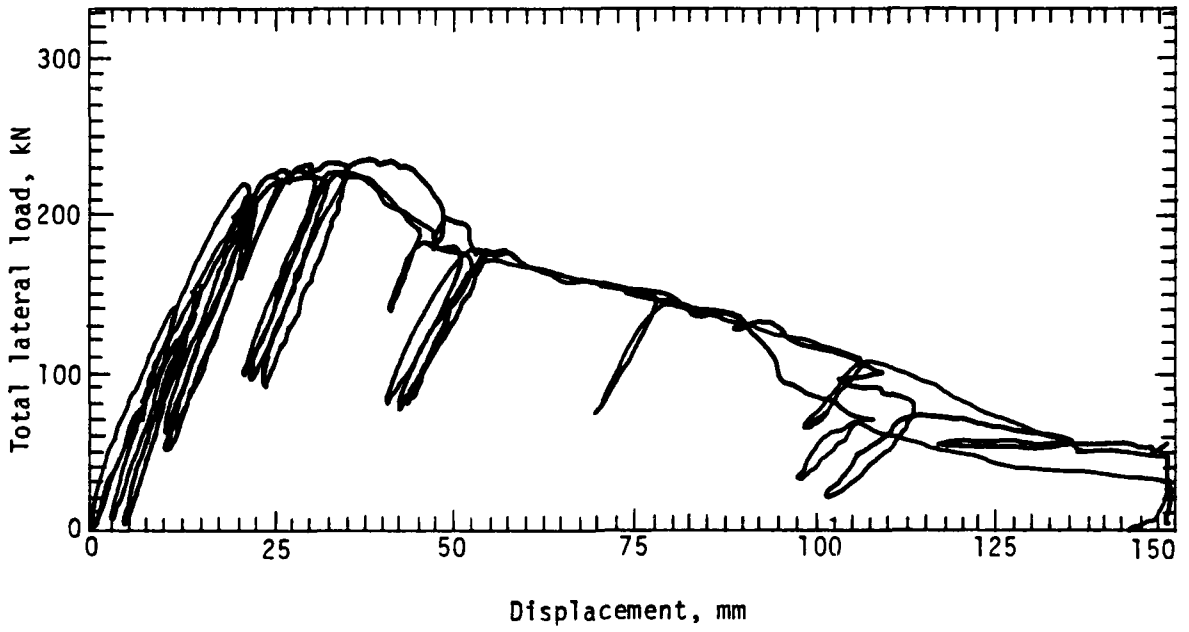

Figure 18. Load-centerline deflection, Series 3.

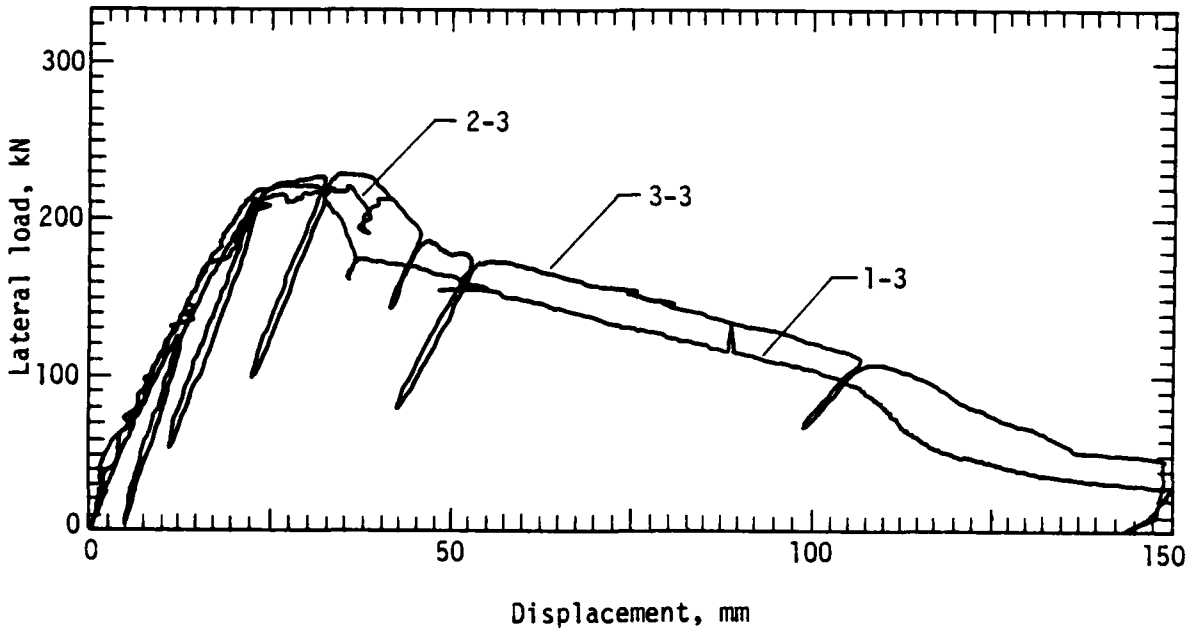

Figure 19. Load-displacement for three beams.

IV. BEAM TESTING CONCLUSIONS

Nine reinforced concrete beams were statically tested under combined axial and lateral load. The beams were laterally loaded by a symmetrical two-point load. The ratio of axial-to-lateral load was constant throughout the tests and had a value of approximately 3.2. Deflection control was used in the loading to failure of the beams. A closed loop system was used to provide the deflection control for the tests.

The beam tests consisted of three series of three beams each. The geometry and longitudinal reinforcement were the same for all beams. However, the Series 2 beams contained no web reinforcement in the shear span. The Series 1 beams were monotonically loaded to a maximum deflection of 150 mm with the failure being flexural tension. The Series 2 beams failed in shear-compression, at a load slightly less than the Series 1 beam. The Series 3 beams were tested under cycles of load-unload with the test being stopped at a maximum deflection of 150 mm. These beams also failed in flexural tension.

The behavior of the Series 1 beams was very similar to the 4-3-1 and 4-3-2 beams of the previous test program reported in Reference 1. The only difference in the two test series was the use of deflection control in this study versus the load control used in the previous study. The similarities in the behavior of the beams indicate that the loading apparatus was stiff enough in the previous test not to alter significantly the behavior at initial crushing of the concrete and into the strain-softening region.

The Series 2 beams, designed to fail in shear, exhibited essentially the same behavior as the Series 1 beams up to just beyond yielding of the tensile reinforcement. At that point, the beams suddenly collapsed as a result of shear-compression failure.

The Series 3 beams, which were loaded cyclically, produced the same envelope load-deflection behavior as the Series 1 beams. The load-unload cycles can be characterized by a slight amount of hysteretics and a degradation with increasing deflection.

CONVERSION FACTORS FOR U.S. CUSTOMARY TO METRIC (SI) UNITS OF MEASUREMENTS

(Symbols of SI units given in parentheses)

To convert from	to	Multiply by
angstrom	meters (m)	1.000 000 X E -10
atmosphere (normal)	kilo pascal (kPa)	1.013 25 X E +2
bar	kilo pascal (kPa)	1.000 000 X E +2
barn	meter^2 (m^2)	1.000 000 X E -28
British thermal unit (thermochemical)	joule (J)	1.054 350 X E +3
calorie (thermochemical)	joule (J)	4.184 000
cal (thermochemical)/cm^2	mega joule/m^2 (MJ/m^2)	4.184 000 X E -2
curie	giga becquerel (GBq)*	3.700 000 X E +1
degree (angle)	radian (rad)	1.745 329 X E -2
degree Fahrenheit	degree kelvin (K)	$t_K = (t_{°F} + 459.67)/1.8$
electron volt	joule (J)	1.602 19 X E -19
erg	joule (J)	1.000 000 X E -7
erg/second	watt (W)	1.000 000 X E -7
foot	meter (m)	3.048 000 X E -1
foot-pound-force	joule (J)	1.355 818
gallon (U.S. liquid)	meter^3 (m^3)	3.785 412 X E -3
inch	meter (m)	2.540 000 X E -2
jerk	joule (J)	1.000 000 X E +9
joule/kilogram (J/kg)(radiation dose absorbed)	Gray (Gy)**	1.000 000
kilotons	terajoules	4.183
kip (1000 lbf)	newton (N)	4.448 222 X E +3
kip/$inch^2$ (ksi)	kilo pascal (kPa)	6.894 757 X E +3
ktap	newton-second/m^2 ($N-s/m^2$)	1.000 000 X E +2
micron	meter (m)	1.000 000 X E -6
mil	meter (m)	2.540 000 X E -5
mile (international)	meter (m)	1.609 344 X E +3
ounce	kilogram (kg)	2.834 952 X E -2
pound-force (lbf avoirdupois)	newton (N)	4.448 222
pound-force inch	newton-meter (N·m)	1.129 848 X E -1
pound-force/inch	newton/meter (N/m)	1.751 268 X E +2
pound-force/$foot^2$	kilo pascal (kPa)	4.788 026 X E -2
pound-force/$inch^2$ (psi)	kilo pascal (kPa)	6.894 757
pound-mass (lbm avoirdupois)	kilogram (kg)	4.535 924 X E -1
pound-mass-$foot^2$ (moment of inertia)	kilogram-$meter^2$ ($kg·m^2$)	4.214 011 X E -2
pound-mass/$foot^3$	kilogram/$meter^3$ (kg/m^3)	1.601 846 X E +1
rad (radiation dose absorbed)	Gray (Gy)**	1.000 000 X E -2
roentgen	coulomb/kilogram (C/kg)	2.579 760 X E -4
shake	second (s)	1.000 000 X E -8
slug	kilogram (kg)	1.459 390 X E +1
torr (mm Hg, 0° C)	kilo pascal (kPa)	1.333 22 X E -1

*The becquerel (Bq) is the SI unit of radioactivity; 1 Bq = 1 event/s.

**The Gray (Gy) is the SI unit of absorbed radiation.

A more complete listing of conversions may be found in "Standard for Metric Practice," ASTM E-380-79, American Society for Testing and Materials.

APPENDIX A. BEAM TEST DATA TRACES

Appendix A presents data from the nine beam tests. For Series 1 and 2, where possible, data traces for symmetric measurement stations are presented on the same graph. However, because of the cyclic nature of the Series 3 data, representative data plots are presented for the various stations. The measurement designation system is shown below.

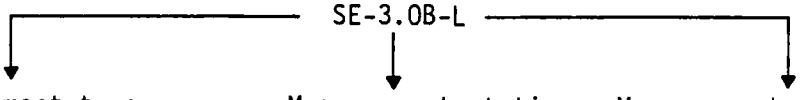

Measurement type		Measurement station and location		Measurement orientation	
SE	Steel strain	B	Bottom	L	Longitudinal
CE	Concrete strain	T	Top	V	Vertical
AD	Absolute displacement	F	Front	T	Tangential
R	Rotation	R	Rear		
		M	Middle		

Sign convention:

Strain: Compression = +
Tension = -

Displacement: Downward = +

SUMMARY OF MEASUREMENTS

Measurement designation	Measurement type	Orientation	X-coordinate, mm	Y-coordinate, mm
AD-0.0-V	Displacement	Vertical	0	178
AD-2.0-V	↓	↓	689	203
AD-3.0-V			1299	203
AD-4.0-V			1910	203
AD-5.0-V			2520	203
AD-6.0-V			3130	203
AD-8.0-V			3820	203
AD-0.0-H	↓	Horizontal	0	178

Measurement designation	Measurement type	Orientation	X-coordinate, mm	Y-coordinate, mm
AD-8.0-H	Displacement	Horizontal	3820	178
SE-2.0B-L	Steel strain	Longitudinal	689	64
SE-3.0B-L			1299	64
SE-4.0B-L			1910	64
SE-5.0B-L			2520	64
SE-6.0B-L			3130	64
SE-2.0TF-L			689	343
SE-3.0TF-L			1299	343
SE-4.0TF-L			1910	343
SE-5.0TF-L			2520	343
SE-6.0TF-L			3130	343
CE-2.0T-L	Concrete strain		689	343
CE-2.0M-L			689	203
CE-3.0T-L			1299	343
CE-3.0M-L			1299	203
CE-4.0T-L			1910	343
CE-4.0M-L			1910	203
CE-5.0T-L			2520	343
CE-5.0M-L			2520	203
CE-6.0T-L			3130	343
CE-6.0M-L			3130	203
SE-2.0F-V	Steel strain	Vertical	689	203
SE-3.0F-V			1299	203
SE-4.0F-V			1910	203
SE-5.0F-V			2520	203
SE-6.0F-V			3130	203
SE-2.0B-T		Transverse	689	64
SE-3.0B-T			1299	64
SE-4.0T-T			1910	343
SE-5.0T-T			2520	343
SE-6.0T-T			3130	343
R-0.0-A	Rotation	Angular	0	178
R-8.0-A	Rotation	Angular	3820	178

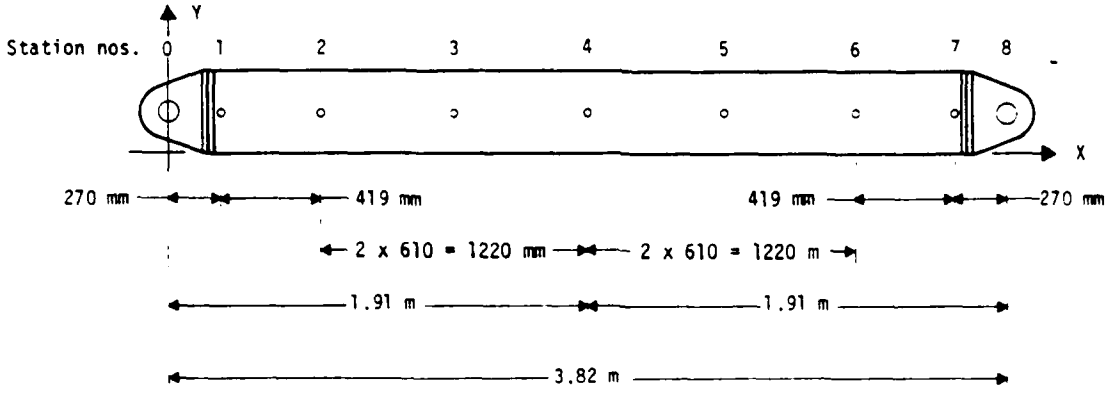

Measurements:
Stations 0 and 8, horizontal and vertical displacement.
Stations 1 and 7, rotation only.
Stations 2 through 6, vertical deflection.
Stations 2 through 6, strain.

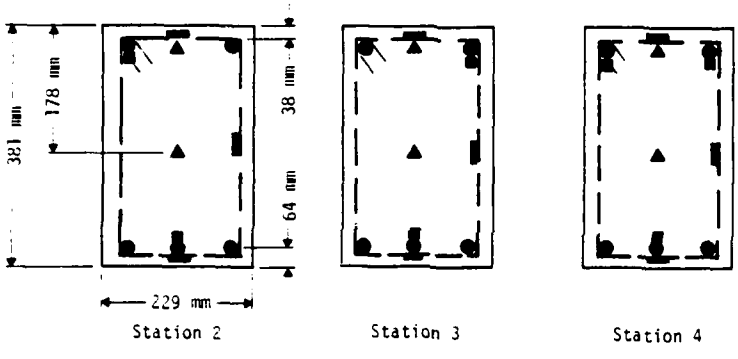

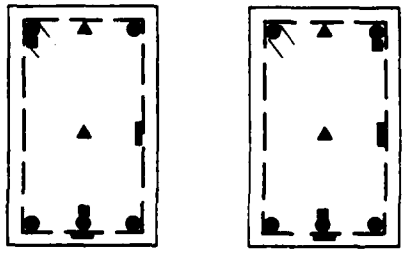

Legend
- ■ Longitudinal steel strain
- ▬ Vertical or transverse steel strain
- ▲ Embedded concrete strain

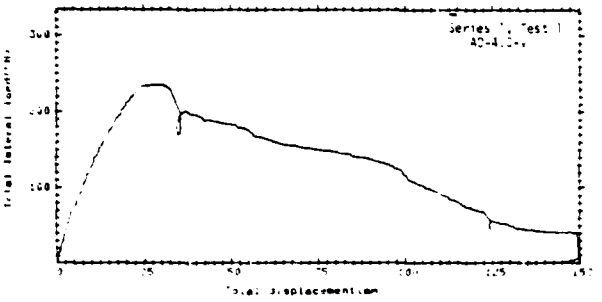

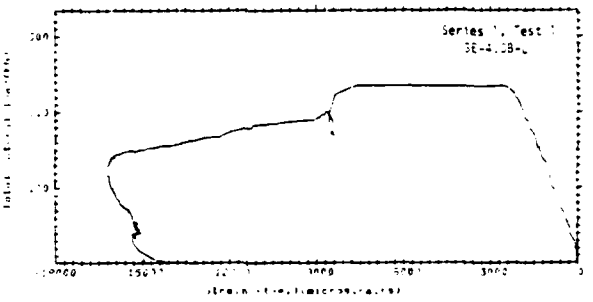

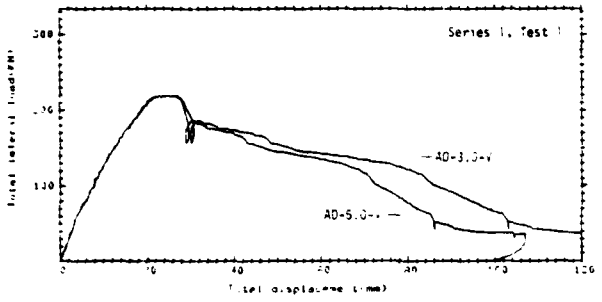
Series 1, Test 1
AD-3.0-v
AD-5.0-v

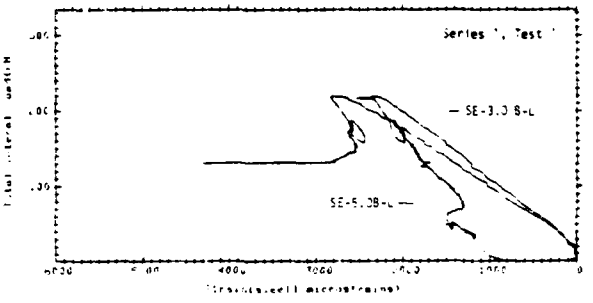
Series 1, Test 1
SE-3.0B-L
SE-5.0B-L

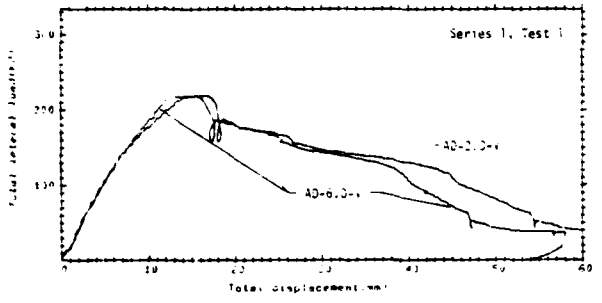
Series 1, Test 1
AD-6.0-v

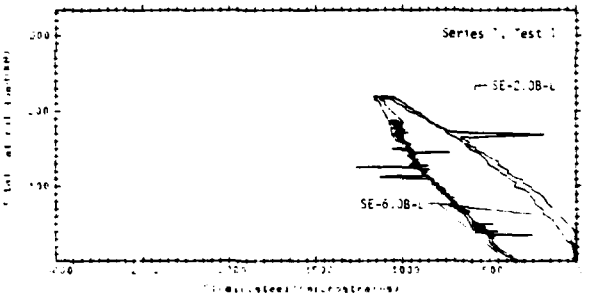
Series 1, Test 1
SE-6.0B-L

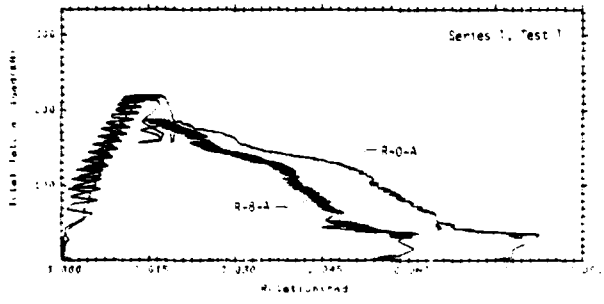
Series 1, Test 1
R-0-A
R-8-A

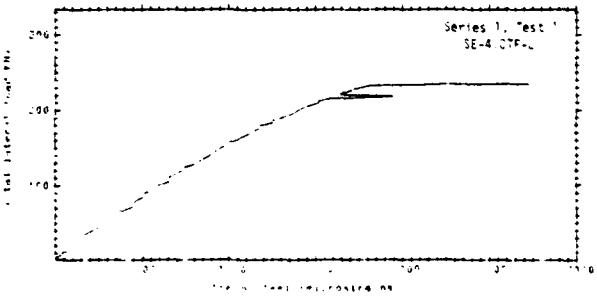
Series 1, Test 1

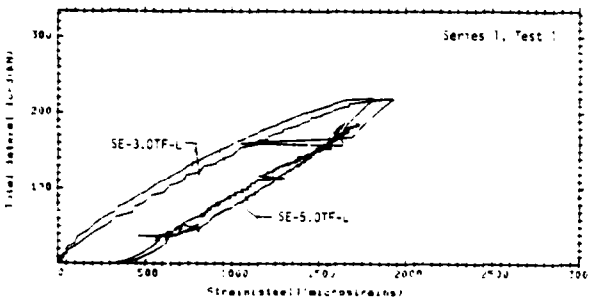
Series 1, Test 1
SE-3.0TF-L
SE-5.0TF-L

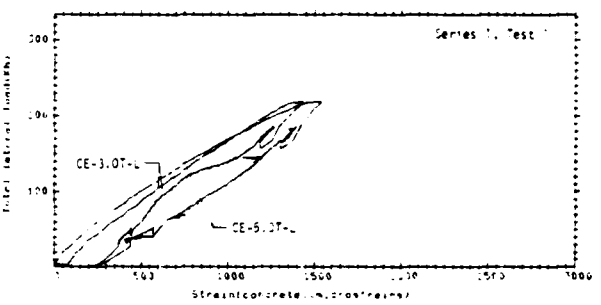
Series 1, Test 1
CE-3.0T-L
CE-5.0T-L

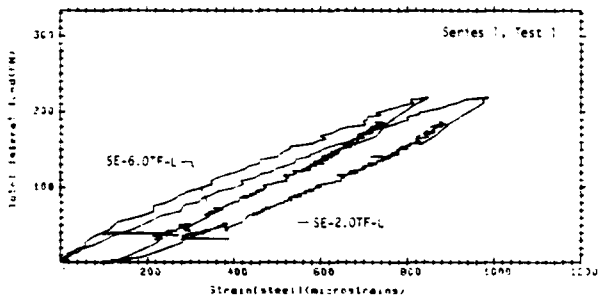
Series 1, Test 1
SE-6.0TF-L
SE-2.0TF-L

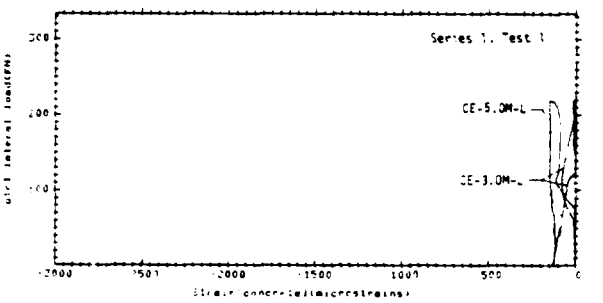
Series 1, Test 1
CE-5.0M-L
CE-3.0M-L

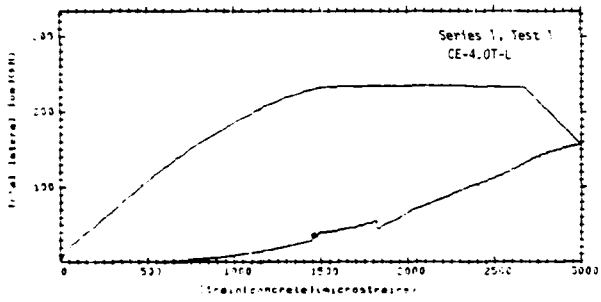
Series 1, Test 1
CE-4.0T-L

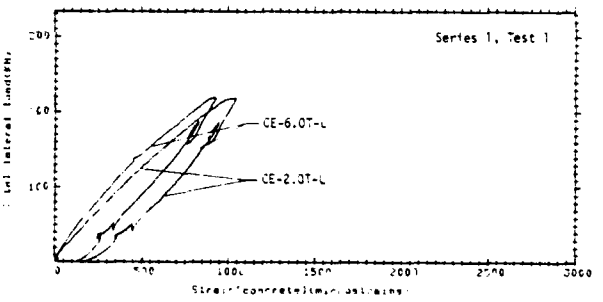
Series 1, Test 1
CE-6.0T-L
CE-2.0T-L

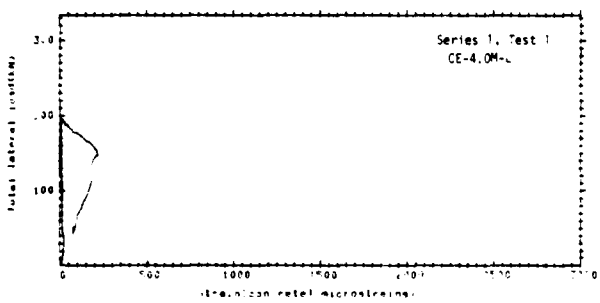
Series 1, Test 1
CE-4.0M-L

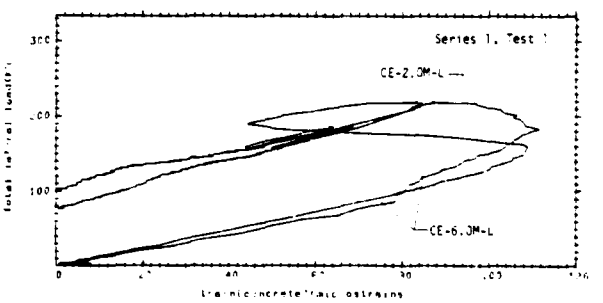
Series 1, Test 1
CE-2.0M-L
CE-6.0M-L

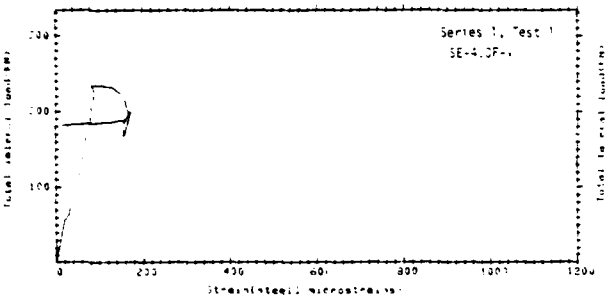
Series 1, Test 1
SE-4.0F-L

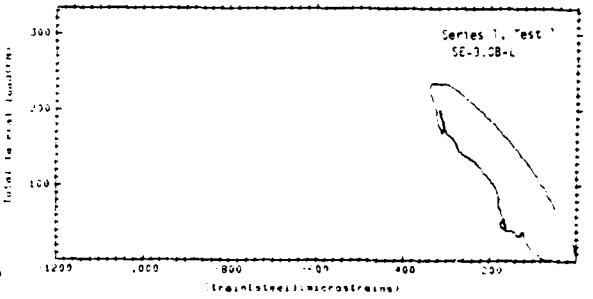
Series 1, Test 1
SE-3.0B-L

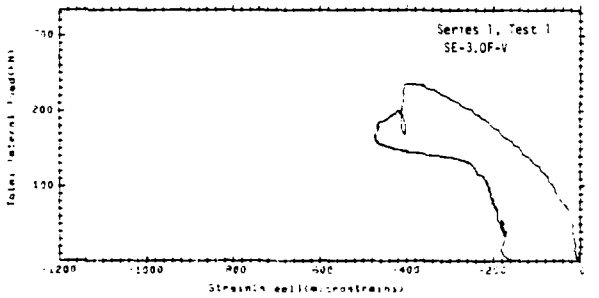
Series 1, Test 1
SE-3.0F-V

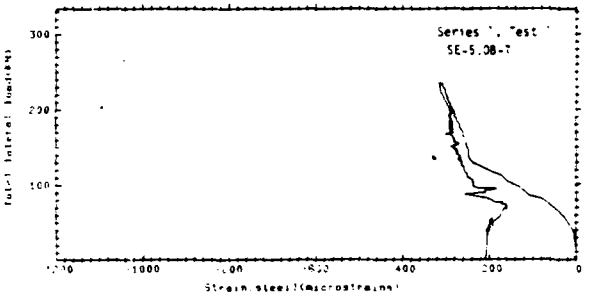
Series 1, Test 1
SE-5.0B-T

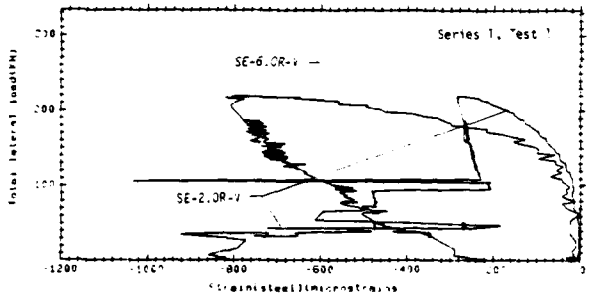
Series 1, Test 1
SE-6.0R-V
SE-2.0R-V

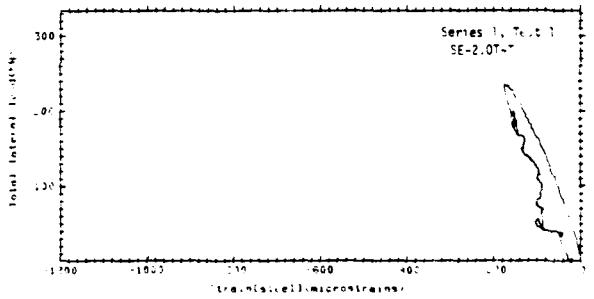
Series 1, Test 1
SE-2.0T-T

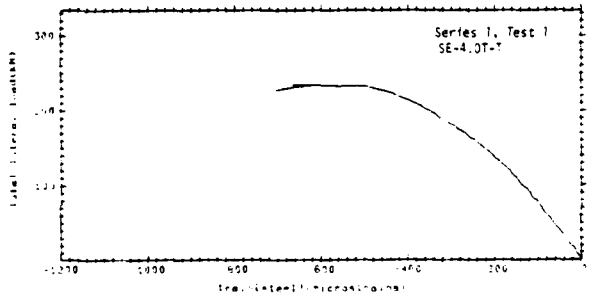
Series 1, Test 1
SE-4.0T-T

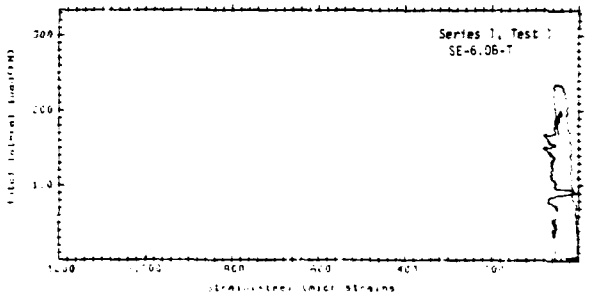
Series 1, Test 1
SE-6.0B-T

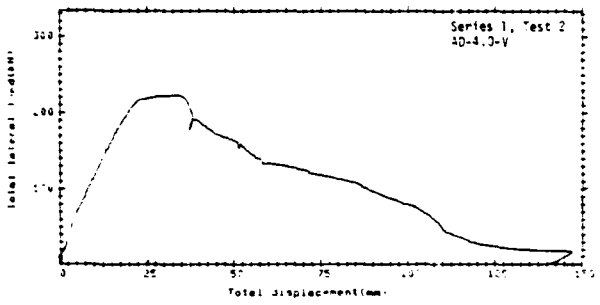
Series 1, Test 2
AD-4.0-V

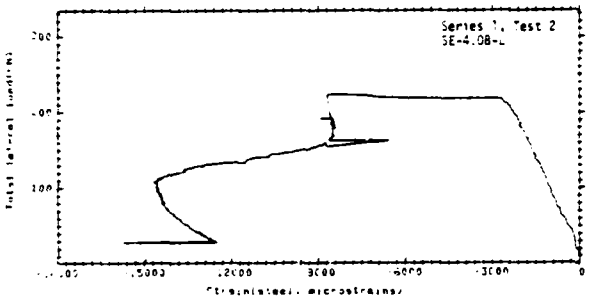
Series 1, Test 2
SE-4.0B-L

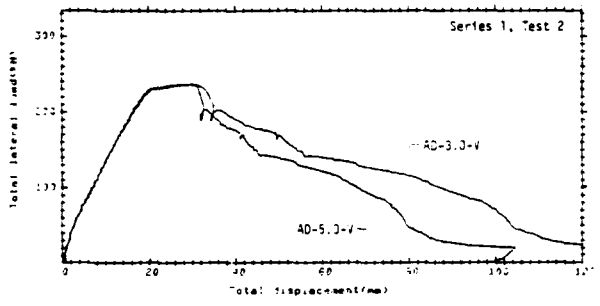
Series 1, Test 2
AD-3.0-V
AD-5.0-V

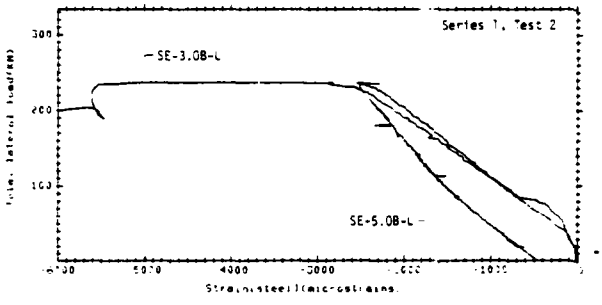
Series 1, Test 2
SE-3.0B-L
SE-5.0B-L

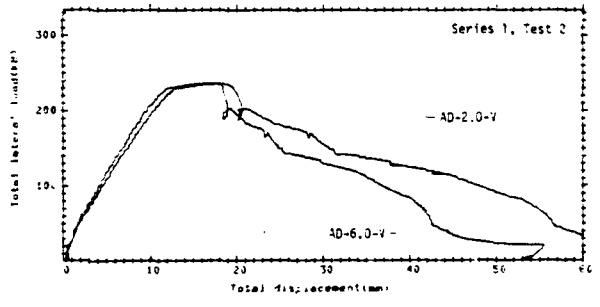
Series 1, Test 2
AD-2.0-V
AD-6.0-V

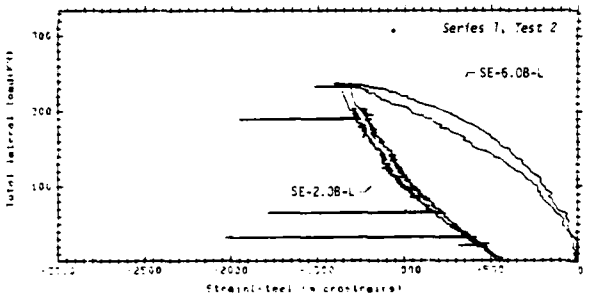
Series 1, Test 2
SE-6.0B-L
SE-2.0B-L

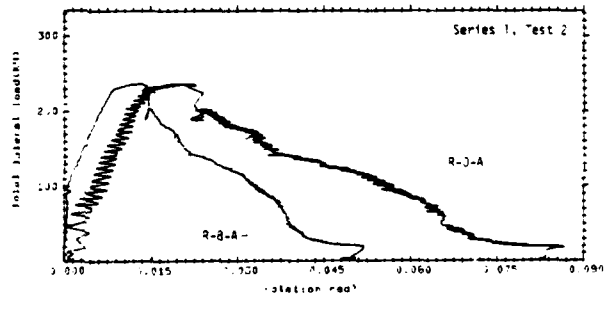
Series 1, Test 2
R-3-A
R-8-A

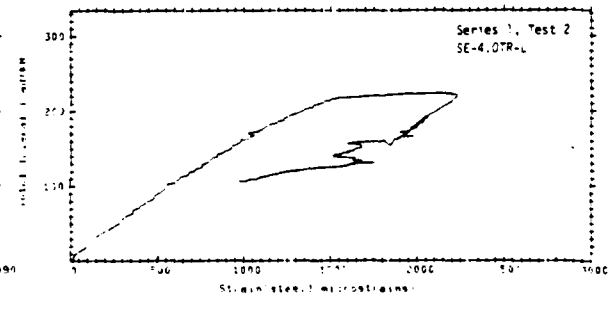
Series 1, Test 2
SE-4.0TR-L

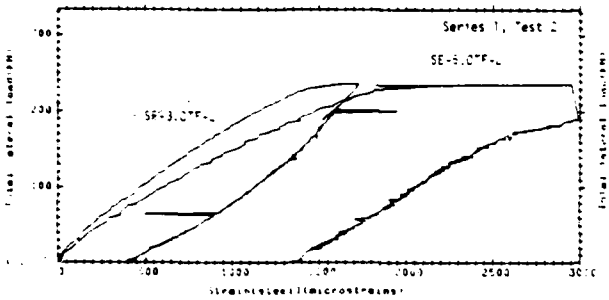
Series 1, Test 2
SE-6.0TF-L
SE-3.0TF-L

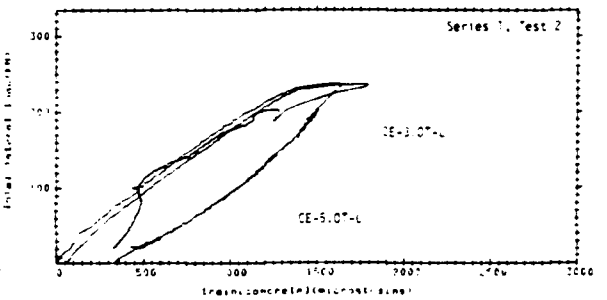
Series 1, Test 2
CE-3.0T-L
CE-6.0T-L

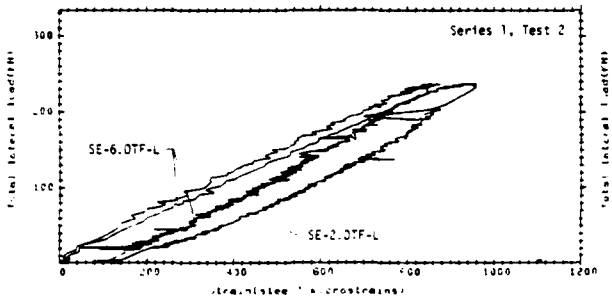
Series 1, Test 2
SE-6.0TF-L
SE-2.0TF-L

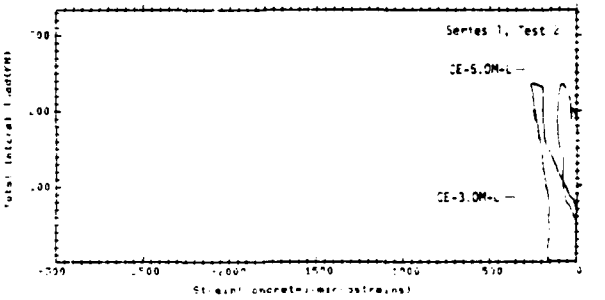
Series 1, Test 2
CE-5.0M-L
CE-3.0M-L

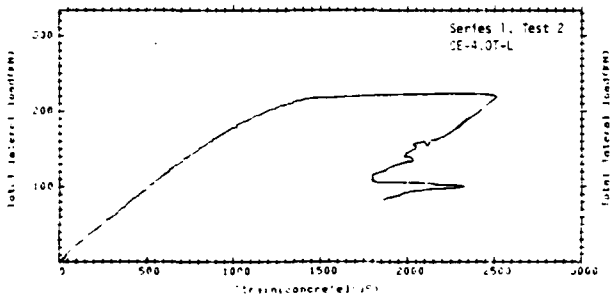
Series 1, Test 2
CE-4.0T-L

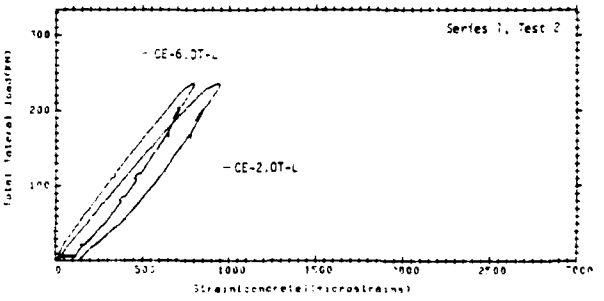
Series 1, Test 2
CE-6.0T-L
CE-2.0T-L

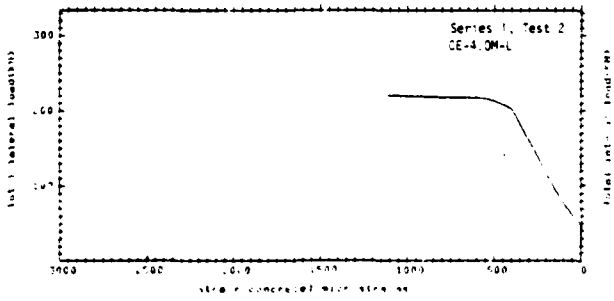
Series 1, Test 2
CE-4.0M-L

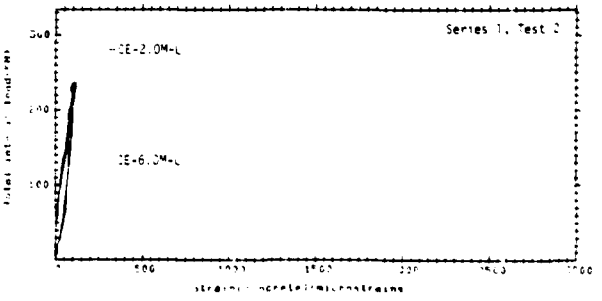
Series 1, Test 2
CE-2.0M-L
CE-6.0M-L

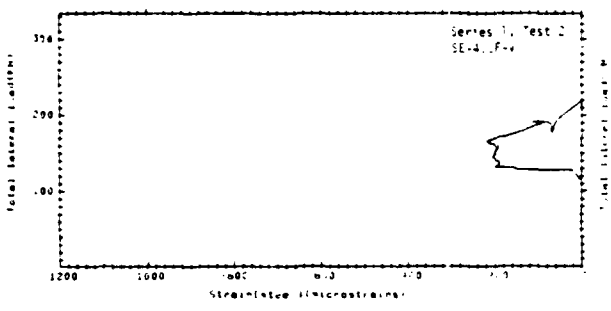
Series 1, Test 2

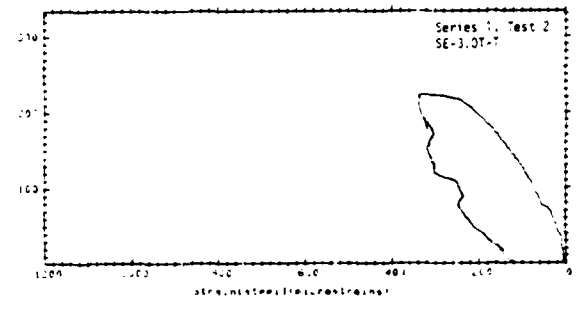
Series 1, Test 2

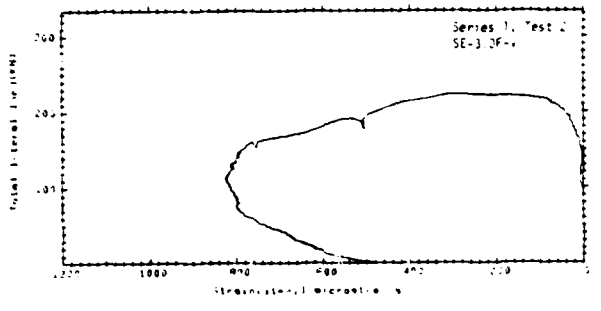
Series 1, Test 2

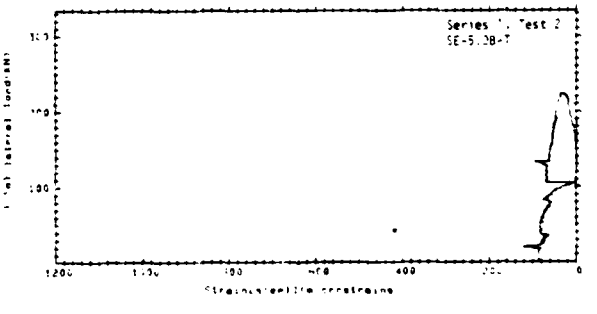
Series 1, Test 2

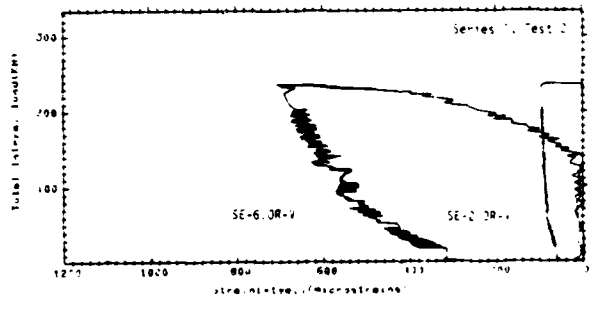
SE-6.0R-V
SE-2.0R-H

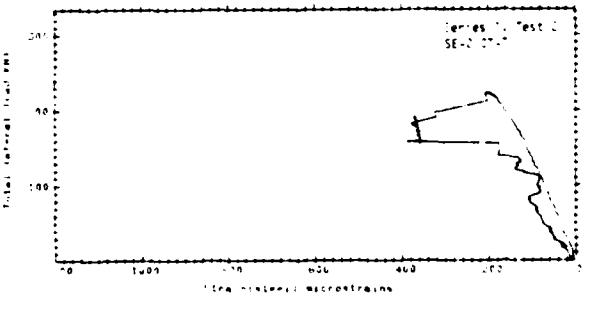

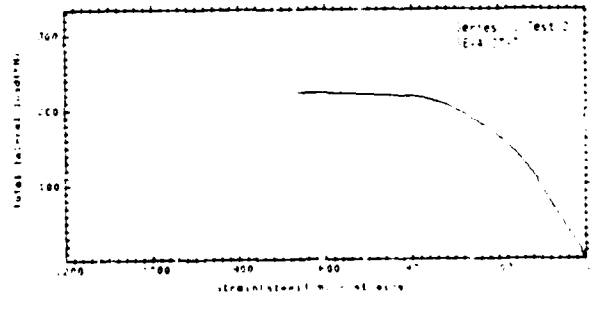

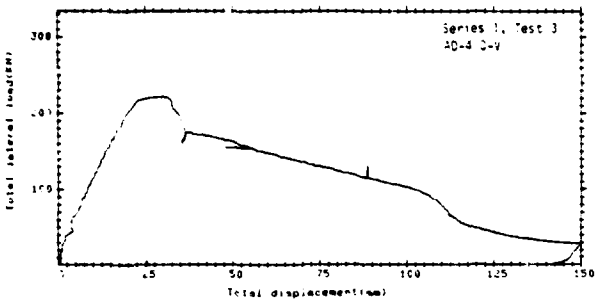
Series 1, Test 3
AD-4.0-V

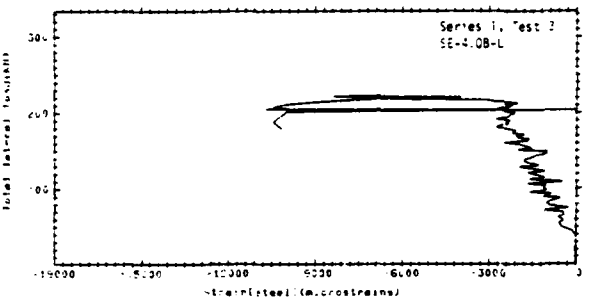
Series 1, Test 3
SE-4.0B-L

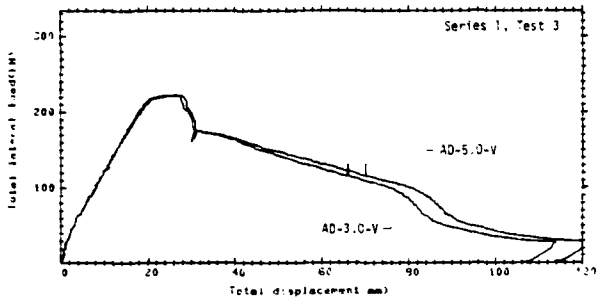
Series 1, Test 3
AD-5.0-V
AD-3.0-V

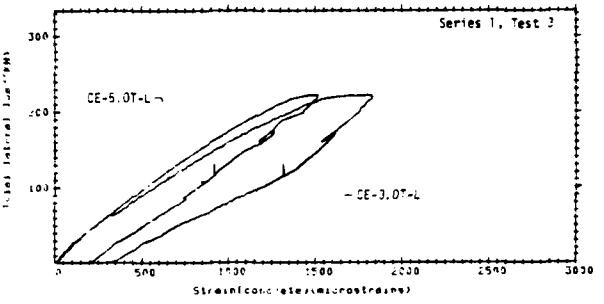
Series 1, Test 3
CE-5.0T-L
CE-3.0T-L

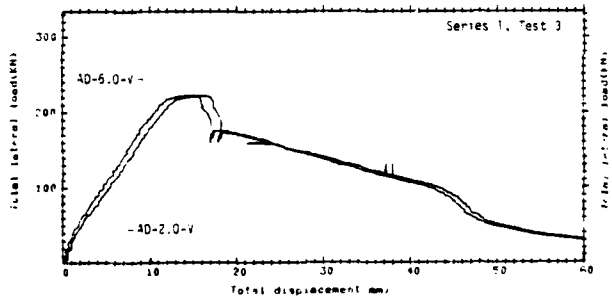
Series 1, Test 3
AD-6.0-V
AD-2.0-V

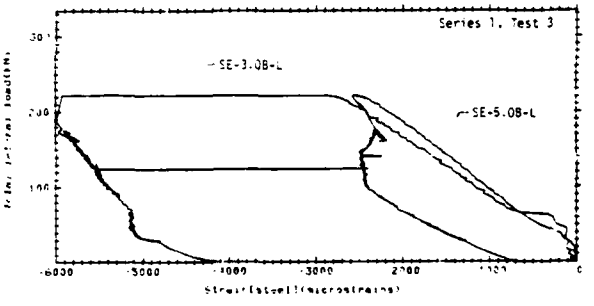
Series 1, Test 3
SE-3.0B-L
SE-5.0B-L

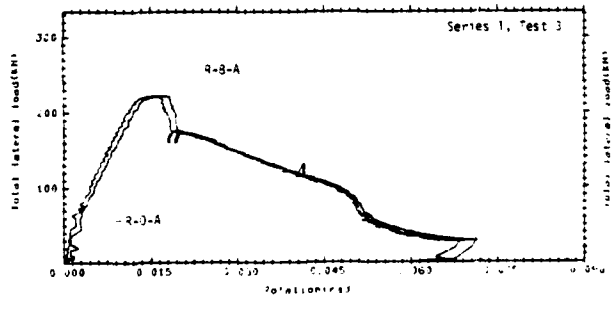
Series 1, Test 3
R-8-A
R-0-A

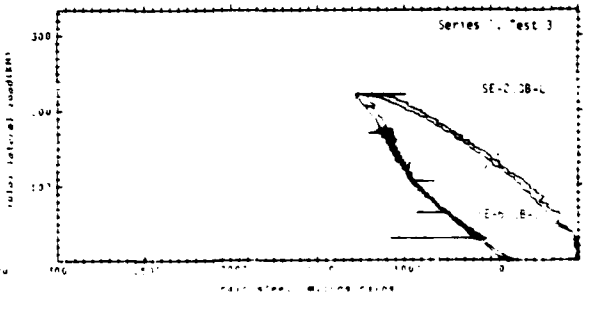
Series 1, Test 3

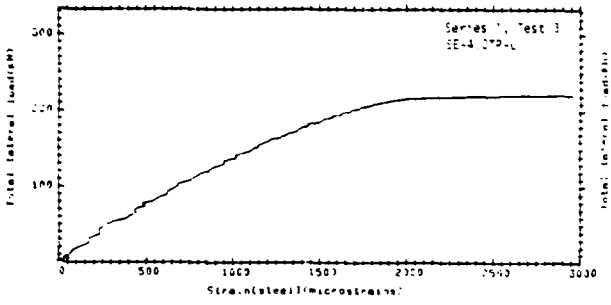
Series 1, Test 3

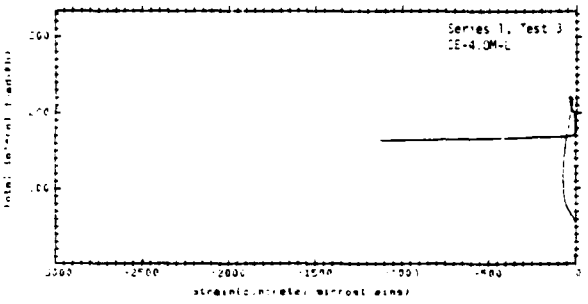
Series 1, Test 3
CE-4.0M-L

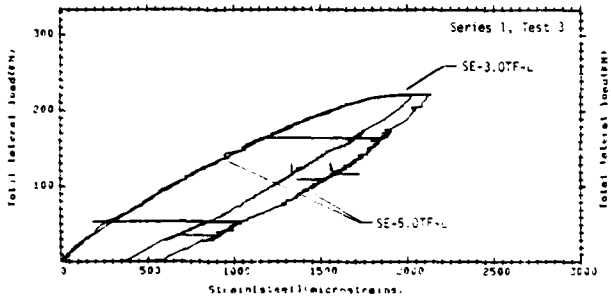
Series 1, Test 3
SE-3.0TF-L
SE-5.0TF-L

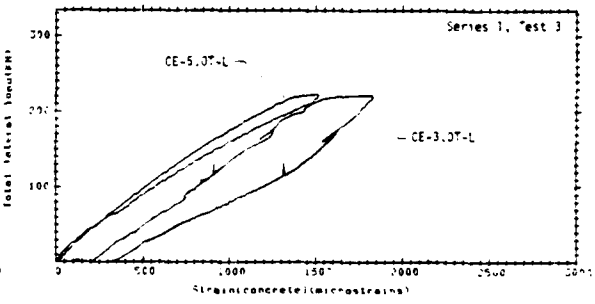
Series 1, Test 3
CE-5.0T-L
CE-3.0T-L

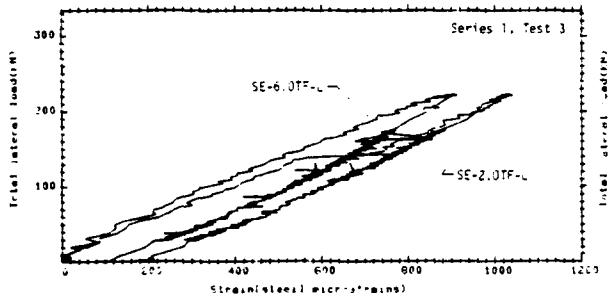
Series 1, Test 3
SE-6.0TF-L
SE-2.0TF-L

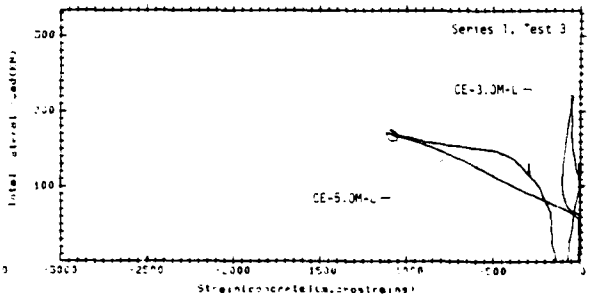
Series 1, Test 3
CE-3.0M-L
CE-5.0M-L

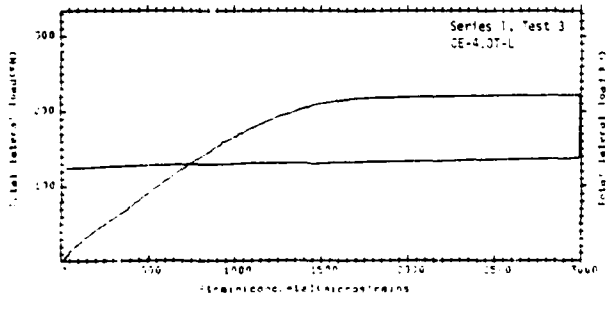
Series 1, Test 3
CE-4.0T-L

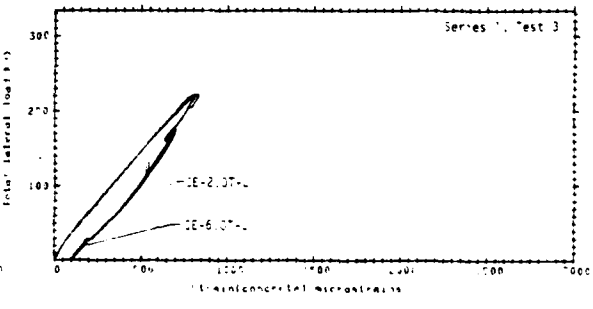
CE-2.0T-L
CE-6.0T-L

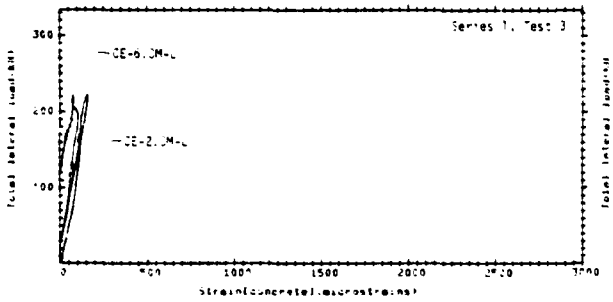
Series 1, Test 3

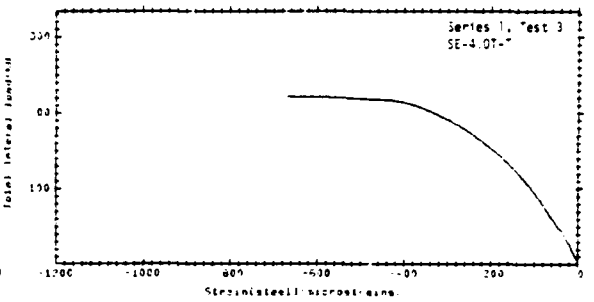
Series 1, Test 3
SE-4.0T-

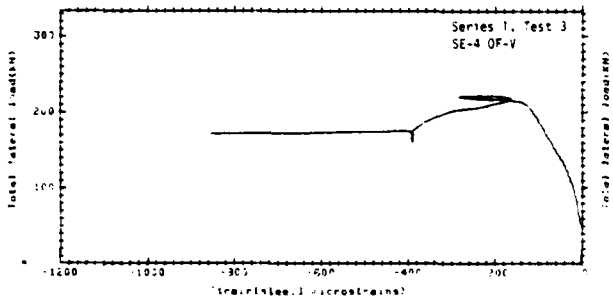
Series 1, Test 3
SE-4 0F-V

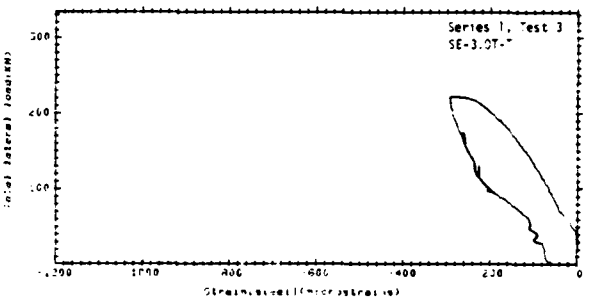
Series 1, Test 3
SE-3.0T-

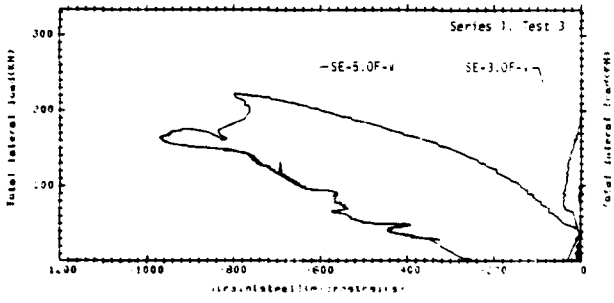
Series 1, Test 3
SE-5.0F-V
SE-3.0F-V

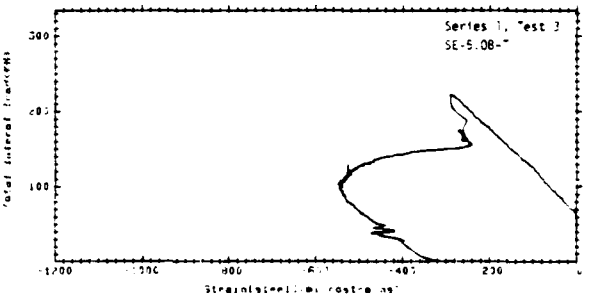
Series 1, Test 3
SE-5.0B-

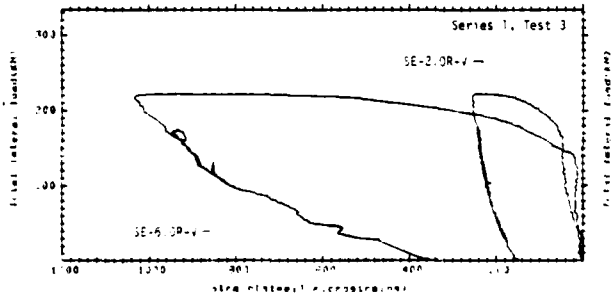
Series 1, Test 3
SE-2.0R-V

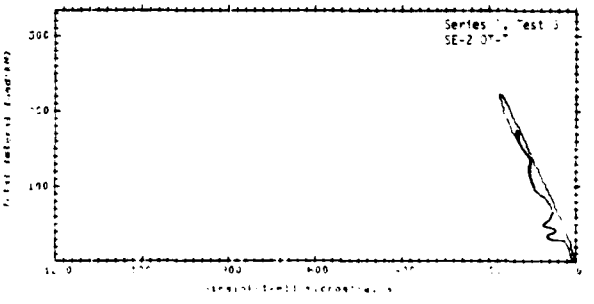
Series 1, Test 3
SE-2.0T-

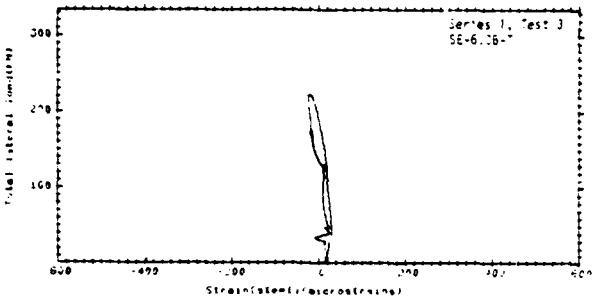
Series 1, Test 3
SE-6.2E-7
300
200
100
-400
0
400

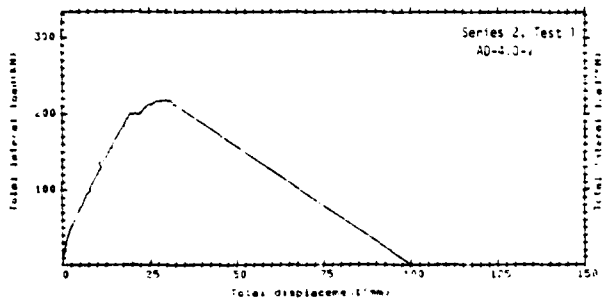
Series 2, Test 1

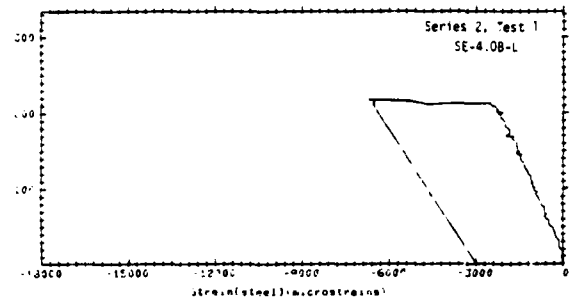
Series 2, Test 1
SE-4.0B-L

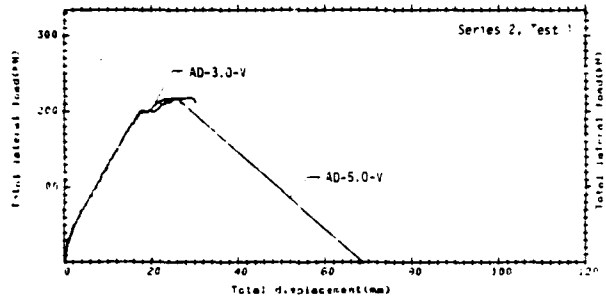
Series 2, Test 1
AD-3.0-V
AD-5.0-V
Total displacement(mm)

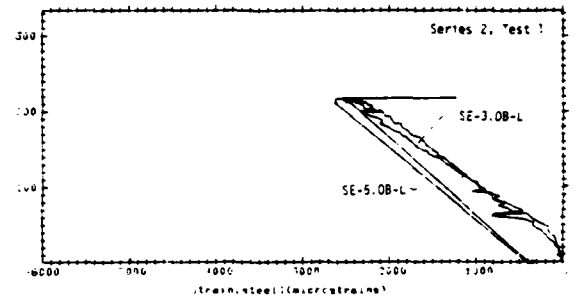
Series 2, Test 1
SE-3.0B-L
SE-5.0B-L

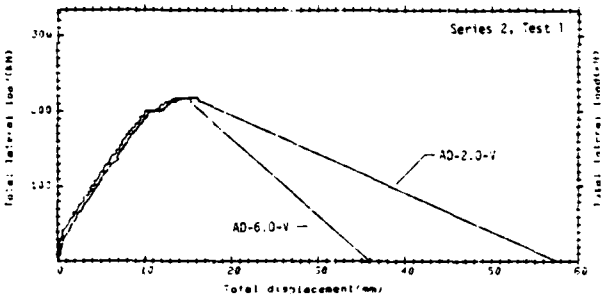
Series 2, Test 1
AD-2.0-V
AD-6.0-V

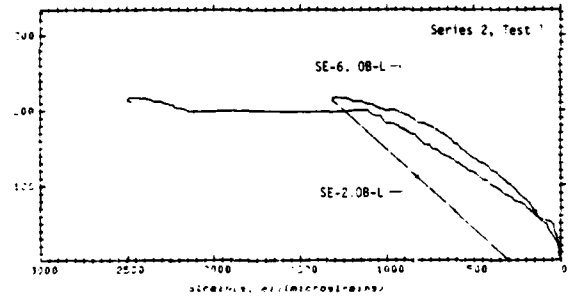
Series 2, Test 1
SE-6.0B-L
SE-2.0B-L

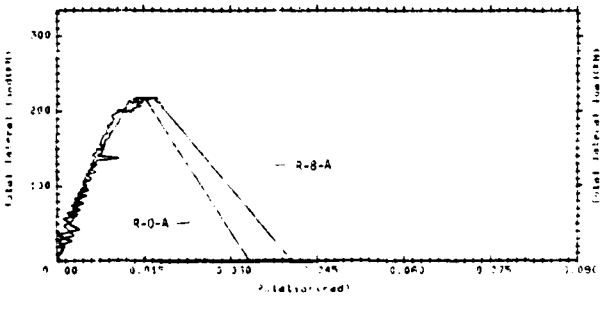
R-8-A
R-0-A

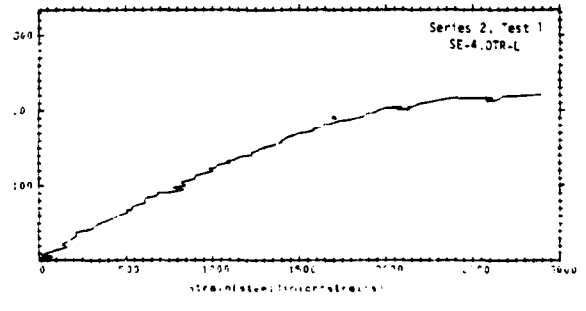
Series 2, Test 1
SE-4.0TR-L

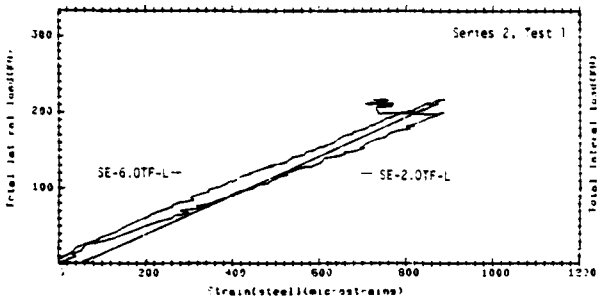
Series 2, Test 1
SE-6.0TF-L
SE-2.0TF-L
Strain(steel)(microstrains)

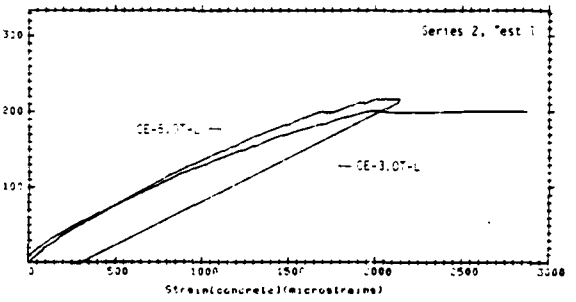
Series 2, Test 1
CE-6.0T-L
CE-3.0T-L
Strain(concrete)(microstrains)

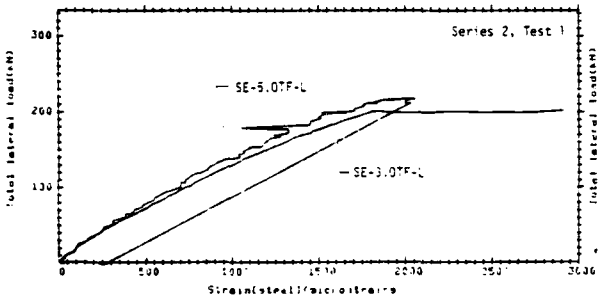
Series 2, Test 1
SE-5.0TF-L
SE-3.0TF-L
Strain(steel)(microstrains)

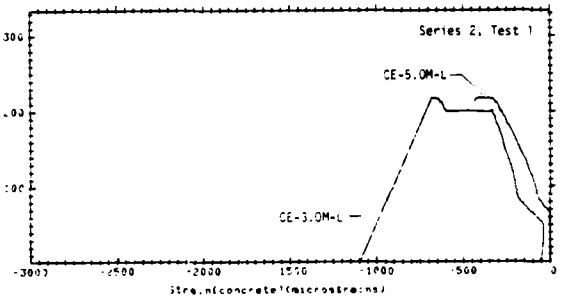
Series 2, Test 1
CE-5.0M-L
CE-3.0M-L

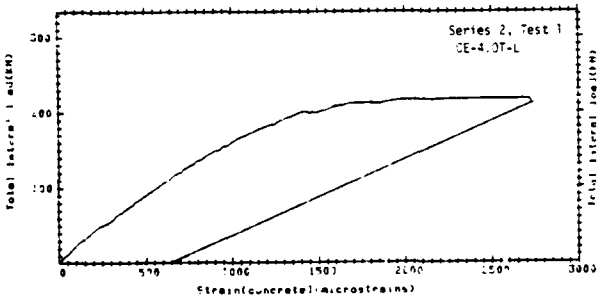
Series 2, Test 1
CE-4.0T-L
Strain(concrete)(microstrains)

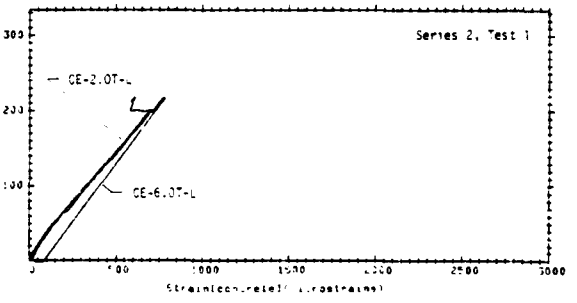
Series 2, Test 1
CE-2.0T-L
CE-6.0T-L

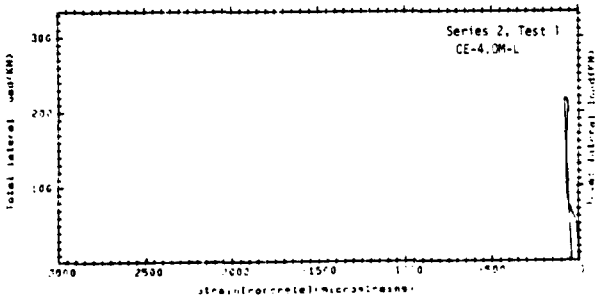
Series 2, Test 1
CE-4.0M-L

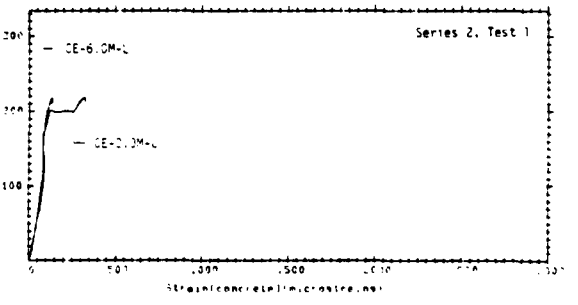
Series 2, Test 1
CE-6.0M-L
CE-2.0M-L

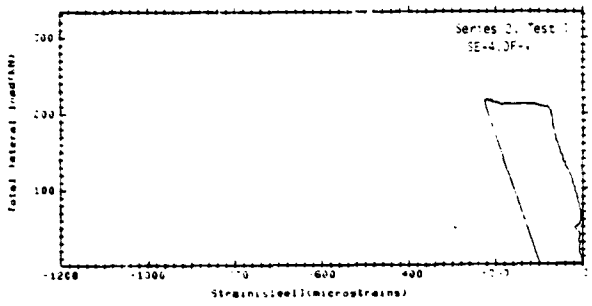
Series 2, Test 1
SE-4.0F-v
Total lateral load(kN)
Strain(steel)(microstrains)

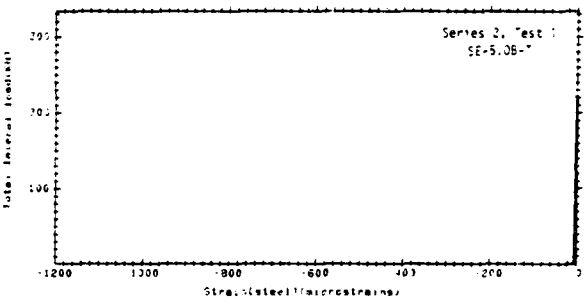
Series 2, Test 1
SE-5.0B-T
Total lateral load(kN)
Strain(steel)(microstrains)

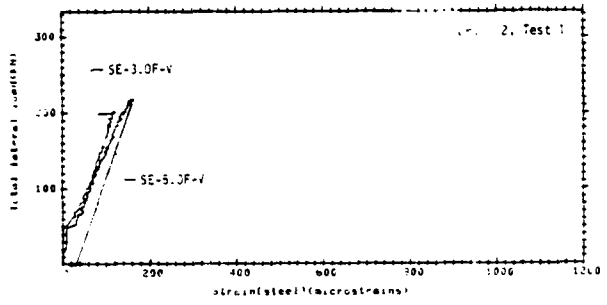
Series 2, Test 1
SE-3.0F-v
SE-5.0F-v
Total lateral load(kN)
Strain(steel)(microstrains)

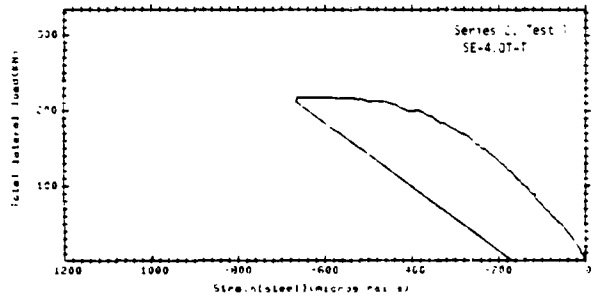
Series 2, Test 1
SE-4.0T-T
Total lateral load(kN)
Strain(steel)(microstrains)

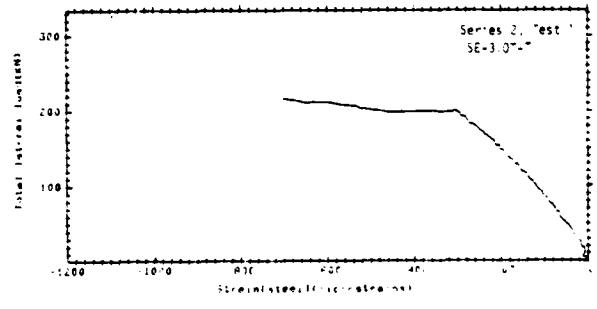
Series 2, Test 1
SE-3.0T-T
Total lateral load(kN)
Strain(steel)(microstrains)

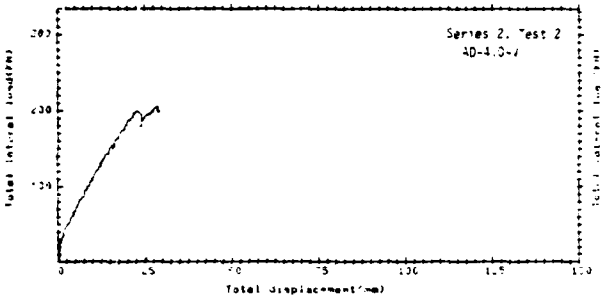
Series 2, Test 2
AD-4.0-V

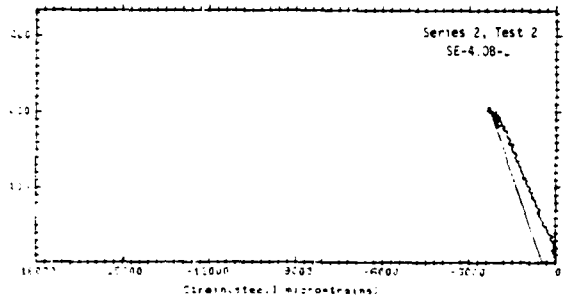
Series 2, Test 2
SE-4.0B-L

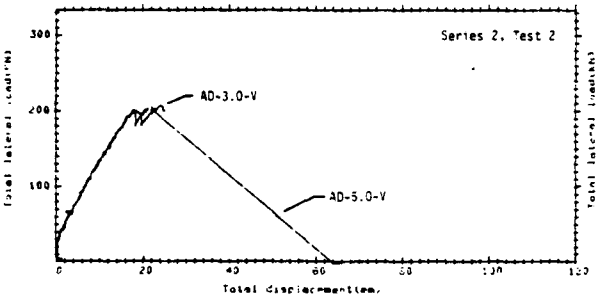
Series 2, Test 2
AD-3.0-V
AD-5.0-V

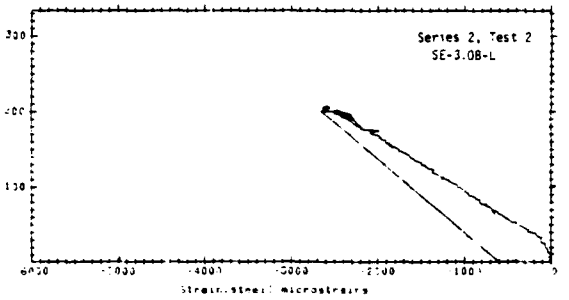
Series 2, Test 2
SE-3.0B-L

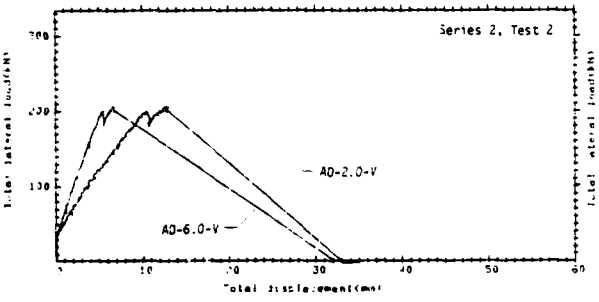
Series 2, Test 2
AD-2.0-V
AD-6.0-V

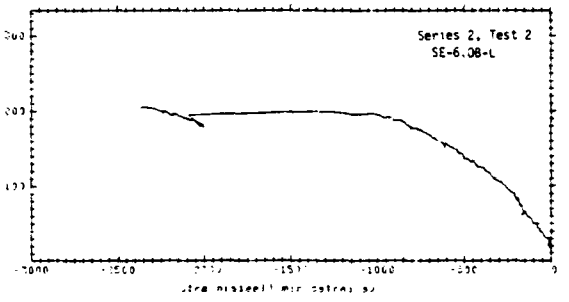
Series 2, Test 2
SE-6.0B-L

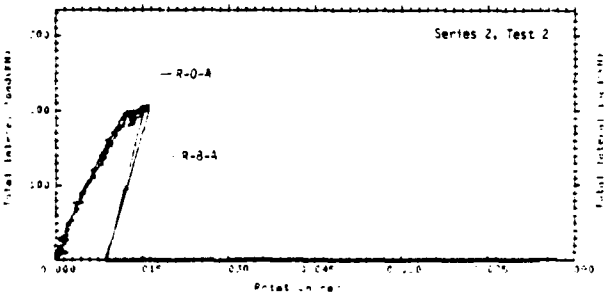
Series 2, Test 2
R-0-A
R-8-A

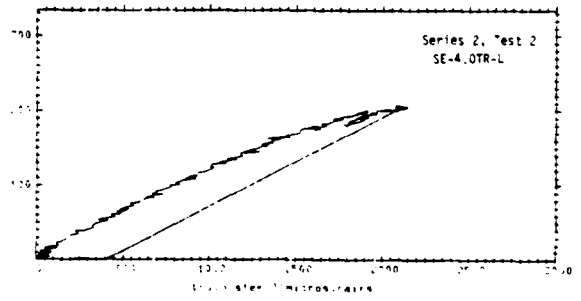
Series 2, Test 2
SE-4.0TR-L

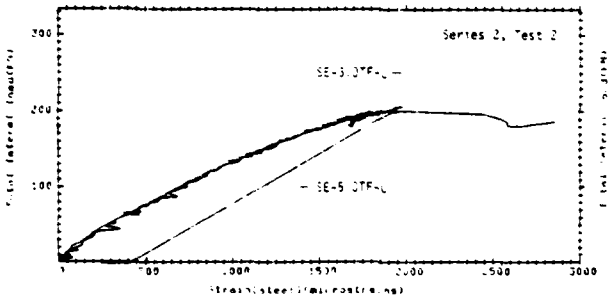
Series 2, Test 2
SE-3.0TF-L
SE-5.0TF-L

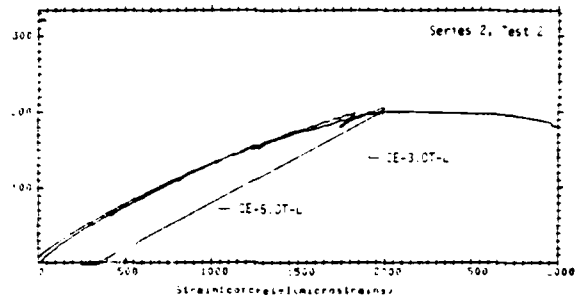
Series 2, Test 2
CE-3.0T-L
CE-5.0T-L

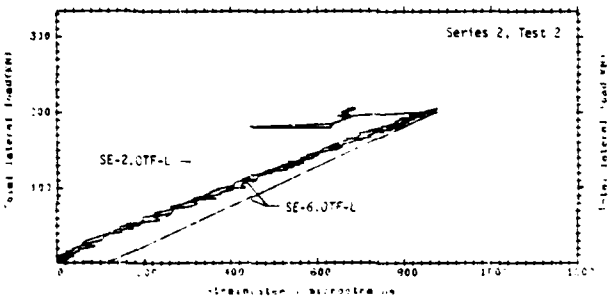
Series 2, Test 2
SE-2.0TF-L
SE-6.0TF-L

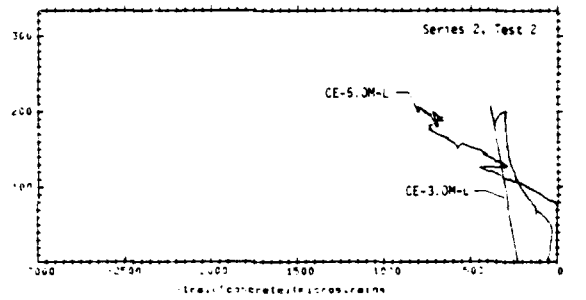
Series 2, Test 2
CE-5.0M-L
CE-3.0M-L

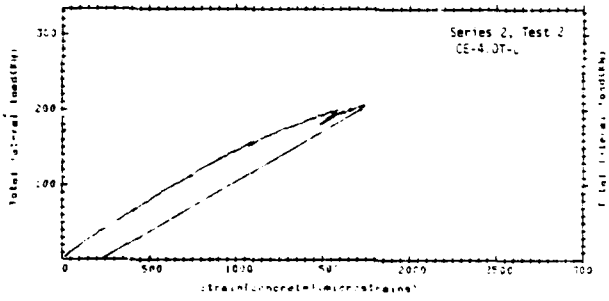
Series 2, Test 2
CE-4.0T-L

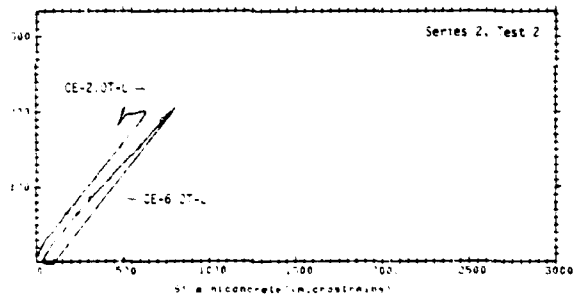
Series 2, Test 2
CE-2.0T-L
CE-6.0T-L

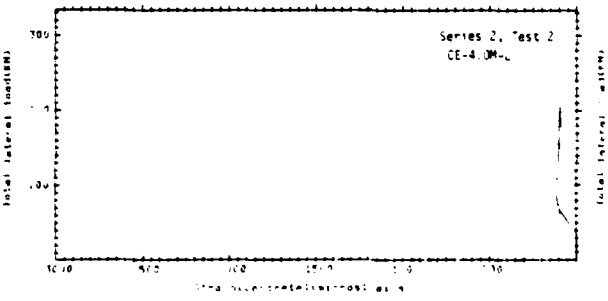
Series 2, Test 2
CE-4.0M-L

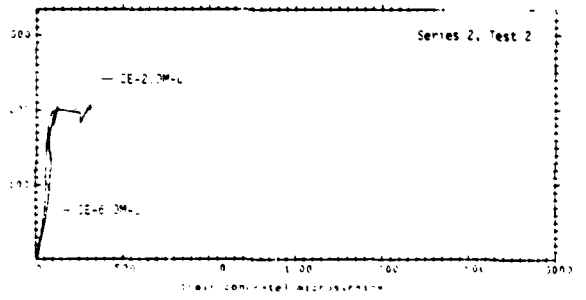
Series 2, Test 2
CE-2.0M-L
CE-6.0M-L

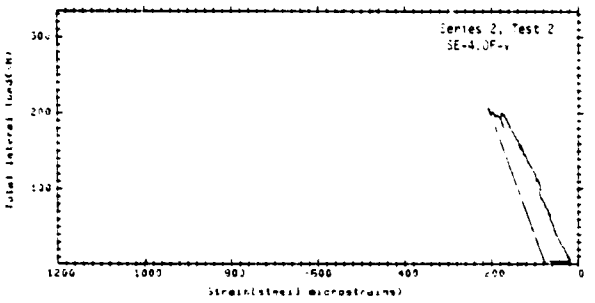
Series 2, Test 2
SE-4.0F-V

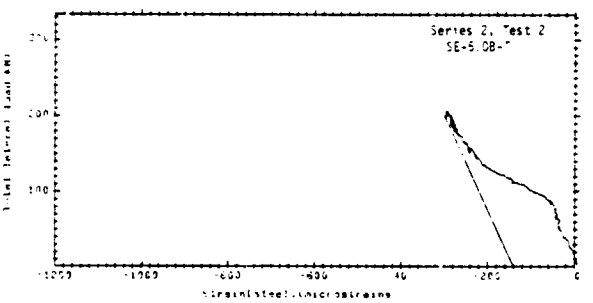
Series 2, Test 2
SE-5.0B-T

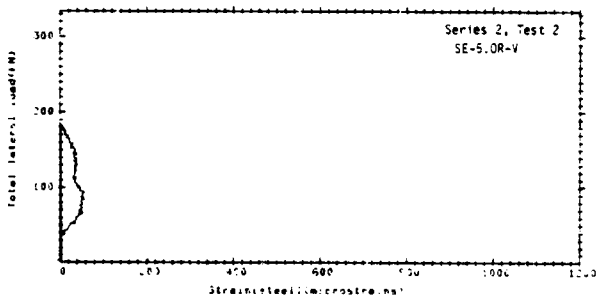
Series 2, Test 2
SE-5.0R-V

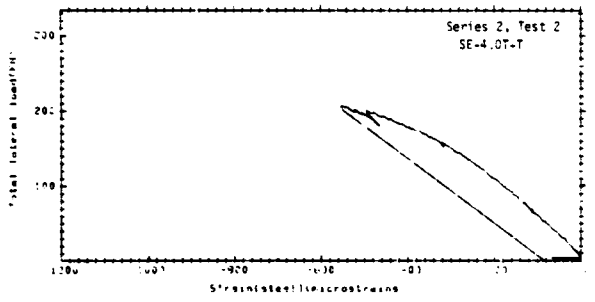
Series 2, Test 2
SE-4.0T-T

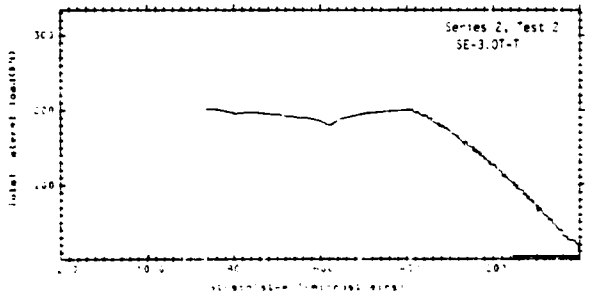
Series 2, Test 2
SE-3.0T-T

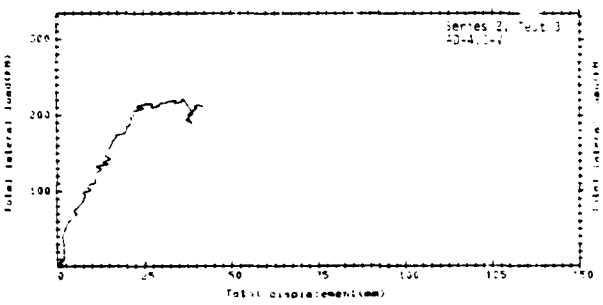
Series 2, Test 3

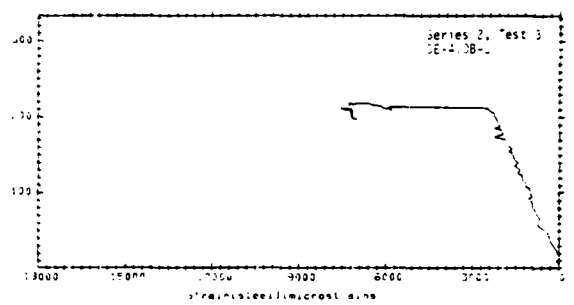
Series 2, Test 3

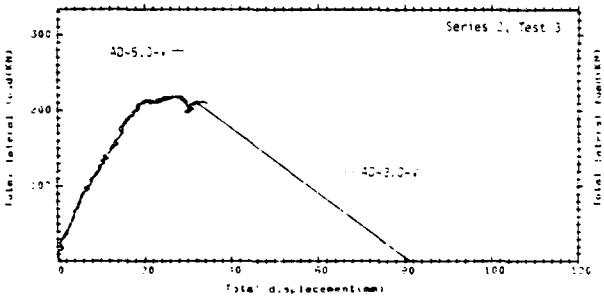
Series 2, Test 3
AD-5.0-L
AD-3.0-L

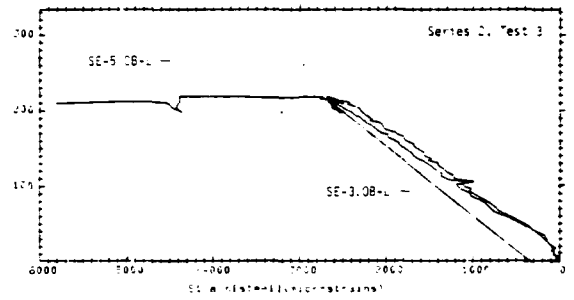
Series 2, Test 3
SE-5.0B-L
SE-3.0B-L

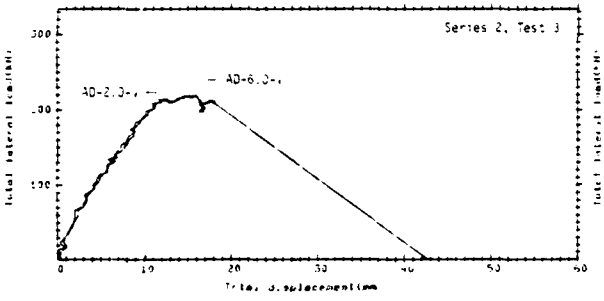
Series 2, Test 3
AD-2.0-L
AD-6.0-L

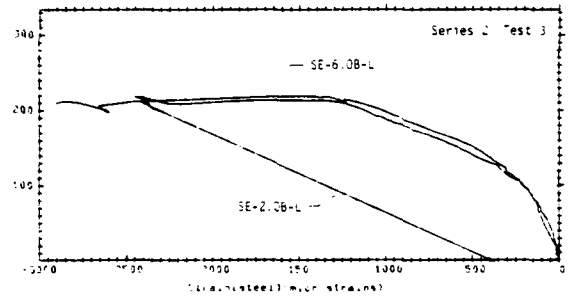
Series 2, Test 3
SE-6.0B-L
SE-2.0B-L

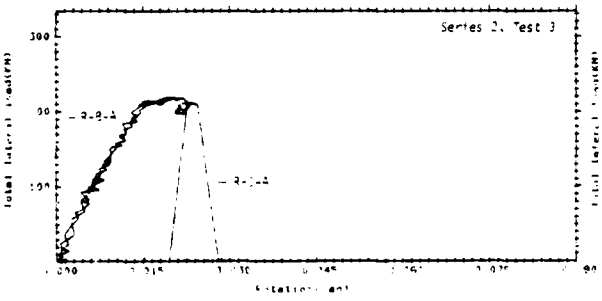
Series 2, Test 3

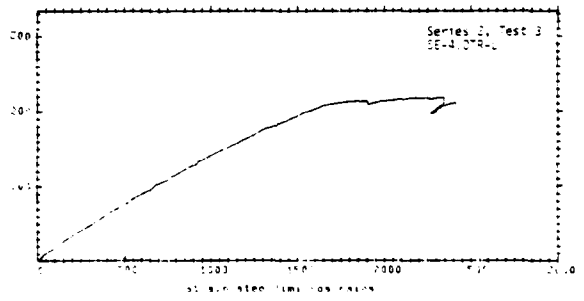
Series 2, Test 3

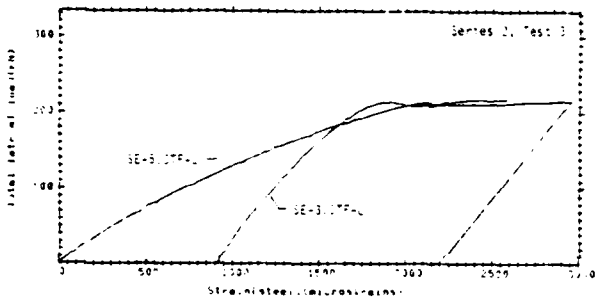
Series 2, Test 3

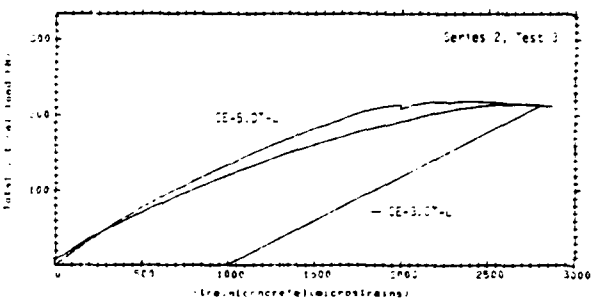
Series 2, Test 3
CE-5.0T-L
CE-3.0T-L

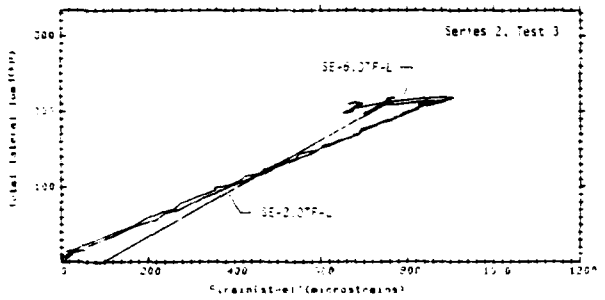
Series 2, Test 3
SE-6.0TF-L
SE-2.0TF-L

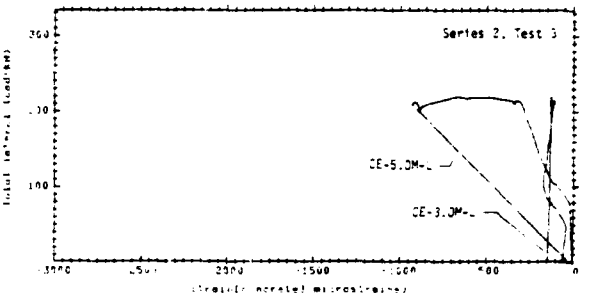
Series 2, Test 3
CE-5.0M-L
CE-3.0M-L

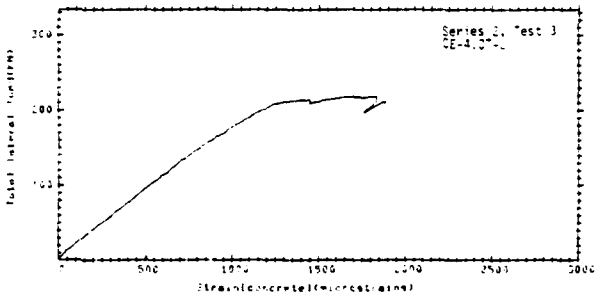
Series 2, Test 3
CE-4.0T-L

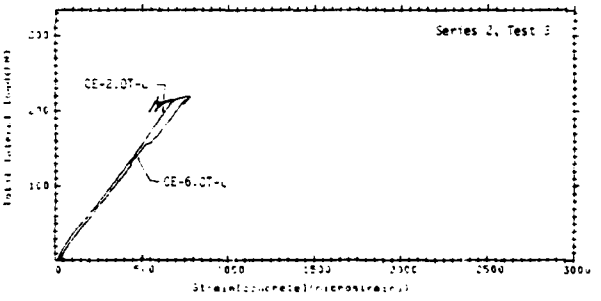
Series 2, Test 3
CE-2.0T-L
CE-6.0T-L

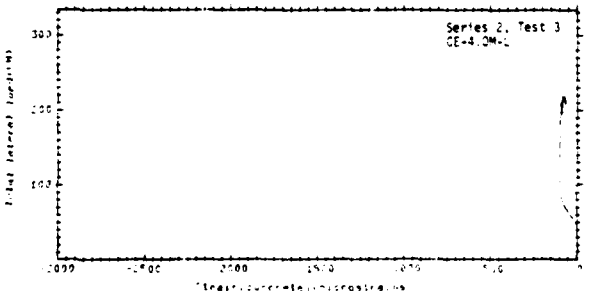
Series 2, Test 3
CE-4.0M-L

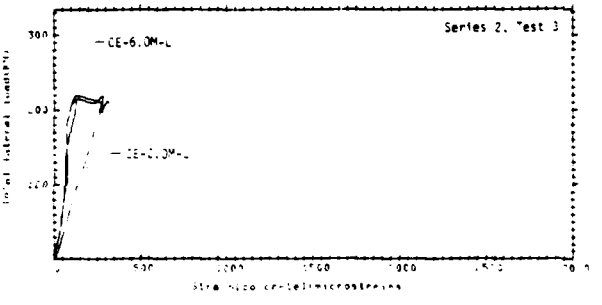
Series 2, Test 3
CE-6.0M-L

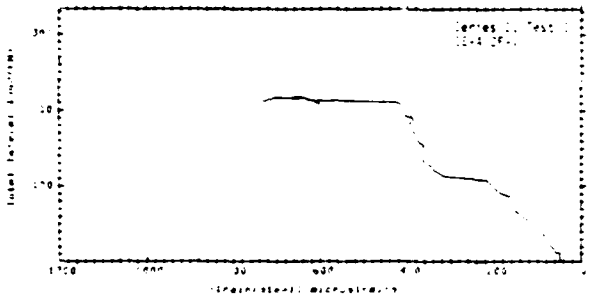

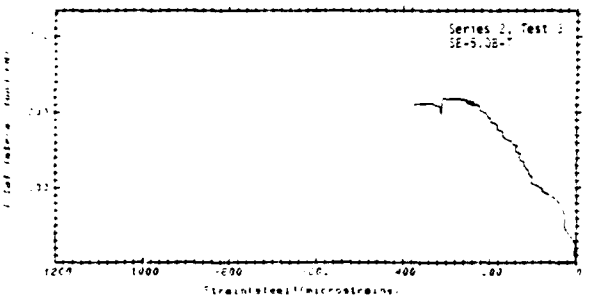
Series 2, Test 3

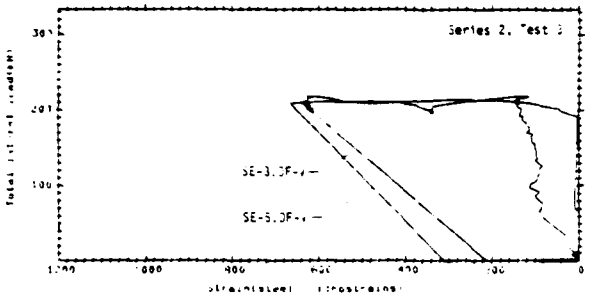
Series 2, Test 3
SE-3.0F-
SE-5.0F-

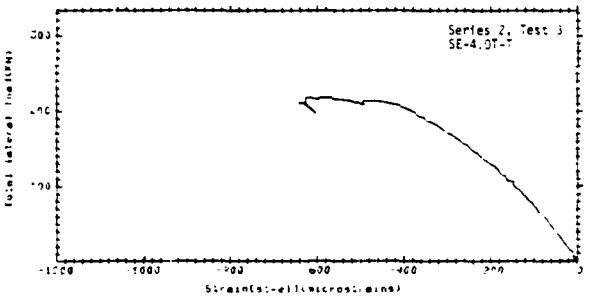
Series 2, Test 3

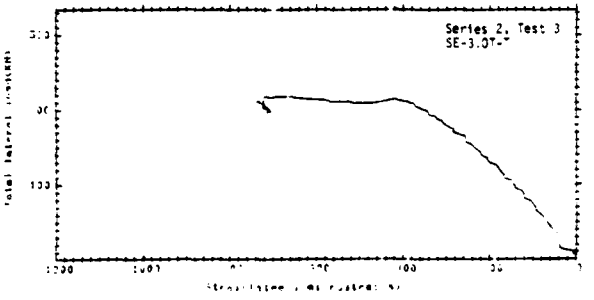
Series 2, Test 3

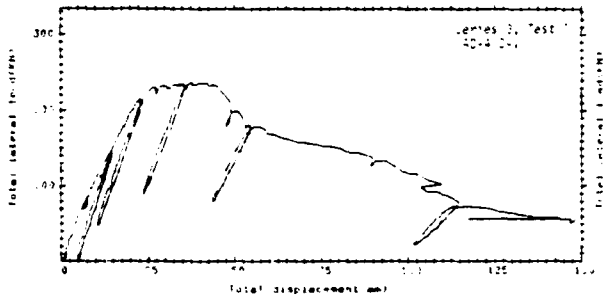

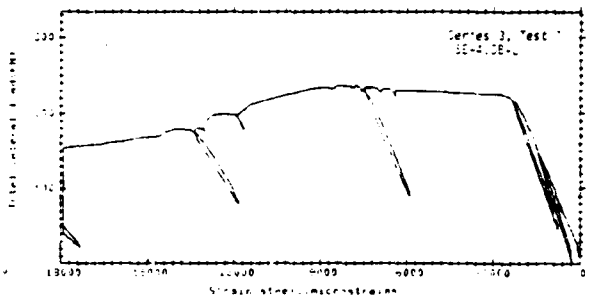

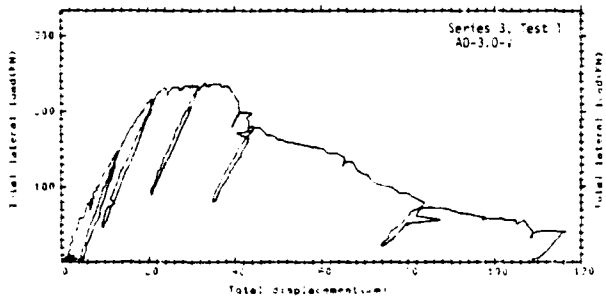
Series 3, Test 1
AD-3.0-L

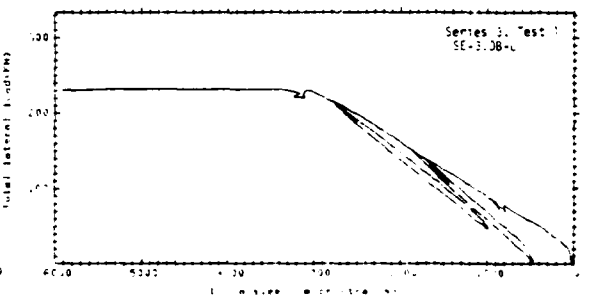
Series 3, Test 1

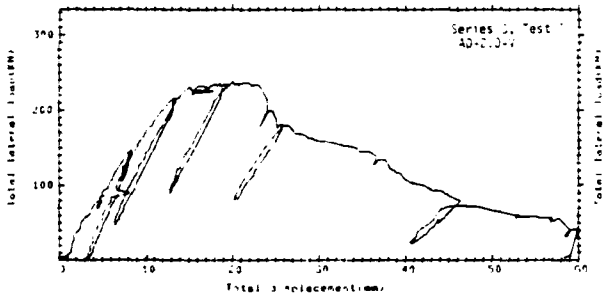
Series 3, Test 1
AD-2.0-L

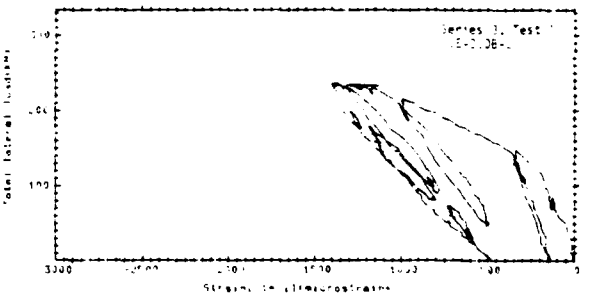
Series 3, Test 1

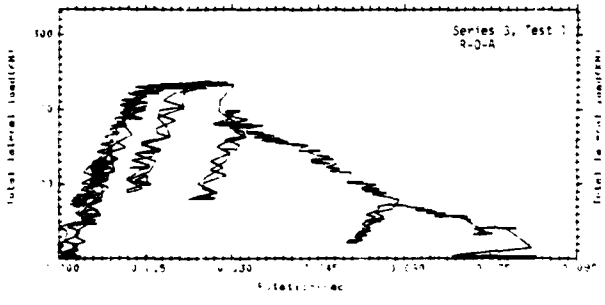
Series 3, Test 1
R-O-A

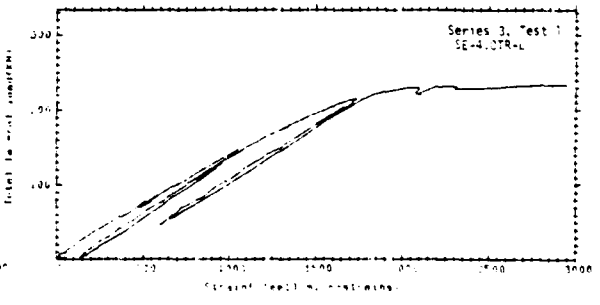
Series 3, Test 1
SE-4.0TR-L

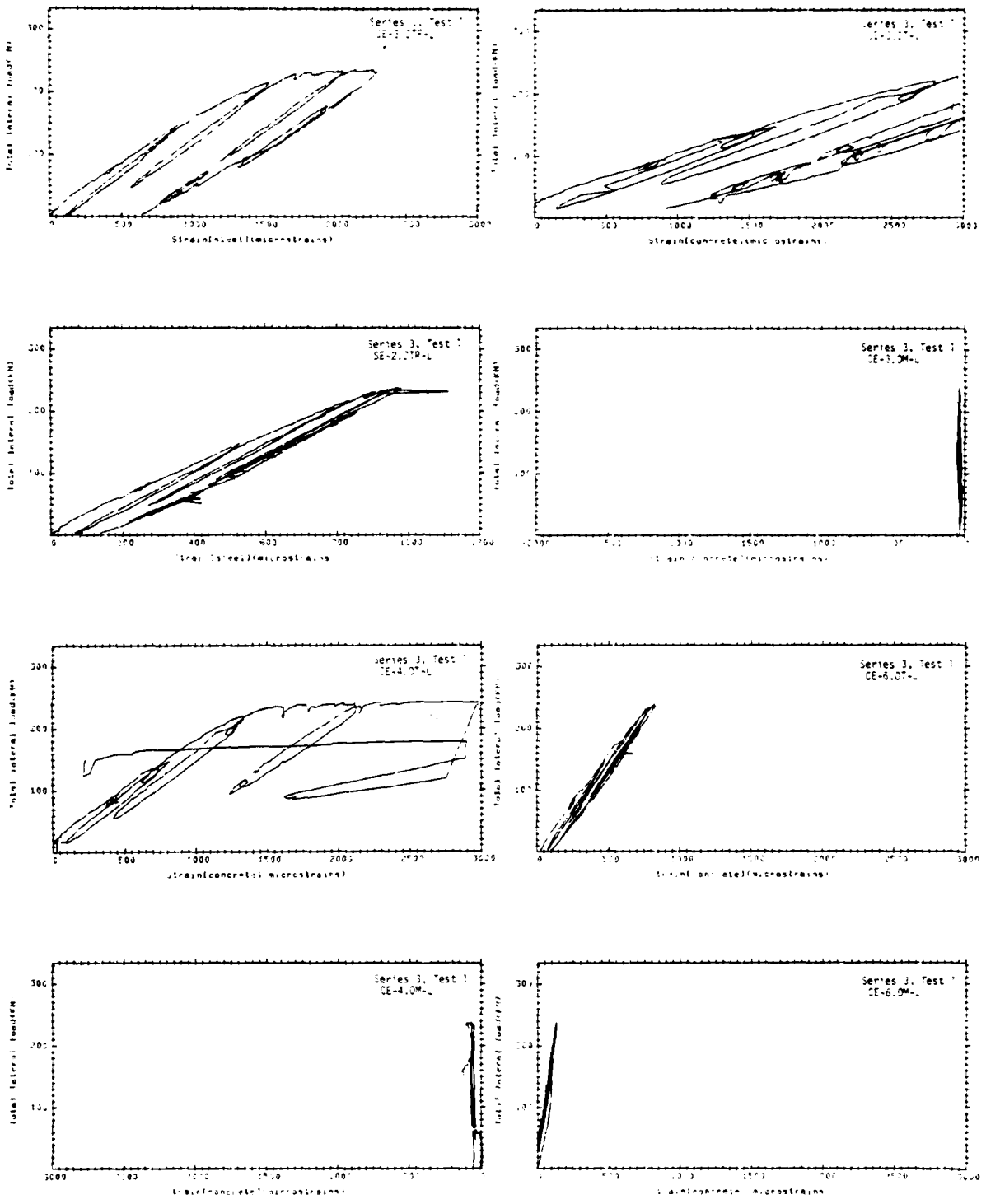
Series 3, Test 1
SE-3.0TP-L
Series 3, Test 1
SE-2.0TP-L
Series 3, Test 1
SE-3.0M-L
Series 3, Test 1
SE-4.0T-L
Series 3, Test 1
SE-6.0T-L
Series 3, Test 1
SE-4.0M-L
Series 3, Test 1
SE-6.0M-L

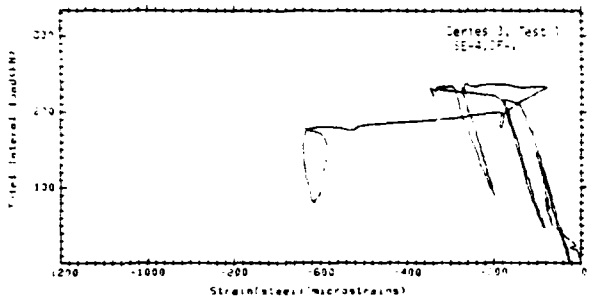
Series 3, Test 1

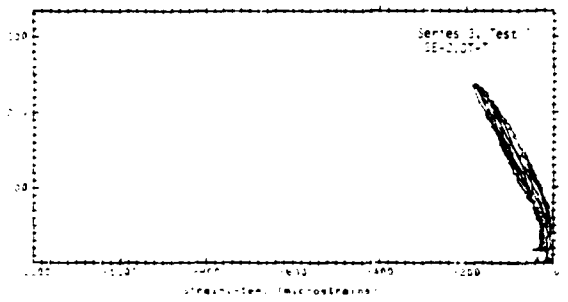
Series 3, Test 1

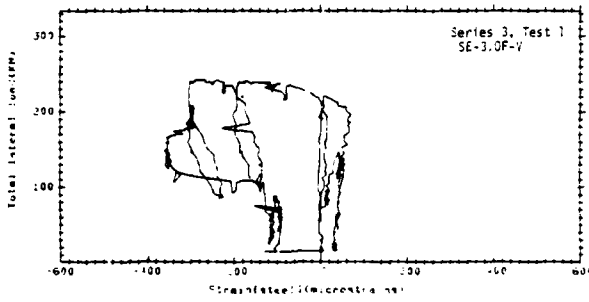
Series 3, Test 1
SE-3.0F-V

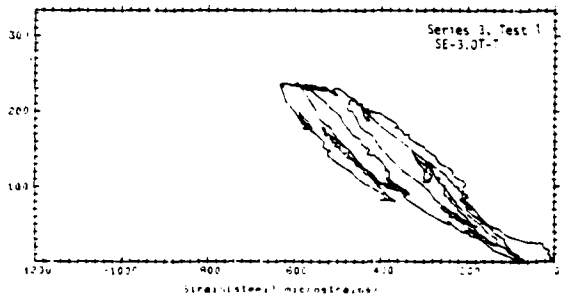
Series 3, Test 1
SE-3.0T-T

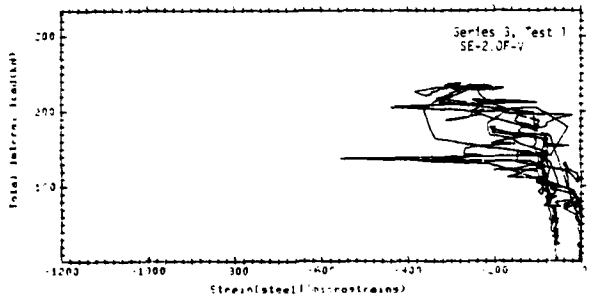
Series 3, Test 1
SE-2.0F-V

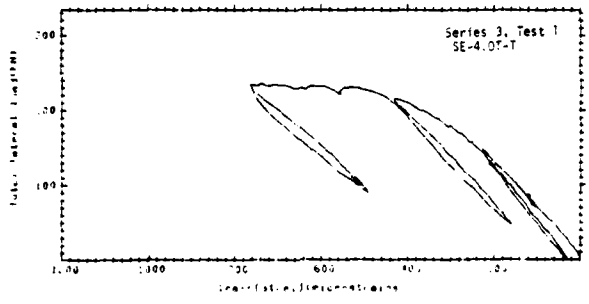
Series 3, Test 1
SE-4.0T-T

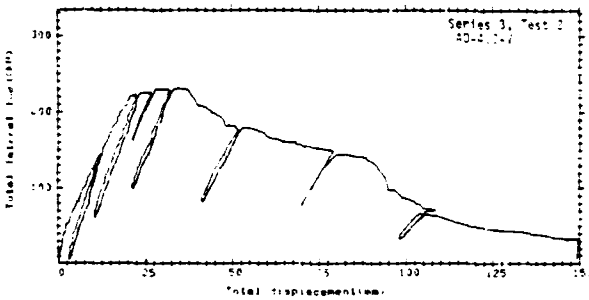
Series 3, Test 2

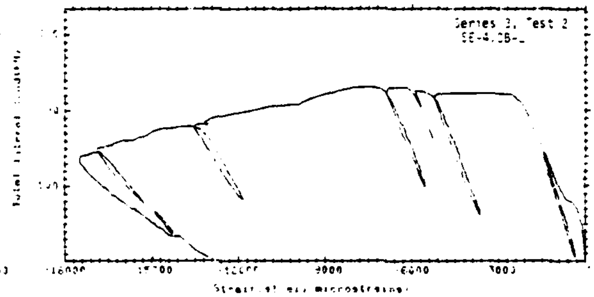
Series 3, Test 2

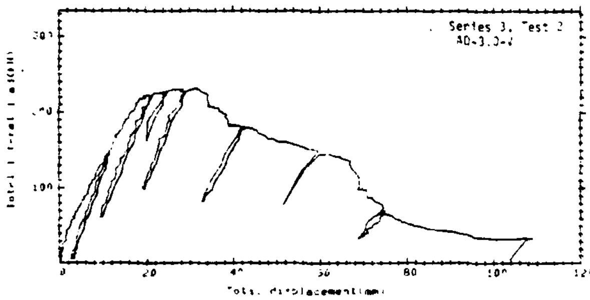
Series 3, Test 2
AD-3.0-V

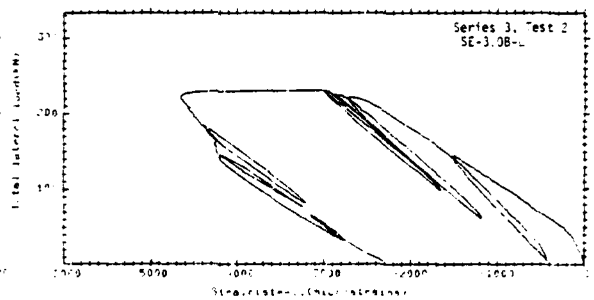
Series 3, Test 2
SE-3.0B-L

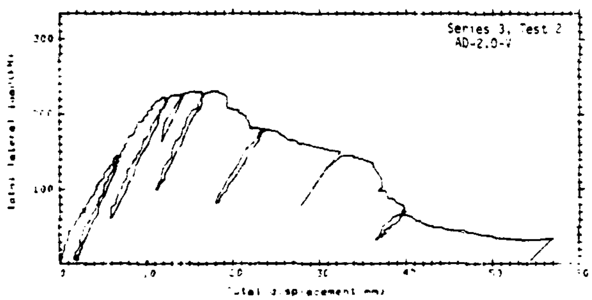
Series 3, Test 2
AD-2.0-V

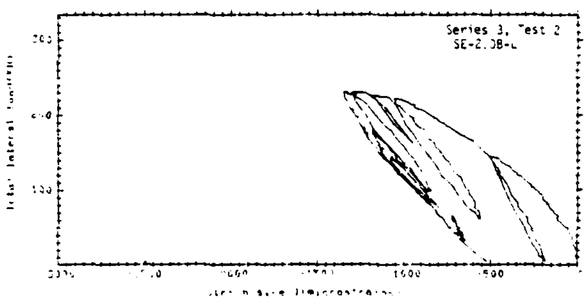
Series 3, Test 2
SE-2.0B-L

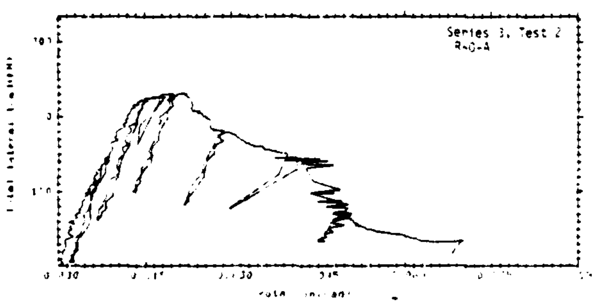
Series 3, Test 2

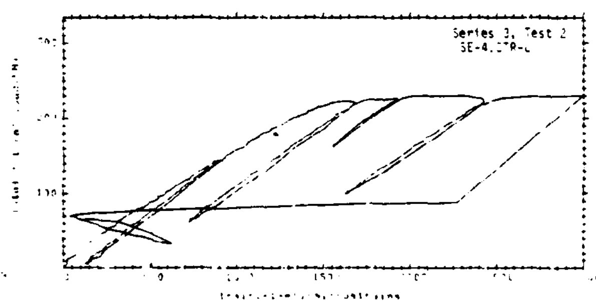
Series 3, Test 2

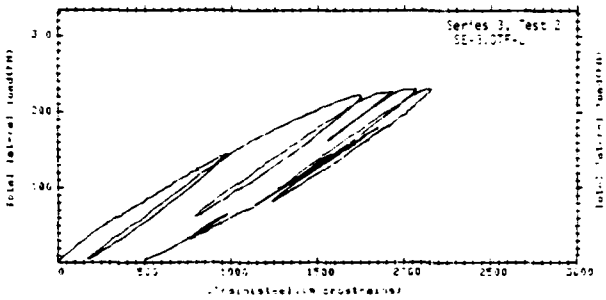
Series 3, Test 2
SE-3.0TF-L

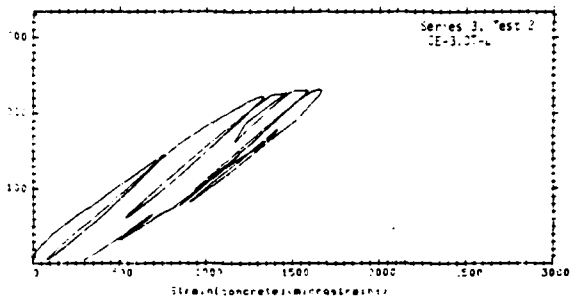
Series 3, Test 2
CE-3.0T-L

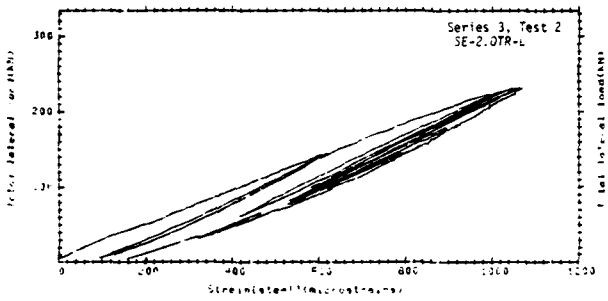
Series 3, Test 2
SE-2.0TR-L

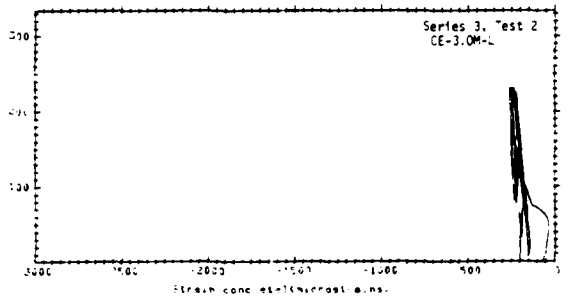
Series 3, Test 2
CE-3.0M-L

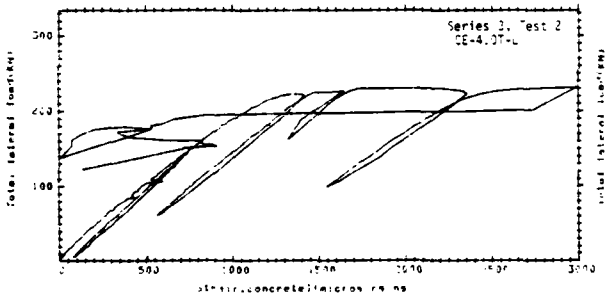
Series 3, Test 2
CE-4.0T-L

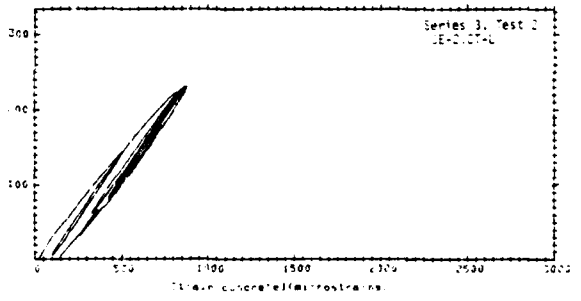
Series 3, Test 2

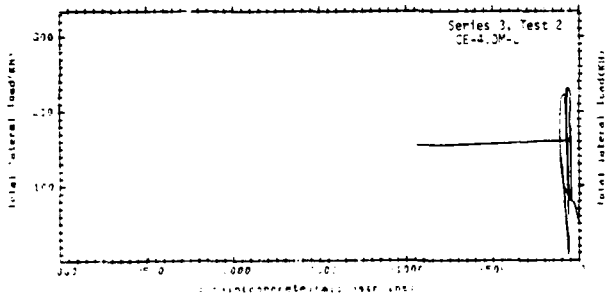
Series 3, Test 2
CE-4.0M-L

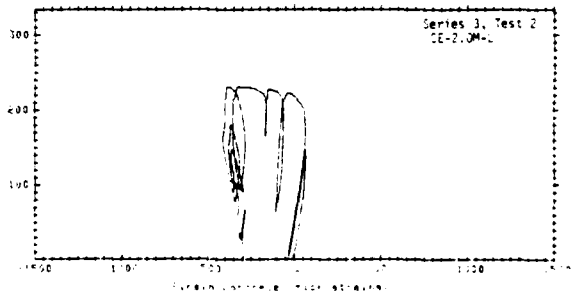
Series 3, Test 2
CE-2.0M-L

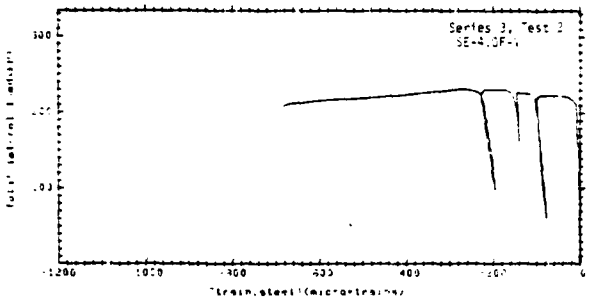
Series 3, Test 2
SE-4.0F-V

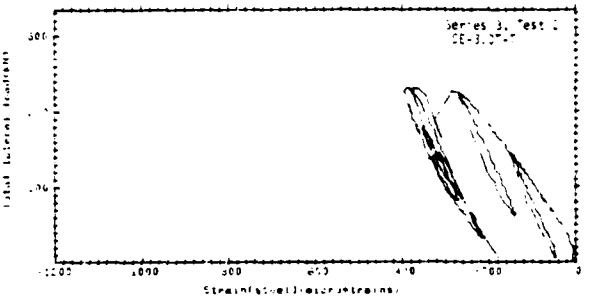
Series 3, Test 2

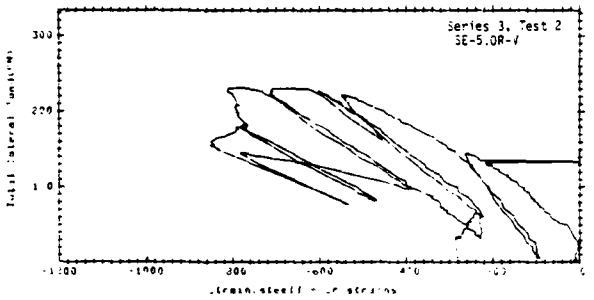
Series 3, Test 2
SE-5.0R-V

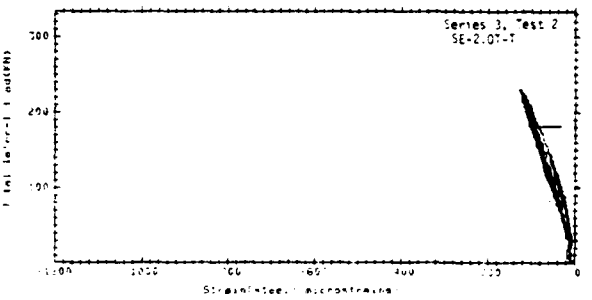
Series 3, Test 2
SE-2.0T-T

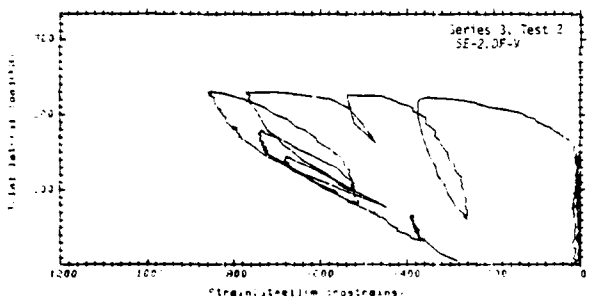
Series 3, Test 2
SE-2.0F-V

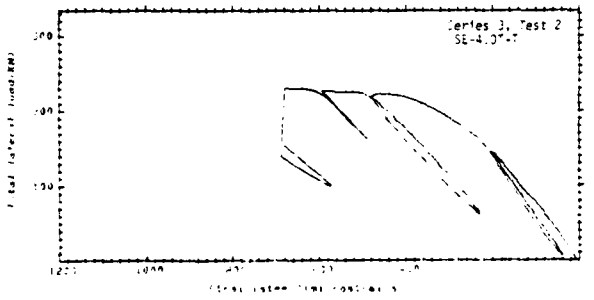
Series 3, Test 2
SE-4.0T-T

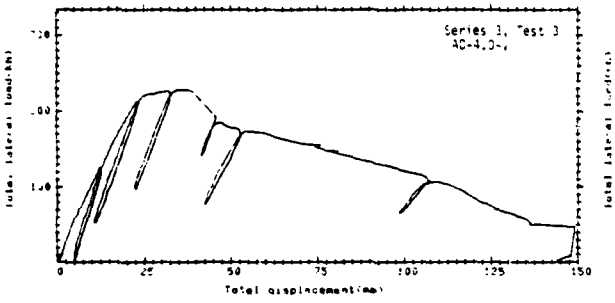
Series 3, Test 3
AD-4.0-L

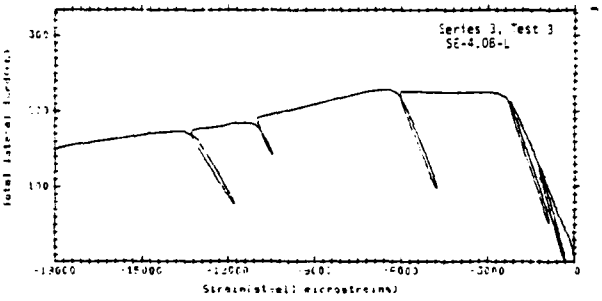
Series 3, Test 3
SE-4.0B-L

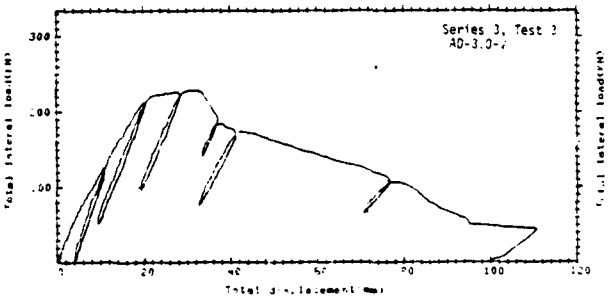
Series 3, Test 3
AD-3.0-L

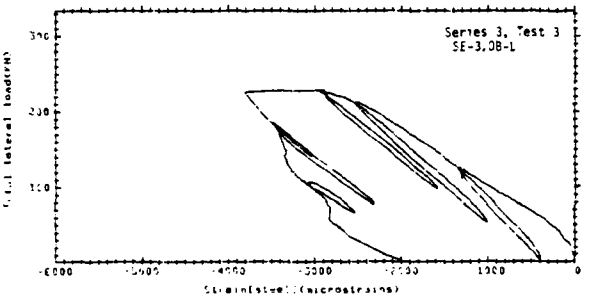
Series 3, Test 3
SE-3.0B-L

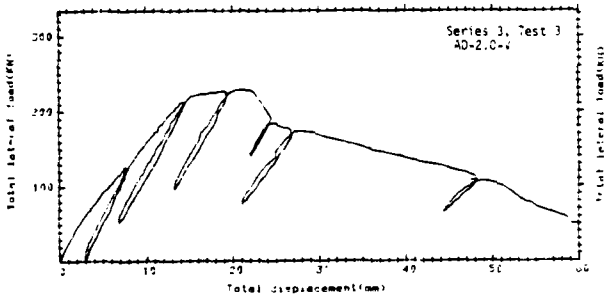
Series 3, Test 3
AD-2.0-L

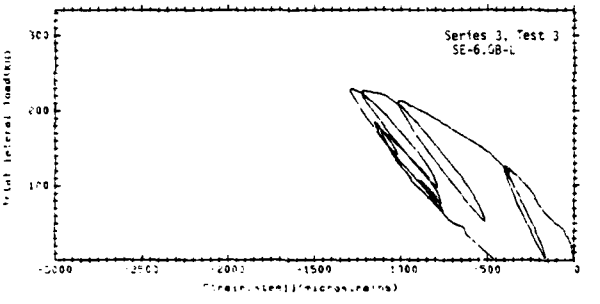
Series 3, Test 3
SE-6.0B-L

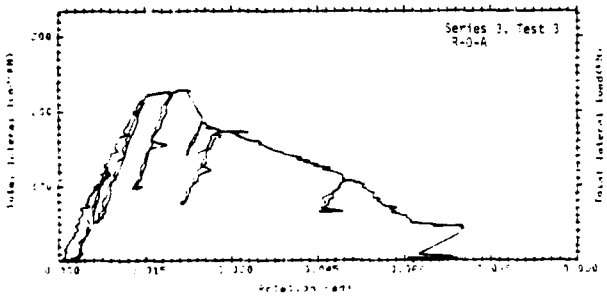
Series 3, Test 3
R-0-A

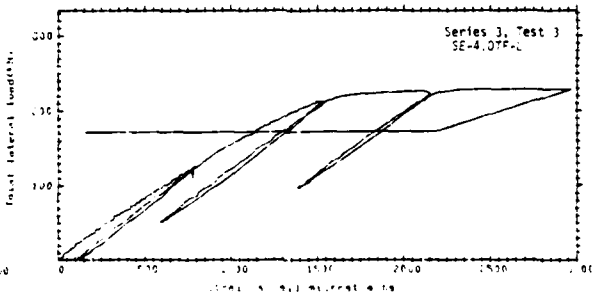
Series 3, Test 3
SE-4.0TF-L

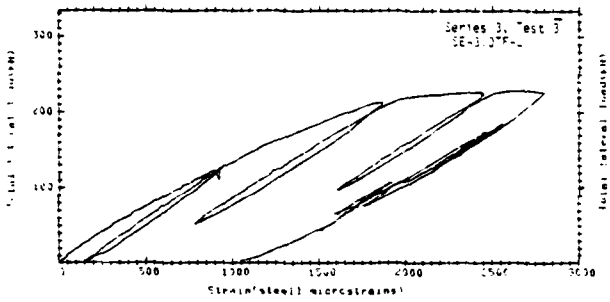
Series 3, Test 3

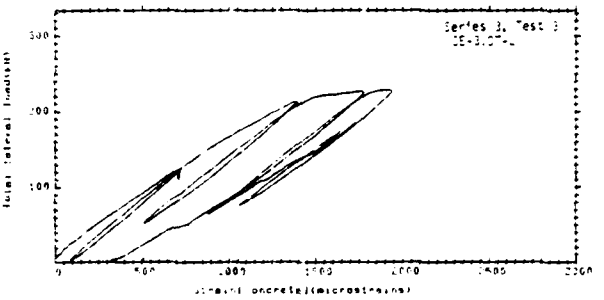
Series 3, Test 3

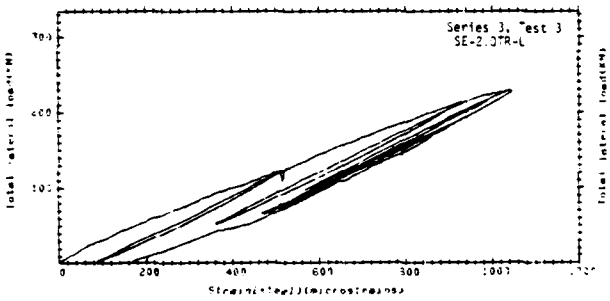
Series 3, Test 3
SE-2.0TR-L

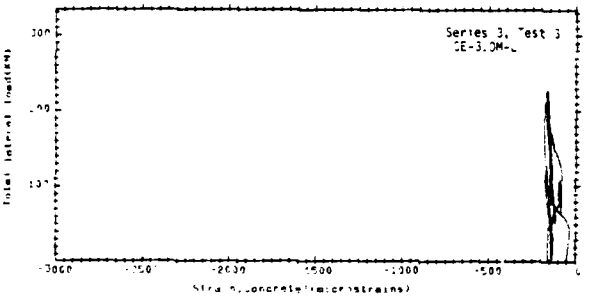
Series 3, Test 3
SE-3.0M-L

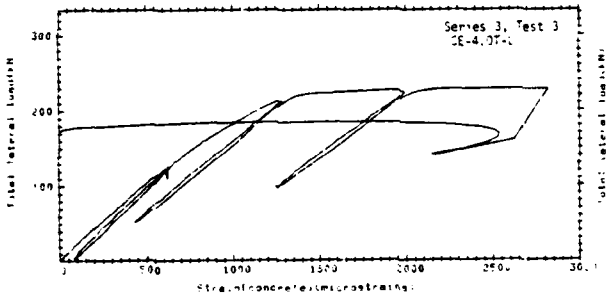
Series 3, Test 3

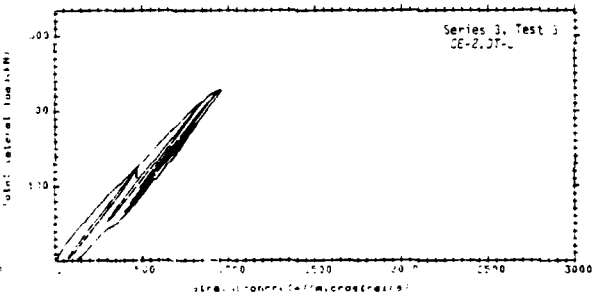
Series 3, Test 3

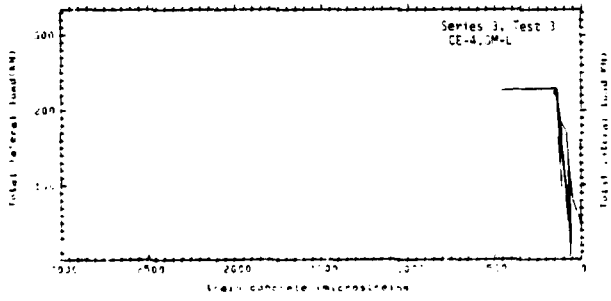
Series 3, Test 3
CE-4.0M-L

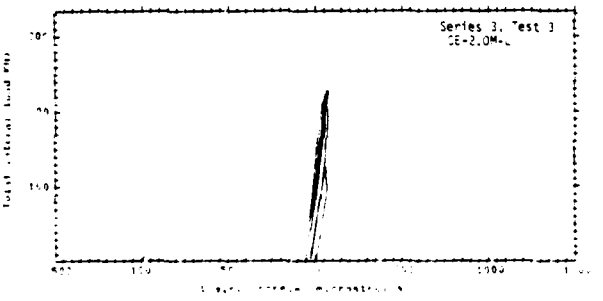
Series 3, Test 3

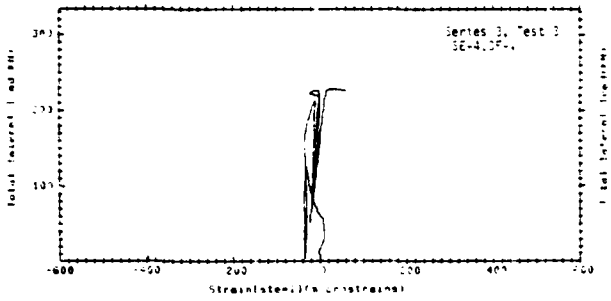
Series 3, Test 3

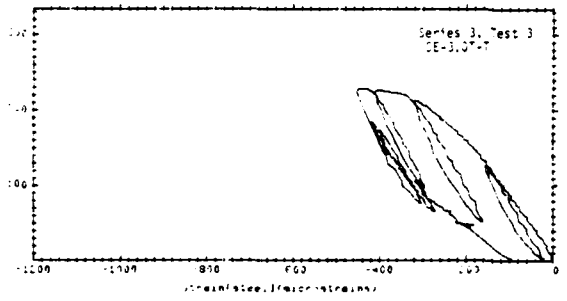
Series 3, Test 3

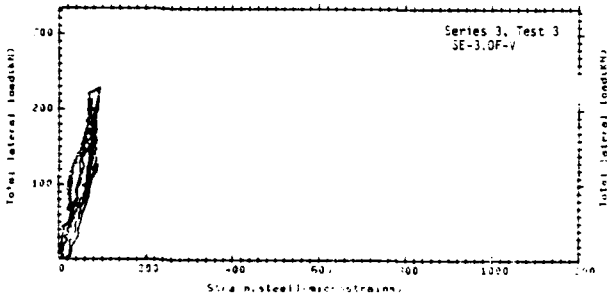
Series 3, Test 3
SE-3.0F-V

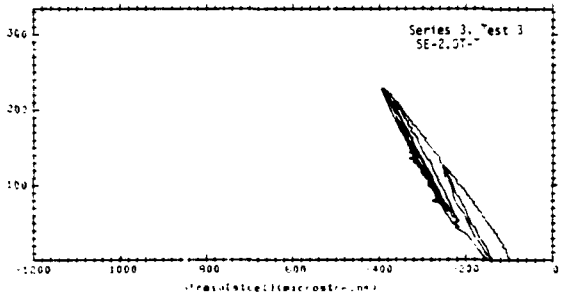
Series 3, Test 3

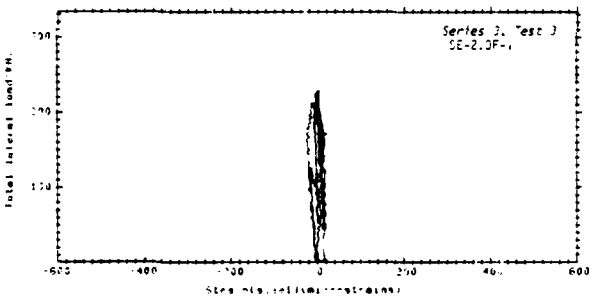
Series 3, Test 3
SE-2.0F-

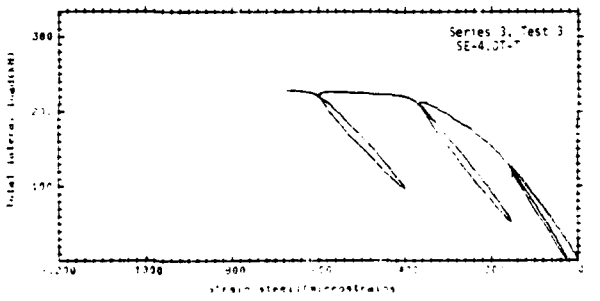
Series 3, Test 3

APPENDIX B

THE EFFECTS OF MULTIAXIAL COMPRESSIVE LOADING ON THE RESIDUAL TENSILE STRENGTH OF PLAIN CONCRETE

by

Roger W. Meier

Kurt H. Gerstle

Hon-Yim Ko

University of Colorado, Boulder, Colorado

Submitted to

New Mexico Engineering Research Institute

University of New Mexico, Albuquerque, New Mexico

June 1981

Note: This appendix is a self-contained document, provided for the reader's information, with its own figures, tables, and appendixes.

INTRODUCTION

A test program had been designed by others to verify general analytical formulation and prediction of the behavior of plain and reinforced concrete under general stress states. This test program consisted of tests on a series of reinforced concrete beams, carried out at the University of New Mexico, and tests on a number of plain concrete specimens cast of identical concrete, carried out at the University of Colorado, in order to obtain the material parameters required for the description of the response of the constituent plain concrete under multi-axial stress states. The results from the plain concrete test program are described herein.

TEST PROGRAM

This test program is intended to dovetail with earlier tests (1, 2, 3) in which a concrete whose strength is similar to that of the concrete used here was tested in both biaxial and triaxial compression using a variety of different stress paths. By duplicating selected stress paths used in the previous study, the results of this test program can be compared to those of the previous program. This makes available a wealth of information which could not be obtained from the present test program alone.

This test program, as well as a portion of the previous program, was performed using a fluid-cushion cubical test cell designed to apply a uniform, homogenous stress state with a minimum of boundary constraint. The test cell, described later in this report and in Ref. 4, is capable of applying three totally independent principal stresses ($\sigma_1 \neq \sigma_2 \neq \sigma_3$).

A total of 24 specimens from each of 4 batches of concrete were available for testing. Originally, four of the specimens from each batch were to be subjected to biaxial compression, six tested triaxially, and two subjected to triaxial load histories which would terminate in a biaxial stress state at failure which duplicated two of the four biaxial tests. Due to a number of complications, enumerated elsewhere in this report, specimens from two of the batches could not be used. With the loss of half of the available specimens, the last two test types had to be dropped from the program.

Table 1 summarizes the loadings used. The four biaxial compression tests include proportional loadings with stress ratios of 0:3, 1:3, 2:3, and 3:3 as shown in Figure 1. The triaxial tests consist of hydrostatic compression to two different levels, which correspond approximately to the uniaxial compressive strength and three-quarters of the uniaxial compressive strength, followed by deviation along three different stress paths at constant mean stress. These are shown in Figure 2. Path 1 is a triaxial compression in the octahedral plane (constant mean stress), Path 2 is a simple shear in the octahedral plane, and Path 3 is a triaxial extension in the octahedral plane. These stress paths will be referred to throughout this report as TC, SS, and TE, respectively.

Failure of specimens in the fluid cushion (cubical) test cell leave a sufficient portion of the specimen intact so that NX-size cores (2-1/8 inch

diameter) can be obtained from the failed specimens for split-cylinder tests to determine the residual tensile strength of the concrete following the compressive load histories in Table 1. The cores are cut into disks which are loaded diametrically to failure along one of two axes as shown in Figure 3. By testing disks from the same core in different directions,

Table 1.

Compressive Test Program

TEST NUMBER	TEST TYPE	LOAD HISTORY	
		PART 1	PART 2*
1	Proportional	$\frac{\sigma_2}{\sigma_1}$ = 0/3	
2	Biaxial to	1/3	
3	*Failure*	2/3	
4		3/3	
5	Triaxial:		Path 1
6	Hydrostatic	σ_o = 3.75 ksi	Path 2
7	Compression		Path 3
8	to σ_o, then		Path 1
9	Deviatoric to	σ_o = 5.00 ksi	Path 2
10	Failure		Path 3

Note: Three-fold replication of all tests.

* Path 1: $\Delta\sigma_1 = \Delta\sigma_2 = -\frac{1}{2}\Delta\sigma_3$

Path 2: $\Delta\sigma_3 = -\Delta\sigma_1$, $\Delta\sigma_2 = 0$

Path 3: $\Delta\sigma_3 = \Delta\sigma_2 = -\frac{1}{2}\Delta\sigma_1$

stress-induced anisotropy may be detected. Comparison of these splitting strengths with the strengths of virgin disks cored from untested secimens will also indicate the tensile strength reductions caused by previous compressive loading.

MULTIAXIAL TEST APPARATUS[1]

The multiaxial test apparatus consists of a rigid cubical space frame and six walls (faces) as shown in Figure 4. The openings in the frame form six identical cavities which, together with the adjoining walls and a pressure seal arrangement, act as six pressure vessels. The 4-inch cubical specimen is placed in the central cavity of the space frame and sealed in by the six walls, which bolt onto the frame. Loads are applied by a hydraulic pressure system which supplies silicone fluid to fluid cushions (membranes) located on the inner face of each wall. Each set of opposing walls is connected to an individual pumping system which regulates the stress level on that axis. By means of a series of valves located on a control panel, the pumping systems can be connected together such that any two axes or all three axes can be controlled by a single pump or the systems can be separated from each other completely to provide three independent principal stresses ($\sigma_1 \neq \sigma_2 \neq \sigma_3$). Proximity-type transducers (probes) are used to measure the deformations in the three principal directions. The test data is monitored and plotted in real time by a microcomputer so the specimen behavior can be observed while the test is in progress. This allows the tests to be stopped exactly at failure (the definition of which is presented later in this report).

[1]This section is rewritten in part from Ref. 4 which includes a more detailed description of the apparatus.

The walls of the test apparatus are composed of two parts. The main frames of the walls serve as the lids of the pressure vessels and include the pressure seals and hydraulic fluid ports. One of the two fluid ports serves as a pressure inlet and the other as an outlet to bleed entrapped air from the pressure vessels. The probe blocks, which bolt on the inside face of the walls, serve as bases for the displacement probes.

Details of the pressure sealing system are shown in section in Figure 5. Two O-ring grooves form the pressure seal between the wall and the frame. The inner groove seats an O-ring which seals the pressure vessel to prevent fluid from escaping outside the apparatus. The outer groove houses the O-ring built into the fluid cushions to prevent fluid from leaking into the sample cavity. Because the aluminum faces expand sideways due to Poisson's effects when fluid pressure is applied in the cavity between the wall and the specimen, the sealing capacity of this arrangement increases with cell pressure.

A polyurethane pad and a leather pad transmit the fluid pressure from the membrane to the specimen. They are flexible enough to follow minor differential distortions on the specimen surface yet provide membrane support to prevent an extrusion from occurring when a large deviator stress is present between two adjacent pressure vessels. The membrane, polyurethane pad, and leather pad are shown in Figure 6. The leather pads are made from 1/4-inch shoe leather to the approximate specifications given in Figure 7. Leather was chosen because it is pervaded by tiny air cells which absorb deformations, thereby reducing the Poisson's effects. This helps to minimize tangential stresses which could be transferred to the specimen. The hole in the center of the pad is to prevent interference between the probes and the specimen, and the 45° bevel along the edges of

the pad prevent interference between the leather pads of adjacent pressure vessels. Because the leather pad is slightly narrower than the cavity, the polyurethane pad, which is built up along its edges, is used to prevent a membrane extrusion into the space between the leather pad and the sides of the cavity.

The deformation measurement system is composed of 18 Bentley-Nevada proximitor probes (three on each face) and their supporting electronics. Each probe, operating on an induction principal, measures the width of the gap between a conductive metal target in contact with the specimen surface and a coil embedded in its tip, without requiring physical contact between itself and the specimen. Each probe is driven by its own external 18 Vdc power supply operating at 25 ma. A signal emitted by the probe is reflected by the metal target and returned to the probe. This signal varies with the distance it travels to the target and back. A data acquisition system, of which the probe drivers are a part, scans through each of the 18 probe channels and rectifies the returning signals into DC voltages. These voltage outputs are equated to gap widths by means of a calibration curve. The calibration curve is stored in the microcomputer memory and, as the voltage readings are transferred to the computer through an interface with the data acquisition system, they are automatically transformed into gap widths.

The probe targets are 4-inch square sheets of 0.012 in. thick brass shim stock. To reduce the transverse stiffness of these sheets so they can conform to the shape of the deformed specimen surfaces, the targets are cut in the pattern shown in Figure 8. The dotted circular areas show the regions at which the proximeter probes are aimed. Note that no slits enter

these regions as they would scatter the signal and cause erroneous deformation readings.

The proximeter probes are positioned so that the probe arrangement on each wall is a mirror image of that on the opposing wall. By comparing the outputs of opposing probes as a test progresses, the deformations of the specimen-apparatus system are determined. Because the probes are mounted on the faces, which deform during a test, the deformations of the apparatus must be subtracted out before the actual specimen deformations can be found. This is discussed in detail in the section titled "Box Calibration". The advantage of using opposing probes to determine deformations is that rigid body translations are automatically eliminated from the calculations. In addition, because the three probes on each face are equidistant from the center of the face and located 120° apart, rigid body rotations can also be eliminated by averaging the three probe readings.

SAMPLE PREPARATION

Concrete specimens to be used in the cubical test cell are cast in steel molds with inside dimensions of 4 inches square by either 4 inches or 4-1/8 inches in height. The concrete is placed without floating or troweling in order that concrete remains above the tops of the mold. This excess concrete is cut off using a diamond-bladed masonry saw to ensure a specimen height of 4.00 $\pm$ 0.02 inches and a completely planar surface.

Because small voids near the surface of the concrete will allow penetration of the flexible membranes, resulting in the rupture of the fluid cushion, the central portion of all six faces are sandblasted to

expose these voids. The sandblasted areas are then filled with a plastic wood filler material (Durham's Rock Hard Water Putty) and smoothed out as much as possible with a 1-inch putty knife and 5-inch broad knife. After drying for 24 hours, the puttied surfaces are belt-sanded. Any holes uncovered by the sanding are reputtied and the surfaces are finished with hand sanding using 400-grit paper. A typical specimen, finished and ready for testing, is shown in Figure 9.

CUBICAL CELL CALIBRATION

An essential component of the data reduction process is the correction for the deformations of the cubical cell itself during a test. These deformations arise from the reaction forces to the fluid pressure on the specimen and the lateral expansion of the cavity which contains the fluid cushion and are of a comparable order of magnitude as the deformations of the concrete specimen.

The cubical cell is calibrated by applying an incremental, monotonically-increasing uniaxial stress to an aluminum specimen with known stress-strain response. Each axis of the cubical cell is loaded separately as the response differs slightly from axis to axis. The pressure is generally increased in load steps of 500 psi up to the maximum stress which can be expected during the test program. For this test program, the maximum expected stress was 15,000 psi which corresponds to the limiting stress state $_1 = 15000$, $_2 = _3 = 0$ in the 5000 psi octahedral plane. Each axis is loaded a minimum of three times using the same load steps each time to ensure that the observed response is truly representative. During the calibration test, at the end of each load step, the total deformation

in terms of changes in gap widths is measured in each of the three axis directions of the cubical cell. By subtracting the calculated response of the aluminum cube from the observed total deformations, the deformations of the cubical cell are computed. For each stress level, s, at which measurements are taken, a calibration array is compiled in the form

$$\begin{bmatrix} d_{xx} & d_{xy} & d_{xz} \\ d_{yx} & d_{yy} & d_{yz} \\ d_{zx} & d_{zy} & d_{zz} \end{bmatrix}^{s}$$

where d_{ij} denotes the deformations of the cubical cell in the i-direction due to an applied stress, s, in the j-direction.

During a test, the cubical cell deformations in any direction, j, are computed by superposition of the terms d_{jx}^{r}, d_{jy}^{s}, and d_{jz}^{t} where r, s and t represent the stress levels in the x, y, and z directions, respectively. Because the response of the cubical cell is nonlinear, superposition is not strictly valid. Triaxial tests on an aluminum specimen with known elastic parameters, however, have shown this method of computing cubical cell deformations to be reasonably accurate. Above approximately 10,000 psi, the cubical cell response is linear and the validity of superposition is no longer in question; thus, the accuracy of the corrected specimen deformations is improved as the stresses approach the failure state.

The cubical cell was calibrated immediately before proceeding with this testing program and during this time, it was observed that the response of the cubical cell at low pressures (below 1000 psi) varied with successive loadings. The variation in the deformations within this stress range is attributed to movement of the probe target before it becomes firmly seated against the specimen, and thus represents neither

deformations of the specimen nor of the cubical cell. Because strain calculations are made using the relative changes in gap width since the start of the test, this initial uncertainty as to the distance from the proximitor probes to the face of the specimen would affect the calculated response of the specimen during the entire test by presenting a false starting point on the stress-strain curve and errant initial moduli.

In order to eliminate these false initial gap width measurements, the cubical cell was completely recalibrated using the gap widths at 100 psi as the reference point for subsequent deformation calculations. It was felt that 100 psi would be sufficient to seat the targets firmly against the specimen and that the continued application of at least 100 psi on all axes (regardless of test type) throughout a test would preclude target movements which were independent of the movement and deformation of the specimen. Furthermore, the deformations of a concrete specimen under a hydrostatic stress of 100 psi are negligible in comparison to the total deformations experienced by the concrete during the rest of a test; thus the gap widths as measured at 100 psi can be assumed to be equal to the gap widths which would have been measured in a completely unloaded state.

It is apparent in the stress-strain curves of Appendix B that most but not all of the uncertainty has been eliminated. Some of the tests show a virtual expansion of the specimen upon first loading. This results from less cubical cell deformation than is allowed for in the calibration array and can be eliminated, when necessary, by shifting the stress-strain curve along the strain axis by the amount required to eliminate the anomaly. It was felt that any attempts to further eliminate these discrepancies by beginning the tests at a stress in excess of 100 psi would not be prudent. Although the results of triaxial tests should not be affected by the use of

a nonzero stress to represent the unloaded condition, the results of biaxial tests might be suspect. Because the minimum pressure of 100 psi must be maintained throughout the test, even on what should be the unloaded axis, a truly biaxial state of stress cannot be achieved. Because the 100 psi reference state on the unloaded axis of a biaxial test is at most only 4 percent of the maximum deviator stress at failure, it was assumed that little effect would be noticed.

STRESS-STRAIN-STRENGTH BEHAVIOR

At the outset of this testing program, it was decided that the specimens should be tested in such a manner that inherent anisotropy may be identified. To this end, a method of labeling the specimens was devised such that the concrete batch as well as the mold used and the orientation of the specimen in the mold could be determined. The first batch of concrete was cast in New Mexico prior to receipt of the labeling instructions, hence Batch 1 specimens were eliminated from the testing program.

Shortly after starting the testing program, some concern arose as to variations in the properties of the remaining three batches of concrete. Because two TE 3750 tests had already been performed which showed a marked dissimilarity in stress-strain behavior between a specimen from Batch 3 and a specimen from Batch 4, a series of TE 3750 tests was begun to investigate the the possibility of a systematic difference. The series was to consist of six tests using two specimens from each of Batches 2, 3, and 4. It soon became apparent that a systematic difference did exist between those specimens taken from Batch 3 and the specimens from Batches 2 and 4. One

of the tests on a specimen from Batch 2 was unsuccessful due to an equipment malfunction, however the very close agreement between tests on the two specimens from Batch 4 and the successful test on one specimen from Batch 2 was deemed sufficient to preclude a third test on a specimen from Batch 2. A third test was performed, however, on another cube from Batch 3 to provide a better statistical average of the stress-strain behavior of specimens from that batch.

Figures 10 and 11 show the results of the three tests on specimens from Batch 3 and the three tests on specimens from Batches 2 and 4, respectively. Although the tests on Batch 3 specimens exhibit considerably more scatter than the tests on Batch 2 and 4 specimens, a comparison of the average response of the two test groups, as shown in Figure 12, indicates the differences in behavior. The specimens from Batch 3 appear to have lower moduli and more ductility (defined here by the maximum deviator strains near failure) than the specimens from Batches 2 and 4, which have nearly identical responses. In addition, specimens from Batch 3 consistently failed at lower values of the maximum principal stress. In Table 2 these differences are quantified as the maximum deviator stress at failure and the maximum deviator strains at σ_1 = 5225 psi, $\sigma_2 = \sigma_3$ = 800 psi, which is the stress state with the greatest deviator stess which all six tests had in common prior to failure. From the averages of these few tests, it appears that the specimens from Batch 3 have approximately 20 percent greater ductility (deviator strains at a given stress level) and 10 percent less strength than the remaining specimens.

Table 2.

BATCH	SPECIMEN	$(\sigma_1 - \sigma_3)_f$ (psi)	$(\varepsilon_1 - \varepsilon_3)^*$ (mils/in)
2	C4	5175	1.464
4	D2	5175	1.450
4	A6	5100	1.270
Average		5150	1.395
3	B5	4650	1.767
3	B6	4200	1.688
3	C2	4875	1.648
Average		4575	1.701

* at $\sigma_1 = 5225$ psi, $\sigma_2 = \sigma_3 = 800$ psi.

Based on these findings, specimens from Batch 3 were also eliminated from further consideration. It should be noted that three other specimens from Batch 3 were used in tests prior to the decision to eliminate that batch. Now that sufficient data has been accumulated on the test types involved, it can be seen that the Batch 3 specimens exhibited greater ductility and lower strengths during these tests as well. The tests involved were a TC 3750, a TC 5000, and a TE 5000. The results of these tests as well as the TE 3750 tests are included in Appendices A and B.

With only two remaining batches from which to obtain test specimens, the goals of the testing program were changed to require only two-fold replication of each test type. Since no systematic differences could be detected between the properties of specimens from Batches 2 and 4, further

testing was performed on cubes selected at random rather than using a cube from each batch for the two-fold replication. In order to compensate for the change in the degree of replication, attempts were made to obtain two tests for each test type for which the results were as nearly identical as possible. In the attempt, three tests were sometimes performed with the result that two tests exhibit quite similar stress-strain behavior while a third test exhibits behavior which is similar but not in as close agreement. Given the statistical nature of concrete, those test types for which three tests were perfomed can be considered to have the three-fold replication which was originally required. Given the limitations on the number of specimens available, however, some tests resulted in close enough behavior agreement that a third test was unwarranted.

In order to investigate the possibility of inherent anisotropy in the specimens, a standard convention was established whereby the z-axis of the cubical cell (the vertical axis) was always the major principal stress axis. In this way, the orientation of the specimen in the cubical cell would determine which axis of the specimen was loaded with the major principal stress. In a similar manner, the x-axis of the cubical cell was always the minor principal stress axis. With this method, any strain anomalies which arose due to inaccurate calibration of the equipment could be seen (for example, if the z-axis of the cell always resulted in the largest strain regardless of cube orientation) and any systematic anisotropy in the specimens could be detected.

Because of the statistical nature of concrete, any quantification of anisotropy must be viewed relative to the overall scatter of results. Table 3 shows the variation in the tangent bulk modulus at a hydrostatic stress of 3500 psi, which is the highest hydrostatic stress common to all

of the triaxial tests. By using the bulk modulus, which in effect averages the strains, the variability of properties from cube to cube can be estimated. The standard deviation of the bulk modulus with respect to the mean is $\pm$15.6 percent. Table 4 shows the greatest difference between any principal strain ε and the average strain $\bar{\varepsilon}$ at the same hydrostatic stress of 3500 psi for each of the tests. This quantity is expressed as a percentage relative to the mean and can be equated to the greatest amount of anisotropy exhibited by the specimen. The average degree of anisotropy is 9 percent. From this it can be assumed that no systematic anisotropy exists since the scatter of strain values within the individual cubes is far exceeded by the scatter of data among all of the cubes. The values listed in Table 4 occurred on various axes of the cubes with no one axis showing a predominance. Therefore these specimens can be considered to be isotropic and the stress-strain behavior of different tests can be compared without regard to specimen orientation.

Table 3.

TEST	K_t* (10^6 psi)	TEST	K_t* (10^6 psi)
5A	1.538	8A	1.483
5B	2.201	8B	1.580
5C	2.355	8E	1.925
6A	1.840	9A	1.994
6B	2.222		
6C	1.890	9C	2.009
7B	1.881	10A	1.519
7F	1.556	10B	1.389
7G	1.609	10C	1.721

Average: 1.807×10^6 psi

Standard Deviation: $\pm$ 0.28% $\times 10^6$ psi (15.6% of mean)

*Tangent Bulk Modulus at σ_{oct} = 3500 psi

Table 4.

TEST	$\frac{(\varepsilon-\bar{\varepsilon})^*}{\bar{\varepsilon}}$ (%)	TEST	$\frac{(\varepsilon-\bar{\varepsilon})^*}{\bar{\varepsilon}}$ (%)
5A	9.39	8A	6.40
5B	15.44	8B	4.97
5C	18.34	8E	17.89
6A	6.48	9A	6.38
6B	13.18		
6C	10.26	9C	7.08
7B	13.18	10A	3.41
7F	6.00	10B	4.00
7G	2.93	10C	6.05

Average: 8.9%
Standard Deviation: $\pm$ 4.8%
(54% of mean)

*at σ_{oct} = 3500 psi

TRIAXIAL TEST RESULTS

Prior to the presentation of the failure results, it is important to define the criterion used in this study. Because of the need to obtain intact cores from the failed specimens, the tests could not be continued to the point at which ultimate strength was reached, i.e., the stress state at which physical separation along a shear surface occurs. Instead, the definition of failure used by Bieniawski (5) to describe brittle failure of rocks and Newman (6) to describe the failure of concrete was applied.

These investigators describe the failure mechanisms of brittle materials (which includes concrete) in three stages. The first stage consists of a nearly linear stress-strain response associated with very small amounts of propogation of pre-existing bond cracks at the mortar-aggregate interface. The second stage, the beginning of which is reflected in a deviation of the stress-strain curve from linearity, is characterized by an increase in the number and length of the bond cracks which propogate in a stable (stress-dependent) manner. This stage proceeds up to approximately 80 percent of the ultimate load. The third stage begins when the bond cracks become unstable, continuing to propogate without an increase in stress, and join together to form mortar cracks. The stress state at the start of this third stage, called the "discontinuity point" by Newman, is taken to be the failure state. The reason for this is that the unstable growth of cracks beginning at this stress level can conceivably continue *until enough cracks join that the specimen* is physically separated; all without a further increase in stress. As these cracks propogate, separating more and more material, the specimen expands. This expansion is reflected in a reversal of the volumetric strain curve. Therefore, the "discontinuity point" is synonymous with the point at which the volumetric curve changes directions. Because this reversal is generally gradual, a more rigorous definition of the discontinuity point is the point at which the volumetric strain curve achieves an instantaneous vertical slope.

Since a stress-strain curve is plotted in real time during a test, the discontinuity point is fairly easily identified and the test can be stopped in order to prevent further damage to the specimen. In order to ensure that this point had actually been reached, the tests were actually taken

one or two load steps (stress increments) further. If the volumetric strain curve continued to show expansion after these load steps, the test was stopped.

The results of the triaxial test series (which can be found in their entirety in Appendix B) are summarized in Figures 13a through 13f. The solid lines in these figures represent the average stress-strain response for each test type up to the point of failure. The shaded regions indicate the range of strains actually observed in the tests. It is evident that a fairly high degree of reproducibility was achieved for every test type.

Tables 5 and 6 summarize the stress states at failure in terms of the octahedral normal stress (whose value is included in the path designation) and two commonly used measures of shear stress - the deviator stress ($\sigma_1 - \sigma_3$) and the octahedral shear stress τ_{oct}. This data is also presented in Figure 14a as failure envelopes in the two octahedral planes investigated. Because the tests were performed using incremental loading, the failure stresses can only be defined to the nearest 100 psi in most cases; thus the deviator stresses are accurate to within 2 percent of the octahedral normal stress values.

It was mentioned earlier that the stress paths and octahedral planes were chosen so as to coincide with a previous test program which included cubical cell testing of a concrete with a uniaxial compressive strength similar to that of the concrete used in this study. The results of standard uniaxial compression tests on 6 in. by 12 in. cylinders performed as part of the testing program undertaken by Gerstle, et al. indicate a strength of 4600 psi. From the results of uniaxial compression tests performed at the University of New Mexico on cylinders cast from Batches 2

Table 5.

(All units are in psi.)

TEST	PATH	$\sigma_1 - \sigma_3$	τ_{oct}
5B	TC 3750	8400	3842
5C		8250	3889
Average		8325	3866
6A	SS 3750	7000	2858
6B		7100	2899
6C		7200	2939
Average		7100	2899
7B	TE 3750	5100	2404
7F		5175	2440
7G		5175	2440
Average		5150	2428

Table 6.

(All units are in psi.)

TEST	PATH	$\sigma_1 - \sigma_3$	τ_{oct}
8B	TC 5000	10200	4808
8E		10350	4879
Average		10275	4844
9A	SS 5000	8800	3593
9C		9200	3756
Average		9000	3675
10A	TE 5000	6750	3182
10C		6975	3288
Average		6850	3235

and 4, a uniaxial strength of 5215 is indicated. Figure 14b shows the failure envelopes in the 5000 psi octahedral plane resulting from the present study (identified as AFWL) and the previous study. The octahedral shear stresses at failure for the concrete used by Gerstle, et al. appear to be approximately 15 percent greater. Some of this difference is due to the slightly greater strength of the concrete, indicated by the higher uniaxial compression strengths, while a portion of the difference is undoubtedly the result of the slightly different definition of failure used in the previous study. Although Starovisky (3) recognized the discontinuity point as an indication that failure had occurred, the data acquisition system did not provide for real time plotting of the stress-strain response when she was doing her testing. With no indication of the strain behavior, she relied on a sudden drop in pressure, which was most likely due to a sudden increase in strain in one direction, to define failure. Although the sudden increase in strain is usually accompanied by a reversal in the volumetric strain curve, the results of many of her tests, once plotted, showed that the discontinuity point had not yet been reached. This could account for much of the remaining difference.

BIAXIAL TEST RESULTS

The results of the biaxial test series, which can be found in Appendices C and D, show much less reproducibility than those of the triaxial tests. This is most evident in the scatter of failure stress states shown in Figure 15. A large amount of scatter is to be expected because the fluid cushions provide little constraint, allowing the specimen to fail in a brittle manner. This brittle failure is dependent on random

weak areas within each specimen; when the weakest portion fails, the entire specimen fails in the absence of any means of stress redistribution. Clearly, three-fold or even four-fold replication would have been preferable in this biaxial test series. Because the entire supply of specimens from Batches 2 and 4 had been exhausted, further testing, however much warranted, was impossible.

For the uniaxial stress path (stress ratio of 0:3), only one successful test was performed using cubes from Batches 2 and 4. Because the supply of cubes had been exhausted, a specimen from Batch 3 was tested in order to provide indirect supportive data. This specimen failed at a stress of approximately 4200 psi as compared to the strength of 4550 psi observed for the specimen from Batch 2 (Test 1A in Table 7). It was previously mentioned that Batch 3 has roughly 10 percent less strength than Batches 2 and 4. This strength difference seems to have been preserved in these tests as well.

Table 7.

STRESS RATIO	BATCH 2,4		BATCH 3	
	TEST NUMBER	σ_{1f} (psi)	TEST NUMBER	σ_{1f} (psi)
0:3	1A	4550	1C	4200
1:3	2B	8400	2A	6900
	2C	7500	2D	6700
Average		7950		6800
2:3	3A	6900		
	3B	9000		
	3C	9000		
Average		8300		
3:3	4A	6300		
	4E	7250		
Average		6775		

Another indication that the single failure point obtained for uniaxial loading is reasonable comes from the previous study. Results of that study indicate that the uniaxial strength of concrete as measured in the cubical cell is approximately 90 percent of the strength as measured using 6 in. by 12 in. cylinders in a conventional testing machine. The strength of 4550 psi measured in the cubical cell is nearly 90 percent of the cylinder strength mentioned previously. This evidence suggests that a fair amount of confidence can be placed in this data point.

Similar supportive data from Batch 3 specimens has been provided for the biaxial tests with a stress ratio of 1:3. Table 7 shows that the average strength of the specimens from Batch 3, expressed as the major principal stress at failure, is 15 percent less than the strength of specimens from Batches 2 and 4. This would suggest that the strength of 8400 psi measured in Test 2B is a reasonable upper limit to the actual strength value.

The two equi-biaxial tests (stress ratio of 3:3) performed show similar stress-strain behavior despite the 1000 psi difference in strengths. It must be noted that Test 4A was never completed due to the rupture of one of the fluid cushions. An extrapolation of the volumetric strain curve would indicate a vertical slope within one or two more load steps. Therefore, the maximum principal stress at the point at which the test was stopped is taken to be the failure stress, although it is more likely that the actual failure stress is a few hundred psi greater.

The average of the biaxial test results is shown in Figure 15a as the solid curve above the equi-biaxial line. Because of the large amount of scatter of the few data points available, which are indicated by the open

circles below the equi-biaxial line , this curve should be looked upon more as just a mathematical average than a representation of the average properties of the concrete. For convenience, however, this average curve has been reproduced in Figure 15b along with the results from the previous testing program. The higher ratios of biaxial strengths to uniaxial strength in the present study are due, in part, to the higher concrete strength and different failure criterion mentioned previously.

Because of the limited amount of data, it is impossible to determine what effect the 100 psi reference stresses had on the strength results. Research is presently underway, however, which will duplicate the biaxial tests performed in the previous study using an identical concrete mix. These tests will be performed with the 100 psi reference state, thus allowing a determination of its effects. An addendum to this report will be provided once the research is completed.

RESIDUAL TENSILE STRENGTH STUDY

TEST PROCEDURES

The original goal of this portion of the testing program was to obtain an NX-size core along the intermediate principal stress axis and to subdivide this core into four 1-inch thick disks. When actual coring was begun, however, it was found that insufficient intact material existed at the points of entry and exit of the coring bit to allow use of the entire 4-inch length of the core. As the core was cut into disks using a masonry saw which had a kerf of slightly more than 1/8 inch, further reduction in the amount of usable length of the core occurred. In order that the disks would have as great of a cross-sectional area as possible while still

providing a measure of redundancy in the testing program, it was decided that three disks would be taken from each core rather than four. Each of these disks would have a one-inch thickness as was originally proposed. Two of the disks from each core were tested immediately and the third was held in reserve. Once all of the disks had been tested, those held in reserve were used to fill any gaps in the data resulting from clearly erroneous results (such as a compressive mode of failure in a disk) and to provide another data point in those instances where the response was not well-defined by only two data points.

Another problem came to light during the coring operation involving the quality of the core geometry. Because of the heterogeneity of the concrete, the coring bit would tend to wander, first in one direction and then in another, depending on the direction which offered the least resistance to cutting. If there were a number of pieces of hard aggregate on one side of the bit but only mortar on the opposing side, the bit would move toward the mortar. The result of the bit taking this "path of least resistance" was a core with irregular sides. Any attempt to perform a tensile splitting test on these disks would result in point loads being applied only at the highest points on the circumference.

It has been estimated (7) that the actual loaded area in the tensile splitting test is approximately 3/16 inch wide for this size core. To eliminate the irregularities along the sides of the disks, a 1/4 inch wide flat was ground on each side of the disk as shown in Figure 16a. This was the narrowest flat which would eliminate all of the irregularities. The work was performed on a milling machine to ensure that the flats would be exactly perpendicular to the desired loading axis. With these flats on the disks, the testing procedure recommended by the International Society of

Rock Mechanics (8) could no longer be used. Instead, the tests would be performed per ASTM C-296 which specifies that the load be applied through an inch-wide strip of wood or masonite which extends over the length of the disk. It was anticipated that any anomalies in the stress field resulting from the shape of the loading area would disappear a short distance into the disk, according to St. Venant's principle, leaving a predominantly tensile stress field across most of the remaining diameter.

Preliminary testing of these modified disks indicated, by the mode of failure of the disks, that a compressive stress regime existed in the loaded disks. The mode of failure observed is illustrated in Figure 16b. Because some of the disks had already been provided with flats, any further modifications to provide tensile splitting had to incorporate the flats. It was decided that a line load would be applied at the center of the flats (and thus exactly in the plane of splitting) by means of a length of 1/8-inch square aluminum key stock. Figure 16c illustrates this method of loading and the resulting failure surface in the disks, which indicates that a tensile splitting failure mode had indeed been established.

Because of this unconventional method of testing, the results of this portion of the testing program cannot be compared to tensile splitting tests performed at the University of New Mexico on cast concrete cylinders. It is possible, however, to compare the results of these tests to each other as all disks were ground and loaded identically using the same key stock and the same rate of loading. In addition, tensile splitting tests on disks taken from previously unloaded specimens were provided as a firm basis for comparison of the tensile splitting strength results.

In order to keep track of the orientation of the tensile failure surfaces with respect to the previous load histories of the specimens, a

notation convention has been established which is based on an arbitrary but fixed orientation of the specimen in physical space. The coordinate axes used to describe physical space are shown in Figure 17a along with the Cartesian coordinate system from which is was adapted. This coordinate system adheres to the right-hand rule of Cartesian coordinates with x, y and z replaced by 1, 2 and 3, respectively. Prior to the beginning of a testing program, the specimens are assigned an orientation in physical space. In this program, for example, the vertical axis of the cubes while still in the molds was designated the 1-axis. The long axis of the molds was chosen to define the 3-axis, and the direction perpendicular to the long axis of the molds in the horizontal plane was designated the 2-axis. This is shown in Figure 17c.

The orientation of the measured tensile splitting strength is denoted within this coordinate framework by t_{ij} (i,j = 1,2,3), the residual tensile strength in the j-direction of a specimen originally subjected to a major principal stress in the i-direction. If the principal stresses are applied in directions which adhere to a right-hand rule, describing the axis of the specimen on which the major principal stress acts automatically reveals the axes of the specimen on which the intermediate and minor principal stresses act.

The advantage of this convention lies in its ability to describe the direction in which tensile strength is measured relative to not only the directions in which stresses were applied during a previous load history but also relative to any directions of inherent anisotropy. A difference between t_{13} and t_{31} would be relevant if, for example, the specimens were inherently stronger in the 1-direction.

Because the specimens in this study exhibit negligible anisotropy, and because the specimens were always cored in the direction of the intermediate principal stress, no attempt will be made to distinguish between t_{13} and t_{31} or t_{11} and t_{33}. Instead, for simplicity, the tensile strength in the direction of the previously applied major principal stress will be denoted by t_{ii} and the tensile strength in the direction of the previously applied minor principal stress will be denoted t_{ij}.

RESIDUAL TENSILE STRENGTH STUDY
TENSILE SPLITTING TEST RESULTS

As a control measure, tensile splitting tests were performed on nine disks cut from three specimens which had not been subjected to previous loads. The results of these nine tests, which had an average strength of 433 psi, are given in Table 9. In order to give a qualitative meaning to the tensile splitting test results, all splitting strengths are normalized with respect to this average control strength. These normalized strengths, t_{ii}/t_c and t_{ij}/t_c, can be viewed as measures of the percentage of strength remaining in a specimen after loading. Conversely, the quantity $(1 - t/t_c)$ expresses the relative amount of degradation resulting from the loading. Table 10 lists all of the splitting test results from specimens which had been loaded triaxially. The results are also expressed in this table as the ratio of the tensile splitting strength in the direction of the major principal stress to the splitting strength in the direction of the minor principal stress, t_{ii}/t_{ij}. This strength ratio is, in effect, a measure of the amount of stress-induced anisotropy.

Because the failure states for any one triaxial test type are almost identical, it would be expected that the splitting test results within any

AD-A114 375 NEW MEXICO ENGINEERING RESEARCH INST ALBUQUERQUE F/G 13/13
REINFORCED CONCRETE BEAMS UNDER COMBINED AXIAL AND LATERAL LOAD--ETC(U)
JAN 82 G E LANE F29601-76-C-0015
UNCLASSIFIED NMERI-SSR-71 AFWL-TR-81-99 NL

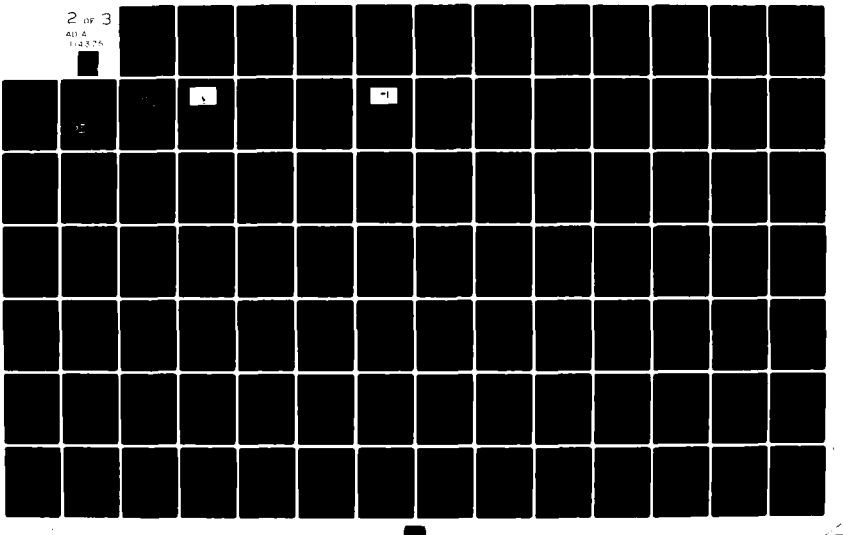

one test type would also be similar. The results in Table 10, however, show considerable scatter. This large amount of scatter can also be seen in the splitting strengths of the control disks. The primary reason for this is the small size of the disks. Because the thickness of the disks is only 2 or 3 times the maximum aggregate size, the percentage of the cross-sectional area occupied by aggregate can vary widely. The amount of aggregate the failure surface must pass through is a controlling factor in the tensile splitting strength of the disk because the tensile strength of the aggregate particles far exceeds the tensile strength of the mortar. Examination of the failure surfaces after the disks had been split showed that in almost every disk the aggregate-mortar bonds were still intact; the failure surface did, indeed, pass through the aggregate.

Because of this variability and the small number of specimens available for testing, any relationships to be established must necessarily be general.

Table 9.

Tensile Splitting Strengths of Control Disks

DISK	STRENGTH	DISK	STRENGTH	DISK	STRENGTH
1a	298	2a	350	3a	529
b	436	b	360	b	468
c	412	c	513	c	534
avg.	382	avg.	408	avg.	510

Mean Strength = 433 psi

Stnd. Dev. = 80 psi (18.5% of the mean)

Table 10.

TEST TYPE	TEST NUMBER	t_{11}/t_c	t_{1j}/t_c	t_{11}/t_{1j}
TC 3750	5A*	0.67	0.62	1.08
	5B	0.64	0.60	1.07
	5C	0.48	0.55	0.87
Average		0.59		1.01
SS 3750	6A	0.82	0.80, 0.96	1.03, 0.85
	6B	0.94	0.79, 0.71	1.33, 1.19
	6C	0.86	0.88, 0.69	1.26, 0.98
Average		0.81		1.11
TE 3750	7A*	0.73	0.90, 0.68	1.08, 0.82
	7B	0.88, 0.86	0.81	1.07, 1.09
	7C*	1.12, 0.89	0.96	0.93, 1.17
	7D*	0.78	0.73	1.07
	7F	1.23, 0.74	0.76	0.98, 1.59
	7G	0.76	0.76	0.99
Average		0.85		1.08
TC 5000	8A*	0.52, 0.61	0.57	1.07, 0.92
	8B	NA	NA	NA
	8E	0.89	0.91	0.97
Average		0.70		0.99
SS 5000	9A	0.82	0.92, 1.09	0.76, 0.90
	9C	0.82	0.74, 0.58	1.43, 1.12
Average		0.83		1.05
TE 5000	10A	NA	0.58	NA
	10B*	NA	NA	NA
	10C	1.17, 1.02	0.81	1.25, 1.44
Average		0.90		1.35

* Specimens from Batch 3

Examining the average values of t/t_c listed in Table 10 without differentiating between t_{ii} and t_{ij}, it appears that for a given test type, the residual tensile strength increases (and conversely, the amount of degradation decreases) as the hydrostatic stress level reached prior to deviating in the octahedral plane increases. One possible explanation for this is that the octahedral shear stress at failure, when normalized with respect to the octahedral normal stress, is lower for tests in the 5000 psi octahedral plane than in the 3750 psi octahedral plane. Table 11 lists the average splitting strength results for each triaxial test performed along with the ratio of τ_{oct} to σ_{oct} at failure. By plotting the average residual tensile strength t/t_c as a function of the ratio τ_{oct}/σ_{oct}, as shown in Figure 18, a fairly good correlation is established which shows a regular decrease in the residual tensile strength (and conversely an increase in the amount of degradation) with increasing relative shear stress. The open circles in this figure represent test results from Batch 2 and 4 specimens and the solid circles indicate the results from tests performed on Batch 3 specimens. The linear relation indicated in the figure, which was found by a linear regression analysis of the data points pertaining to Batches 2 and 4, is meant only to show that a decreasing trend exists. The actual functional relation would most likely not be linear because the residual tensile strength cannot exceed 1.0 ($t = t_c$). Scematically the relation might be as shown in Figure 19 with the function asymptotically approaching $t/t_c = 1.0$. Further triaxial testing in higher octahedral planes would be needed to determine the actual relation.

Table 11.

TEST TYPE	TEST NUMBER	$\frac{\tau_{oct}}{\sigma_{oct}}$	t/t_c	t_{11}/t_c	t_{ij}/t_c	t_{11}/t_{ij}
TC 3750	5A*	0.98	0.65	0.67	0.62	1.08
	5B	1.06	0.62	0.64	0.60	1.07
	5C	1.04	0.52	0.48	0.55	0.87
SS 3750	6A	0.75	0.86	0.82	0.88	0.94
	6B	0.79	0.81	0.94	0.75	1.26
	6C	0.78	0.81	0.86	0.79	1.12
TE 3750	7A*	0.64	0.77	0.73	0.79	0.95
	7B	0.64	0.85	0.87	0.81	1.08
	7C*	0.58	0.99	1.01	0.96	1.05
	7D*	0.53	0.76	0.78	0.73	1.07
	7F	0.68	0.91	0.99	0.76	1.29
	7G	0.68	0.76	0.76	0.76	0.99
TC 5000	8A*	0.88	0.57	0.57	0.57	1.00
	8B	0.98	NA	NA	NA	NA
	8E	0.98	0.90	0.89	0.91	0.97
SS 5000	9A	0.73	0.94	0.82	1.01	0.83
	9C	0.75	0.71	0.82	0.66	1.28
TE 5000	10A	0.61	NA	NA	0.58	NA
	10B*	0.64	NA	NA	NA	NA
	10C	0.66	1.00	1.10	0.81	1.35

* Specimens from Batch 3.

It is interesting to note that the data points corresponding to Batch 3 specimens generally fall below those of Batch 2 and 4 specimens. The splitting strengths of the Batch 3 disks were normalized with respect to the average splitting strengths of the control disks, all of which were cored from Batch 2 and 4 specimens. Therefore, this data would also suggest that Batch 3 had less strength than Batches 2 and 4.

Figures 20a and 20b show the individual relations t_{ii} vs. τ_{oct}/σ_{oct} and t_{ij} vs. τ_{oct}/σ_{oct}. The slightly different slopes of the trend lines suggest that the residual tensile strength in one direction is affected more than in the other, which is equivalent to saying that stress-induced anisotropy does exist and may vary with the relative amount of shearing produced by the previous load history. The amount of stress-induced anisotropy (expressed as the ratio t_{ii}/t_{ij}) is plotted against τ_{oct}/σ_{oct} in Figure 21. The low value of the correlation coefficient suggests that either no correlation exists between stress-induced anisotropy and previous shear stress history or that there is insufficient data available to clearly establish a trend. If the indicated trend does have some significance, however slight, it appears, quite surprisingly, that the amount of stress-induced anisotropy actually decreases as the amount of previous shearing increases. This phenomenon can be better explained by examining the variation in the tensile strength ratio between the different test types.

Figure 22 shows the individual test results and averages of t_{ii}/t_{ij} for the different test types. There is a regular progression in the amount of anisotropy from the triaxial compression test through the simple shear to the triaxial extension test. It is possible to explain these changes from one test type to another in terms of the mechanics involved in each

test. In the triaxial compression test, one of the specimen axes is loaded and the other two are relieved once the octahedral plane is reached. Thus, energy is being applied in one direction and dissipated in two directions as the specimen expands against the decreasing forces. Equate this with the specimen having two "degrees of freedom". In the triaxial extension test, two axes are loaded and only one is relieved. Let this represent one "degree of freedom". It would be suspected that a greater amount of expansion would have to occur on the one unloaded axis of a triaxial extension test than would be necessary on each of the two unloaded axes of a triaxial compression test. This is, of course, obvious from the rates of expansion shown by the stress-strain curves of the different tests. As the specimen expands, cracks propagate within planes which are perpendicular to the direction of expansion. The greater the amount of expansion, the more the cracks propagate, and the more these cracks propagate, the less intact material remains to support a tensile stress. Thus, the greater amount of crack propagation associated with lower "degrees of freedom" can be equated with lower tensile strengths in the direction of the unloaded axes. The result of this would be that the amount of anisotropy exhibited by specimens subjected to triaxial extension loading would exceed that exhibited by specimens subjected to triaxial compression histories. Because the simple shear test includes one axis which is neither loaded nor unloaded, the amount of anisotropy should be halfway between those of the other two tests. These are exactly the results shown in Figure 22. Thus it would appear that the energy distribution (force x displacement) rather than just the force distribution may be what produces stress-induced anisotropy.

The tensile splitting test results from specimens tested biaxially are given in Table 12. With such a small number of data points, the results could not be analyzed using regression analysis. Instead, bar charts are shown in Figures 23 and 24 which indicate the average results of each test type. For the 1:3 stress ratio tests, the Batch 3 results are included and indicated by an asterisk. Their average is shown by the dashed horizontal line while the solid horizontal line shows the average from Batch 2 and 4 specimens.

In Figure 23 there is no apparent trend relating residual strength to stress ratio. It does appear, however, that the residual strength of the biaxially-loaded specimens is consistently above 90 percent of the control disk strengths, a level achieved by only three of the triaxially-loaded specimens. This greater residual strength may relate to the lower stress levels achieved in biaxial testing.

Figure 24 also shows no apparent trends. It is interesting to note, however, that the tensile strength ratio of the one uniaxial test indicates that more damage was done in the direction of the major principal stress than was done in the minor principal stress direction. This test has the highest degree of freedom, as defined before, of the biaxial tests and, in fact, the uniaxial test represents exactly two degrees of freedom, as did the triaxial compression test. The tensile strength ratio of the TC test also indicated that slightly more damage had been done in the major principal stress direction. The remaining biaxial stress ratios show tensile strength ratios above unity (if the one very low value is discarded) but there is no regular increase in the tensile strength ratio from test to test.

Table 12

TEST NUMBER	STRESS RATIO	t_{11}/t_c	t_{1j}/t_c	t_{11}/t_{1j}
1A	0:3	0.90, 0.79	1.06	0.85, 0.75
2A*	1:3	0.79	0.87	0.91
2B		1.03	0.88, 1.09	1.17, 0.94
2C		1.23, 0.76	0.82	1.50, 0.93
2D*		0.95	1.17, 0.77	0.81, 1.23
3A	2:3	1.26	1.23	1.02
3B		0.65	0.64	1.02
3C		0.68	1.32	0.52
4E		1.35	1.27	1.06

* Specimens from Batch 3.

CONCLUSION

It is felt that sufficient reproducibility of triaxial stress-strain-strength behavior has been achieved to allow material characterization based on the results of these tests. Unfortunately the biaxial test series did not include enough successful tests that as high of a level of confidence can be had in its results. Comparisons between the results of this test program and those of the previous program may be made, however the differences in concrete strengths and the slightly different failure criterion must be kept in mind.

The results of the tensile splitting test series have shown that load histories do affect the residual tensile strength of a specimen and the amount of stress-induced anisotropy, indicating future research along these lines is warranted. Specifically, research utilizing a greater number of specimens is needed to more completely investigate the trends suggested here. The effects of the "degrees of freedom" of a test on the relative amount of stress-induced anisotropy can be better studied using more triaxial stress paths to fill in the gaps between those paths used in this program. Further biaxial testing with more stress ratios would also be helpful since the concept of energy distribution based on "degrees of freedom" also extends to biaxial tests. Similarly, additional triaxial testing at higher octahedral stress values would more clearly establish the relationship between the amount of octahedral shear stress relative to the level of octahedral normal stress and the amount of residual tensile strength. Triaxial testing at lower octahedral normal stress levels would

also aid in this investigation, however failure states cannot yet be achieved in lower octahedral planes because the failure envelope extends beyond the compression-compression-compression octant of stress space. A multiaxial testing cell with tension capabilities is being developed at the present time which could aid in such a study.

REFERENCES

1. Gerstle, K. H., et al., "Strength of Concrete under Multiaxial Stress States", Proc. Douglas McHenry Symposium, ACI, Pub. SP55, 1978, p. 103.

2. Gerstle, K. H., et al., "Behavior of Concrete under Multiaxial Stress States", Journal Engg. Mech. Div., ASCE, Vol. 106, No. EM6, December 1980, p. 1383.

3. Starovisky, P. "Response of Concrete to Multiaxial Compression", M.S. Thesis, University of Colorado, Boulder, Colorado, 1976.

4. Egging, D. "Constitutive Relations of Fiber-Reinforced Concrete under True Triaxial Loading", M.S. Thesis, University of Colorado, Boulder, Colorado, 1981.

5. Bieniawski, Z.T., "Mechanics of Brittle Fracture of Rock", Int. Jour. Rock Mech., Vol. 4, 1967, p. 395.

6. Newman, K., "Criteria for the Behavior of Plain Concrete under Complex States of Stress", Proc. Int. Conf. on Structure of Concrete, Cement and Concrete Association, London, 1968, p. 255.

7. Fairhurst, C., "On the validity of the 'Brazilian' Test for Brittle Materials", Int. Jour. Rock Mech., Vol. 1, 1964, p. 535.

8. Int. Soc. Rock Mech. "Suggested Method for Determining the Tensile Strength of Rock Materials", Int. Jour. Rock Mech., Vol. 15, 1978, p. 99.

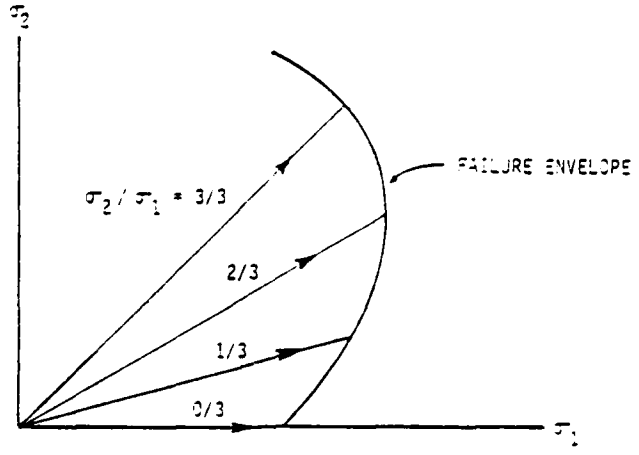

Figure 1. Biaxial Stress Paths

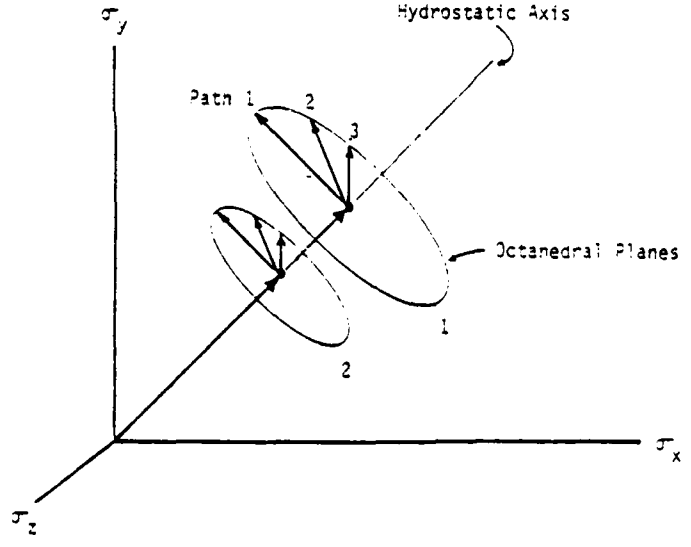

Figure 2. Triaxial Stress Paths in two octahedral planes.

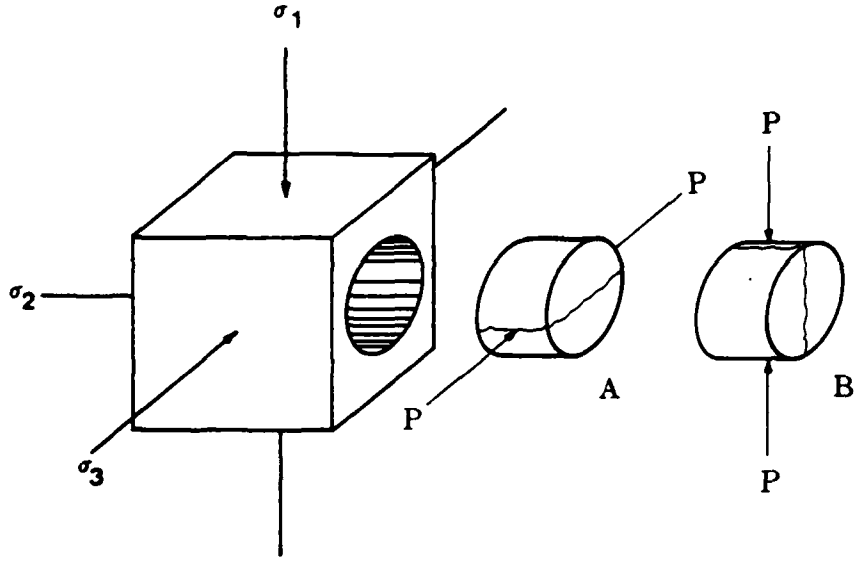

Figure 3. Orientation of tensile splitting test disks cored from cubical cell specimens.
Disk A - Tensile splitting in the direction of previously applied major principal stress.
Disk B - Tensile splitting in the direction of previously applied minor principal stress.

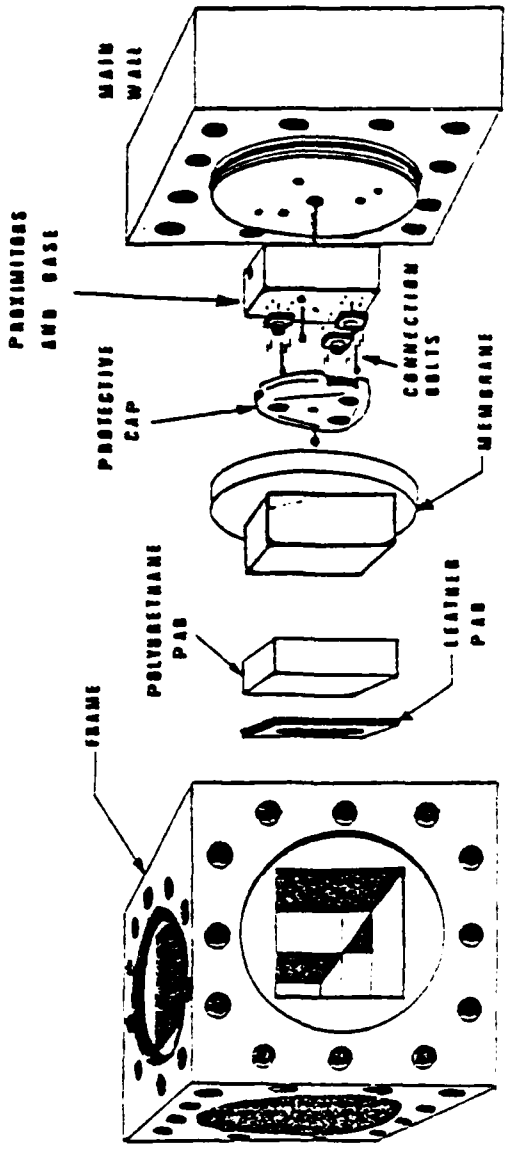

Figure 4. Exploded view of the cubical cell frame and one wall.

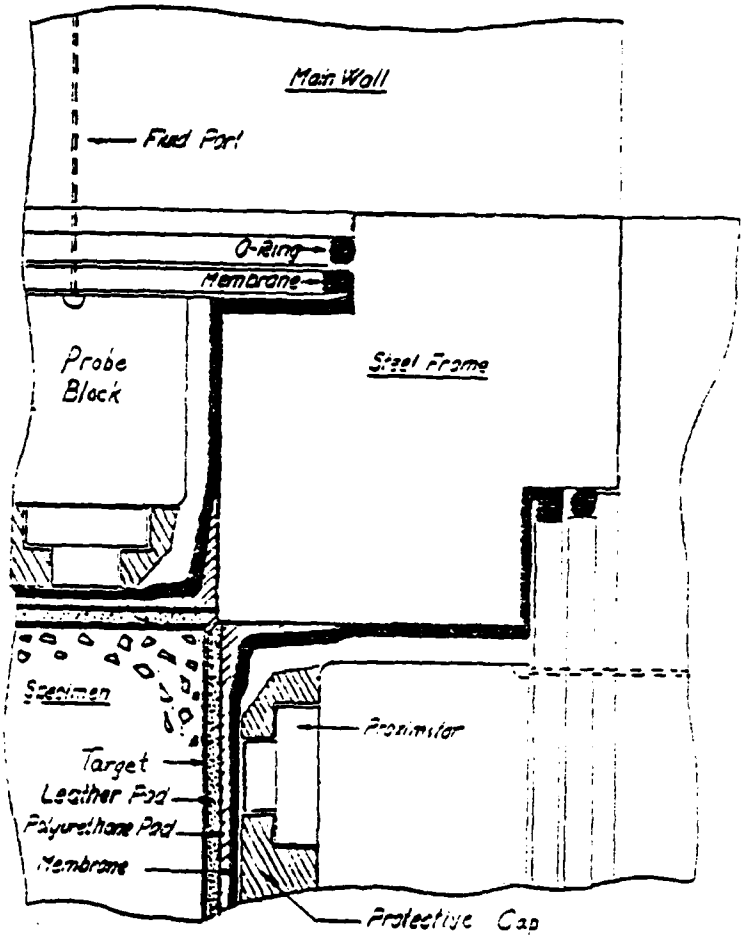

Figure 5. Section through one corner of the assembled cubical cell.

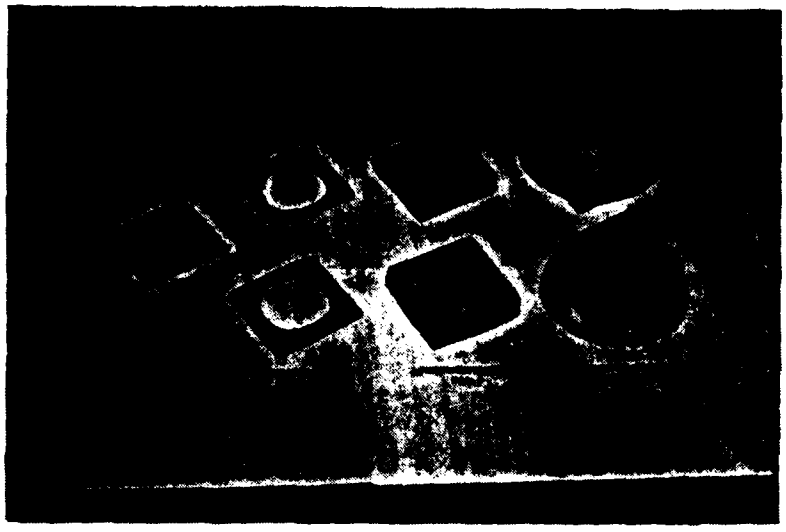

Figure 6. Photograph of (in order of insertion into pressure vessel) brass probe target (far left), protective leather pad, protective polyurethane pad, and fluid cushion membrane. (Bottom half of photo shows components as viewed from within the cubical cell, upper half shows components as viewed from the inside face of the walls)

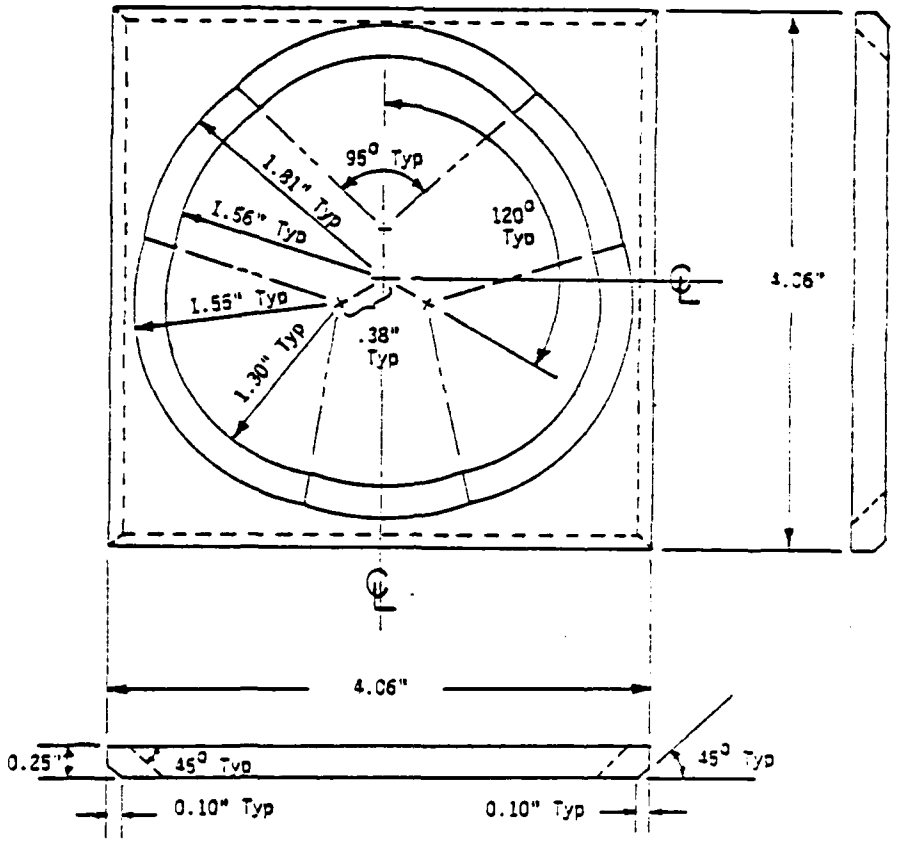

Figure 7. Specifications for the leather pads showing beveled center hole and beveled edges.

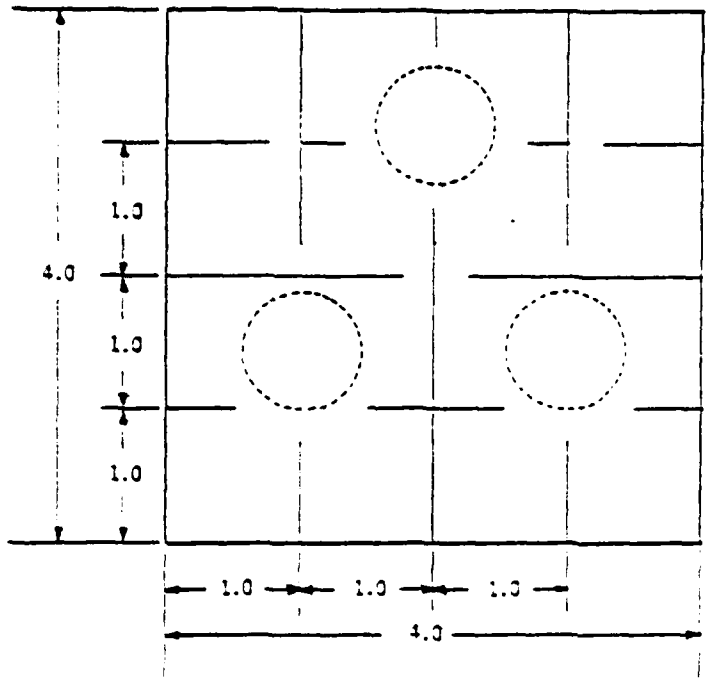

Figure 8. Pattern of slits cut in probe targets to allow flexibility. (Dashed circles show the areas at which the proximitor probes aim.)

Figure 9. Cubical cell concrete specimen ready for testing.
(Note circular patches on each face)

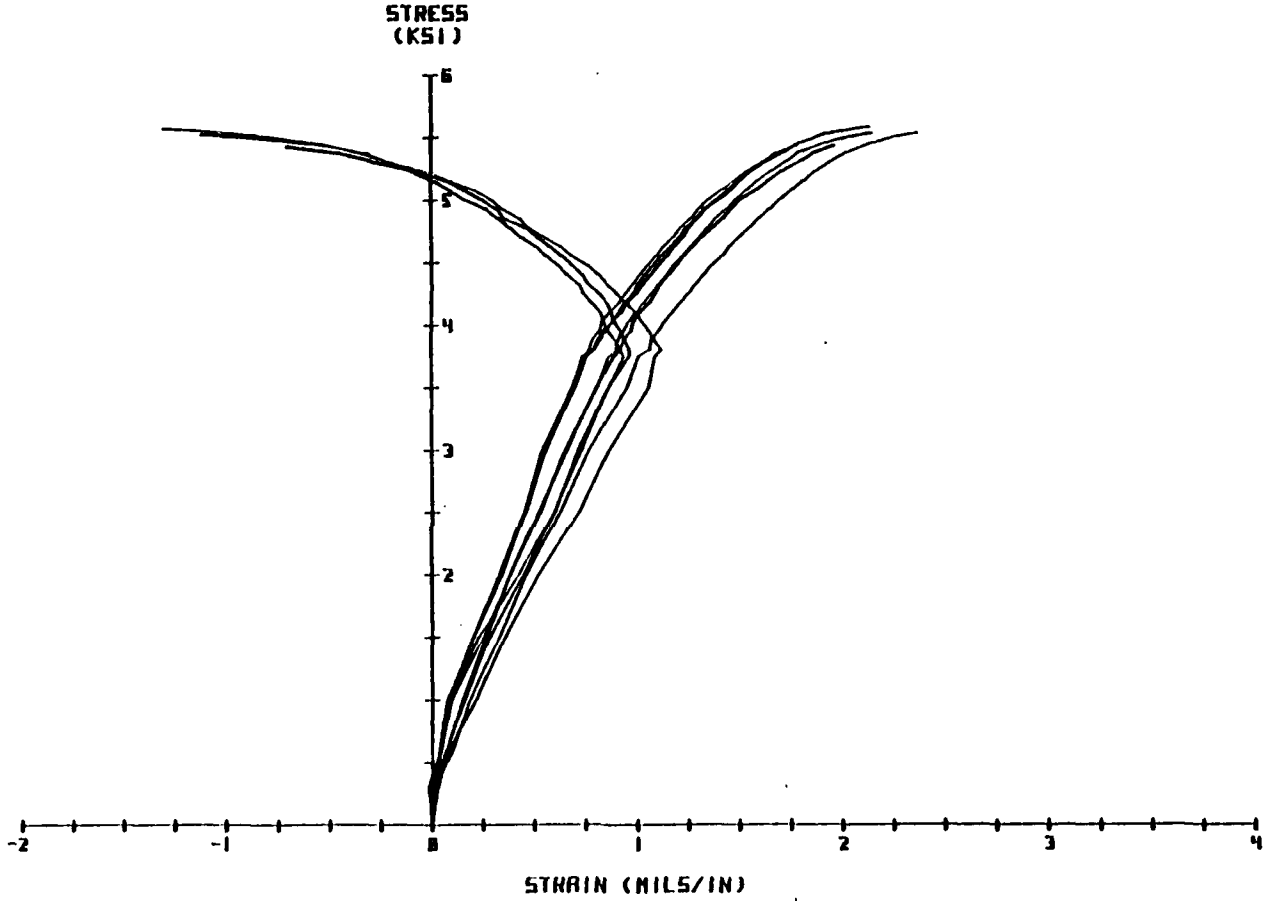

Figure 10. Stress-strain curves from all three triaxial extension tests on specimens from Batch 3.

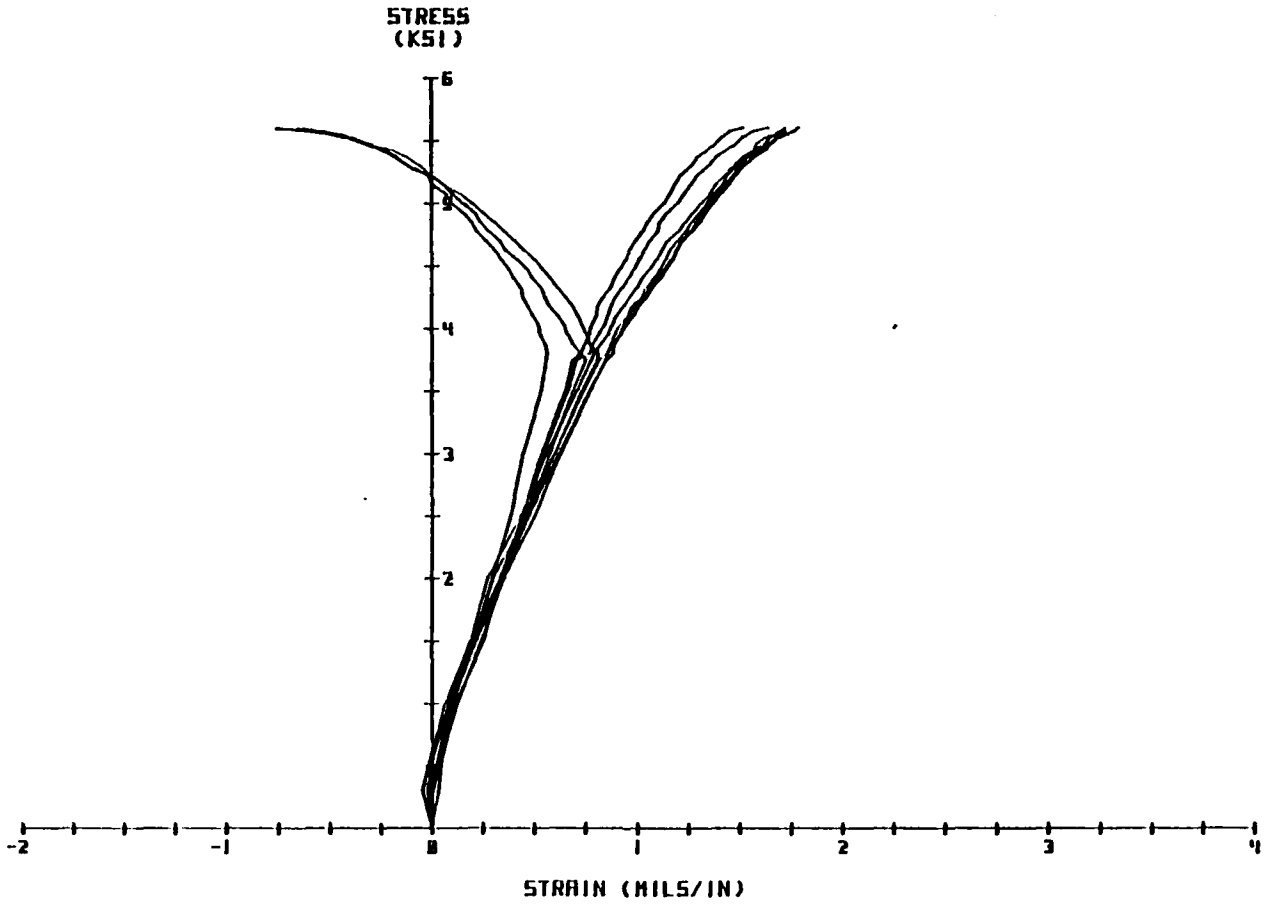

Figure 11. Stress-strain curves from all three triaxial extension tests on specimens from Batches 2 and 4.

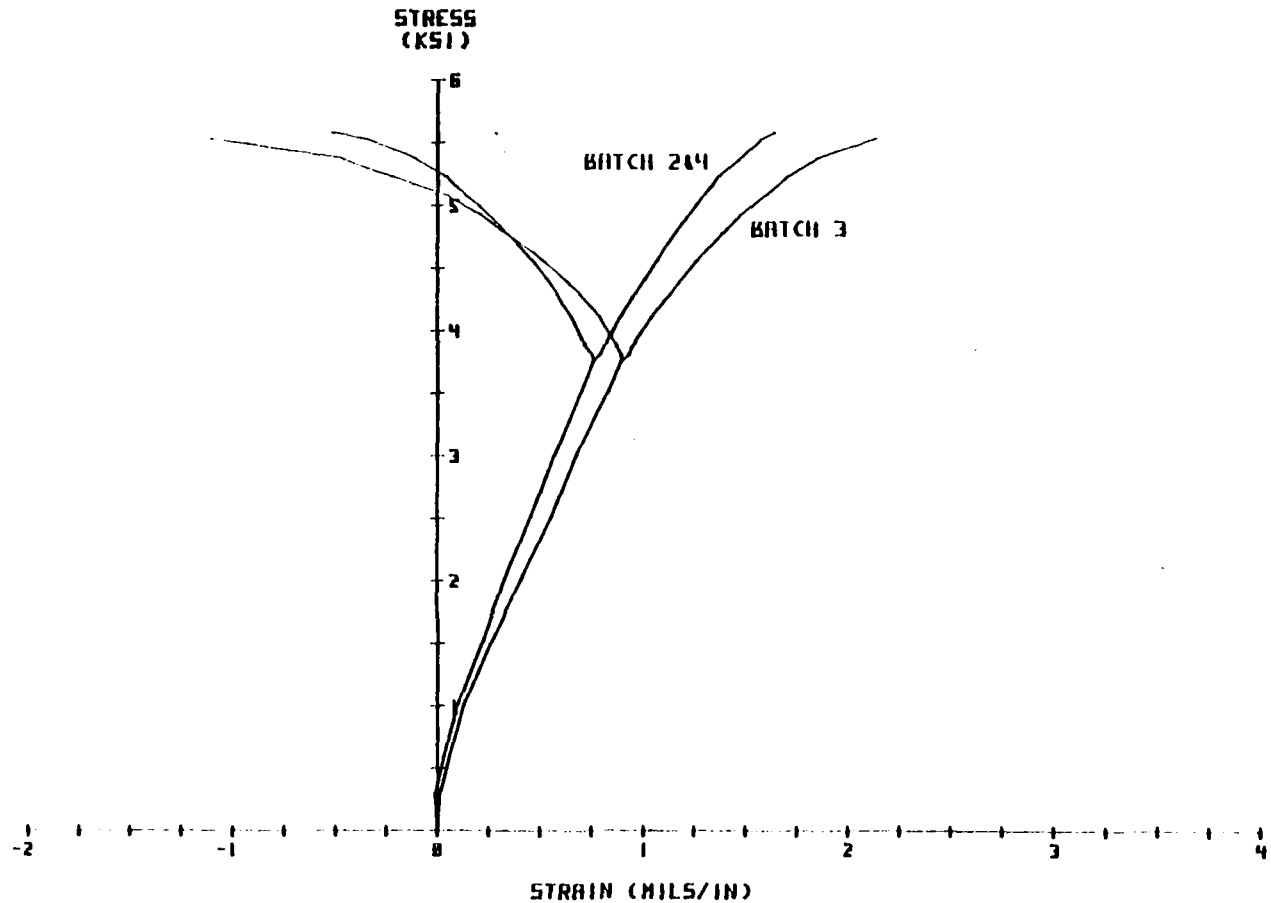

Figure 12. Average behavior in triaxial extension of specimens from Batch 3 and specimens from Batches 2 and 4.

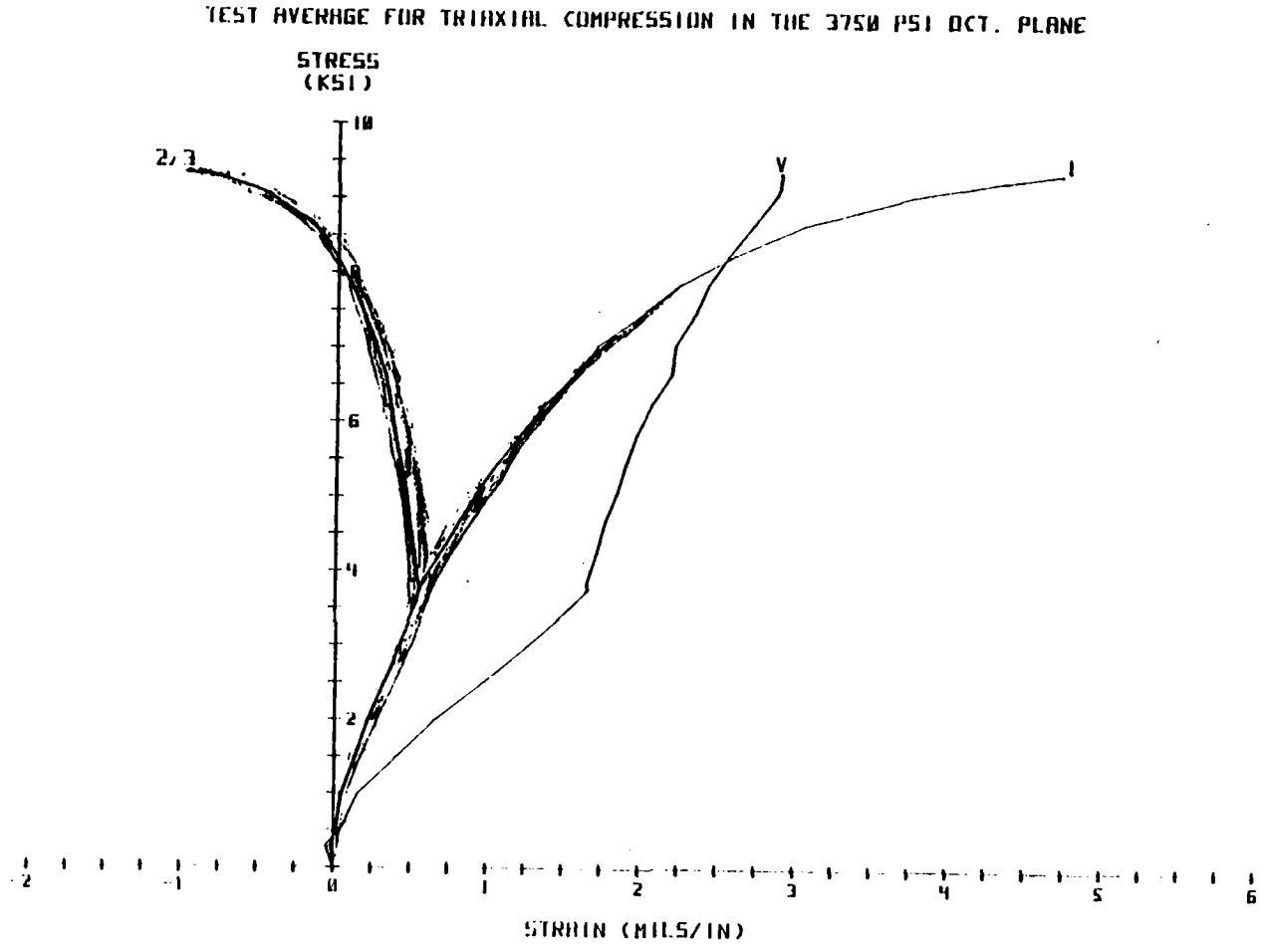

Figure 13a. IC 3750

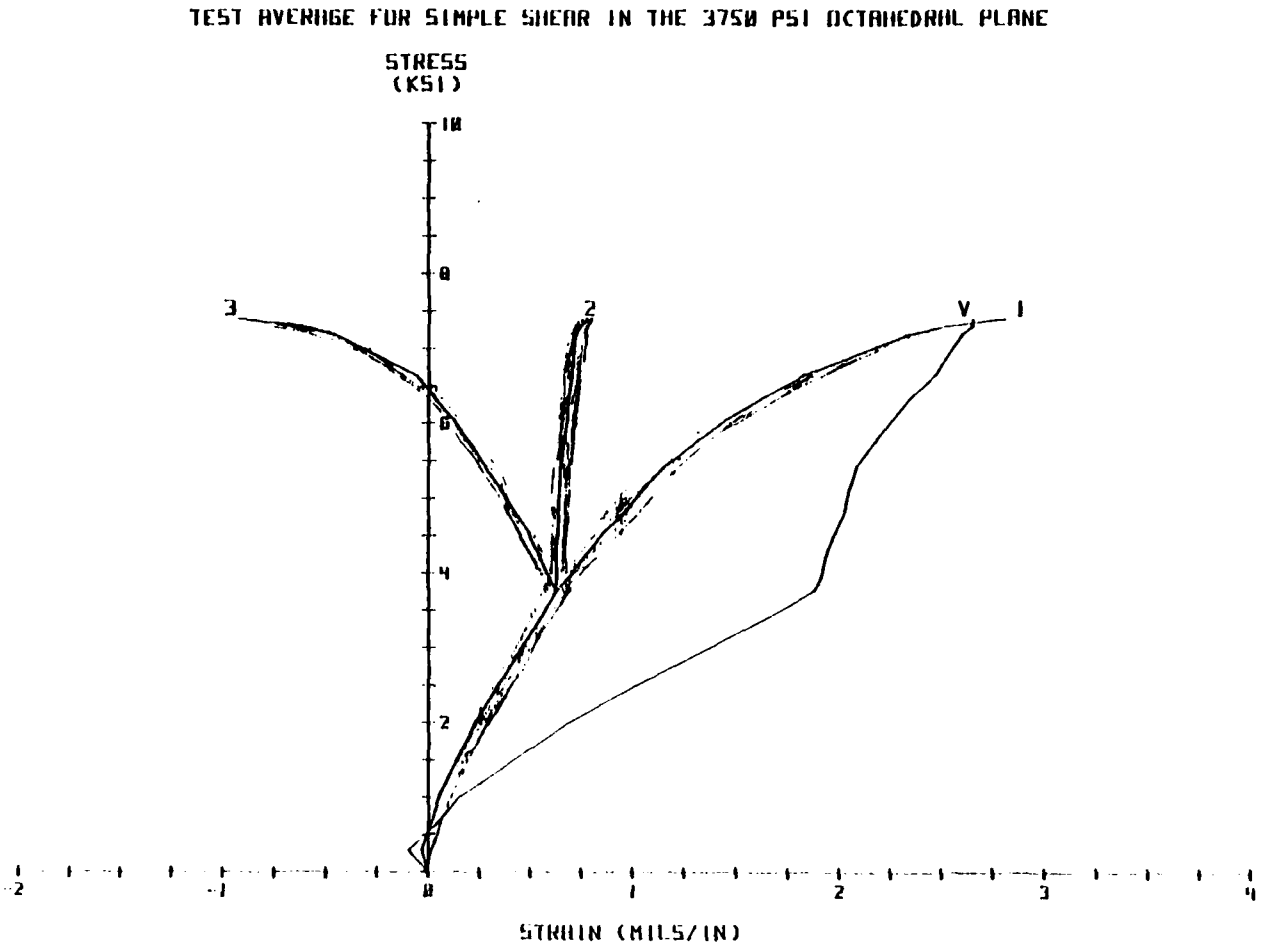

Figure 13b. SS 3750

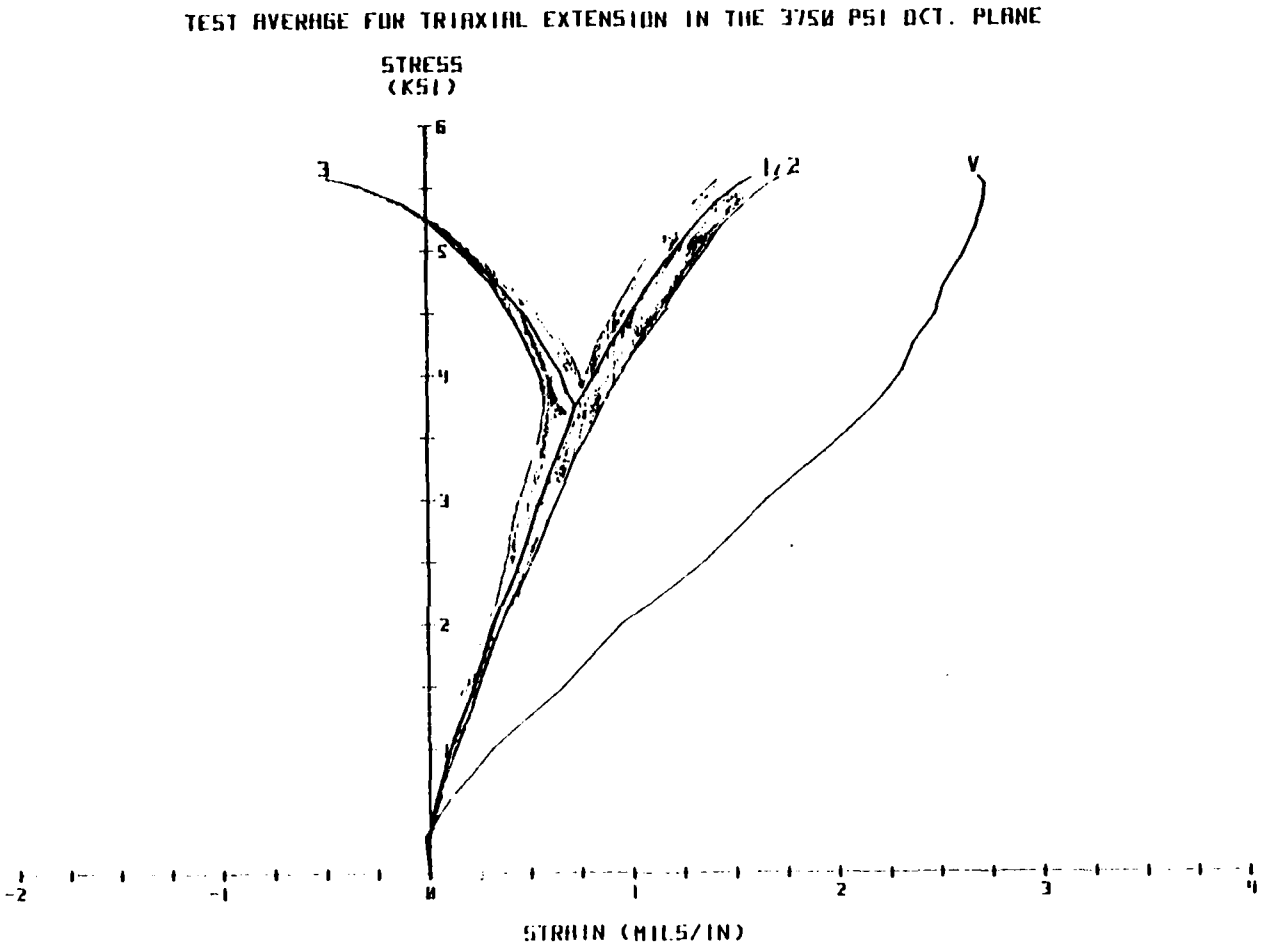

Figure 13c. TE 3750

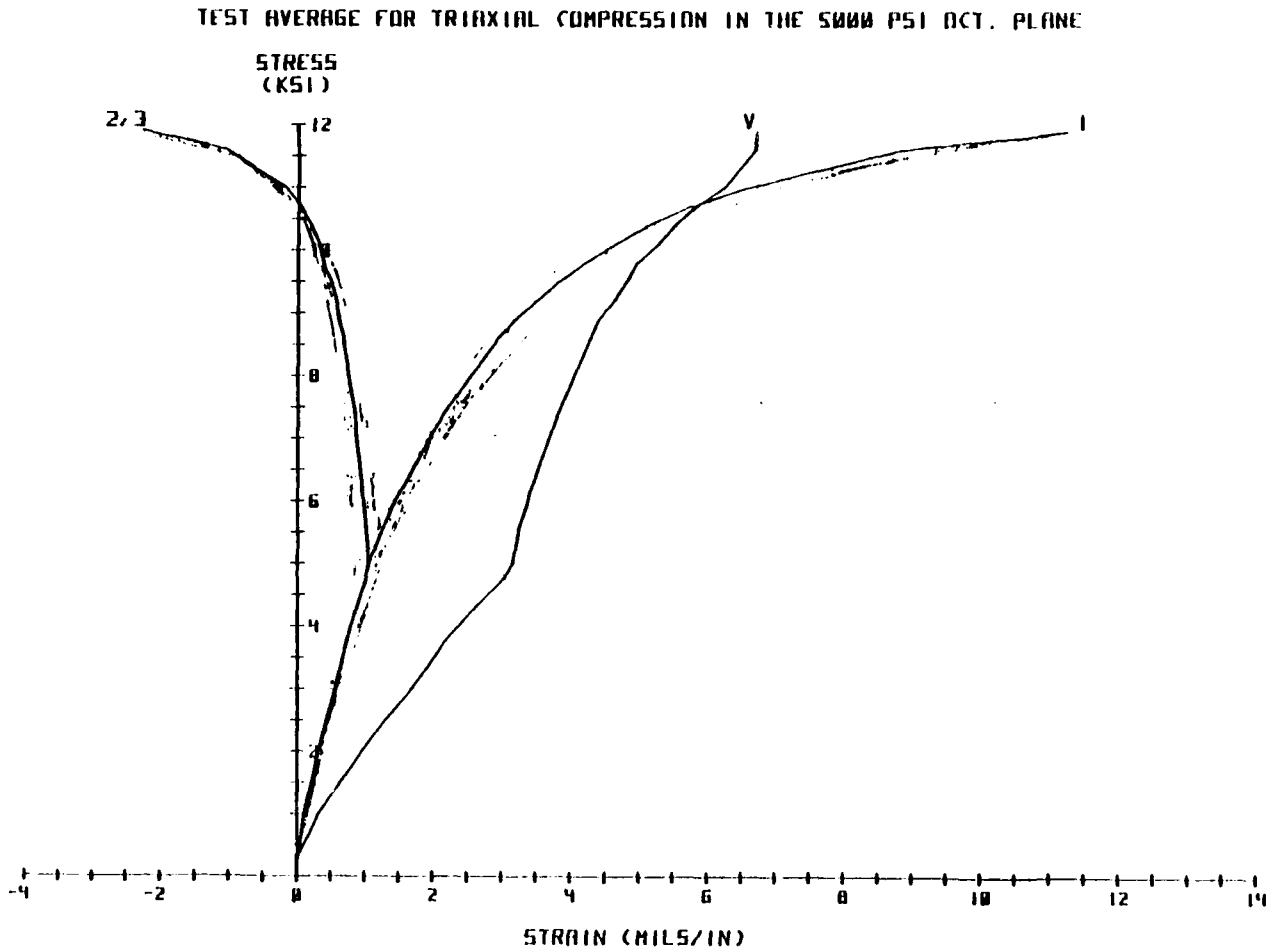

Figure 13d. IC 5000

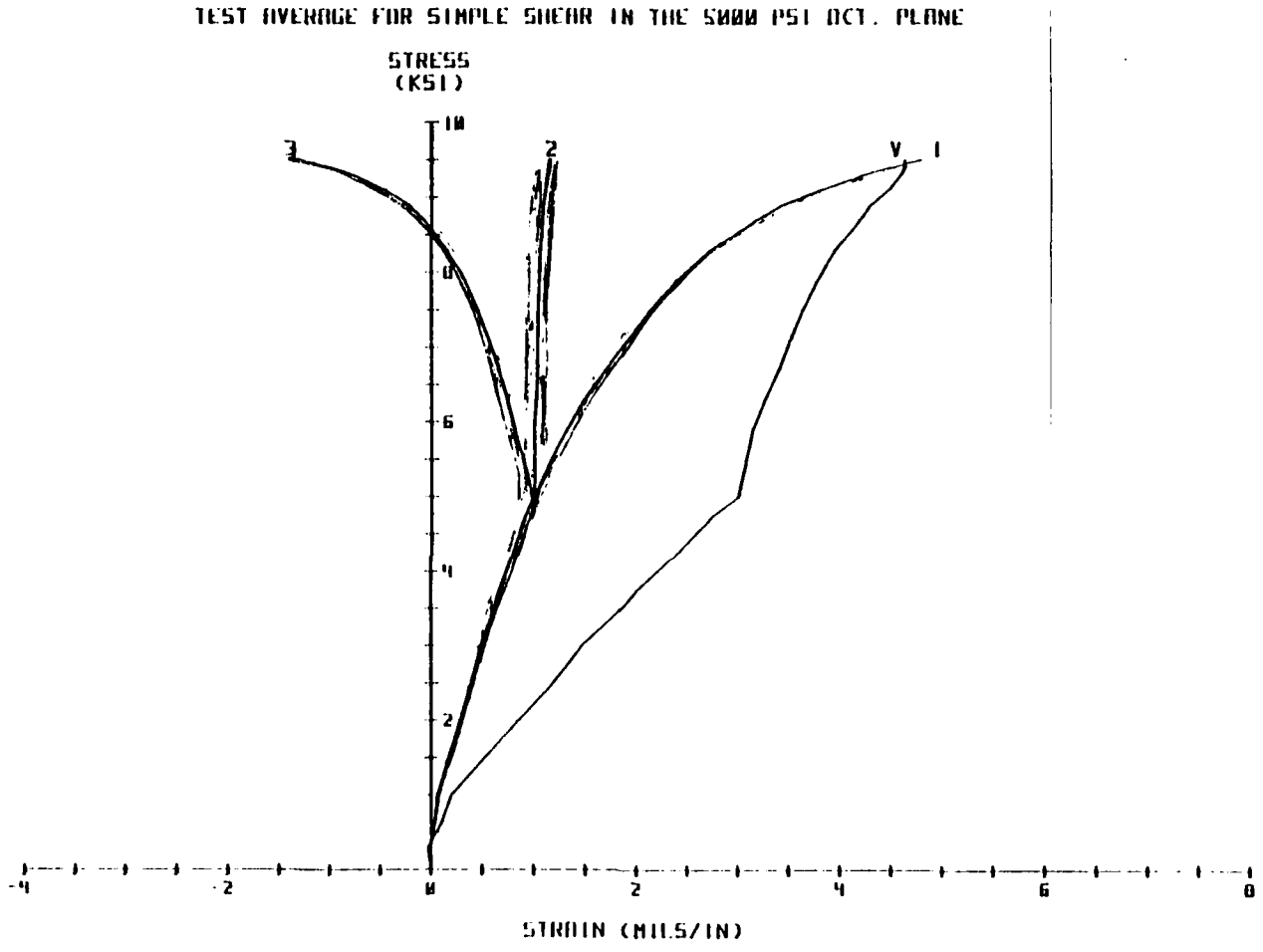

Figure 13e. SS 5000

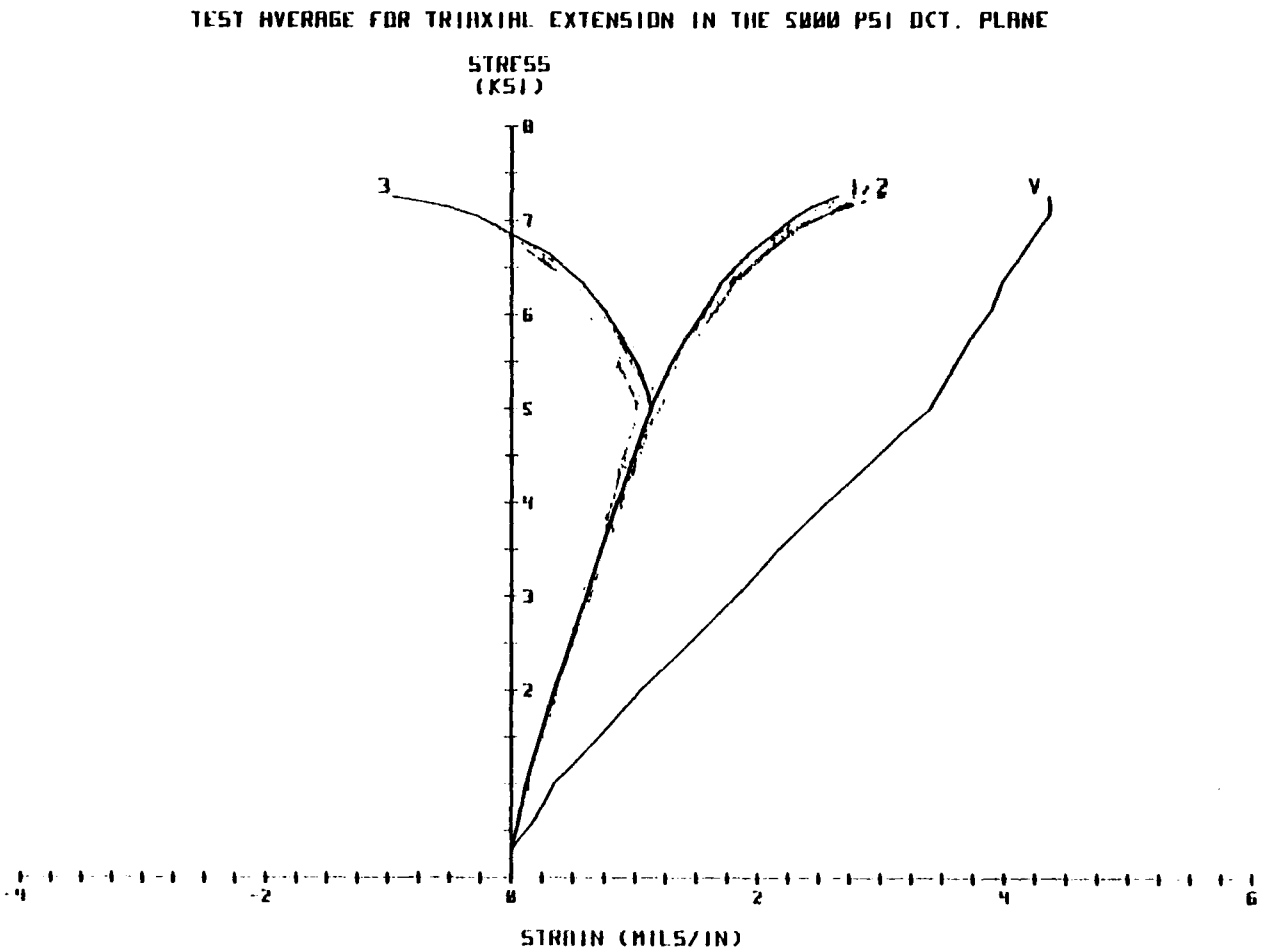

Figure 13f. TE 5000

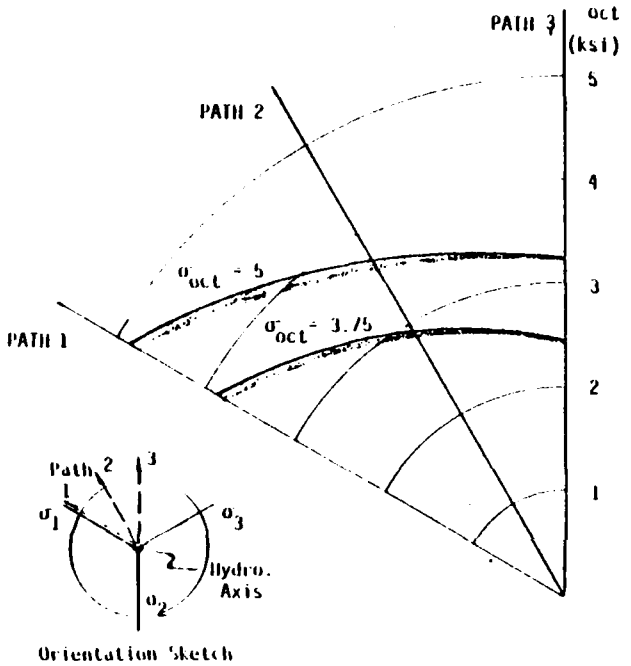

Orientation Sketch

Figure 14a. Failure envelopes in the σ_{oct} = 5 ksi and σ_{oct} = 3.75 ksi octahedral planes.

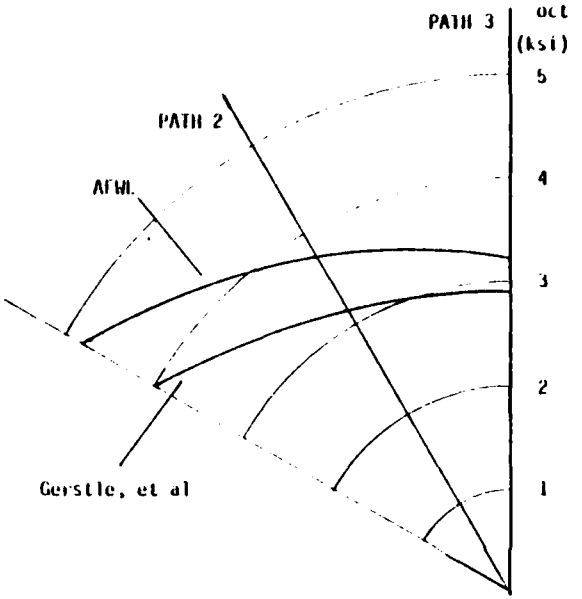

Figure 14b. Failure envelopes from this study and fluid cushion testing by Gerstle, et al. in the σ_{oct} = 5 ksi octahedral plane.

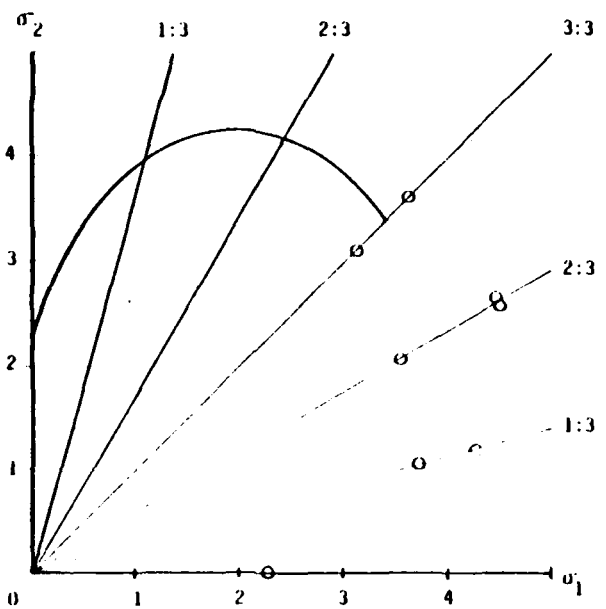

Figure 15a. Biaxial compressive strength results

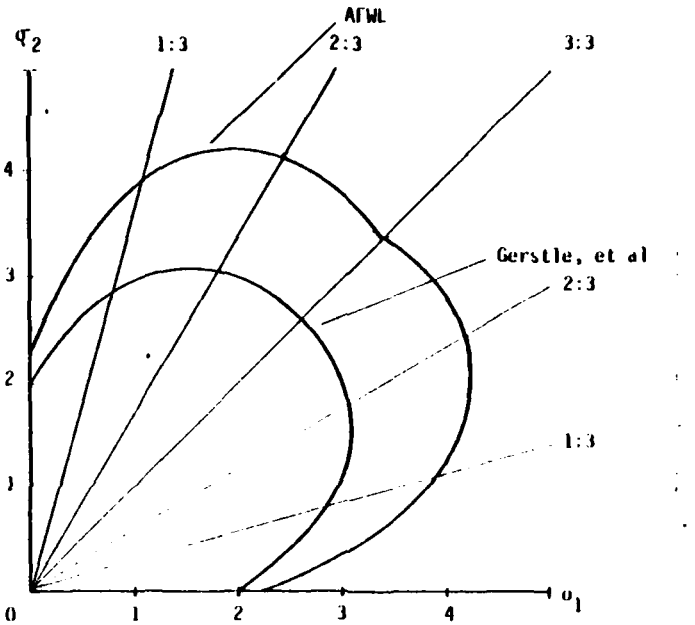

Figure 15b. Biaxial strength results from this study and fluid cushion testing by Gerstle, et al.

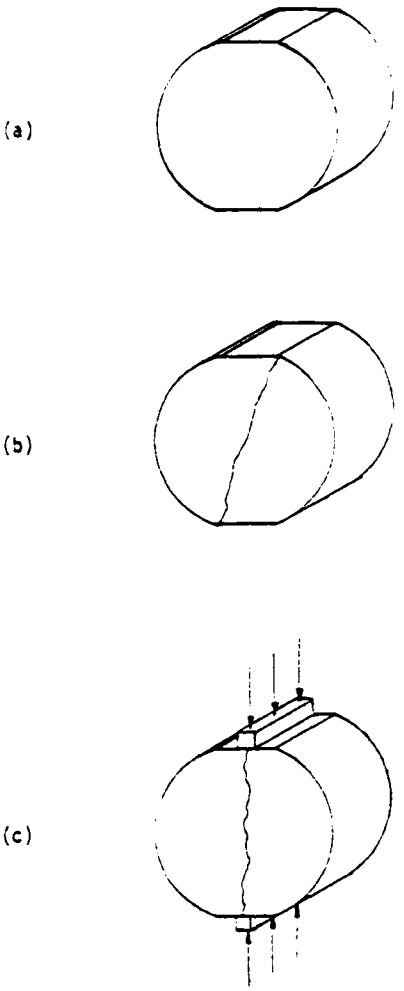

Figure 16. (a) Modification of tensile splitting test disk specimen; (b) Compressive failure mode of modified disk: (c) Use of steel bars to ensure a line load in the plane of splitting.

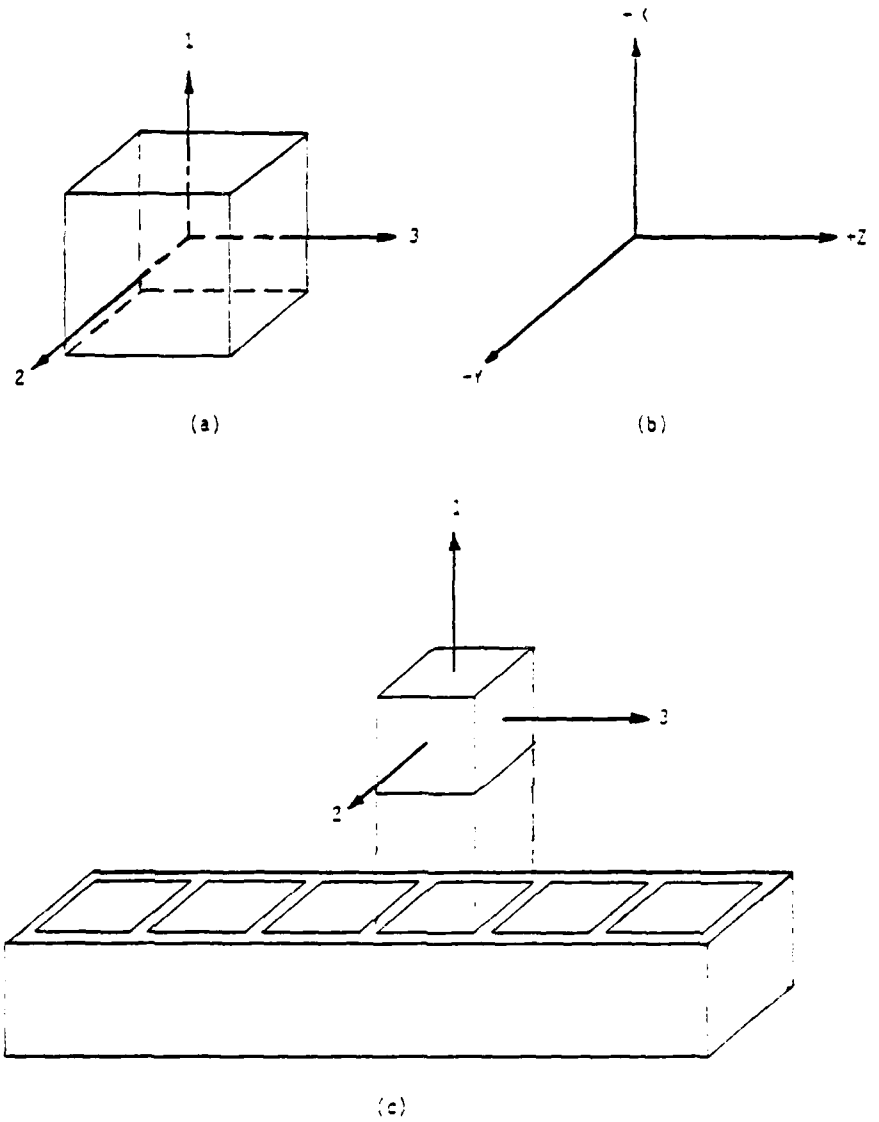

Figure 17. (a) The 1,2 and 3 coordinate axes used to describe physical space and (b) the x,y and z axes of Cartesian coordinates; (c) specimen axes chosen to relate to the axes of the concrete molds.

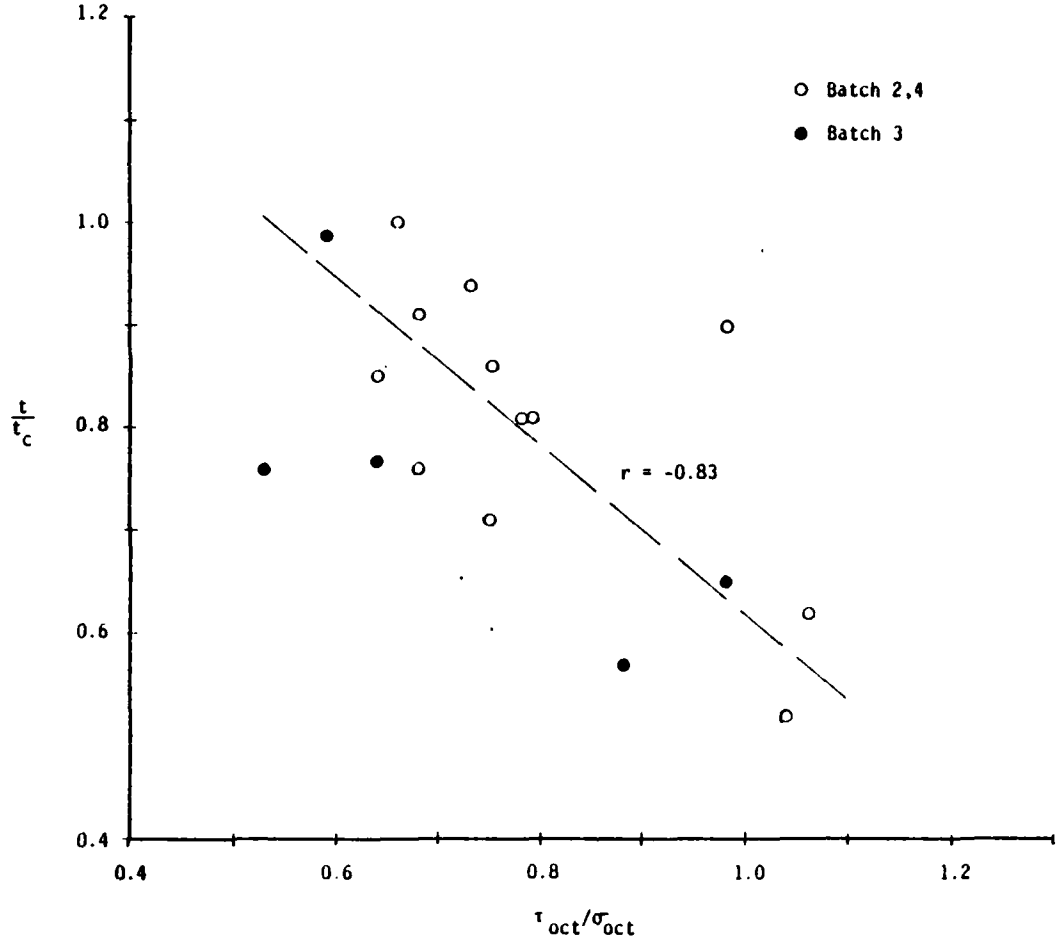

Figure 18. Residual tensile strength as a function of the normalized shear stress at failure.

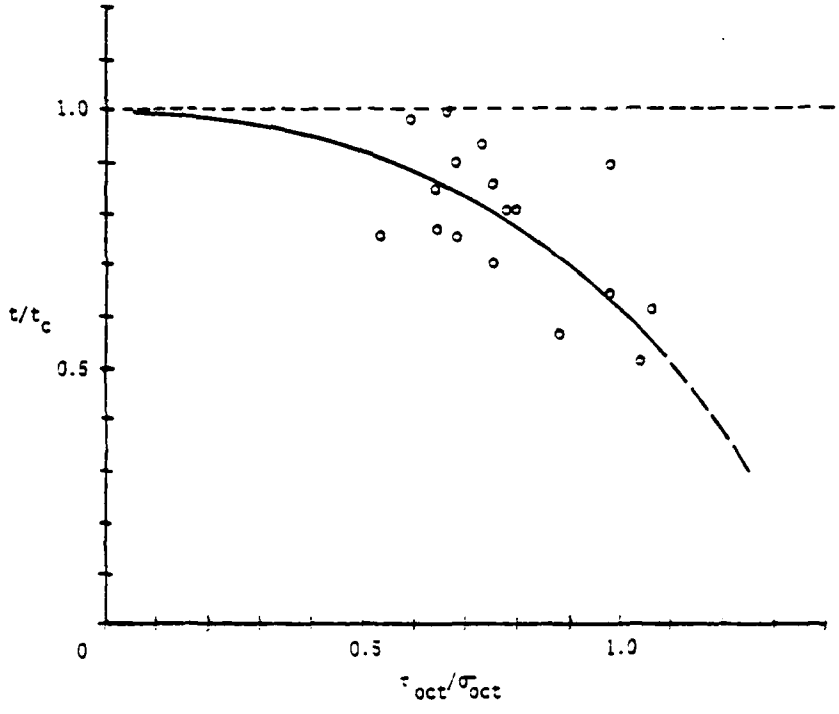

Figure 19. A possible relationship between residual tensile strength and the normalized octahedral shear stress at failure.

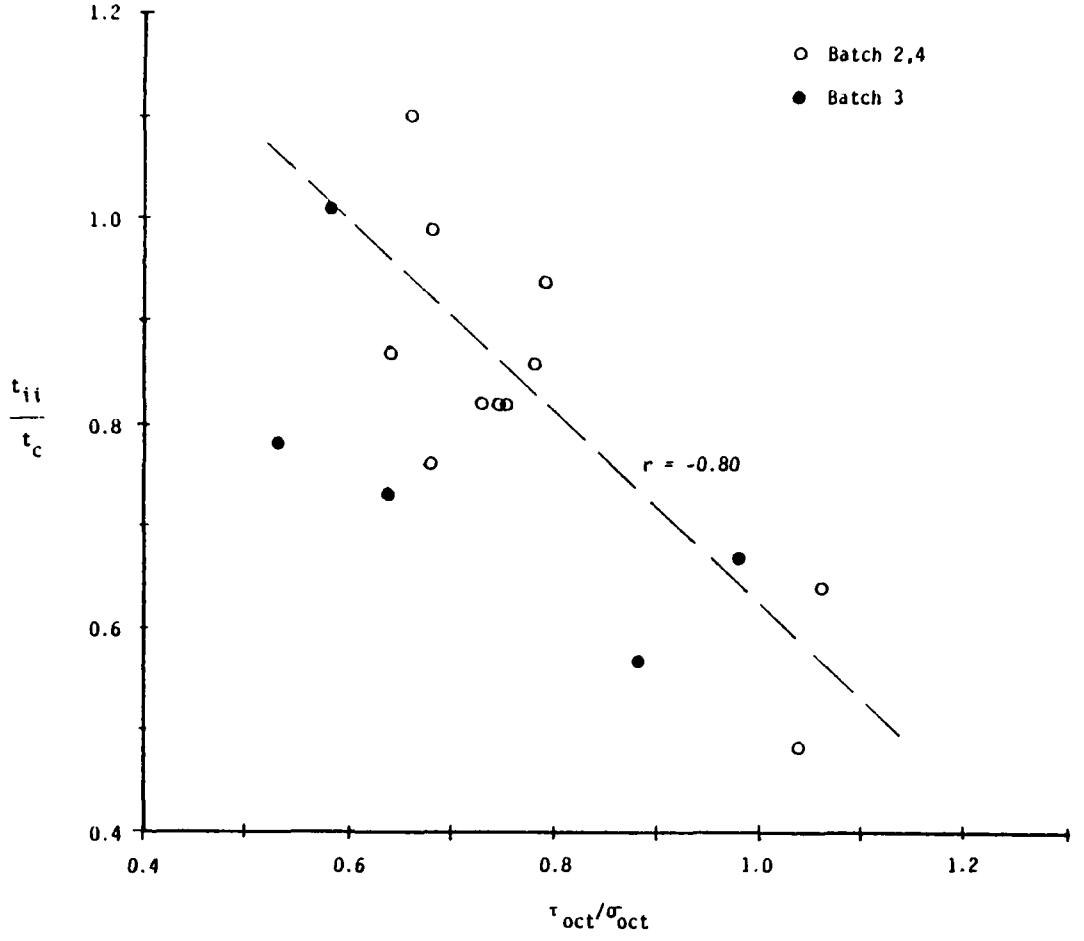

Figure 20a. Residual tensile strength in the direction of the previously applied major principal stress as a function of the normalized octahedral shear stress at failure.

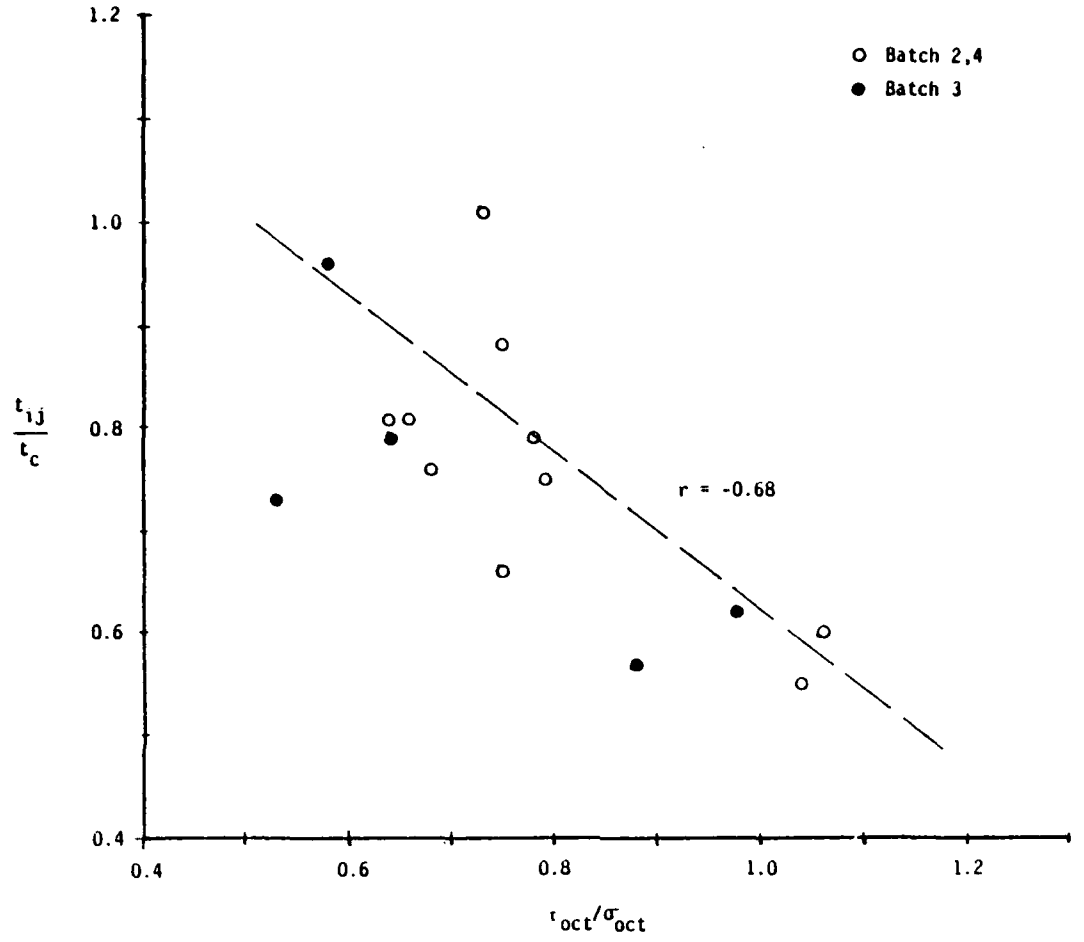

Figure 20b. Residual tensile strength in the direction of the previously applied minor principal stress as a function of the normalized octahedral shear stress at failure.

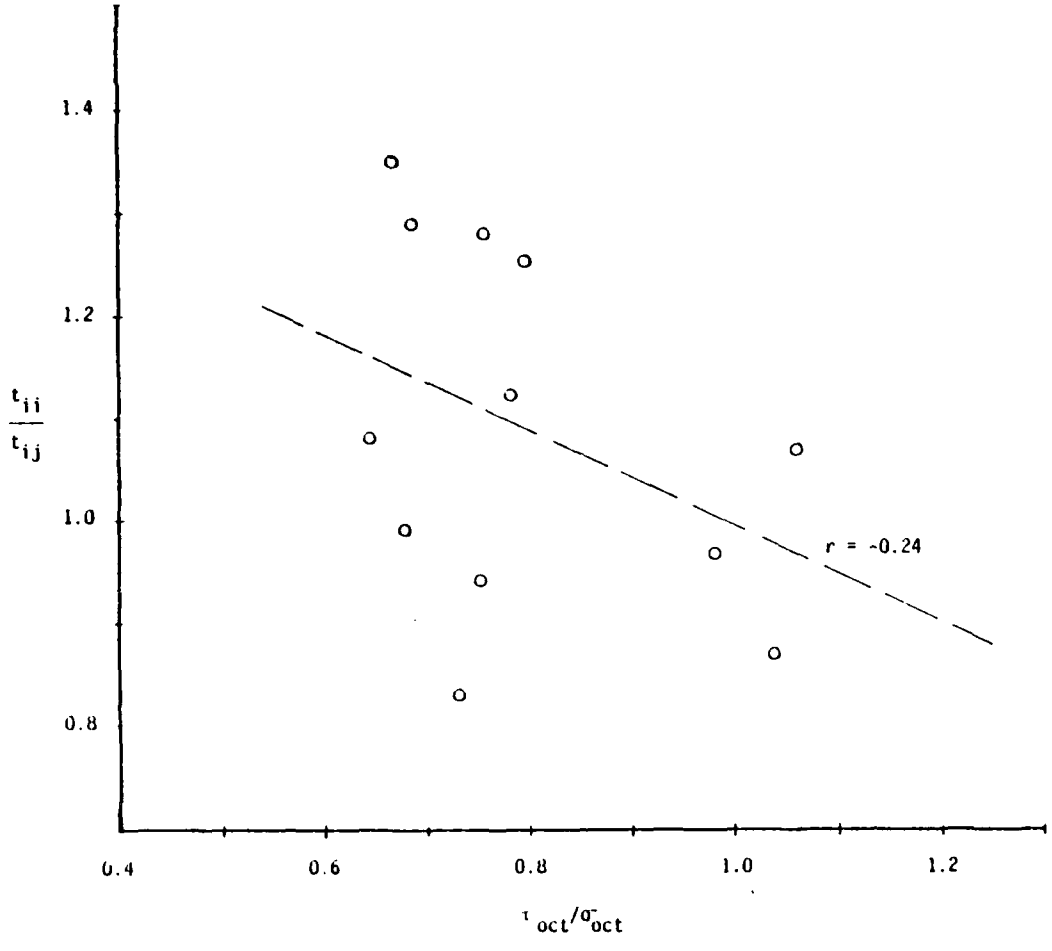

Figure 21. Tensile strength ratio as a function of the normalized octahedral shear stress at failure.

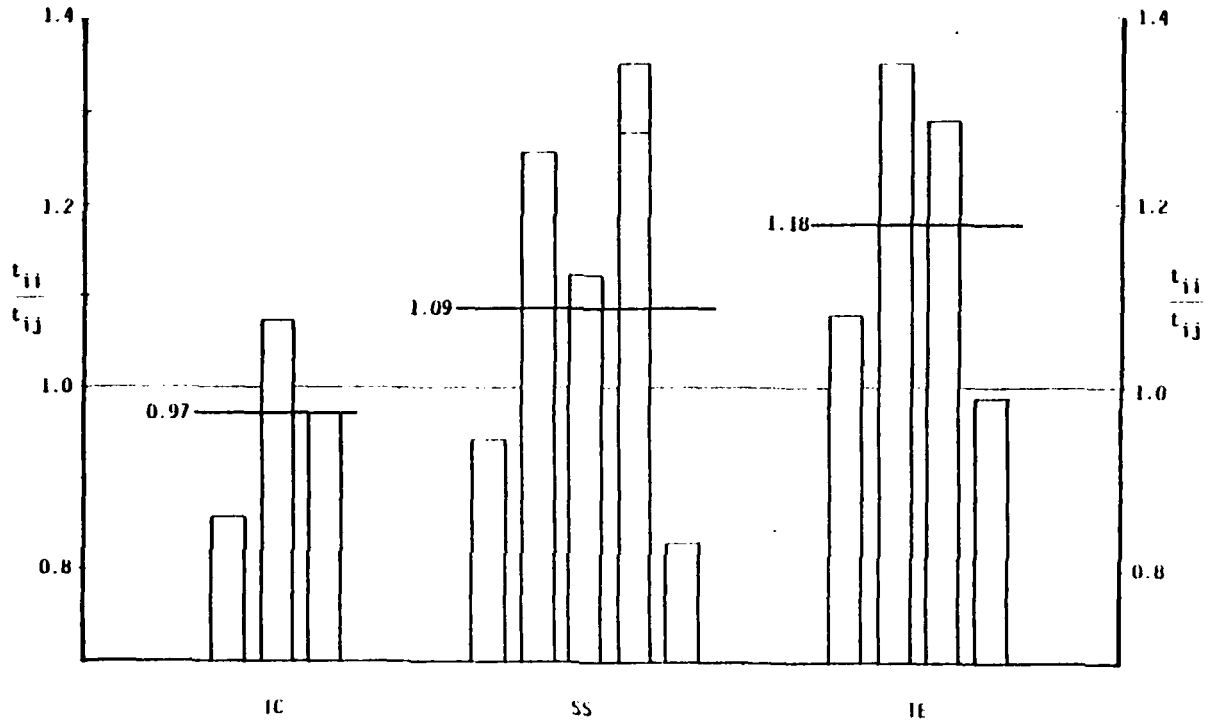

Figure 22. Tensile strength ratios of the various triaxial tests.

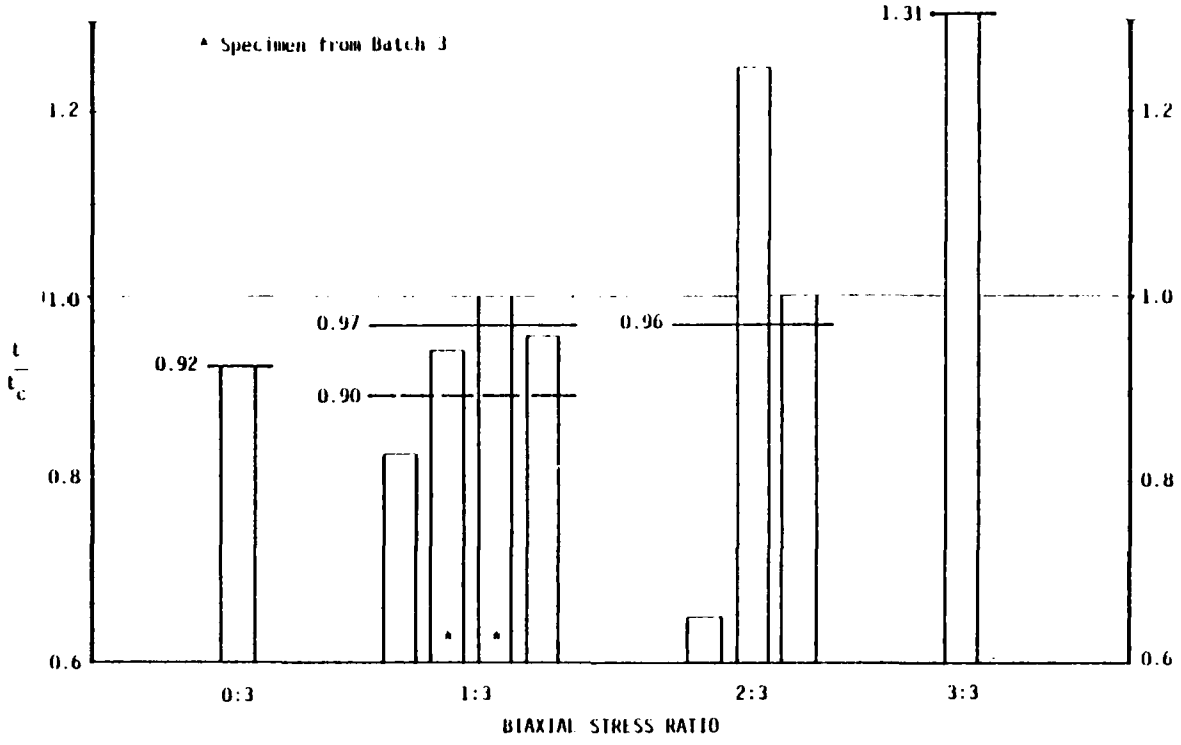

Figure 23. Residual tensile strengths of the various biaxial tests.

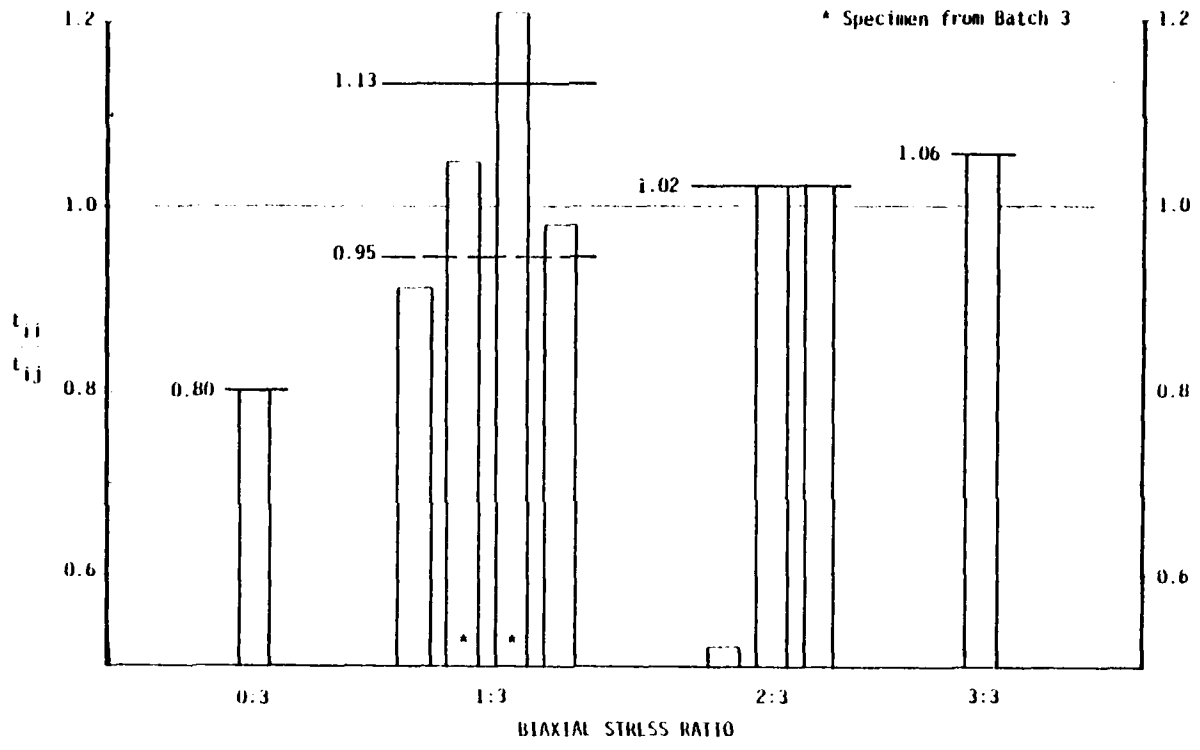

Figure 24. Tensile strength ratios of the various biaxial tests.

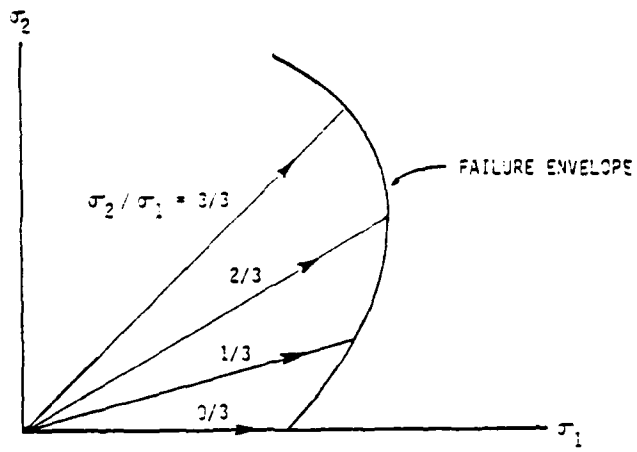

Figure 1. Biaxial Stress Paths

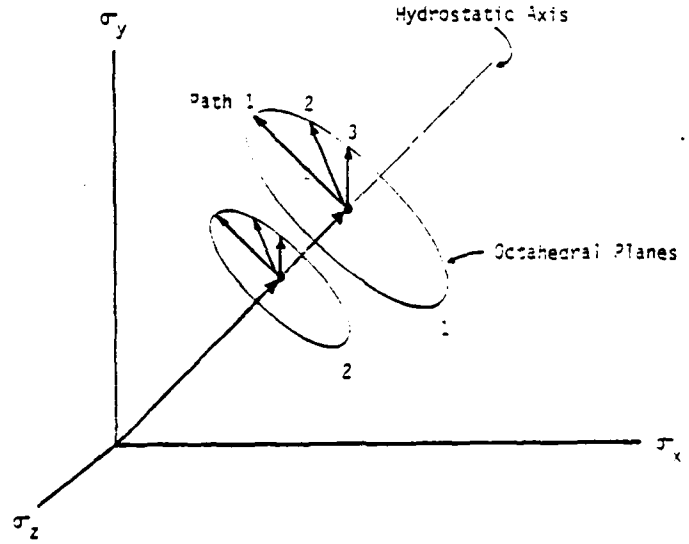

Figure 2. Triaxial Stress Paths in two octahedral planes.

APPENDIX A.

STRESS-STRAIN DATA FOR TRIAXIAL TESTS

This appendix contains the stress-strain data for each successful triaxial test. The data sheets are arranged in order of test number beginning with Test 5A. The axes which head the columns are the axes of the cubical cell. Stresses are given in psi and strains are given in mils/in. 1 mil/in = 0.1% strain = 10^{-3} in/in.

STRESS - STRAIN DATA

X-AXIS		Y-AXIS		Z-AXIS	
STRESS (PSI)	STRAIN (MILS/IN)	STRESS (PSI)	STRAIN (MILS/IN)	STRESS (PSI)	STRAIN (MILS/IN)
0	0.0000	0	0.0000	0	0.0000
300	0.0080	300	-0.0177	300	-0.0058
600	0.0531	600	0.0558	600	0.0592
1000	0.1186	1000	0.1330	1000	0.1611
1500	0.2242	1500	0.2527	1500	0.2907
2000	0.3309	2000	0.3468	2000	0.4128
2500	0.4448	2500	0.4803	2500	0.5654
3000	0.5719	3000	0.6403	3000	0.7000
3500	0.6875	3500	0.7620	3500	0.8268
3750	0.7338	3750	0.8196	3750	0.8993
3700	0.7290	3700	0.8330	3850	0.9356
3600	0.7065	3600	0.8043	4050	1.0077
3500	0.7091	3500	0.8013	4250	1.0882
3400	0.6952	3400	0.7851	4450	1.1791
3300	0.6786	3300	0.7620	4650	1.2555
3200	0.6651	3200	0.7433	4850	1.3436
3100	0.6378	3100	0.7188	5050	1.4293
3000	0.6109	3000	0.6980	5250	1.5373
2800	0.6043	2800	0.6650	5650	1.7147
2700	0.5722	2700	0.6306	5850	1.8535
2600	0.5394	2600	0.5938	6050	1.9940
2500	0.5181	2500	0.5622	6250	2.1230
2400	0.4898	2400	0.5047	6450	2.2348
2300	0.4416	2300	0.4733	6650	2.3583
2200	0.3905	2200	0.4214	6850	2.5073
2100	0.3427	2100	0.3611	7050	2.6863
2000	0.1282	2000	0.1355	7250	3.3408
1900	0.1122	1900	0.1186	7450	3.4433
1800	0.0753	1800	0.0829	7650	3.5581
1700	0.0172	1700	0.0174	7850	3.7903
1600	-0.1734	1600	-0.1915	8050	4.3007
1500	-0.2440	1500	-0.2612	8250	4.5802
1400	-0.3630	1400	-0.3843	8450	4.9783
1300	-0.9081	1300	-0.9555	8650	6.1597
1250	-0.9984	1250	-1.0552	8750	6.4399
1200	-1.1291	1200	-1.1824	8850	6.7368
1150	-1.4264	1150	-1.4826	8950	7.3930
1100	-1.6796	1100	-1.7077	9050	7.7569
1050	-2.3530	1050	-2.3747	9150	8.9083
1000	-2.9744	1000	-3.9567	9250	11.1324

TENSILE STRENGTHS

THE DIRECTION OF THE MAXIMUM PRINCIPAL STRESS = 290 PSI
THE DIRECTION OF THE MINIMUM PRINCIPAL STRESS = 265 PSI

TEST 55 ... TC 1750 SPECIMEN 02, BATCH 3 12/20/80

STRESS - STRAIN DATA

X-AXIS		Y-AXIS		Z-AXIS	
STRESS (PSI)	STRAIN (MILS/IN)	STRESS (PSI)	STRAIN (MILS/IN)	STRESS (PSI)	STRAIN (MILS/IN)
0	0.0000	0	0.0000	0	0.0000
300	0.0209	300	-0.0299	300	-0.0368
600	0.0577	600	0.0173	600	-0.0006
1000	0.0885	1000	0.0357	1000	0.0299
1500	0.1717	1500	0.1125	1500	0.0931
2000	0.2713	2000	0.1788	2000	0.1633
2500	0.3794	2500	0.2670	2500	0.2793
3000	0.4777	3000	0.3800	3000	0.3643
3500	0.6118	3500	0.5033	3500	0.4748
3750	0.6724	3750	0.5583	3750	0.5246
3700	0.6586	3700	0.5403	3850	0.5417
3600	0.6359	3600	0.5144	4050	0.6076
3500	0.6139	3500	0.4964	4250	0.6579
3400	0.6017	3400	0.4813	4450	0.7113
3300	0.5826	3300	0.4671	4650	0.7639
3200	0.5641	3200	0.4473	4850	0.8098
3100	0.5560	3100	0.4355	5050	0.8709
3000	0.5293	3000	0.4058	5250	0.9370
2900	0.5181	2900	0.4028	5450	1.0120
2800	0.4918	2800	0.3662	5650	1.0703
2700	0.4841	2700	0.3545	5850	1.1906
2600	0.4586	2600	0.3315	6050	1.2397
2500	0.4513	2500	0.3184	6250	1.3330
2400	0.4274	2400	0.3024	6450	1.4541
2300	0.4192	2300	0.2952	6650	1.5571
2200	0.3884	2200	0.2612	6850	1.6729
2100	0.3490	2100	0.2242	7050	1.7554
2000	0.3051	2000	0.1839	7250	1.8573
1900	0.2527	1900	0.1268	7450	1.9879
1800	0.2194	1800	0.0960	7650	2.0970
1700	0.1708	1700	0.0422	7850	2.2601
1600	0.1190	1600	-0.0057	8050	2.4283
1500	0.0624	1500	-0.0675	8250	2.5869
1400	-0.0020	1400	-0.1393	8450	2.8073
1300	-0.0893	1300	-0.2207	8650	3.0753
1200	-0.2128	1200	-0.3528	8850	3.3871
1100	-0.3475	1100	-0.4989	9050	3.7526
1050	-0.4678	1050	-0.6290	9150	4.0425
1000	-0.5924	1000	-0.7544	9250	4.3154
950	-0.7343	950	-0.8928	9350	4.6217

TEST SB ... TC 3750 SPECIMEN CB, BATCH 3 12/23/90

(CONTINUED)

X-AXIS		Y-AXIS		Z-AXIS	
STRESS (PSI)	STRAIN (MILS/IN)	STRESS (PSI)	STRAIN (MILS/IN)	STRESS (PSI)	STRAIN (MILS/IN)
900	-0.9343	900	-1.1035	9450	4.9961
850	-1.2160	850	-1.3669	9550	5.4689
800	-1.6508	800	-1.7982	9650	6.1700

TENSILE STRENGTHS

IN THE DIRECTION OF THE MAXIMUM PRINCIPAL STRESS = 278 PSI
IN THE DIRECTION OF THE MINIMUM PRINCIPAL STRESS = 260 PSI

TEST SC ... TC 8750 SPECIMEN A4, BATCH 4 1-05-91

STRESS - STRAIN DATA

X-AXIS		Y-AXIS		Z-AXIS	
STRESS (PSI)	STRAIN (MILS/IN)	STRESS (PSI)	STRAIN (MILS/IN)	STRESS (PSI)	STRAIN (MILS/IN)
0	0.0000	0	0.0000	0	0.0000
500	0.0337	500	0.0258	500	-0.0253
750	0.0530	750	0.0465	750	0.0005
1000	0.0780	1000	0.0465	1000	0.0408
1500	0.1561	1500	0.1349	1500	0.1547
2000	0.2408	2000	0.2035	2000	0.2628
2500	0.3333	2500	0.2951	2500	0.3878
3000	0.4093	3000	0.3950	3000	0.5064
3500	0.4506	3500	0.4494	3500	0.5863
3750	0.4666	3750	0.4838	3750	0.6113
3700	0.4533	3700	0.4695	3850	0.6283
3600	0.4570	3600	0.4584	4050	0.6932
3500	0.4513	3500	0.4529	4250	0.7552
3400	0.4341	3400	0.4458	4450	0.8106
3300	0.4153	3300	0.4183	4650	0.8833
3200	0.4238	3200	0.4237	4850	0.9418
3100	0.4155	3100	0.4032	5050	1.0031
3000	0.3979	3000	0.3928	5250	1.0799
2900	0.3693	2900	0.3618	5450	1.1400
2800	0.3485	2800	0.3318	5650	1.1973
2700	0.3309	2700	0.3078	5850	1.2705
2600	0.3167	2600	0.2861	6050	1.3493
2500	0.3119	2500	0.2839	6250	1.4318
2400	0.2920	2400	0.2598	6450	1.4957
2300	0.2727	2300	0.2327	6650	1.6040
2200	0.2421	2200	0.2079	6850	1.6880
2100	0.2201	2100	0.1809	7050	1.7985
2000	0.1964	2000	0.1409	7250	1.9016
1900	0.1701	1900	0.1229	7450	2.0168
1800	0.1295	1800	0.0874	7650	2.1245
1700	0.0750	1700	0.0434	7850	2.2573
1600	0.0346	1600	0.0051	8050	2.4631
1500	-0.0287	1500	-0.0776	8250	2.6368
1400	-0.0845	1400	-0.1268	8450	2.8030
1300	-0.1644	1300	-0.2191	8650	3.0313
1200	-0.3074	1200	-0.3613	8850	3.3972
1100	-0.4713	1100	-0.5339	9050	3.8122
1050	-0.6055	1050	-0.6912	9150	4.1289
1000	-0.7566	1000	-0.8594	9250	4.4247
950	-0.9809	950	-1.0753	9350	4.8519

TEST SC ... TC ST50 SPECIMEN A4, CATCH 4 1 05 81

(CONTINUED)

X-AXIS		Y-AXIS		Z-AXIS	
STRESS (PSI)	STRAIN (MILS/IN)	STRESS (PSI)	STRAIN (MILS/IN)	STRESS (PSI)	STRAIN (MILS/IN)
900	-1.3653	900	-1.4738	9450	5.5258

TENSILE STRENGTHS

IN THE DIRECTION OF THE MAXIMUM PRINCIPAL STRESS = 208 PSI
IN THE DIRECTION OF THE MINIMUM PRINCIPAL STRESS = 240 PSI

TEST SE ... 8 3750 SPECIMEN 55, BATCH 2 1/13/81

STRESS - STRAIN DATA

X-AXIS		Y-AXIS		Z-AXIS	
STRESS (PSI)	STRAIN (MILS/IN)	STRESS (PSI)	STRAIN (MILS/IN)	STRESS (PSI)	STRAIN (MILS/IN)
0	0.0000	0	0.0000	0	0.0000
300	-0.0024	300	-0.0446	300	-0.0594
600	0.0243	600	-0.0146	600	-0.0356
1000	0.0813	1000	0.0254	1000	0.0199
1500	0.1765	1500	0.1017	1500	0.0999
2000	0.2756	2000	0.1642	2000	0.1917
2500	0.3829	2500	0.2549	2500	0.3005
3000	0.4979	3000	0.3865	3000	0.4213
3500	0.5941	3500	0.4803	3500	0.5003
3750	0.6530	3750	0.5385	3750	0.5605
3750	0.6679	3650	0.5275	3850	0.5954
3750	0.6885	3550	0.5114	3950	0.6213
3750	0.6569	3400	0.4721	4100	0.6440
3750	0.6528	3250	0.4804	4250	0.6982
3750	0.6586	3100	0.4562	4400	0.7448
3750	0.6765	2950	0.4230	4550	0.7835
3750	0.6971	2800	0.3989	4700	0.8296
3750	0.6649	2650	0.3420	4850	0.8703
3750	0.6834	2500	0.3200	5000	0.9056
3750	0.6715	2350	0.2793	5150	0.9459
3750	0.6556	2200	0.2086	5300	0.9862
3750	0.6685	2050	0.1834	5450	1.0527
3750	0.6805	1900	0.1690	5600	1.1164
3750	0.6870	1750	0.1308	5750	1.1827
3750	0.6959	1600	0.0832	5900	1.2654
3750	.7096	1450	0.0484	6050	1.3403
3750	0.7167	1300	0.0058	6200	1.4339
3750	0.7227	1150	-0.0396	6350	1.5048
3750	0.7260	1000	-0.0886	6500	1.6110
3750	0.7483	850	-0.1404	6650	1.7196
3750	0.7428	700	-0.2214	6800	1.8455
3750	0.7411	600	-0.2887	6900	1.9290
3750	0.7387	500	-0.3559	7000	2.0347
3750	0.7513	300	-0.5841	7200	2.2642
3750	0.7872	200	-0.7892	7300	2.4685
3750	0.8030	100	-0.9554	7400	2.6785
3750	0.8183	100	-1.0563	7400	2.8142
3750	0.8188	100	-1.1524	7400	2.8554

TENSILE STRENGTHS

IN THE DIRECTION OF THE MAXIMUM PRINCIPAL STRESS = 408 PSI
IN THE DIRECTION OF THE MINIMUM PRINCIPAL STRESS = 329 PSI

TEST 61 ... 08 3750 SPECIMEN D2, BATCH 2 1 35 61

STRESS - STRAIN DATA

X-AXIS		Y-AXIS		Z-AXIS	
STRESS (PSI)	STRAIN (MILS/IN)	STRESS (PSI)	STRAIN (MILS/IN)	STRESS (PSI)	STRAIN (MILS/IN)
0	0.0000	0	0.0000	0	0.0000
300	0.0187	300	-0.0423	300	-0.0648
600	0.0763	600	0.0151	600	-0.0170
1000	0.1206	1000	0.0291	1000	0.0308
1500	0.2167	1500	0.1190	1500	0.1235
2000	0.3119	2000	0.2056	2000	0.2202
2500	0.4331	2500	0.3099	2500	0.3500
3000	0.5367	3000	0.4316	3000	0.4675
3500	0.6807	3500	0.5706	3500	0.6008
3750	0.7272	3750	0.6218	3750	0.6456
3750	0.7187	3650	0.6086	3850	0.6735
3750	0.7104	3550	0.5869	3950	0.7088
3750	0.7218	3400	0.5518	4100	0.7557
3750	0.7239	3250	0.5216	4250	0.8057
3750	0.7243	3100	0.4929	4400	0.8585
3750	0.7212	2950	0.4668	4550	0.8910
3750	0.7447	2800	0.4304	4700	0.9291
3750	0.7442	2650	0.4046	4850	1.0321
3750	0.7532	2500	0.3513	5000	1.0685
3750	0.7516	2350	0.3338	5150	1.1238
3750	0.7642	2200	0.2917	5300	1.1820
3750	0.7643	2050	0.2738	5450	1.2338
3750	0.7644	1900	0.2262	5600	1.3243
3750	0.7732	1750	0.1846	5750	1.3784
3750	0.7860	1600	0.1498	5900	1.4586
3750	0.7877	1450	0.1057	6050	1.5248
3750	0.7847	1300	0.0566	6200	1.6136
3750	0.7827	1150	0.0097	6350	1.7141
3750	0.7801	1000	-0.0406	6500	1.7777
3750	0.7862	850	-0.0731	6650	1.8899
3750	0.7885	750	-0.1288	6750	1.9584
3750	0.7940	650	-0.1704	6850	2.0341
3750	0.8164	550	-0.2156	6950	2.1359
3750	0.8208	450	-0.2868	7050	2.2155
3750	0.8226	400	-0.3374	7100	2.2908
3750	0.8309	300	-0.4357	7200	2.3750
3750	0.8333	250	-0.5232	7250	2.4379
3750	0.8333	200	-0.6075	7300	2.5476
3750	0.8511	150	-0.6933	7350	2.6247
3750	0.8678	100	-0.7962	7400	2.7018

(CONTINUED)

X-AXIS		Y-AXIS		Z-AXIS	
STRESS (PSI)	STRAIN (MILS/IN)	STRESS (PSI)	STRAIN (MILS/IN)	STRESS (PSI)	STRAIN (MILS/IN)
3750	0.8792	50	-0.9354	7450	2.7949

TENSILE STRENGTHS

IN THE DIRECTION OF THE MAXIMUM PRINCIPAL STRESS = 373 PSI
IN THE DIRECTION OF THE MINIMUM PRINCIPAL STRESS = 340 PSI

TEST [illegible] ... TE 1750 SPECIMEN 66 BATCH 3 10 24 80

STRESS - STRAIN DATA

X-AXIS		Y-AXIS		Z-AXIS	
STRESS (PSI)	STRAIN (MILS/IN)	STRESS (PSI)	STRAIN (MILS/IN)	STRESS (PSI)	STRAIN (MILS/IN)
0	0.0000	0	0.0000	0	0.0000
300	0.0166	300	-0.0215	300	0.0080
600	0.0482	600	0.0391	600	0.0669
1000	0.0998	1000	0.0913	1000	0.1620
1500	0.2038	1500	0.2047	1500	0.2833
2000	0.3457	2000	0.3318	2000	0.4517
2500	0.4628	2500	0.4543	2500	0.6041
3000	0.5627	3000	0.5447	3000	0.7167
3500	0.7039	3500	0.6918	3500	0.8654
3750	0.7630	3750	0.7403	3750	0.9414
3800	0.7978	3800	0.7903	3650	0.9197
3875	0.8266	3875	0.8157	3500	0.8994
3950	0.8537	3950	0.8411	3350	0.8631
4025	0.8839	4025	0.8820	3200	0.8385
4100	0.9286	4100	0.9130	3050	0.8232
4175	0.9583	4175	0.9429	2900	0.7815
4250	1.0000	4250	0.9823	2750	0.7423
4325	1.0292	4325	1.0053	2600	0.7174
4400	1.0722	4400	1.0438	2450	0.6590
4475	1.1059	4475	1.0818	2300	0.6201
4550	1.1493	4550	1.1203	2150	0.5620
4625	1.1846	4625	1.1687	2000	0.5134
4700	1.2289	4700	1.2082	1850	0.4417
4775	1.2571	4775	1.2440	1700	0.3866
4850	1.2961	4850	1.2989	1550	0.3298
4925	1.3359	4925	1.3386	1400	0.2675
5000	1.3982	5000	1.4065	1250	0.1640
5075	1.4513	5075	1.4615	1100	0.0938
5150	1.4981	5150	1.5071	950	0.0141
5225	1.5528	5225	1.5598	800	-0.0919
5300	1.6169	5300	1.6333	650	-0.1960
5375	1.7081	5375	1.7207	500	-0.3535
5450	1.7982	5450	1.7998	350	-0.5383
5525	1.9135	5525	1.9315	200	-0.8540
5575	2.1166	5575	2.1329	100	-1.3021

TENSILE STRENGTHS

IN THE DIRECTION OF THE MAXIMUM PRINCIPAL STRESS = 313 PSI
IN THE DIRECTION OF THE MINIMUM PRINCIPAL STRESS = 295 PSI

STRESS - STRAIN DATA

X-AXIS		Y-AXIS		Z-AXIS	
STRESS (PSI)	STRAIN (MILS/IN)	STRESS (PSI)	STRAIN (MILS/IN)	STRESS (PSI)	STRAIN (MILS/IN)
0	0.0000	0	0.0000	0	0.0000
300	0.0367	300	0.0094	300	-0.0343
600	0.0527	600	0.0528	600	0.0097
1000	0.1059	1000	0.1171	1000	0.0895
1500	0.2055	1500	0.2577	1500	0.2188
2000	0.2984	2000	0.3852	2000	0.3345
2500	0.3883	2500	0.4452	2500	0.4648
3000	0.4504	3000	0.5338	3000	0.5479
3500	0.5385	3500	0.6546	3500	0.6676
3750	0.5620	3750	0.6887	3750	0.7093
3650	0.5668	3800	0.7275	3800	0.7717
3500	0.5530	3875	0.7483	3875	0.7881
3350	0.5298	3950	0.7714	3950	0.8157
3200	0.5243	4025	0.7833	4025	0.8447
3050	0.4959	4100	0.8076	4100	0.8612
2900	0.4696	4175	0.8114	4175	0.8768
2750	0.4450	4250	0.8389	4250	0.8887
2600	0.4372	4325	0.8744	4325	0.9291
2450	0.4016	4400	0.8930	4400	0.9619
2300	0.3766	4475	0.9192	4475	0.9894
2150	0.3381	4550	0.9471	4550	1.0108
2000	0.3108	4625	0.9685	4625	1.0402
1850	0.2683	4700	0.9963	4700	1.0651
1700	0.2220	4775	1.0296	4775	1.1029
1550	0.1946	4850	1.0552	4850	1.1137
1400	0.1554	4925	1.0855	4925	1.1501
1250	0.0993	5000	1.1348	5000	1.1968
1100	0.0708	5075	1.1611	5075	1.2311
950	0.0031	5150	1.1840	5150	1.2629
800	-0.0185	5225	1.2124	5225	1.2912
650	-0.1132	5300	1.2651	5300	1.3511
500	-0.1834	5375	1.2992	5375	1.3918
350	-0.2732	5450	1.3659	5450	1.4659
200	-0.4186	5525	1.4139	5525	1.5130
100	-0.5648	5575	1.4561	5575	1.5679
50	-0.7552	5600	1.5190	5600	1.6330

TENSILE STRENGTHS

IN THE DIRECTION OF THE MAXIMUM PRINCIPAL STRESS = 374 PSI
IN THE DIRECTION OF THE MINIMUM PRINCIPAL STRESS = 350 PSI

TEST [illegible] SPECIMEN 85, BATCH 3 [illegible]

STRESS - STRAIN DATA

X-AXIS		Y-AXIS		Z-AXIS	
STRESS (PSI)	STRAIN (MILS/IN)	STRESS (PSI)	STRAIN (MILS/IN)	STRESS (PSI)	STRAIN (MILS/IN)
0	0.0000	0	0.0000	0	0.0000
300	0.0037	300	0.0134	300	0.0051
600	0.0806	600	0.1038	600	0.0833
1000	0.1501	1000	0.1869	1000	0.2153
1500	0.2691	1500	0.3308	1500	0.3584
2000	0.3880	2000	0.4663	2000	0.5249
2500	0.5032	2500	0.6296	2500	0.7200
3000	0.6334	3000	0.7728	3000	0.8693
3500	0.8126	3500	0.9542	3500	1.0586
3750	0.8699	3750	1.0114	3750	1.0913
3800	0.9049	3800	1.0638	3650	1.1230
3875	0.9108	3875	1.0744	3500	1.0989
3950	0.9378	3950	1.1068	3350	1.0596
4025	0.9623	4025	1.1369	3200	1.0245
4100	0.9977	4100	1.1753	3050	0.9957
4175	1.0358	4175	1.2127	2900	0.9475
4250	1.0738	4250	1.2524	2750	0.9074
4325	1.1059	4325	1.2857	2600	0.8558
4400	1.1483	4400	1.3270	2450	0.8145
4475	1.1750	4475	1.3655	2300	0.7629
4550	1.2265	4550	1.4181	2150	0.6863
4625	1.2643	4625	1.4523	2000	0.6329
4775	1.3467	4775	1.5518	1700	0.4783
4850	1.3904	4850	1.5977	1550	0.4345
4925	1.4413	4925	1.6534	1400	0.3540
5000	1.4859	5000	1.7030	1250	0.2997
5075	1.5435	5075	1.7621	1100	0.2123
5150	1.5934	5150	1.8182	950	0.1008
5225	1.6578	5225	1.8719	800	-0.0024
5300	1.7308	5300	1.9469	650	-0.1954
5375	1.7938	5375	2.0232	500	-0.3147
5450	1.9242	5450	2.1527	350	-0.5789
5500	2.0392	5500	2.2693	250	-0.8556
5525	2.1448	5525	2.3650	200	-1.1154

TENSILE STRENGTHS

IN THE DIRECTION OF THE MAXIMUM PRINCIPAL STRESS = 437 PSI
IN THE DIRECTION OF THE MINIMUM PRINCIPAL STRESS = 416 PSI

[illegible]

STRESS - STRAIN DATA

X-AXIS		Y-AXIS		Z-AXIS	
STRESS (PSI)	STRAIN (MILS/IN)	STRESS (PSI)	STRAIN (MILS/IN)	STRESS (PSI)	STRAIN (MILS/IN)
0	0.0000	0	0.0000	0	0.0000
300	0.0097	300	-0.0158	300	-0.0510
600	0.0477	600	0.0495	600	-0.0031
1000	0.0979	1000	0.1012	1000	0.0659
1500	0.2206	1500	0.2105	1500	0.1886
2000	0.3566	2000	0.3393	2000	0.3350
2500	0.4739	2500	0.4478	2500	0.4595
3000	0.6242	3000	0.6007	3000	0.6045
3500	0.7711	3500	0.7432	3500	0.7333
3750	0.8545	3750	0.8188	3750	0.8115
3800	0.8857	3800	0.8559	3650	0.8163
3875	0.8916	3875	0.8733	3500	0.7896
3950	0.9209	3950	0.8941	3350	0.7537
4025	0.9501	4025	0.9186	3200	0.7348
4100	0.9881	4100	0.9570	3050	0.7135
4175	1.0078	4175	0.9755	2900	0.6891
4250	1.0488	4250	1.0221	2750	0.6532
4325	1.0740	4325	1.0440	2600	0.6158
4400	1.1160	4400	1.0797	2450	0.5785
4475	1.1447	4475	1.1124	2300	0.5435
4550	1.1753	4550	1.1400	2150	0.5034
4625	1.1980	4625	1.1630	2000	0.4551
4700	1.2264	4700	1.1979	1850	0.4090
4775	1.2651	4775	1.2398	1700	0.3569
4850	1.2931	4850	1.2680	1550	0.3068
4925	1.3209	4925	1.3055	1400	0.2522
5000	1.3571	5000	1.3405	1250	0.1978
5075	1.3893	5075	1.3728	1100	0.1424
5150	1.4306	5150	1.4176	950	0.0584
5225	1.4726	5225	1.4404	800	0.0064
5300	1.5057	5300	1.4903	650	-0.0541
5375	1.5493	5375	1.5279	500	-0.1253
5425	1.5993	5425	1.5705	400	-0.1933
5475	1.6550	5475	1.6277	300	-0.3107
5525	1.6854	5525	1.6478	200	-0.3879
5550	1.7350	5550	1.6980	150	-0.4711
5575	1.7701	5575	1.7246	100	-0.6096

TENSILE STRENGTHS

IN THE DIRECTION OF THE MAXIMUM PRINCIPAL STRESS = 412 PSI
IN THE DIRECTION OF THE MINIMUM PRINCIPAL STRESS = 123 PSI

TEST [illegible] SPECIMEN 14, BATCH 1 11 01 80

STRESS - STRAIN DATA

X-AXIS		Y-AXIS		Z-AXIS	
STRESS (PSI)	STRAIN (MILS/IN)	STRESS (PSI)	STRAIN (MILS/IN)	STRESS (PSI)	STRAIN (MILS/IN)
0	0.0000	0	0.0000	0	0.0000
300	0.0005	300	-0.0224	300	-0.0485
600	0.0577	600	0.0338	600	0.0014
1000	0.1280	1000	0.0844	1000	0.0874
1500	0.2449	1500	0.1922	1500	0.2083
2000	0.3539	2000	0.2759	2000	0.3016
2500	0.5048	2500	0.4341	2500	0.4620
3000	0.6327	3000	0.5610	3000	0.5783
3500	0.7763	3500	0.7104	3500	0.6915
3750	0.8523	3750	0.7817	3750	0.7561
3800	0.8588	3800	0.7942	3650	0.7264
3875	0.8889	3875	0.8254	3500	0.6867
3950	0.9202	3950	0.8603	3350	0.6626
4025	0.9426	4025	0.8825	3200	0.6472
4100	0.9639	4100	0.9036	3050	0.6179
4175	0.9936	4175	0.9358	2900	0.5767
4250	1.0089	4250	0.9681	2750	0.5521
4325	1.0653	4325	1.0004	2600	0.5376
4400	1.0919	4400	1.0256	2450	0.4932
4475	1.1353	4475	1.0626	2300	0.4659
4550	1.1645	4550	1.0940	2150	0.4191
4625	1.1962	4625	1.1257	2000	0.3631
4700	1.2223	4700	1.1515	1850	0.3354
4775	1.2694	4775	1.2028	1700	0.2820
4850	1.3050	4850	1.2370	1550	0.2385
4925	1.3339	4925	1.2735	1400	0.2093
5000	1.3716	5000	1.3139	1250	0.1551
5075	1.4082	5075	1.3543	1100	0.1016
5150	1.4483	5150	1.3838	950	0.0581
5225	1.4804	5225	1.4306	800	-0.0085
5275	1.5068	5275	1.4576	700	-0.0875
5325	1.5441	5325	1.4989	600	-0.1351
5375	1.5756	5375	1.5206	500	-0.1742
5425	1.6273	5425	1.5698	400	-0.2353
5475	1.6499	5475	1.5850	300	-0.2968
5525	1.6917	5525	1.6306	200	-0.3869
5550	1.7217	5550	1.6566	150	-0.4386
5575	1.7607	5575	1.6915	100	-0.5280
5600	1.7894	5600	1.7200	50	-0.6491

TENSILE STRENGTHS

IN THE DIRECTION OF THE MAXIMUM PRINCIPAL STRESS = 327 PSI
IN THE DIRECTION OF THE MINIMUM PRINCIPAL STRESS = 330 PSI

STRESS - STRAIN DATA

X-AXIS STRESS (PSI)	X-AXIS STRAIN (MILS/IN)	Y-AXIS STRESS (PSI)	Y-AXIS STRAIN (MILS/IN)	Z-AXIS STRESS (PSI)	Z-AXIS STRAIN (MILS/IN)
0	0.0000	0	0.0000	0	0.0000
300	0.0227	300	0.0113	300	-0.0233
600	0.0556	600	0.0875	600	0.0237
1000	0.1103	1000	0.1439	1000	0.0990
1500	0.2239	1500	0.2631	1500	0.2293
2000	0.3386	2000	0.3749	2000	0.3702
2500	0.4614	2500	0.5087	2500	0.5249
3000	0.5779	3000	0.6372	3000	0.6655
3500	0.7364	3500	0.7919	3500	0.8320
4000	0.8603	4000	0.9137	4000	0.9734
4500	1.0176	4500	1.0739	4500	1.1453
5000	1.1948	5000	1.2524	5000	1.3053
4950	1.1856	4950	1.2575	5100	1.3453
4850	1.1566	4850	1.2295	5300	1.5144
4700	1.1354	4700	1.1993	5600	1.5688
4550	1.1136	4550	1.1649	5900	1.7188
4400	1.0713	4400	1.1308	6200	1.8998
4250	1.0293	4250	1.0845	6500	2.0907
4100	0.9921	4100	1.0493	6800	2.2211
3950	0.9462	3950	1.0226	7100	2.4094
3800	0.8855	3800	0.9522	7400	2.6030
3650	0.8551	3650	0.9285	7700	2.8413
3500	0.7973	3500	0.8669	8000	3.1165
3350	0.7535	3350	0.8253	8300	3.3533
3050	0.6255	3050	0.7014	8900	4.0450
2900	0.5580	2900	0.6224	9200	4.3658
2700	0.4423	2700	0.5058	9600	4.9838
2500	0.2715	2500	0.3252	10000	5.6347
2300	0.0106	2300	0.0684	10400	6.6778
2100	-0.4529	2100	-0.4066	10800	8.1462
1900	-1.3133	1900	-1.2632	11200	10.3530
1700	-3.0479	1700	-2.9608	11600	13.7616

TENSILE STRENGTHS

IN THE DIRECTION OF THE MAXIMUM PRINCIPAL STRESS = 244 PSI
IN THE DIRECTION OF THE MINIMUM PRINCIPAL STRESS = 245 PSI

TEST 88 ... PI 5010 SPECIMEN A5, RATIO 4 , 3 07:81

STRESS - STRAIN DATA

X-AXIS		Y-AXIS		Z-AXIS	
STRESS (PSI)	STRAIN (MILS/IN)	STRESS (PSI)	STRAIN (MILS/IN)	STRESS (PSI)	STRAIN (MILS/IN)
0	0.0000	0	0.0000	0	0.0000
300	0.0341	300	0.0136	300	-0.0322
600	0.0899	600	0.0766	600	0.0257
1000	0.1332	1000	0.1006	1000	0.0847
1500	0.2349	1500	0.1964	1500	0.2110
2000	0.3151	2000	0.2610	2000	0.3320
2500	0.3892	2500	0.3479	2500	0.4628
3000	0.4798	3000	0.4542	3000	0.6010
3500	0.5522	3500	0.5515	3500	0.7145
3750	0.5600	3750	0.5692	3750	0.7572
4250	0.6439	4250	0.6846	4250	0.9145
4750	0.7352	4750	0.7985	4750	1.0396
5000	0.7435	5000	0.8389	5000	1.0806
4900	0.7323	4900	0.8105	5200	1.1449
4800	0.7136	4800	0.7748	5400	1.2031
4700	0.6925	4700	0.7462	5600	1.2666
4550	0.6993	4550	0.7301	5900	1.3875
4400	0.6695	4400	0.6966	6200	1,5085
4250	0.6563	4250	0.6752	6500	1.6308
4100	0.6411	4100	0.6578	6800	1.8015
3950	0.6371	3950	0.6449	7100	1.9076
3800	0.6055	3800	0.6233	7400	2.0722
3650	0.5947	3650	0.5999	7700	2.2352
3500	0.5592	3500	0.5593	8000	2.3841
3350	0.5250	3350	0.5193	8300	2.5818
3200	0.4764	3200	0.4741	8600	2.7827
3050	0.4384	3050	0.4396	8900	2.9875
2900	0.3875	2900	0.3848	9200	3.2635
2750	0.3244	2750	0.3081	9500	3.5693
2600	0.2491	2600	0.2298	9800	3.8710
2450	0.1771	2450	0.1493	10100	4.2922
2300	0.0704	2300	0.0572	10400	4.7572
2150	-0.0666	2150	-0.0896	10700	5.2446
2000	-0.2937	2000	-0.3376	11000	5.7765
1850	-0.5834	1850	-0.6122	11300	6.9462
1700	-1.1765	1700	-1.2018	11600	8.3334
1550	-2.4780	1550	-2.5070	11900	11.0143
1500	-2.9933	1500	-3.0110	12000	11.9307
1450	-3.5390	1450	-3.5331	12100	12.8892

TENSILE STRENGTHS

IN THE DIRECTION OF THE MAXIMUM PRINCIPAL STRESS = 385 PSI
IN THE DIRECTION OF THE MINIMUM PRINCIPAL STRESS = 196 PSI

TEST [illegible] 5000 SPECIMEN [illegible] BATCH 4 [illegible]

STRESS - STRAIN DATA

X-AXIS		Y-AXIS		Z-AXIS	
STRESS (PSI)	STRAIN (MILS/IN)	STRESS (PSI)	STRAIN (MILS/IN)	STRESS (PSI)	STRAIN (MILS/IN)
0	0.0000	0	0.0000	0	0.0000
300	0.0416	300	0.0188	300	-0.0541
600	0.0730	600	0.0818	600	-0.0128
1000	0.0856	1000	0.0753	1000	0.0240
1500	0.1812	1500	0.1878	1500	0.1639
2000	0.2772	2000	0.2843	2000	0.2849
2500	0.3557	2500	0.3568	2500	0.4059
3000	0.4348	3000	0.4601	3000	0.5129
3500	0.5478	3500	0.5743	3500	0.6333
4000	0.6258	4000	0.6723	4000	0.7545
4500	0.7710	4500	0.7960	4500	0.9046
4750	0.7682	4750	0.7969	4750	0.8992
5000	0.8300	5000	0.8688	5000	0.9679
5000	0.8159	4900	0.8539	5100	1.0158
5000	0.8168	4700	0.8271	5300	1.0522
5000	0.8183	4500	0.7818	5500	1.1024
5000	0.8195	4300	0.7453	5700	1.2099
5000	0.8293	4100	0.7076	5900	1.2549
5000	0.8263	3900	0.6674	6100	1.3530
5000	0.8277	3700	0.6289	6300	1.4032
5000	0.8220	3500	0.5935	6500	1.5244
5000	0.8553	3300	0.5566	6700	1.5977
5000	0.8521	3100	0.5104	6900	1.6934
5000	0.8447	2900	0.4598	7100	1.7937
5000	0.8468	2700	0.4126	7300	1.9095
5000	0.8658	2500	0.3669	7500	2.0392
5000	0.8676	2300	0.3138	7700	2.1263
5000	0.8624	2100	0.2411	7900	2.2566
5000	0.8638	1900	0.1588	8100	2.3779
5000	0.8883	1700	0.0810	8300	2.5529
5000	0.8810	1500	-0.0394	8500	2.7666
5000	0.8799	1300	-0.1628	8700	2.9999
5000	0.8766	1100	-0.2953	8900	3.2017
5000	0.8734	900	-0.5012	9100	3.5545
5000	0.8858	700	-0.8623	9300	4.0249
5000	0.8969	600	-1.1123	9400	4.2744
5000	0.9059	500	-1.4951	9500	4.5641

TENSILE STRENGTHS

IN THE DIRECTION OF THE MAXIMUM PRINCIPAL STRESS = 357 PSI
IN THE DIRECTION OF THE MINIMUM PRINCIPAL STRESS = 404 PSI

STRESS - STRAIN DATA

X-AXIS		Y-AXIS		Z-AXIS	
STRESS (PSI)	STRAIN (MILS/IN)	STRESS (PSI)	STRAIN (MILS/IN)	STRESS (PSI)	STRAIN (MILS/IN)
0	0.0000	0	0.0000	0	0.0000
300	0.0143	300	-0.0333	300	-0.0610
600	0.0552	600	0.0256	600	-0.0253
1000	0.1054	1000	0.0645	1000	0.0317
1500	0.1917	1500	0.1527	1500	0.1238
2000	0.2875	2000	0.2328	2000	0.2222
2500	0.3875	2500	0.3377	2500	0.3522
3000	0.4599	3000	0.4117	3000	0.4103
3500	0.6217	3500	0.5662	3500	0.5539
3750	0.6676	3750	0.6170	3750	0.6064
4250	0.7934	4250	0.7223	4250	0.7076
4750	0.9260	4750	0.8380	4750	0.8129
5000	1.0146	5000	0.9251	5000	0.8914
5000	1.0192	4900	0.8944	5100	0.9305
5000	1.0108	4700	0.8485	5300	0.9952
5000	1.0041	4500	0.8450	5500	1.0879
5000	0.9901	4300	0.7987	5700	1.1102
5000	0.9932	4100	0.7531	5900	1.2093
5000	1.0637	3900	0.7319	6100	1.3009
5000	1.0667	3700	0.6906	6300	1.3739
5000	1.0640	3500	0.6576	6500	1.4582
5000	1.0773	3300	0.6092	6700	1.5545
5000	1.0719	3100	0.5649	6900	1.6384
5000	1.0770	2900	0.5112	7100	1.7619
5000	1.0795	2700	0.4431	7300	1.8323
5000	1.0682	2500	0.3971	7500	1.9123
5000	1.0760	2300	0.3272	7700	2.0671
5000	1.0889	2100	0.2730	7900	2.1905
5000	1.0937	1900	0.1892	8100	2.3503
5000	1.0932	1700	0.0921	8300	2.5148
5000	1.1001	1500	-0.0092	8500	2.7351
5000	1.1126	1300	-0.1132	8700	2.9653
5000	1.1288	1100	-0.3045	8900	3.2019
5000	1.1353	1100	-0.6602	9100	3.6533
5000	1.1329	800	-0.7083	9200	3.8155
5000	1.1358	700	-0.8734	9300	4.0109
5000	1.1975	600	-1.0651	9400	4.2314
5000	1.3735	500	-1.3769	9500	4.5129
5000	1.4036	400	-1.7023	9600	4.8414
5000	1.4287	300	-2.2243	9700	5.1882

TENSILE STRENGTHS

IN THE DIRECTION OF THE MAXIMUM PRINCIPAL STRESS = 356 PSI
IN THE DIRECTION OF THE MINIMUM PRINCIPAL STRESS = 284 PSI

STRESS - STRAIN DATA

X-AXIS		Y-AXIS		Z-AXIS	
STRESS (PSI)	STRAIN (MILS/IN)	STRESS (PSI)	STRAIN (MILS/IN)	STRESS (PSI)	STRAIN (MILS/IN)
0	0.0000	0	0.0000	0	0.0000
300	0.0285	300	-0.0050	300	-0.0016
600	0.0673	600	0.0576	600	0.0450
1000	0.1267	1000	0.1168	1000	0.0834
1500	0.2524	1500	0.2471	1500	0.2528
2000	0.3706	2000	0.3734	2000	0.3808
2500	0.4919	2500	0.5110	2500	0.5309
3000	0.6125	3000	0.6565	3000	0.6494
3500	0.7420	3500	0.7899	3500	0.7727
4000	0.8534	4000	0.9194	4000	0.9124
4500	1.0082	4500	1.0641	4500	1.0395
4750	1.0691	4750	1.1560	4750	1.1097
5000	1.1386	5000	1.2357	5000	1.1947
5075	1.1797	5075	1.2789	4850	1.2004
5150	1.1883	5150	1.2987	4700	1.1847
5250	1.2474	5250	1.3579	4500	1.1572
5350	1.2741	5350	1.3855	4300	1.1367
5450	1.3096	5450	1.4186	4100	1.1187
5550	1.3430	5550	1.4555	3900	1.0689
5650	1.4041	5650	1.5140	3700	1.0281
5750	1.4457	5750	1.5495	3500	0.9959
5850	1.5176	5850	1.6289	3300	0.9408
5950	1.5512	5950	1.6628	3100	0.8866
6050	1.5987	6050	1.7283	2900	0.8491
6150	1.6390	6150	1.7639	2700	0.7912
6250	1.6857	6250	1.8191	2500	0.7331
6350	1.7346	6350	1.8736	2300	0.6333
6450	1.8022	6450	1.9452	2100	0.5581
6550	1.8597	6550	2.0071	1900	0.4626
6650	1.9557	6650	2.1242	1700	0.3418
6750	2.0197	6750	2.1961	1500	0.2415
6950	2.2609	6950	2.4911	1100	-0.2069
7050	2.3419	7050	2.6087	900	-0.3174
7150	2.4291	7150	2.7956	700	-0.6155
7250	2.7006	7250	3.0504	500	-1.1514
7350	2.9686	7350	3.3856	300	-2.1678

TENSILE STRENGTHS

IN THE DIRECTION OF THE MAXIMUM PRINCIPAL STRESS = 0 PSI
IN THE DIRECTION OF THE MINIMUM PRINCIPAL STRESS = 253 PSI

TEST 102 ... TE 5000 SPECIMEN CS- BATCH 3 10 29 80

STRESS - STRAIN DATA

X-AXIS		Y-AXIS		Z-AXIS	
STRESS (PSI)	STRAIN (MILS/IN)	STRESS (PSI)	STRAIN (MILS/IN)	STRESS (PSI)	STRAIN (MILS/IN)
0	0.0000	0	0.0000	0	0.0000
300	0.0309	300	-0.0015	300	-0.0188
600	0.0779	600	0.0617	600	0.0248
1000	0.1625	1000	0.1348	1000	0.1146
1500	0.2911	1500	0.2560	1500	0.2345
2000	0.4475	2000	0.3927	2000	0.3885
2500	0.5729	2500	0.5091	2500	0.5201
3000	0.7111	3000	0.6624	3000	0.6638
3500	0.8738	3500	0.8182	3500	0.8287
4000	1.0252	4000	0.9570	4000	0.9811
4500	1.1998	4500	1.1278	4500	1.1539
5000	1.3533	5000	1.3075	5000	1.3095
4850	1.3520	5075	1.3929	5075	1.3871
4700	1.3154	5150	1.4209	5150	1.4238
4500	1.2861	5250	1.4640	5250	1.4723
4300	1.2298	5350	1.5281	5350	1.5261
4100	1.1653	5450	1.5585	5450	1.5759
3900	1.1065	5550	1.6116	5550	1.6281
3700	1.0592	5650	1.6808	5650	1.7018
3500	0.9851	5750	1.7491	5750	1.7753
3300	0.9869	5850	1.8026	5850	1.8277
3100	0.9291	5950	1.8515	5950	1.8856
2900	0.8556	6050	1.9313	6050	1.9722
2700	0.7551	6150	2.0143	6150	2.0524
2500	0.7084	6250	2.0850	6250	2.1440
2300	0.6111	6350	2.1480	6350	2.2071
2100	0.5004	6450	2.2500	6450	2.3027
1900	0.3950	6550	2.3744	6550	2.4313
1700	0.2902	6650	2.4633	6650	2.5239
1500	0.1640	6750	2.5828	6750	2.6445
1100	-0.3510	6950	3.0282	6950	3.1191
900	-0.5161	7050	3.1562	7050	3.3659
700	-0.8793	7150	3.3318	7150	3.4543
500	-1.2975	7250	3.5774	7250	3.7230
300	-2.3382	7350	4.0151	7350	4.3044

TENSILE STRENGTHS

IN THE DIRECTION OF THE MAXIMUM PRINCIPAL STRESS = 0 PSI
IN THE DIRECTION OF THE MINIMUM PRINCIPAL STRESS = 0 PSI

STRESS - STRAIN DATA

X-AXIS		Y-AXIS		Z-AXIS	
STRESS (PSI)	STRAIN (MILS/IN)	STRESS (PSI)	STRAIN (MILS/IN)	STRESS (PSI)	STRAIN (MILS/IN)
0	0.0000	0	0.0000	0	0.0000
300	0.0249	300	-0.0245	300	-0.0279
600	0.0955	600	0.0700	600	0.0426
1000	0.1477	1000	0.1105	1000	0.1110
1500	0.2488	1500	0.2016	1500	0.2152
2000	0.3495	2000	0.3014	2000	0.3112
2500	0.4775	2500	0.4279	2500	0.4490
3000	0.6010	3000	0.5635	3000	0.5615
3500	0.7158	3500	0.6807	3500	0.6367
4000	0.8614	4000	0.8227	4000	0.7631
4500	1.0159	4500	0.9673	4500	0.8583
4750	1.0754	4750	1.0415	4750	0.8937
5000	1.1407	5000	1.1343	5000	0.9580
5075	1.1549	5075	1.1377	4850	0.9232
5150	1.1778	5150	1.1622	4700	0.9054
5250	1.2015	5250	1.1887	4500	0.8959
5350	1.2405	5350	1.2290	4300	0.8446
5450	1.2703	5450	1.2478	4100	0.8169
5550	1.3082	5550	1.2927	3900	0.7789
5650	1.3559	5650	1.3438	3700	0.7192
5750	1.3921	5750	1.3842	3500	0.6814
5850	1.4368	5850	1.4355	3300	0.6311
5950	1.4695	5950	1.4679	3100	0.6027
6050	1.5274	6050	1.5362	2900	0.5501
6150	1.5676	6150	1.5805	2700	0.5033
6250	1.6036	6250	1.6253	2500	0.4516
6350	1.6513	6350	1.6771	2300	0.3853
6450	1.7204	6450	1.7563	2100	0.3179
6550	1.7733	6550	1.8150	1900	0.2281
6650	1.8363	6650	1.8845	1700	0.1431
6750	1.9011	6750	1.9543	1500	0.0489
6850	1.9704	6850	2.0426	1300	-0.0817
6950	2.0785	6950	2.1576	1100	-0.1844
7050	2.1652	7050	2.2711	900	-0.3520
7150	2.2649	7150	2.3785	700	-0.5745
7250	2.4209	7250	2.5639	500	-0.8879
7325	2.5824	7325	2.7370	350	-1.2414
7375	2.6838	7375	2.8614	250	-1.5757
7425	2.8218	7425	3.0115	150	-2.0860

TENSILE STRENGTHS

IN THE DIRECTION OF THE MAXIMUM PRINCIPAL STRESS = 473 PSI
IN THE DIRECTION OF THE MINIMUM PRINCIPAL STRESS = 351 PSI

APPENDIX B.

STRESS-STRAIN CURVES FOR TRIAXIAL TESTS

This appendix contains the stress-strain curves generated during each successful triaxial test. The ordinate values are mils/in. of strain and the values on the abscissa are the maximum principal stress in ksi. The numbers 1, 2 and 3 marked on the curves represent the principal strains and the curve marked "V" is the volumetric strain curve.

TEST SA ...: TC 3750

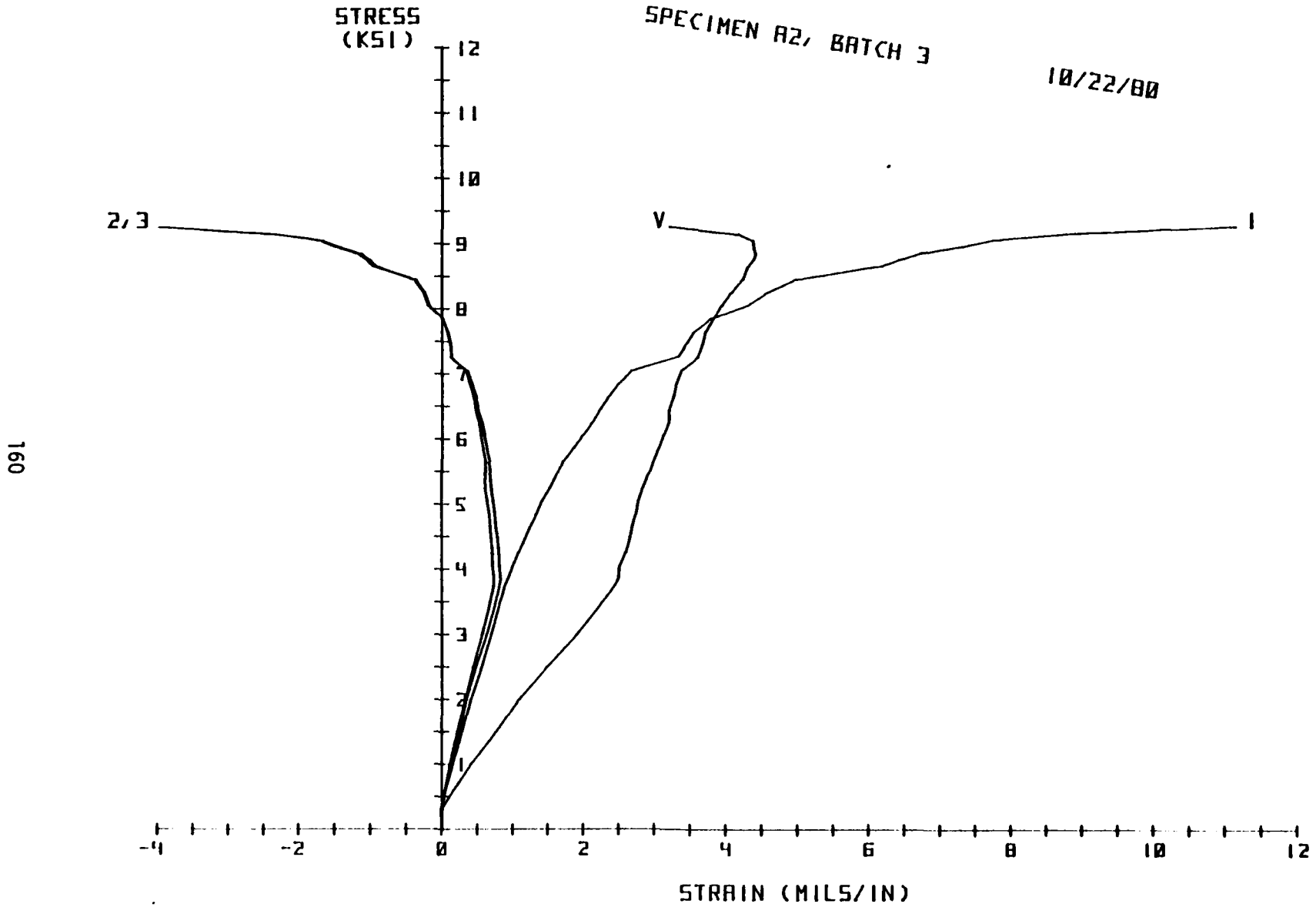

160

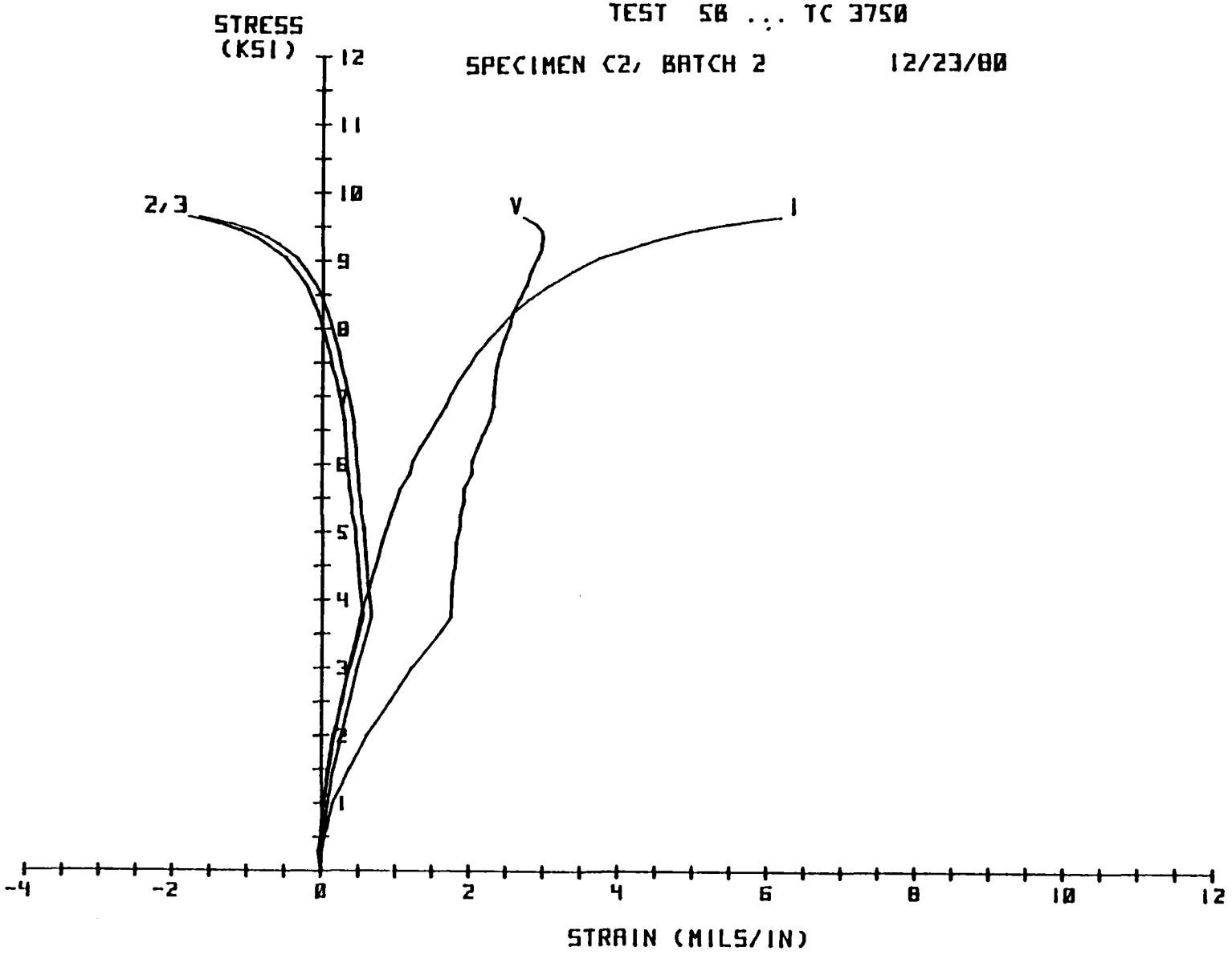
TEST 5B ... TC 3750
SPECIMEN C2, BATCH 2
12/23/80
STRESS
(KSI)
12
11
10
9
8
7
6
5
4
3
2
1
2,3
V
I
-4
-2
0
2
4
6
8
10
12
STRAIN (MILS/IN)

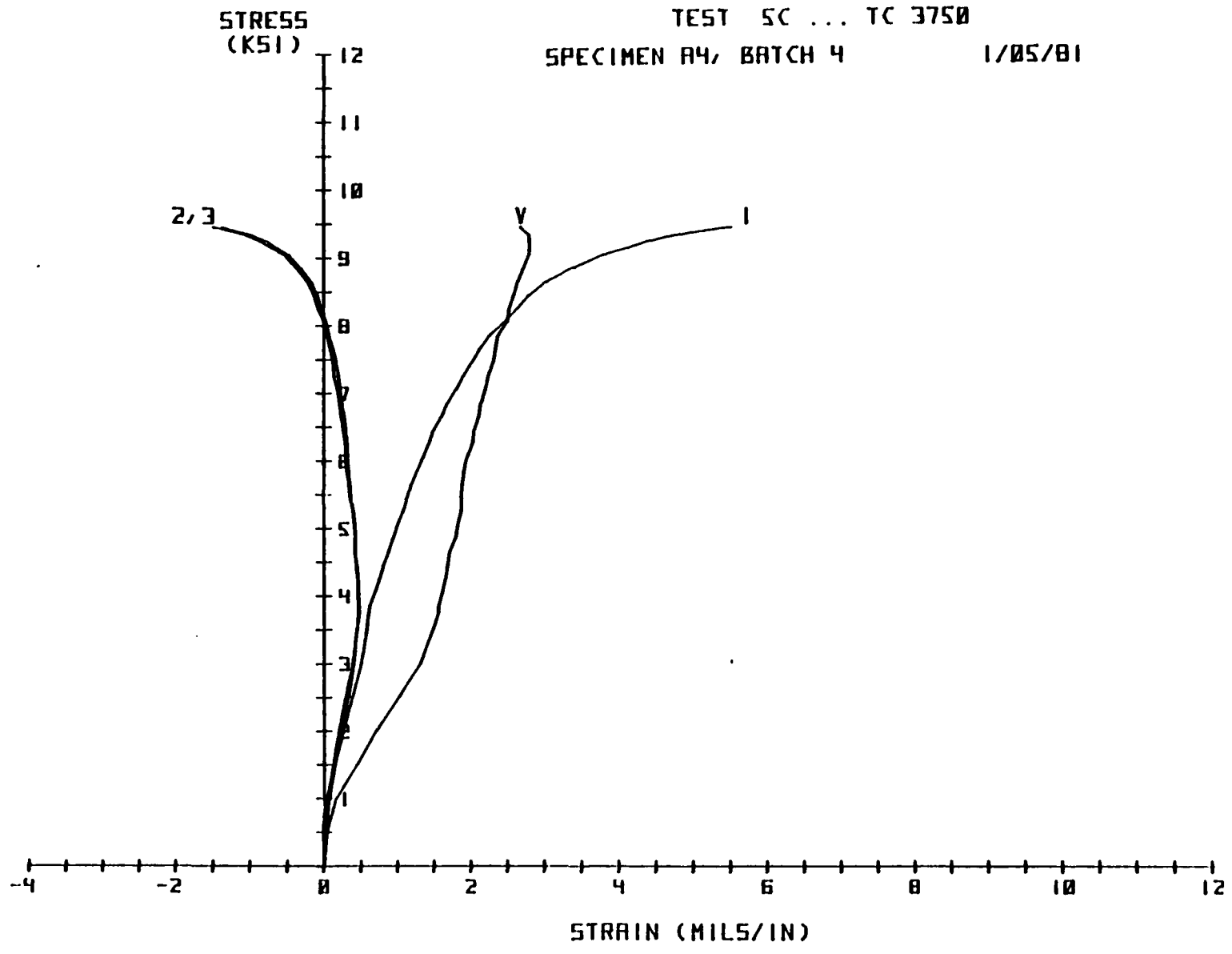
STRESS
(KSI)
TEST SC ... TC 3750
SPECIMEN A4, BATCH 4
1/05/81
12
11
10
9
8
7
6
5
4
3
2
1
2,3
V
I
-4
-2
0
2
4
6
8
10
12
STRAIN (MILS/IN)

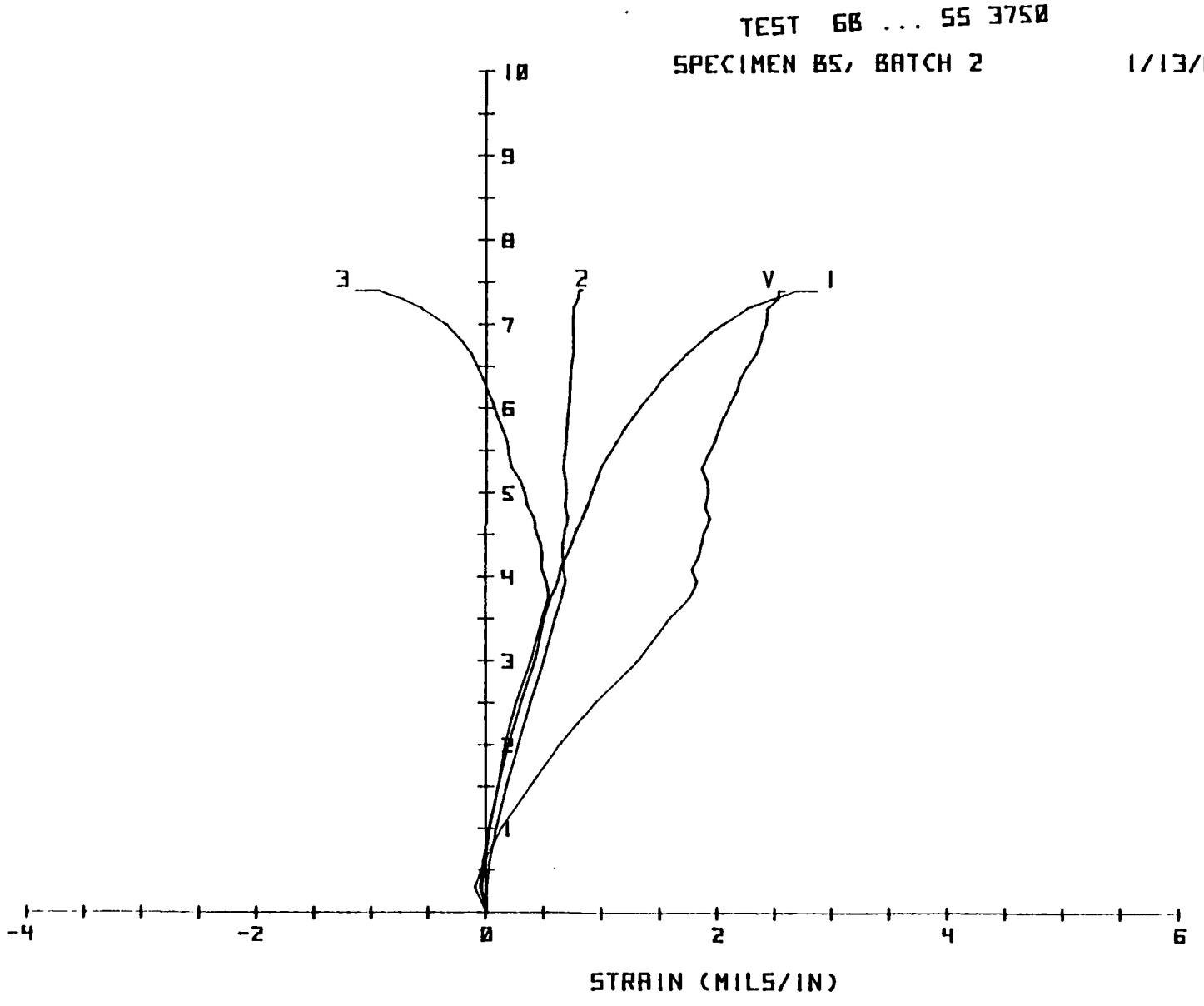
TEST 68 ... SS 3750
SPECIMEN B5, BATCH 2
1/13/81
10
9
8
7
6
5
4
3
2
1
3
2
V
1
-4
-2
0
2
4
6
STRAIN (MILS/IN)

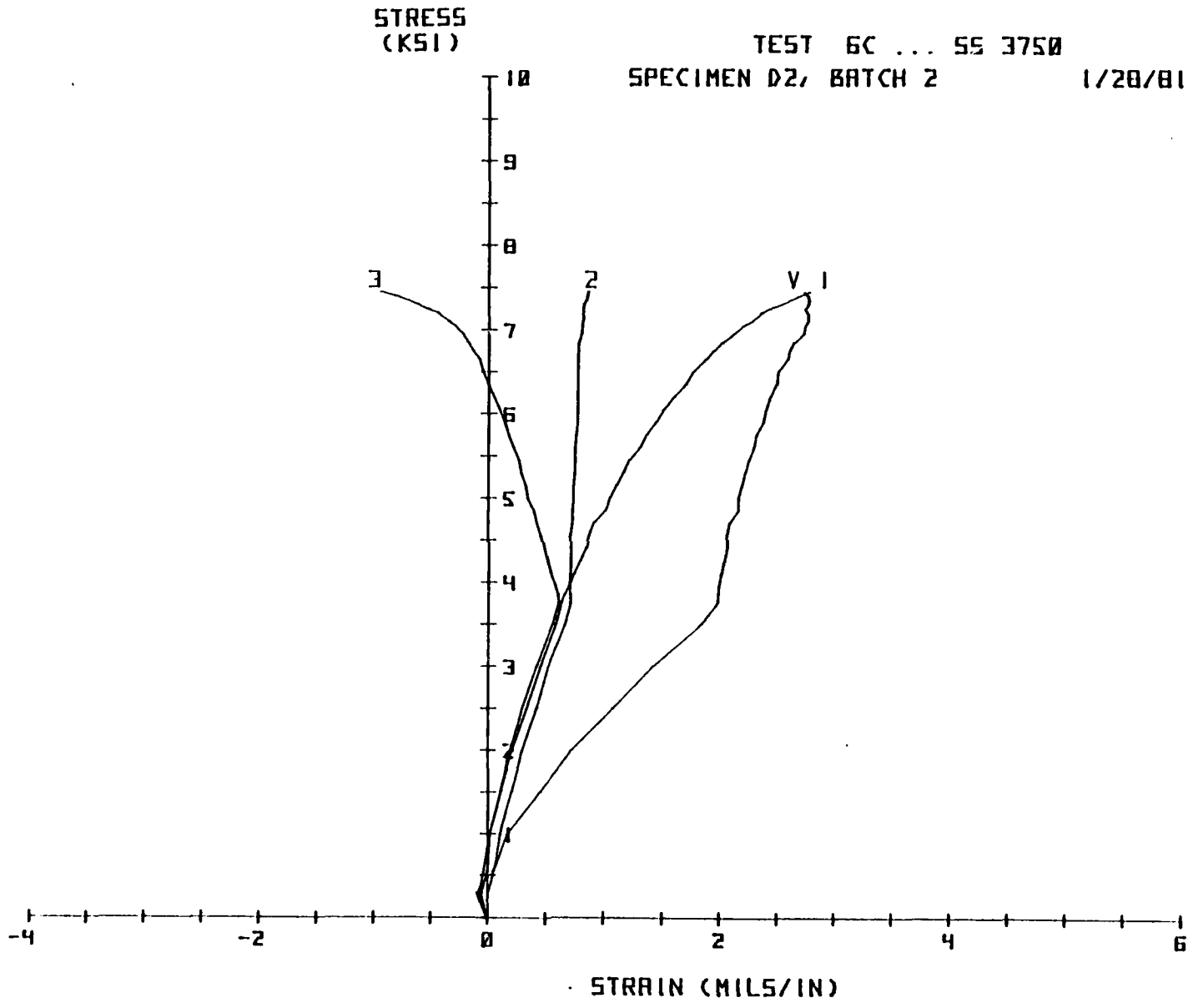
STRESS
(KSI)
TEST 6C ... SS 3750
SPECIMEN D2, BATCH 2
1/20/81
10
9
8
7
6
5
4
3
2
1
3
2
1
-4
-2
0
2
4
6
STRAIN (MILS/IN)

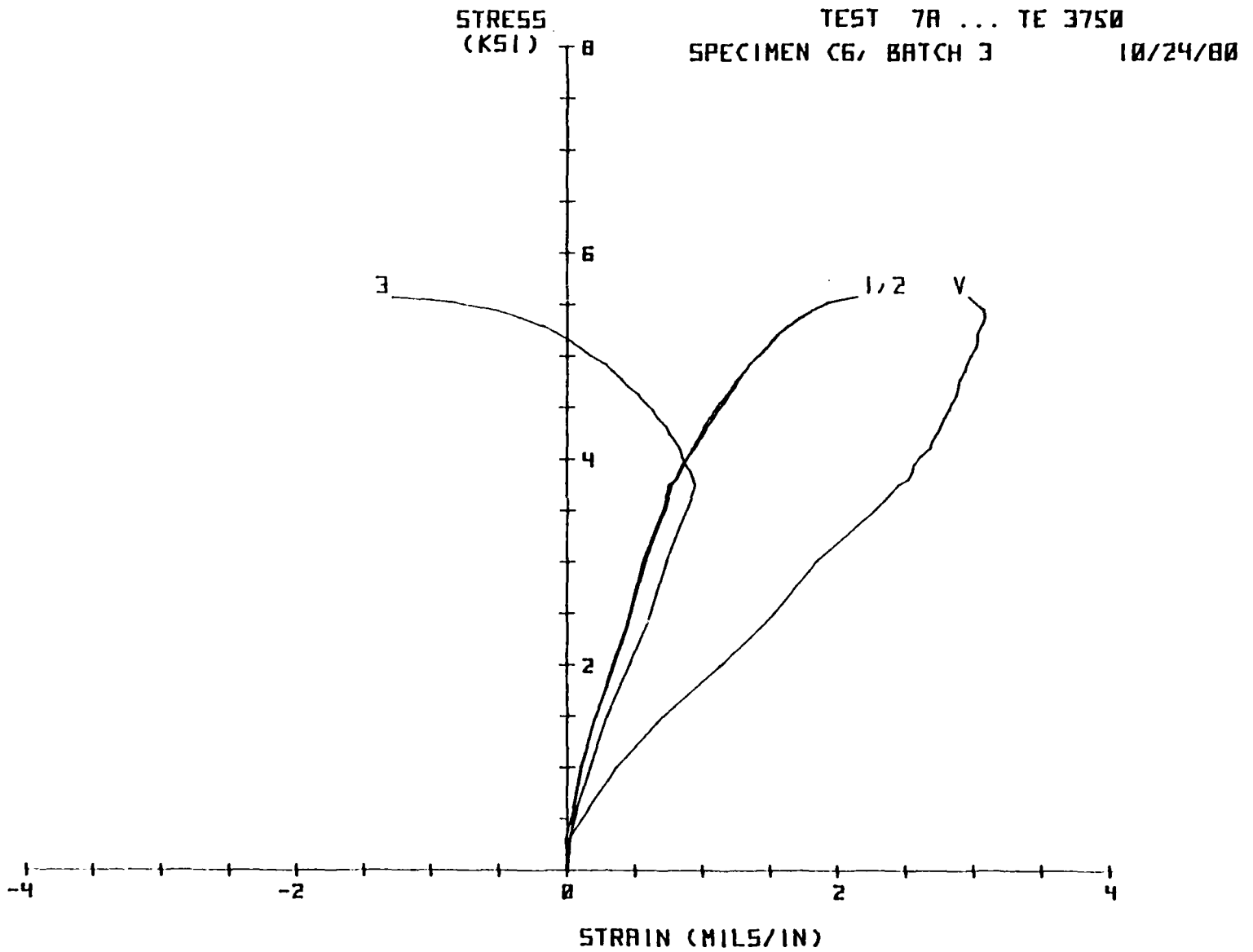
STRESS
(KSI)
TEST 7A ... TE 3750
SPECIMEN C6, BATCH 3
10/24/80
8
6
4
2
3
1,2
V
-4
-2
0
2
4
STRAIN (MILS/IN)

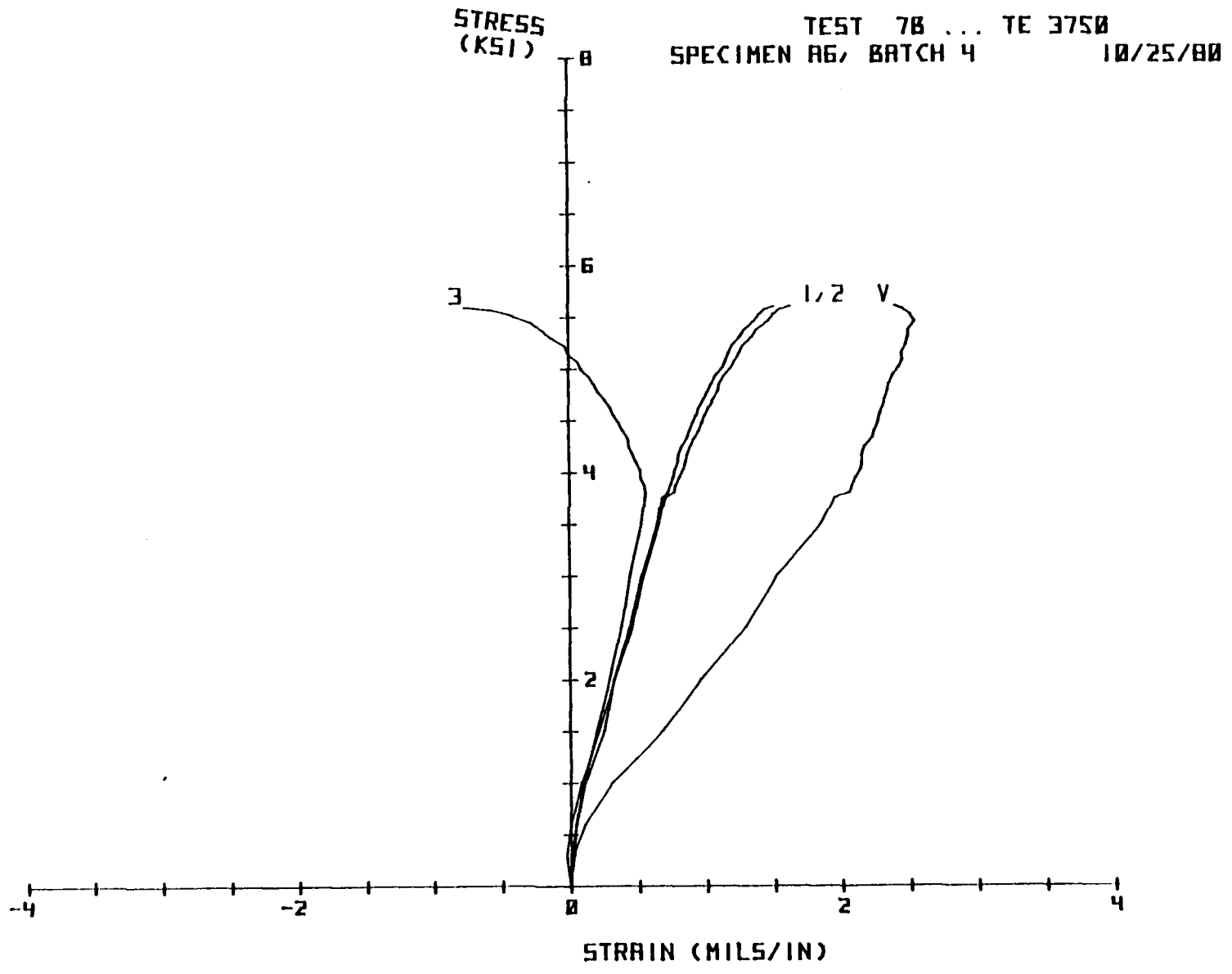
STRESS
(KSI)
TEST 7B ... TE 3750
SPECIMEN B6, BATCH 4
10/25/80
8
6
4
2
3
1,2 V
-4
-2
0
2
4
STRAIN (MILS/IN)

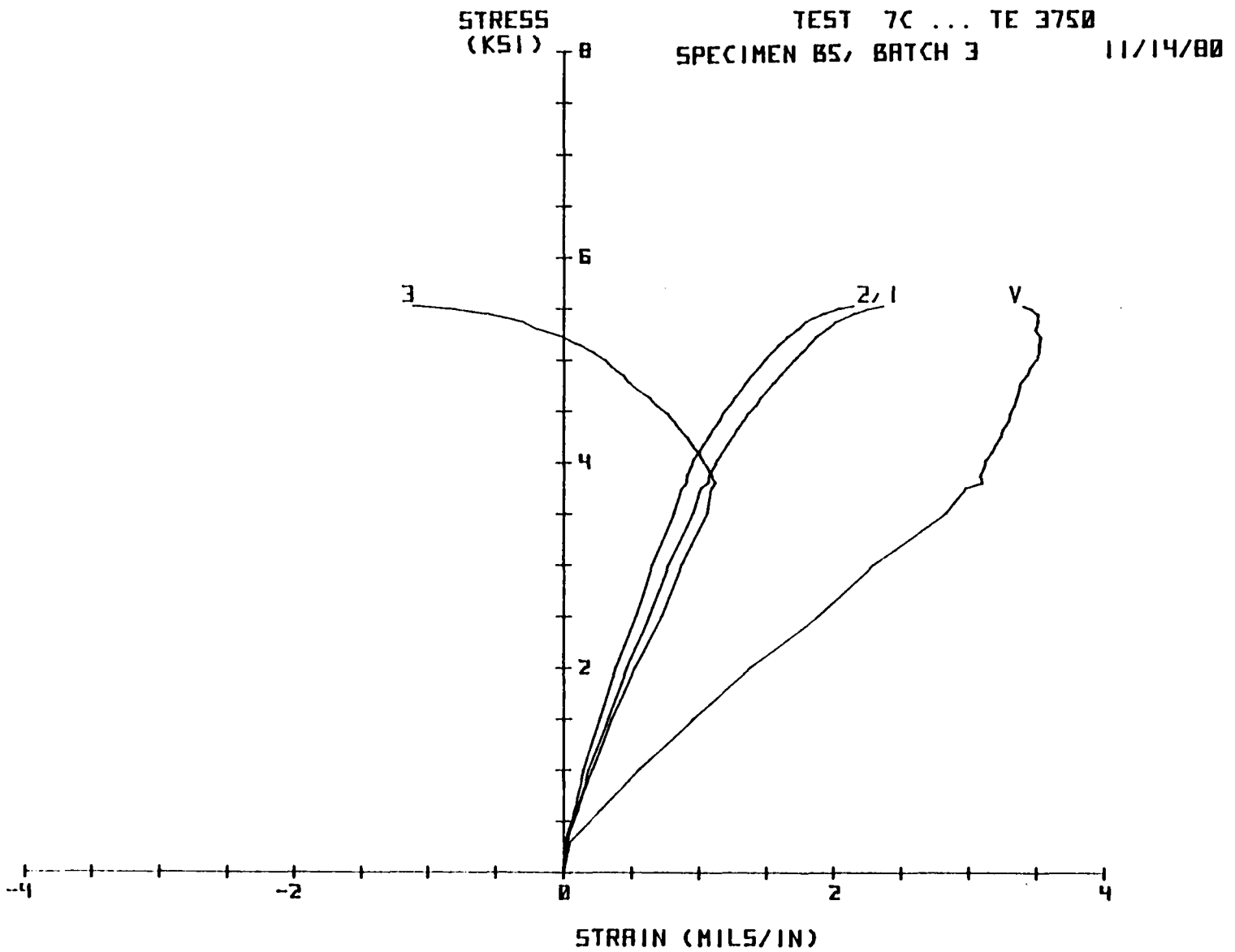
STRESS
(KSI)
TEST 7C ... TE 3750
SPECIMEN B5, BATCH 3
11/14/80
8
6
4
2
3
2, 1
V
-4
-2
0
2
4
STRAIN (MILS/IN)

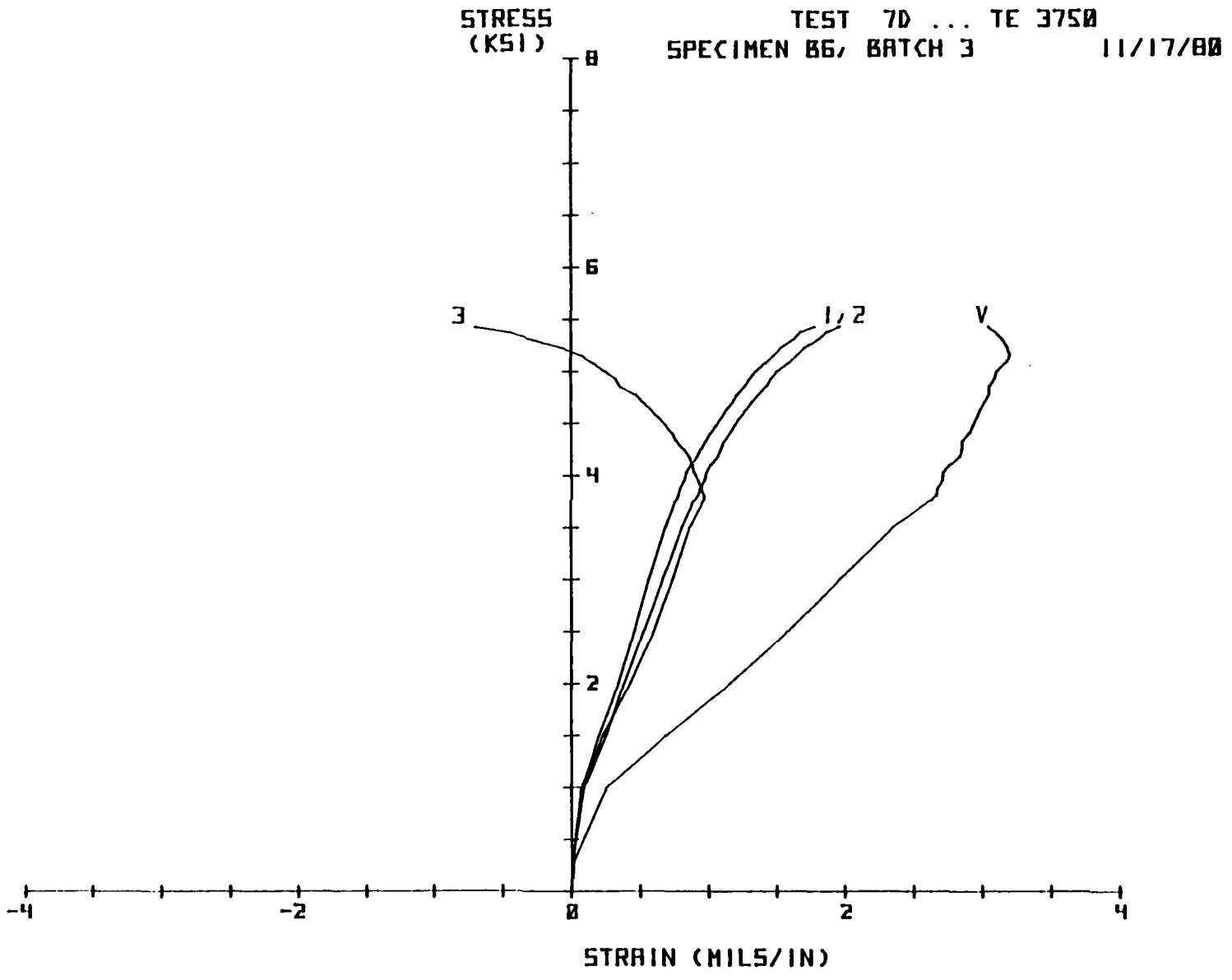
STRESS
(KSI)
TEST 7D ... TE 3750
SPECIMEN B6, BATCH 3
11/17/80
8
6
4
2
3
1,2
V
-4
-2
0
2
4
STRAIN (MILS/IN)

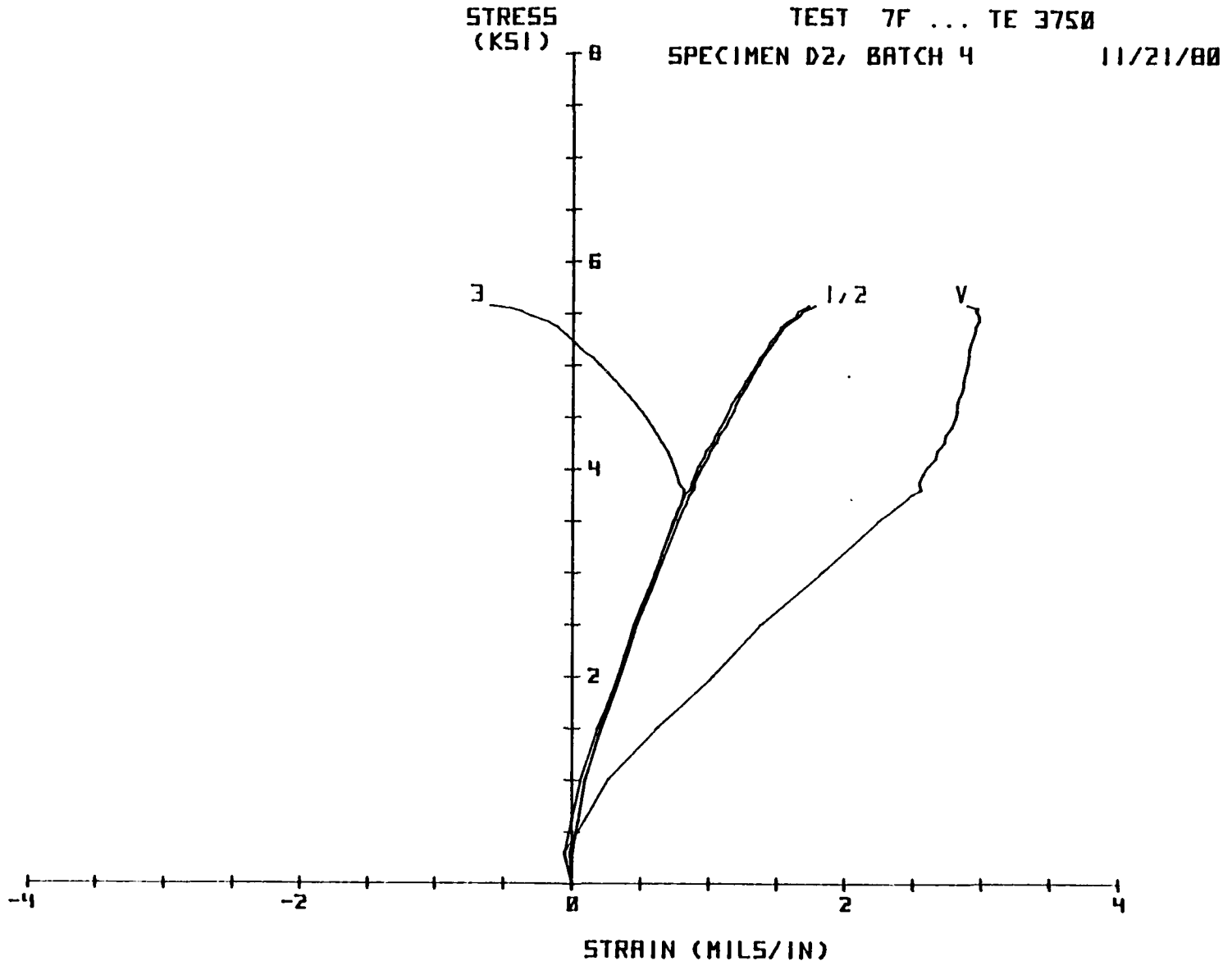
STRESS
(KSI)
TEST 7F ... TE 3750
SPECIMEN D2, BATCH 4
11/21/80
8
6
4
2
3
1/2
V
-4
-2
0
2
4
STRAIN (MILS/IN)

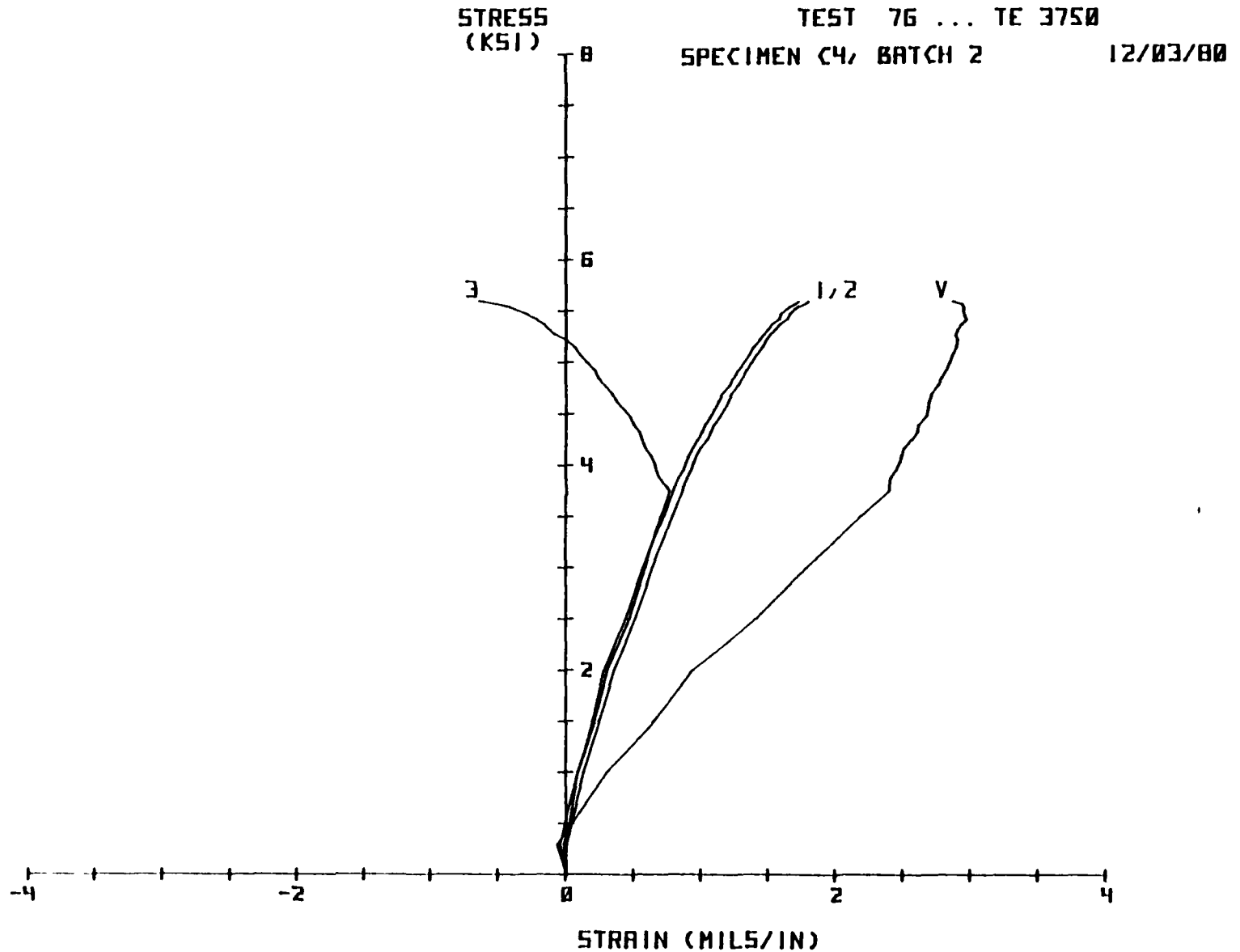
STRESS
(KSI)
TEST 76 ... TE 3750
SPECIMEN C4, BATCH 2
12/03/80
8
6
4
2
3
1,2
V
-4
-2
0
2
4
STRAIN (MILS/IN)

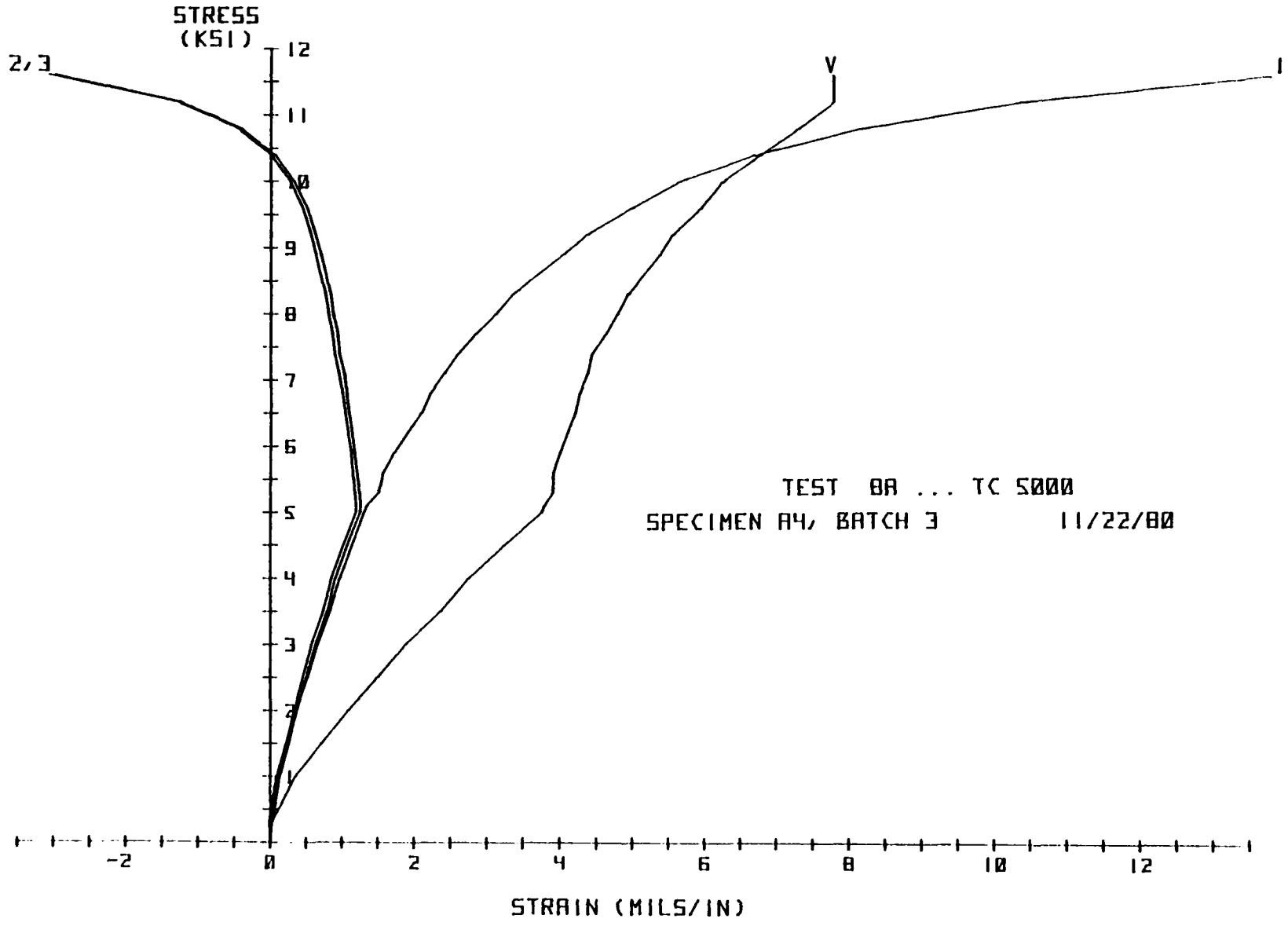
STRESS
(KSI)
12
11
10
9
8
7
6
5
4
3
2
1
2,3
V
I
TEST 8A ... TC 5000
SPECIMEN A4, BATCH 3 11/22/80
-2
0
2
4
6
8
10
12
STRAIN (MILS/IN)

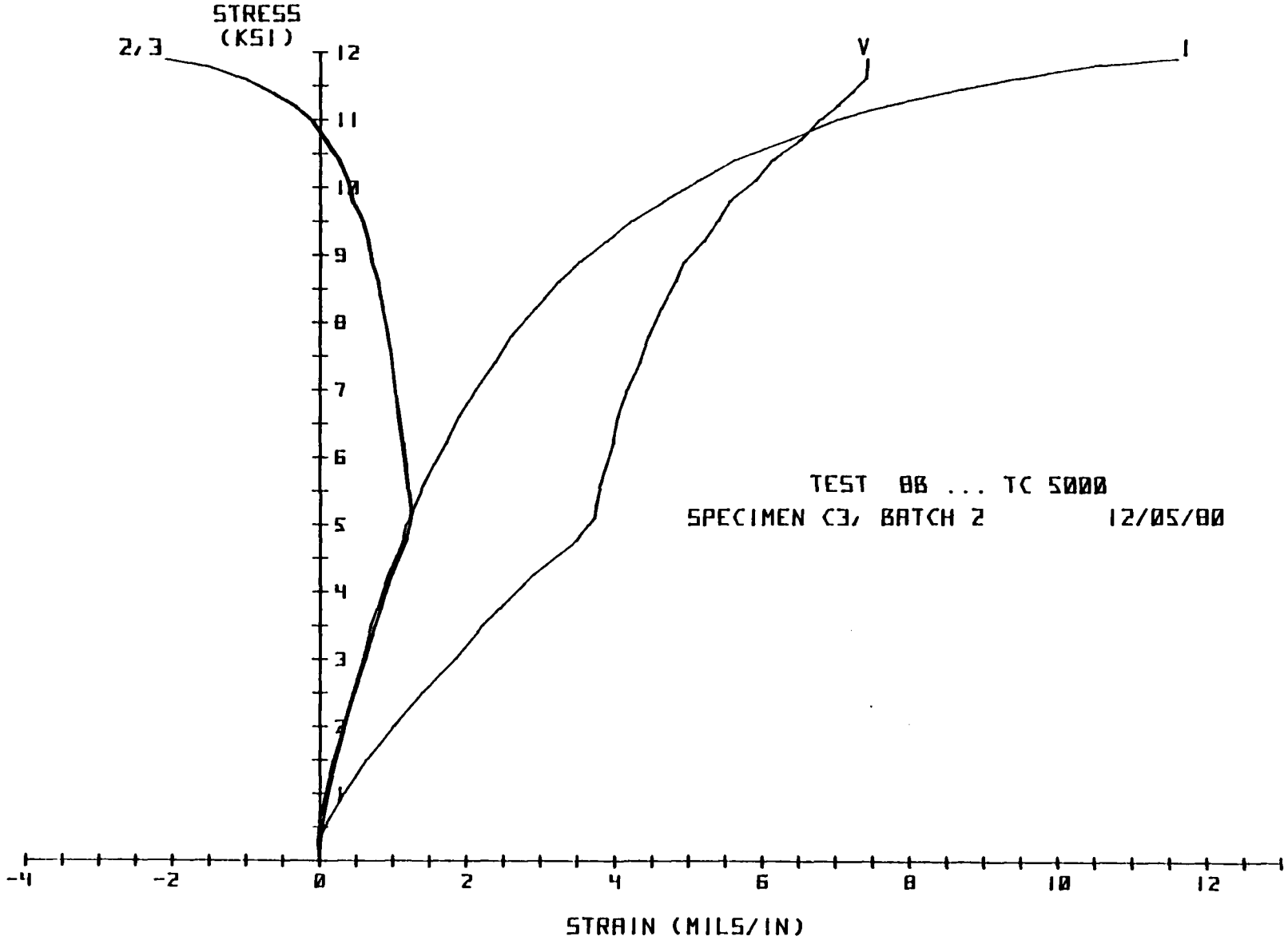
STRESS
(KSI)
2,3
V
1
12
11
10
9
8
7
6
5
4
3
2
1
-4
-2
0
2
4
6
8
10
12
STRAIN (MILS/IN)
TEST 88 ... TC 5000
SPECIMEN (3, BATCH 2
12/05/80

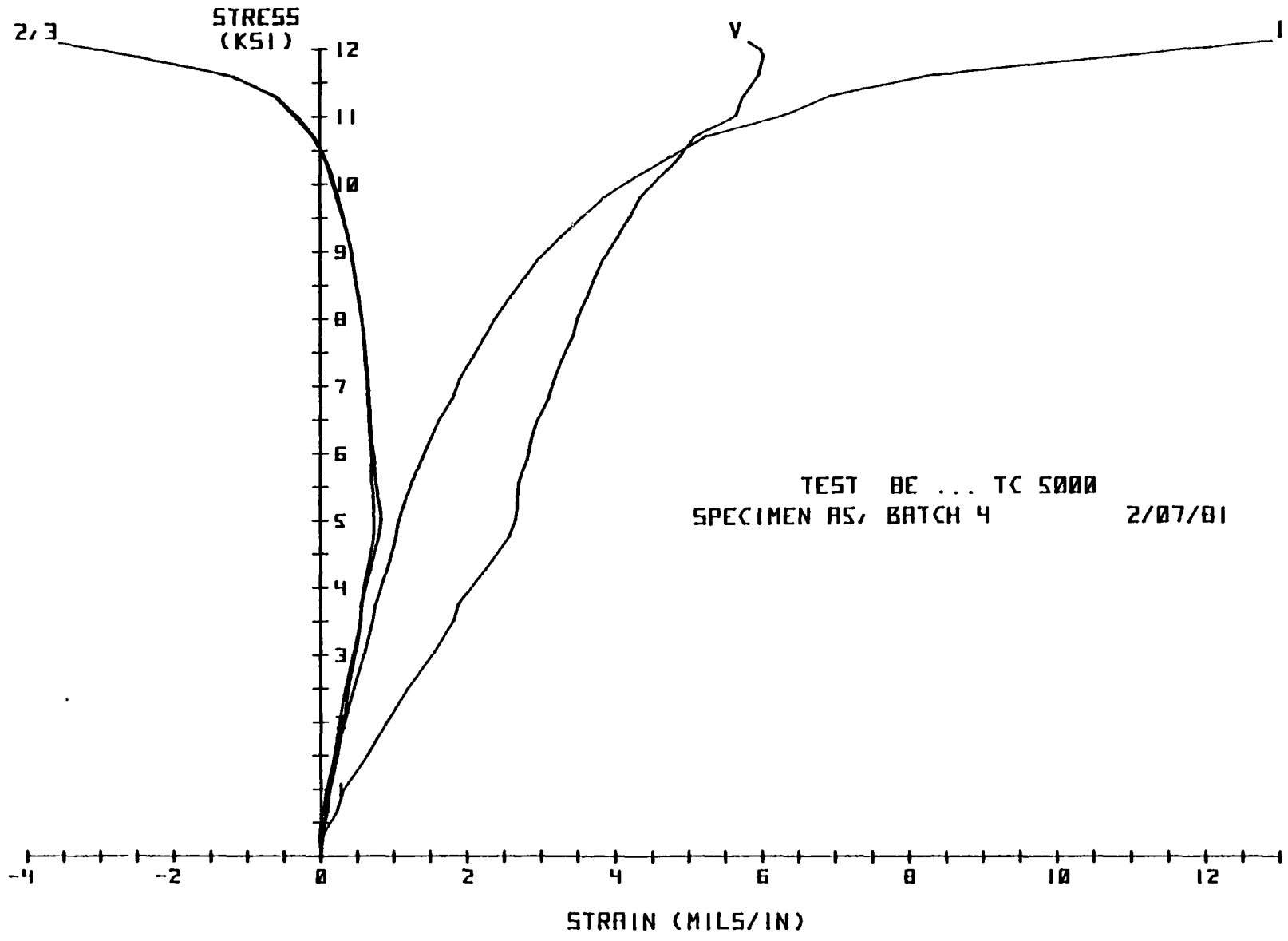
STRESS
(KSI)
2,3
V
1
12
11
10
9
8
7
6
5
4
3
2
1
-4
-2
0
2
4
6
8
10
12
STRAIN (MILS/IN)
TEST BE ... TC 5000
SPECIMEN A5, BATCH 4
2/07/81

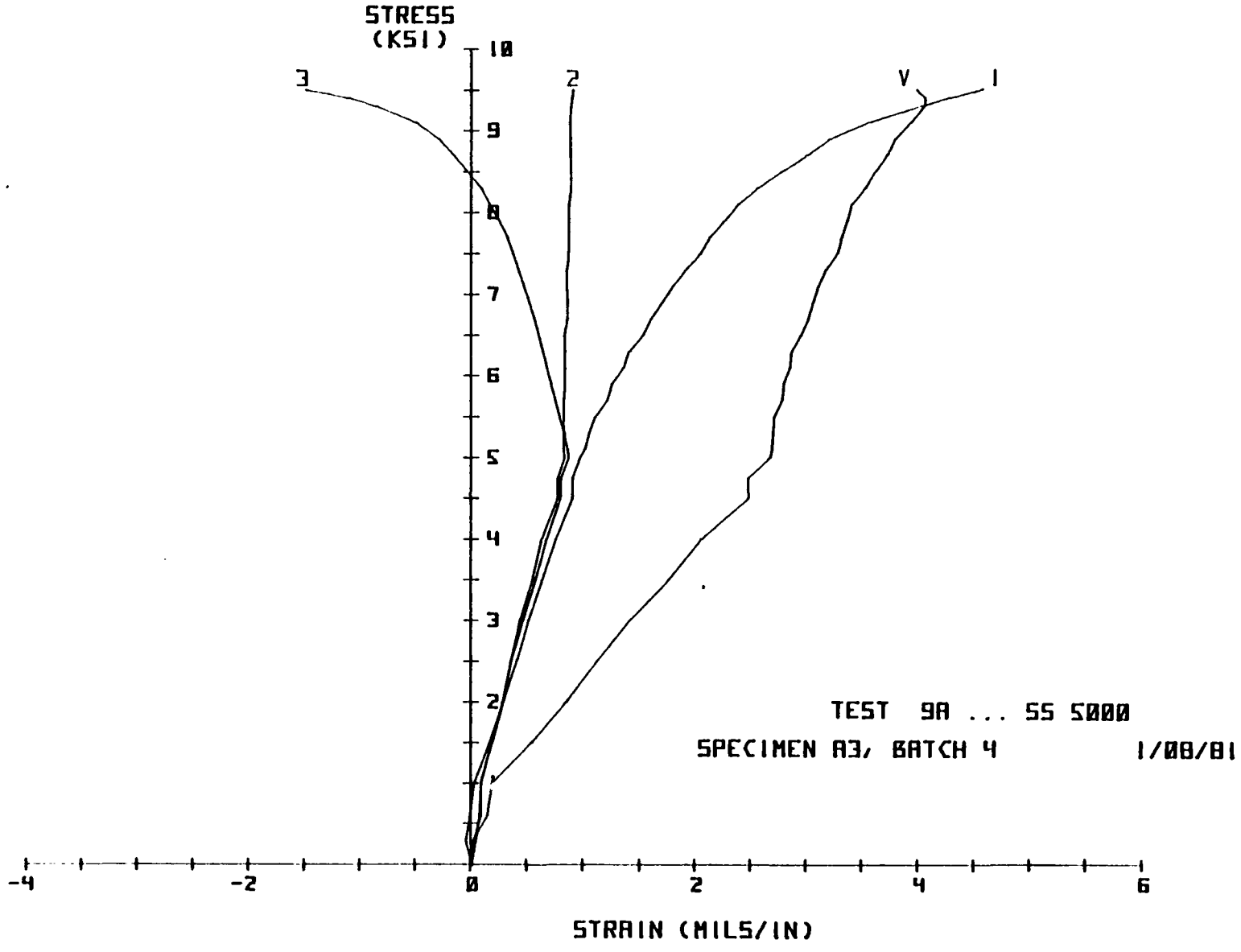
STRESS
(KSI)
10
9
8
7
6
5
4
3
2
3
2
V
1
-4
-2
0
2
4
6
STRAIN (MILS/IN)
TEST 9A ... 55 5000
SPECIMEN A3, BATCH 4
1/08/81

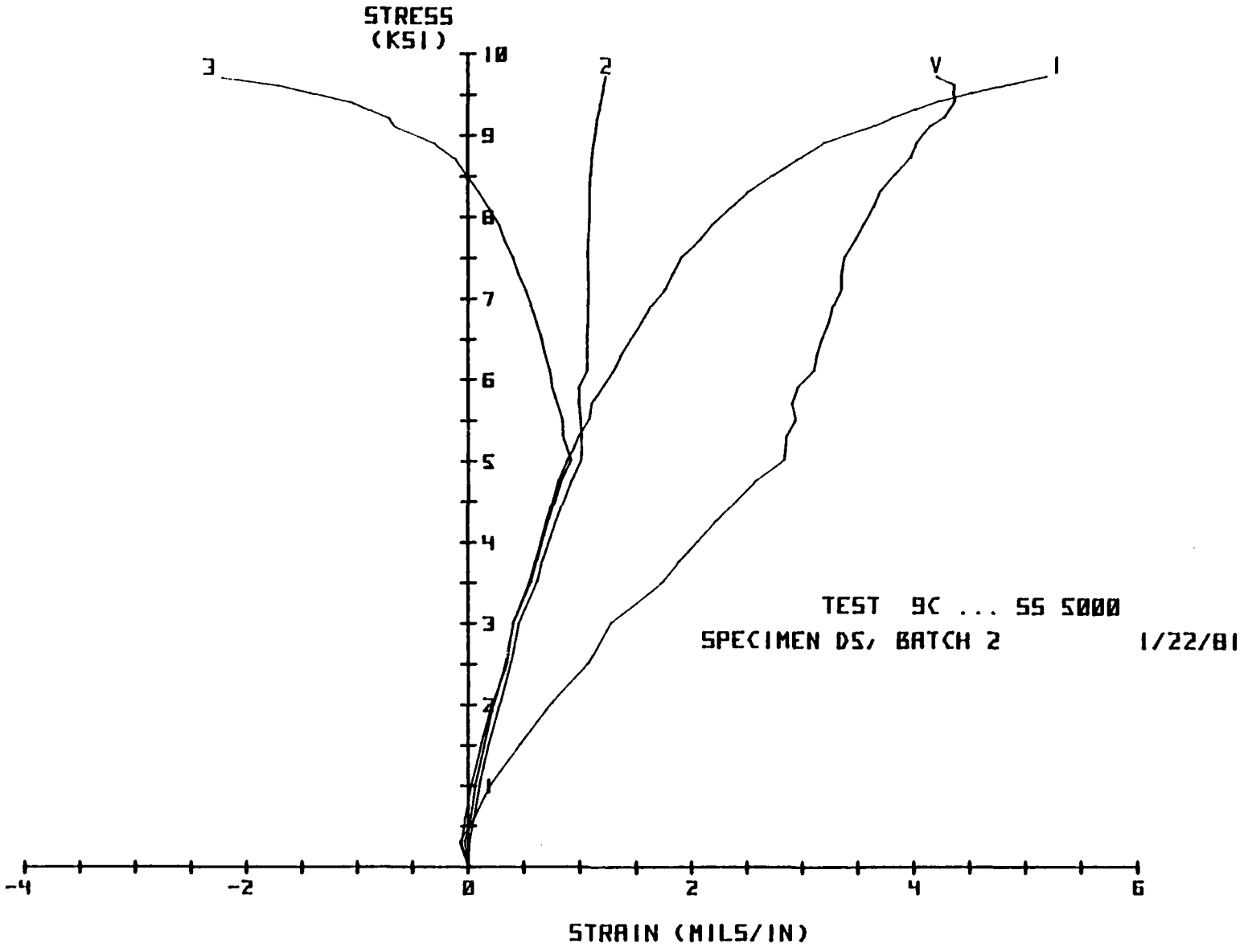
STRESS
(KSI)
10
9
8
7
6
5
4
3
2
1
3
2
V
1
TEST 9C ... SS 5000
SPECIMEN DS, BATCH 2
1/22/81
-4
-2
0
2
4
6
STRAIN (MILS/IN)

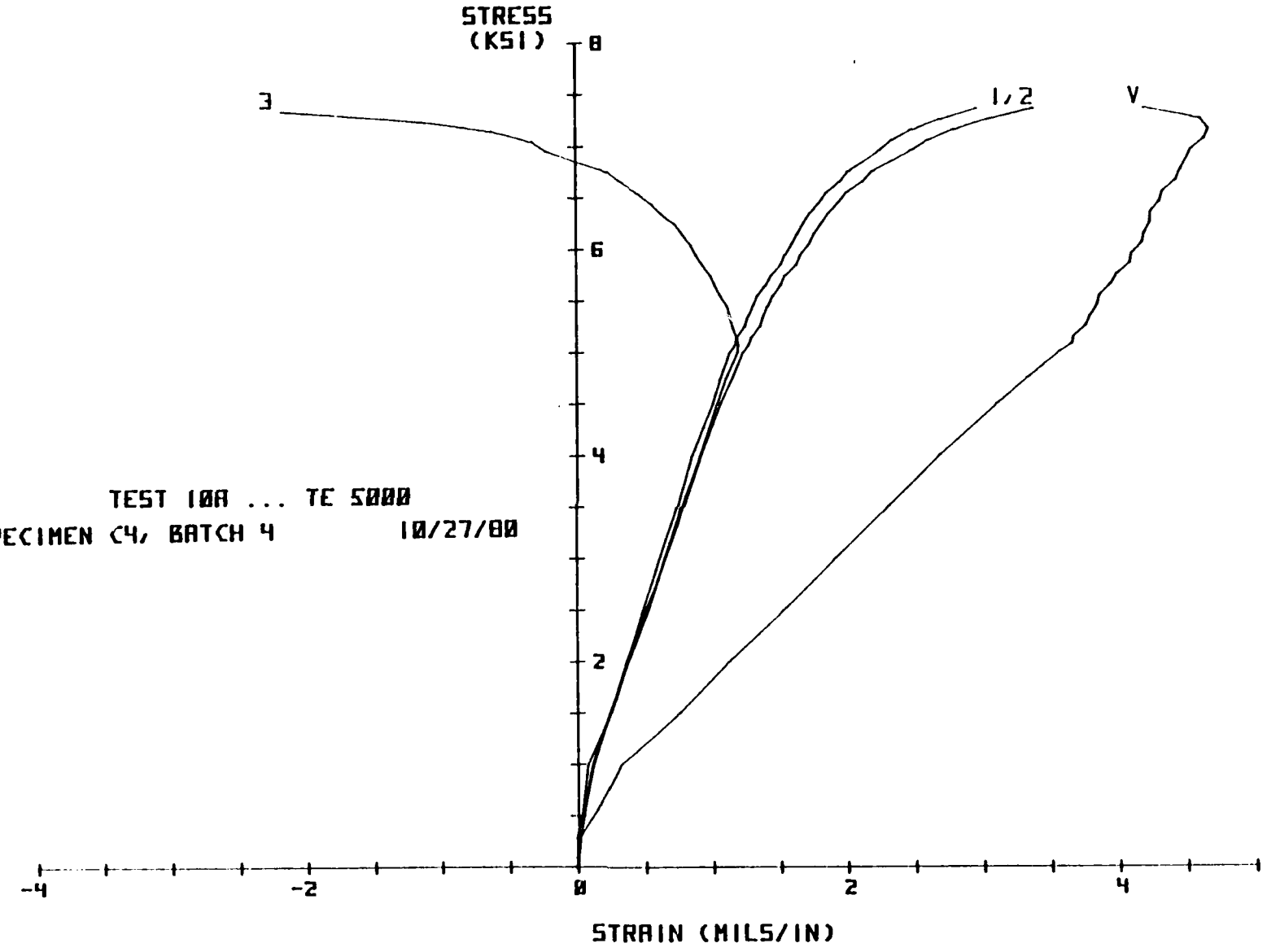
STRESS
(KSI)
8
6
4
2
3
1,2
V
TEST 10A ... TE 5000
SPECIMEN C4, BATCH 4
10/27/80
-4
-2
0
2
4
STRAIN (MILS/IN)

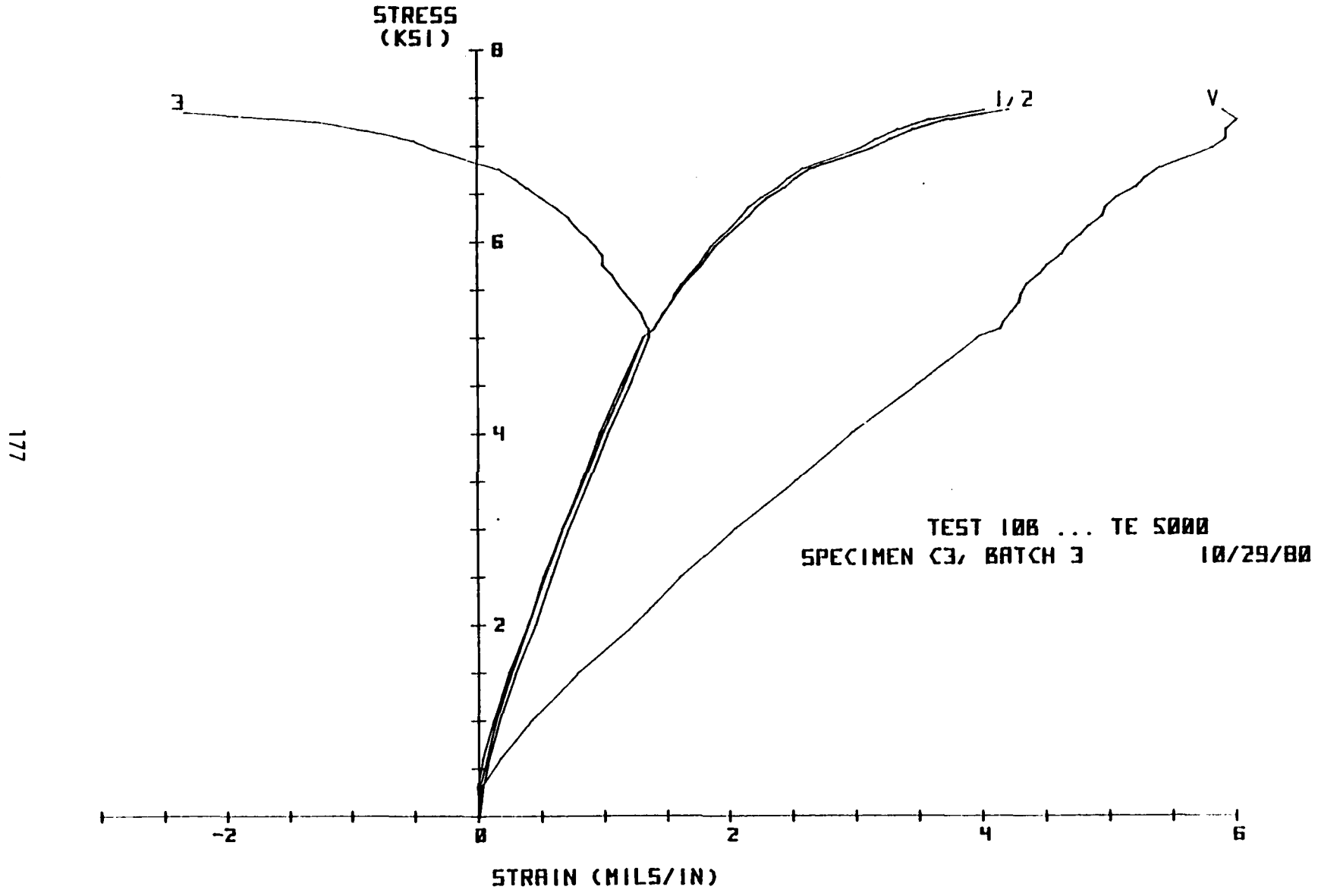
STRESS
(KSI)
8
6
4
2
3
1, 2
V
TEST 108 ... TE 5000
SPECIMEN (3, BATCH 3
10/29/80
-2
0
2
4
6
STRAIN (MILS/IN)

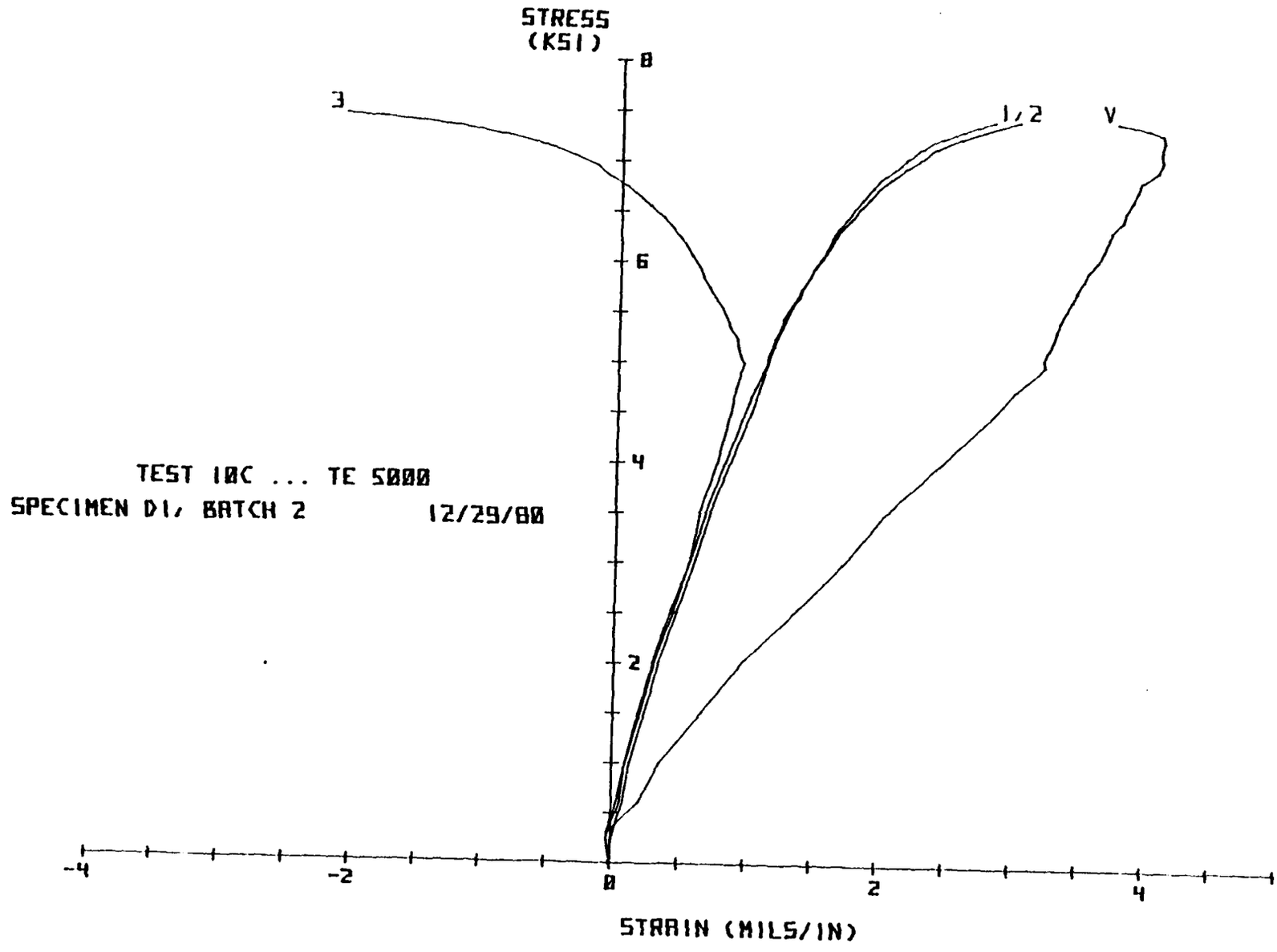
STRESS
(KSI)
8
6
4
2
3
1, 2
V
TEST 10C ... TE 5000
SPECIMEN D1, BATCH 2
12/29/80
-4
-2
0
2
4
STRAIN (MILS/IN)

APPENDIX C.

STRESS-STRAIN DATA FOR BIAXIAL TESTS

This appendix contains the stress-strain data for each successful biaxial tests. The data sheets are arranged in order of test number. The axes which head the columns are the axes of the cubical cell. Stresses are given in psi and strains are given in mils/in. 1 mil/in. = 0.1% strain = 10^{-3} in/in.

STRESS - STRAIN DATA

X-AXIS		Y-AXIS		Z-AXIS	
STRESS (PSI)	STRAIN (MILS/IN)	STRESS (PSI)	STRAIN (MILS/IN)	STRESS (PSI)	STRAIN (MILS/IN)
0	0.0000	0	0.0000	0	0.0000
0	0.0044	0	0.0068	200	-0.0307
0	-0.0001	0	0.0035	350	-0.0306
0	-0.0145	0	-0.0008	500	-0.0175
0	-0.0146	0	-0.0016	650	0.0249
0	-0.0251	0	-0.0106	800	0.0548
0	-0.0312	0	-0.0209	950	0.1006
0	-0.0385	0	-0.0308	1100	0.1498
0	-0.0427	0	-0.0365	1250	0.1951
0	-0.0543	0	-0.0448	1400	0.2363
0	-0.0630	0	-0.0598	1550	0.2663
0	-0.0707	0	-0.0630	1700	0.3176
0	-0.0836	0	-0.0717	1850	0.3583
0	-0.0853	0	-0.0772	2000	0.4124
0	-0.0903	0	-0.0848	2150	0.4648
0	-0.0967	0	-0.0942	2300	0.5267
0	-0.1127	0	-0.1069	2450	0.5829
0	-0.1317	0	-0.1244	2600	0.6203
0	-0.1334	0	-0.1369	2750	0.6802
0	-0.1412	0	-0.1404	2900	0.7418
0	-0.1426	0	-0.1502	3050	0.8125
0	-0.1620	0	-0.1650	3200	0.8973
0	-0.1720	0	-0.1792	3350	0.9538
0	-0.2001	0	-0.2024	3500	1.0543
0	-0.2291	0	-0.2319	3650	1.1554
0	-0.2744	0	-0.2671	3800	1.2382
0	-0.3076	0	-0.3092	3950	1.3584
0	-0.3466	0	-0.3400	4100	1.4807
0	-0.4100	0	-0.3972	4250	1.6227
0	-0.4840	0	-0.4553	4400	1.7793
0	-0.5731	0	-0.5395	4550	1.9545
0	-0.6756	0	-0.6305	4650	2.1332
0	-0.7979	0	-0.7402	4750	2.3113

TENSILE STRENGTHS

IN THE DIRECTION OF THE MAXIMUM PRINCIPAL STRESS = 301 PSI
IN THE DIRECTION OF THE MINIMUM PRINCIPAL STRESS = 374 PSI

TEST [illegible] UNIAXIAL SPECIMEN SIZ- BATCH 3 3 18 8.

STRESS - STRAIN DATA

X-AXIS		Y-AXIS		Z-AXIS	
STRESS (PSI)	STRAIN (MILS/IN)	STRESS (PSI)	STRAIN (MILS/IN)	STRESS (PSI)	STRAIN (MILS/IN)
0	0.0000	0	0.0000	0	0.0000
0	-0.0006	0	0.0046	200	-0.0174
0	-0.0046	0	0.0108	350	0.0005
0	0.0020	0	0.0119	500	0.0568
0	-0.0024	0	0.0084	650	0.0966
0	-0.0053	0	-0.0030	800	0.1437
0	-0.0080	0	-0.0073	950	0.1999
0	-0.0107	0	-0.0116	1100	0.2018
0	-0.0131	0	-0.0182	1250	0.2721
0	-0.0222	0	-0.0225	1400	0.3001
0	-0.0300	0	-0.0308	1550	0.3477
0	-0.0360	0	-0.0359	1700	0.4092
0	-0.0444	0	-0.0437	1850	0.4503
0	-0.0469	0	-0.0582	2000	0.5221
0	-0.0634	0	-0.0728	2150	0.5326
0	-0.0773	0	-0.0857	2300	0.6097
0	-0.0852	0	-0.0924	2450	0.6333
0	-0.0964	0	-0.1020	2600	0.6948
0	-0.1094	0	-0.1116	2750	0.7451
0	-0.1183	0	-0.1316	2900	0.7892
0	-0.1348	0	-0.1452	3050	0.8488
0	-0.1488	0	-0.1657	3200	0.9051
0	-0.1647	0	-0.1774	3350	0.9445
0	-0.1970	0	-0.2031	3500	1.0323
0	-0.2177	0	-0.2247	3650	1.1033
0	-0.2561	0	-0.2537	3800	1.2015
0	-0.2866	0	-0.2846	3950	1.2752
0	-0.3557	0	-0.3361	4100	1.2954
0	-0.4721	0	-0.4227	4250	1.5140
0	-0.5534	0	-0.4843	4400	1.6213

TENSILE STRENGTHS

IN THE DIRECTION OF THE MAXIMUM PRINCIPAL STRESS = 358 PSI
IN THE DIRECTION OF THE MINIMUM PRINCIPAL STRESS = 271 PSI

TEST IA ... BIAXIAL SPECIMEN AI- SATCH 1 [10 80

STRESS - STRAIN DATA

X-AXIS		Y-AXIS		Z-AXIS	
STRESS (PSI)	STRAIN (MILS/IN)	STRESS (PSI)	STRAIN (MILS/IN)	STRESS (PSI)	STRAIN (MILS/IN)
0	0.0000	0	0.0000	0	0.0000
0	-0.0000	600	0.0001	200	-0.0001
0	-0.0202	900	0.1368	300	-0.0653
0	-0.0349	1200	0.2068	400	-0.0603
0	-0.0548	1500	0.3033	500	-0.0426
0	-0.0638	1800	0.4074	600	-0.0255
0	-0.0693	2250	0.5442	750	-0.0328
0	-0.1212	2700	0.7000	900	0.0250
0	-0.1534	3150	0.8728	1050	0.0445
0	-0.1857	3600	1.0213	1200	0.0806
0	-0.2196	4050	1.2363	1350	0.1115
0	-0.2798	4500	1.4262	1500	0.1323
0	-0.3487	4950	1.7132	1650	0.1853
0	-0.4501	5400	1.9693	1800	0.2074
0	-0.6106	5850	2.2473	1950	0.2274
0	-0.8746	6300	2.7196	2100	0.2503
0	-1.2666	6750	3.1808	2250	0.2730
0	-3.1524	7200	4.2909	2400	0.2267

TENSILE STRENGTHS

IN THE DIRECTION OF THE MAXIMUM PRINCIPAL STRESS = 366 PSI
IN THE DIRECTION OF THE MINIMUM PRINCIPAL STRESS = 308 PSI

TEST 35 ... TRI-BIAXIAL SPECIMEN 35, BATCH 1 3-24-80

STRESS - STRAIN DATA

X-AXIS		Y-AXIS		Z-AXIS	
STRESS (PSI)	STRAIN (MILS/IN)	STRESS (PSI)	STRAIN (MILS/IN)	STRESS (PSI)	STRAIN (MILS/IN)
0	0.0000	0	0.0000	0	0.0000
0	-0.0290	200	-0.0576	600	0.0529
0	-0.0420	300	-0.0685	900	0.1231
0	-0.1708	400	-0.0479	1200	0.1686
0	-0.1744	500	-0.0322	1500	0.2429
0	-0.1988	600	-0.0509	1800	0.2968
0	-0.2191	700	-0.0528	2100	0.3538
0	-0.2257	800	-0.0612	2400	0.4174
0	-0.2535	900	-0.0640	2700	0.4964
0	-0.2620	1000	-0.0493	3000	0.5740
0	-0.2769	1100	-0.0134	3300	0.6800
0	-0.2992	1200	-0.0033	3600	0.7782
0	-0.3129	1300	-0.0013	3900	0.8879
0	-0.3281	1400	0.0348	4200	0.9992
0	-0.3510	1500	0.0567	4500	1.1162
0	-0.3793	1600	0.0747	4800	1.2203
0	-0.4231	1700	0.0845	5100	1.3180
0	-0.4704	1800	0.0932	5400	1.4239
0	-0.5300	1900	0.1015	5700	1.5661
0	-0.5900	2000	0.1168	6000	1.7017
0	-0.6715	2100	0.1170	6300	1.8589
0	-0.7243	2150	0.1272	6450	1.9695
0	-0.7735	2200	0.1539	6600	2.0445
0	-0.8209	2250	0.1472	6750	2.1453
0	-0.8720	2300	0.1641	6900	2.2255
0	-0.9473	2350	0.1719	7050	2.3630
0	-1.0145	2400	0.1874	7200	2.4635
0	-1.1079	2450	0.1828	7350	2.5945
0	-1.1894	2500	0.1966	7500	2.6896
0	-1.2748	2550	0.1897	7650	2.8122
0	-1.3772	2600	0.1887	7800	2.9502
0	-1.4948	2650	0.2024	7950	3.0957
0	-1.6413	2700	0.2151	8100	3.2541
0	-1.8207	2750	0.2122	8250	3.4432
0	-2.0051	2800	0.2271	8400	3.6294
0	-2.2580	2850	0.2171	8550	3.8465
0	-2.5498	2900	0.2303	8700	4.0831
0	-2.9607	2950	0.2326	8850	4.4112

TENSILE STRENGTHS

IN THE DIRECTION OF THE MAXIMUM PRINCIPAL STRESS = 363 PSI
IN THE DIRECTION OF THE MINIMUM PRINCIPAL STRESS = 149 PSI

TEST [illegible] BIAXIAL SPECIMEN DS4 SHIM 4 3-30-84

STRESS - STRAIN DATA

X-AXIS		Y-AXIS		Z-AXIS	
STRESS (PSI)	STRAIN (MILS/IN)	STRESS (PSI)	STRAIN (MILS/IN)	STRESS (PSI)	STRAIN (MILS/IN)
0	0.0000	0	0.0000	0	0.0000
0	-0.0248	200	-0.0750	600	0.0487
0	-0.0394	300	-0.0637	900	0.1401
0	-0.0543	400	-0.0416	1200	0.1635
0	-0.0603	500	-0.0314	1500	0.2941
0	-0.0765	600	-0.0396	1800	0.4108
0	-0.0951	700	-0.0248	2100	0.4851
0	-0.1236	800	-0.0495	2400	0.5740
0	-0.1299	900	-0.0294	2700	0.6544
0	-0.1564	1000	-0.0289	3000	0.7730
0	-0.1784	1100	-0.0041	3300	0.8382
0	-0.2124	1200	-0.0025	3600	0.9532
0	-0.2295	1300	0.0094	3900	1.0639
0	-0.2557	1400	0.0256	4200	1.1828
0	-0.2840	1500	0.0422	4500	1.2963
0	-0.3367	1600	0.0575	4800	1.3929
0	-0.3759	1700	0.0721	5100	1.5456
0	-0.4341	1800	0.0762	5400	1.6885
0	-0.5078	1900	0.0795	5700	1.8479
0	-0.6017	2000	0.1009	6000	2.0454
0	-0.7163	2100	0.1172	6300	2.2129
0	-0.8466	2200	0.1279	6600	2.4304
0	-1.0391	2300	0.1425	6900	2.7002
0	-1.2962	2400	0.1576	7200	3.0060
0	-1.6425	2500	0.1826	7500	3.3609
0	-2.1567	2600	0.1919	7800	3.7673
0	-2.4270	2650	0.2030	7950	3.9543
0	-2.7898	2700	0.1966	8100	4.1611

TENSILE STRENGTHS

IN THE DIRECTION OF THE MAXIMUM PRINCIPAL STRESS = 158 PSI
IN THE DIRECTION OF THE MINIMUM PRINCIPAL STRESS = 292 PSI

TEST 3A ... 3/8 DIA.CAL SPECIMEN 02, BATCH 4 3-31-80

STRESS - STRAIN DATA

X-AXIS		Y-AXIS		Z-AXIS	
STRESS (PSI)	STRAIN (MILS/IN)	STRESS (PSI)	STRAIN (MILS/IN)	STRESS (PSI)	STRAIN (MILS/IN)
0	0.0000	0	0.0000	0	0.0000
0	-0.0096	200	-0.0548	300	0.0408
0	-0.0171	400	-0.0360	600	0.1191
0	-0.0334	600	0.0047	900	0.1821
0	-0.0417	800	0.0229	1200	0.2474
0	-0.0602	1000	0.0395	1500	0.3074
0	-0.0786	1200	0.0631	1800	0.3686
0	-0.1011	1400	0.0968	2100	0.4572
0	-0.1225	1600	0.1283	2400	0.5045
0	-0.1424	1800	0.1643	2700	0.6468
0	-0.1578	2000	0.2039	3000	0.7076
0	-0.1944	2200	0.2737	3300	0.7840
0	-0.2217	2400	0.3030	3600	0.8733
0	-0.2554	2600	0.3767	3900	0.9985
0	-0.2837	2800	0.4185	4200	1.0754
0	-0.3429	3000	0.5032	4500	1.1684
0	-0.4032	3200	0.5237	4800	1.2716
0	-0.4875	3400	0.6078	5100	1.3550
0	-0.6031	3600	0.6661	5400	1.5320
0	-0.6809	3800	0.7007	5700	1.6192
0	-0.8263	4000	0.7812	6000	1.7613
0	-0.9896	4200	0.8791	6300	1.9321
0	-1.2197	4400	0.9648	6600	2.1401
0	-1.4767	4600	1.0610	6900	2.3309
0	-1.6747	4700	1.1356	7050	2.4251
0	-1.8204	4800	1.1490	7200	2.4970
0	-2.0024	4900	1.2098	7350	2.4792
0	-2.2543	5000	1.2742	7500	2.6534
0	-2.4753	5100	1.3118	7650	2.6957
0	-2.7038	5200	1.3445	7800	2.7839
0	-3.0703	5300	1.4485	7950	2.8710

TENSILE STRENGTHS

IN THE DIRECTION OF THE MAXIMUM PRINCIPAL STRESS = 446 PSI
IN THE DIRECTION OF THE MINIMUM PRINCIPAL STRESS = 389 PSI

STRESS - STRAIN DATA

X-AXIS		Y-AXIS		Z-AXIS	
STRESS (PSI)	STRAIN (MILS/IN)	STRESS (PSI)	STRAIN (MILS/IN)	STRESS (PSI)	STRAIN (MILS/IN)
0	0.0000	0	0.0000	0	0.0000
0	-0.0027	200	-0.0232	300	-0.0263
0	-0.0123	400	0.0078	600	0.0439
0	-0.0282	600	0.0523	900	0.0565
0	-0.0414	800	0.0697	1200	0.1445
0	-0.0466	1000	0.0866	1500	0.1941
0	-0.0645	1200	0.1574	1800	0.2843
0	-0.0934	1400	0.1530	2100	0.3703
0	-0.1057	1600	0.2171	2400	0.4542
0	-0.1173	1800	0.2358	2700	0.5266
0	-0.1379	2000	0.3048	3000	0.5878
0	-0.1687	2200	0.3419	3300	0.6860
0	-0.1923	2400	0.4108	3600	0.7562
0	-0.2345	2600	0.4683	3900	0.8668
0	-0.2642	2800	0.5262	4200	0.9710
0	-0.3061	3000	0.6003	4500	1.0764
0	-0.3546	3200	0.6544	4800	1.1673
0	-0.4076	3400	0.7072	5100	1.2903
0	-0.4709	3600	0.7841	5400	1.4275
0	-0.5473	3800	0.8502	5700	1.5489
0	-0.6419	4000	0.9186	6000	1.7113
0	-0.7623	4200	1.0004	6300	1.8991
0	-0.8841	4400	1.0831	6600	2.0338
0	-1.0446	4600	1.1613	6900	2.2996
0	-1.2471	4800	1.2621	7200	2.4905
0	-1.4638	5000	1.3639	7500	2.7253
0	-1.7247	5200	1.4846	7800	3.0787
0	-2.0628	5400	1.6152	8100	3.4126
0	-2.6664	5600	1.8314	8400	3.9121
0	-2.9632	5700	1.9425	8550	4.1219
0	-3.2355	5800	2.0143	8700	4.3265
0	-3.5074	5900	2.0988	8850	4.5495
0	-3.8465	6000	2.2015	9000	4.7780
0	-4.2915	6100	2.3038	9150	5.1070
0	-4.9043	6200	2.4628	9300	5.5545
0	-5.2924	6300	2.5583	9450	5.7730
0	-5.7538	6400	2.6808	9600	6.0894

TENSILE STRENGTHS

IN THE DIRECTION OF THE MAXIMUM PRINCIPAL STRESS = 324 PSI
IN THE DIRECTION OF THE MINIMUM PRINCIPAL STRESS = 227 PSI

TEST 02 ... ... BIAXIAL SPECIMEN 01 BATCH 4 1 07 91

STRESS - STRAIN DATA

X-AXIS		Y-AXIS		Z-AXIS	
STRESS (PSI)	STRAIN (MILS/IN)	STRESS (PSI)	STRAIN (MILS/IN)	STRESS (PSI)	STRAIN (MILS/IN)
0	0.0000	0	0.0000	0	0.0000
0	-0.0154	200	-0.0546	300	-0.0297
0	-0.0328	400	-0.0311	600	0.0413
0	-0.0449	600	-0.0160	900	0.1062
0	-0.0576	800	0.0195	1200	0.1849
0	-0.0743	1000	-0.0019	1500	0.2896
0	-0.0918	1200	0.0753	1800	0.3861
0	-0.1209	1400	0.0878	2100	0.4657
0	-0.1349	1600	0.1172	2400	0.5443
0	-0.1597	1800	0.1745	2700	0.6429
0	-0.1747	2000	0.2055	3000	0.7551
0	-0.2011	2200	0.2504	3300	0.8147
0	-0.2273	2400	0.3118	3600	0.9617
0	-0.2566	2600	0.3803	3900	1.0660
0	-0.2964	2800	0.4429	4200	1.2153
0	-0.3358	3000	0.5138	4500	1.3422
0	-0.3743	3200	0.5530	4800	1.4856
0	-0.4296	3400	0.6243	5100	1.6628
0	-0.4848	3600	0.6889	5400	1.7912
0	-0.5577	3800	0.7652	5700	1.9610
0	-0.6365	4000	0.8493	6000	2.1245
0	-0.7461	4200	0.9107	6300	2.3432
0	-0.8734	4400	0.9921	6600	2.5467
0	-1.0611	4600	1.0835	6900	2.8377
0	-1.2640	4800	1.1811	7200	3.0520
0	-1.4801	5000	1.2471	7500	3.3527
0	-1.8040	5200	1.3454	7800	3.6854
0	-2.1960	5400	1.4674	8100	4.0795
0	-2.6029	5600	1.5999	8400	4.4857
0	-3.1786	5800	1.7483	8700	4.9460
0	-3.6236	5900	1.8547	8850	5.3602
0	-4.4195	6000	2.0053	9000	5.9588
0	-5.5267	6100	2.1709	9150	6.3900

TENSILE STRENGTHS

IN THE DIRECTION OF THE MAXIMUM PRINCIPAL STRESS = 191 PSI
IN THE DIRECTION OF THE MINIMUM PRINCIPAL STRESS = 467 PSI

TEST 4A ... 13 BIAXIAL SPECIMEN D4, BATCH 2 1/14/81

STRESS - STRAIN DATA

X-AXIS		Y-AXIS		Z-AXIS	
STRESS (PSI)	STRAIN (MILS/IN)	STRESS (PSI)	STRAIN (MILS/IN)	STRESS (PSI)	STRAIN (MILS/IN)
0	0.0000	0	0.0000	0	0.0000
0	-0.0067	300	-0.0267	300	-0.0662
0	-0.0245	600	0.0153	600	0.0029
0	-0.0417	900	0.0486	900	0.0555
0	-0.0628	1200	0.1046	1200	0.1283
0	-0.0804	1500	0.1723	1500	0.2042
0	-0.1061	1800	0.2437	1800	0.2880
0	-0.1238	2100	0.3299	2100	0.3887
0	-0.1550	2400	0.4286	2400	0.5015
0	-0.1926	2700	0.5044	2700	0.5993
0	-0.2379	3000	0.5985	3000	0.6803
0	-0.2756	3300	0.7095	3300	0.7927
0	-0.3275	3600	0.8550	3600	0.9551
0	-0.3967	3900	1.0108	3900	1.1305
0	-0.4836	4200	1.1514	4200	1.3046
0	-0.5968	4500	1.3303	4500	1.5205
0	-0.7718	4800	1.5687	4800	1.8090
0	-0.9624	5100	1.7958	5100	2.0645
0	-1.1765	5400	2.0210	5400	2.3395
0	-1.5000	5700	2.3981	5700	2.7543
0	-1.8752	6000	2.7598	6000	3.1079
0	-2.1997	6150	3.0645	6150	3.4362
0	-2.4884	6300	3.3451	6300	3.7165
0	-2.7382	6450	3.5569	6450	3.9540
0	-3.0061	6600	3.7780	6600	4.1670
0	-3.2947	6750	4.0374	6750	4.4408
0	-3.9380	6900	4.3755	6900	4.7713
0	-4.3626	7050	4.6643	7050	5.0678
0	-4.9308	7200	4.9733	7200	5.4045

TENSILE STRENGTHS

IN THE DIRECTION OF THE MAXIMUM PRINCIPAL STRESS = 343 PSI
IN THE DIRECTION OF THE MINIMUM PRINCIPAL STRESS = 255 PSI

TEST 42 ... 3.3 BIAXIAL SPECIMEN A3, BATCH 2 2/21/81

STRESS - STRAIN DATA

X-AXIS		Y-AXIS		Z-AXIS	
STRESS (PSI)	STRAIN (MILS/IN)	STRESS (PSI)	STRAIN (MILS/IN)	STRESS (PSI)	STRAIN (MILS/IN)
0	0.0000	0	0.0000	0	0.0000
300	0.0749	300	-0.0235	0	-0.0168
600	0.1038	600	0.0041	0	-0.0272
900	0.1708	900	0.0795	0	-0.0462
1200	0.2448	1200	0.1397	0	-0.0785
1500	0.2782	1500	0.1864	0	-0.0964
1800	0.2857	1800	0.1879	0	-0.1235
2100	0.3891	2100	0.2915	0	-0.1688
2400	0.4719	2400	0.3807	0	-0.2061
2700	0.5383	2700	0.4571	0	-0.2444
3000	0.6286	3000	0.5550	0	-0.2948
3300	0.6800	3300	0.6187	0	-0.3616
3600	0.7446	3600	0.6880	0	-0.4286
3900	0.8509	3900	0.8188	0	-0.5115
4200	0.9462	4200	0.9100	0	-0.6028
4500	1.0669	4500	1.0332	0	-0.7563
4800	1.2277	4800	1.2014	0	-0.9539
5100	1.3767	5100	1.3773	0	-1.2164
5400	1.5438	5400	1.5579	0	-1.4771
5700	1.8202	5700	1.8465	0	-1.9763
6000	2.1154	6000	2.1595	0	-2.5901
6300	2.4338	6300	2.4923	0	-3.2975
6600	2.7812	6600	2.8736	0	-4.1237

TENSILE STRENGTHS

IN THE DIRECTION OF THE MAXIMUM PRINCIPAL STRESS = 476 PSI
IN THE DIRECTION OF THE MINIMUM PRINCIPAL STRESS = 303 PSI

APPENDIX D.

STRESS-STRAIN CURVES FOR BIAXIAL TESTS

This appendix contains the stress-strain curves generated during each successful biaxial test. The ordinate values are mils/in. of strain and the values on the abscissa are the maximum principal stress in ksi. The numbers 1, 2 and 3 marked on the curves represent the principal strains and the curve marked "V" is the volumetric strain curve.

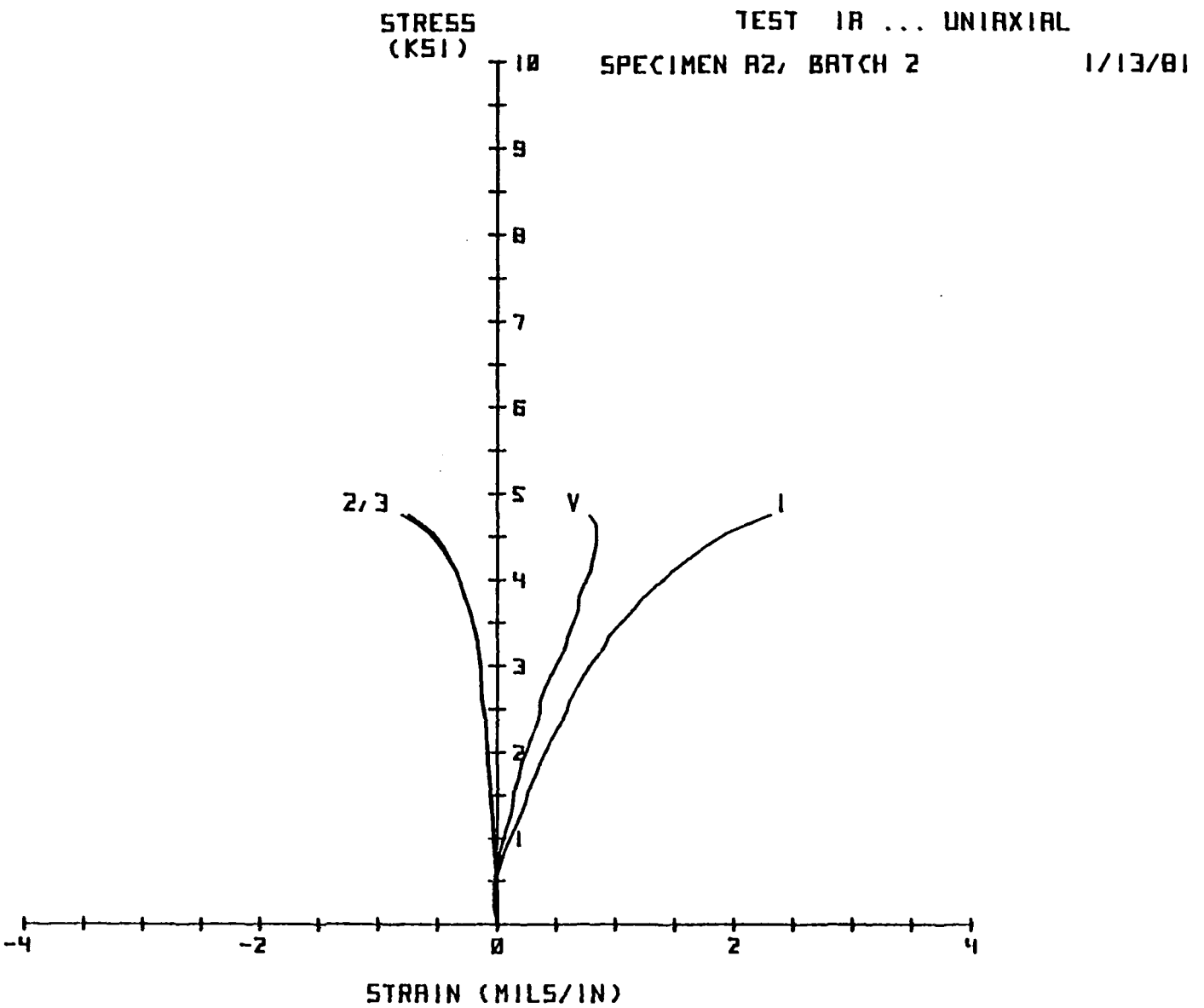
STRESS
(KSI)
TEST 1A ... UNIAXIAL
SPECIMEN A2, BATCH 2
1/13/81
10
9
8
7
6
5
4
3
2
1
2,3
V
1
-4
-2
0
2
4
STRAIN (MILS/IN)

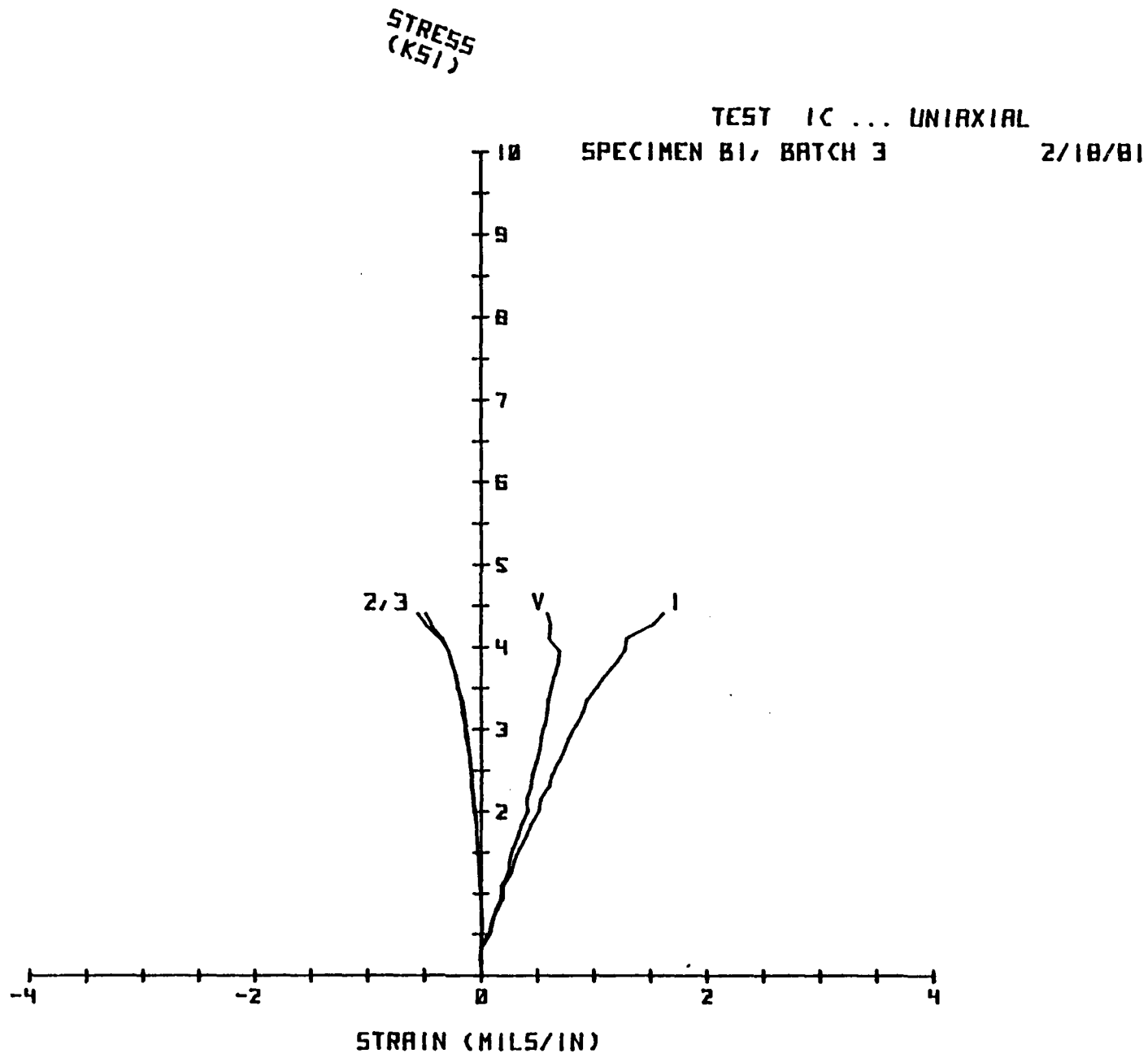
STRESS
(KSI)
TEST IC ... UNIAXIAL
SPECIMEN B1, BATCH 3
2/18/81
10
9
8
7
6
5
4
3
2
2,3
V
1
-4
-2
0
2
4
STRAIN (MILS/IN)

AD-A114 375 NEW MEXICO ENGINEERING RESEARCH INST ALBUQUERQUE F/G 13/13
REINFORCED CONCRETE BEAMS UNDER COMBINED AXIAL AND LATERAL LOAD--ETC(U)
JAN 82 G E LANE F29601-76-C-0015
UNCLASSIFIED NMERI-SSR-71 AFWL-TR-81-99 NL

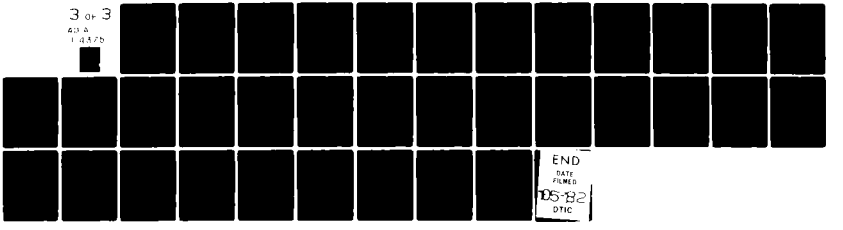

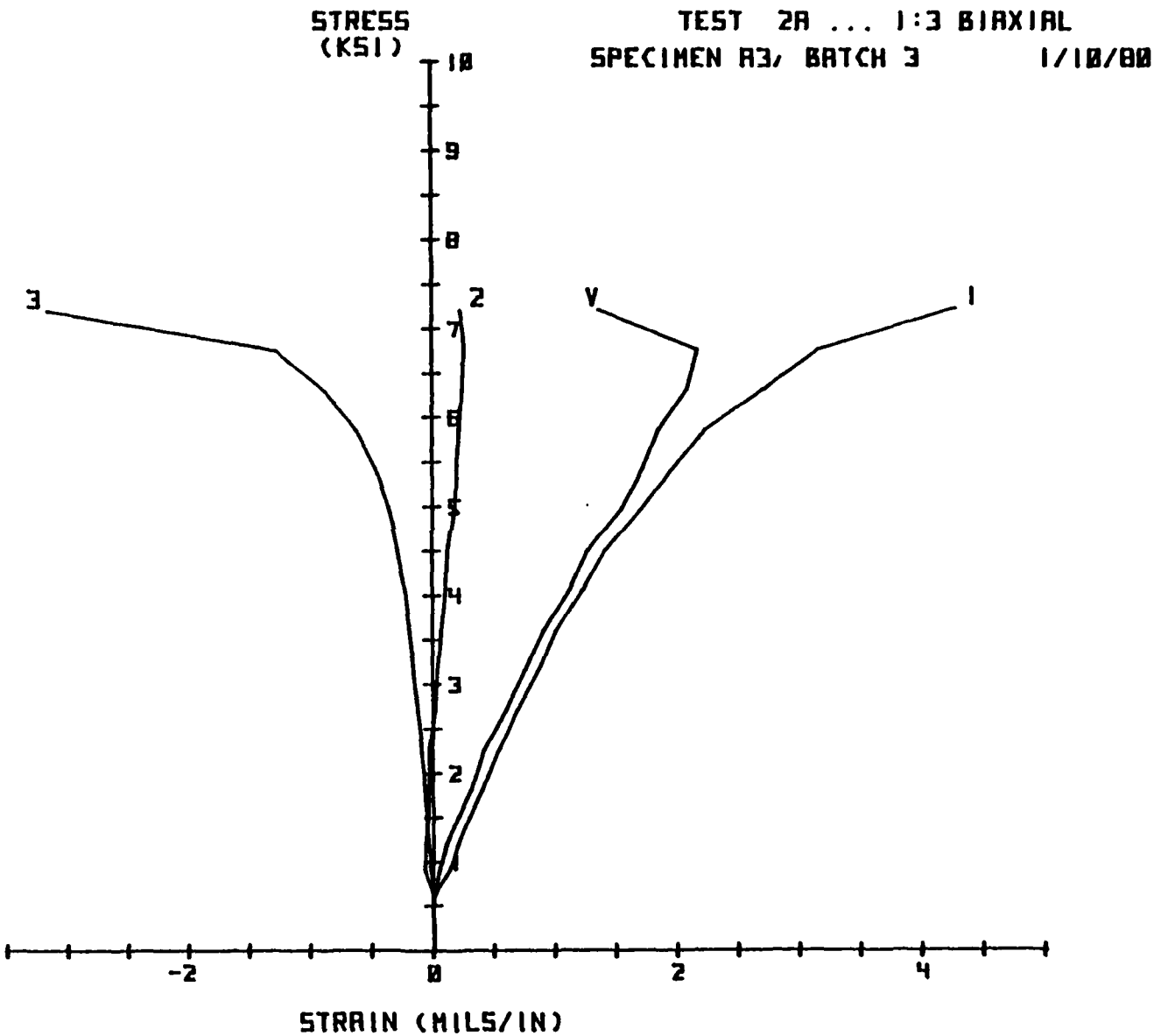
STRESS
(KSI)
TEST 2A ... 1:3 BIAXIAL
SPECIMEN R3, BATCH 3
1/10/80
10
9
8
7
6
5
4
3
2
1
3
2
V
1
-2
0
2
4
STRAIN (MILS/IN)

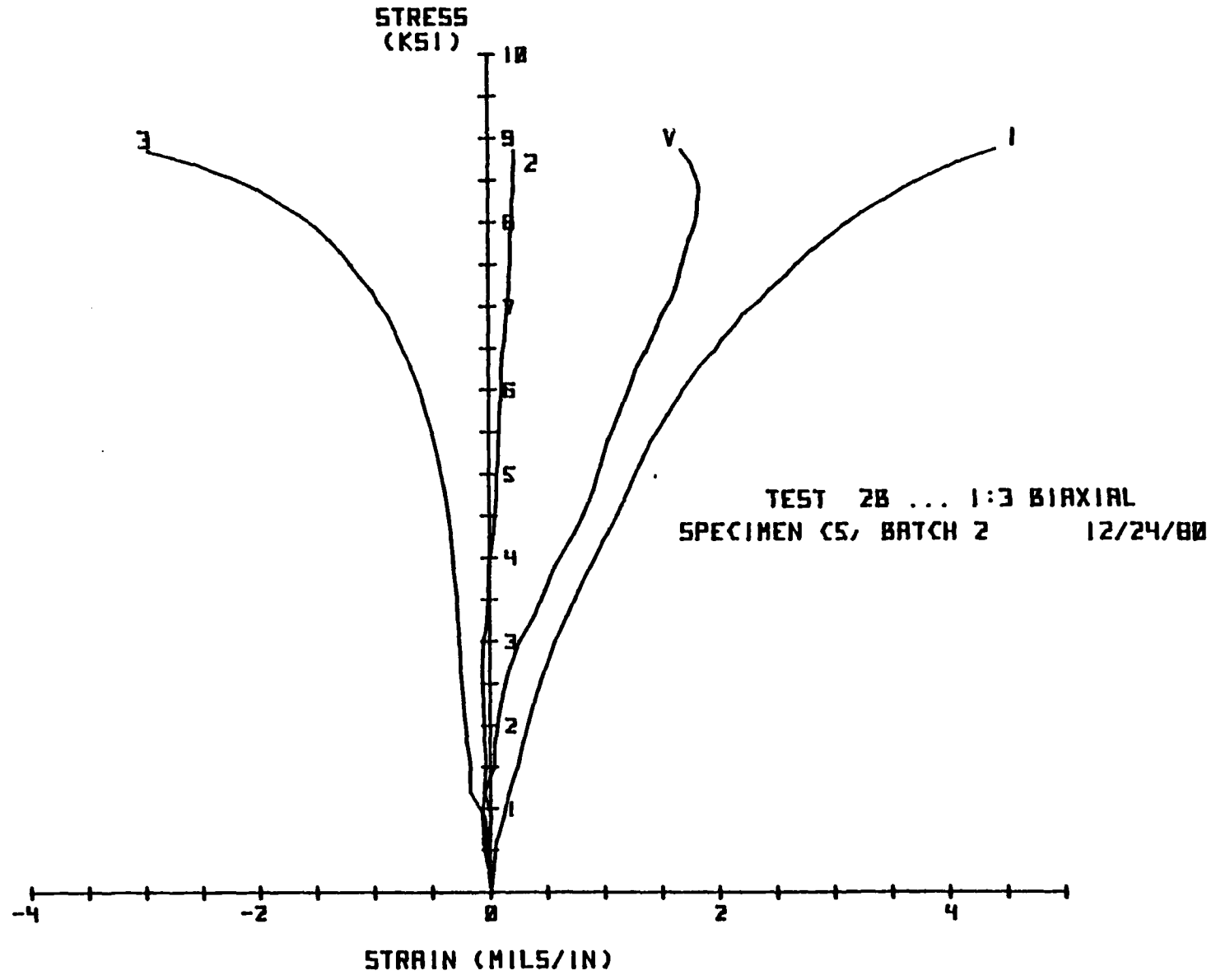
STRESS
(KSI)
10
9
8
7
6
5
4
3
2
1
-4
-2
0
2
4
STRAIN (MILS/IN)
III
II
V
I
TEST 28 ... 1:3 BIAXIAL
SPECIMEN C5, BATCH 2 12/24/80

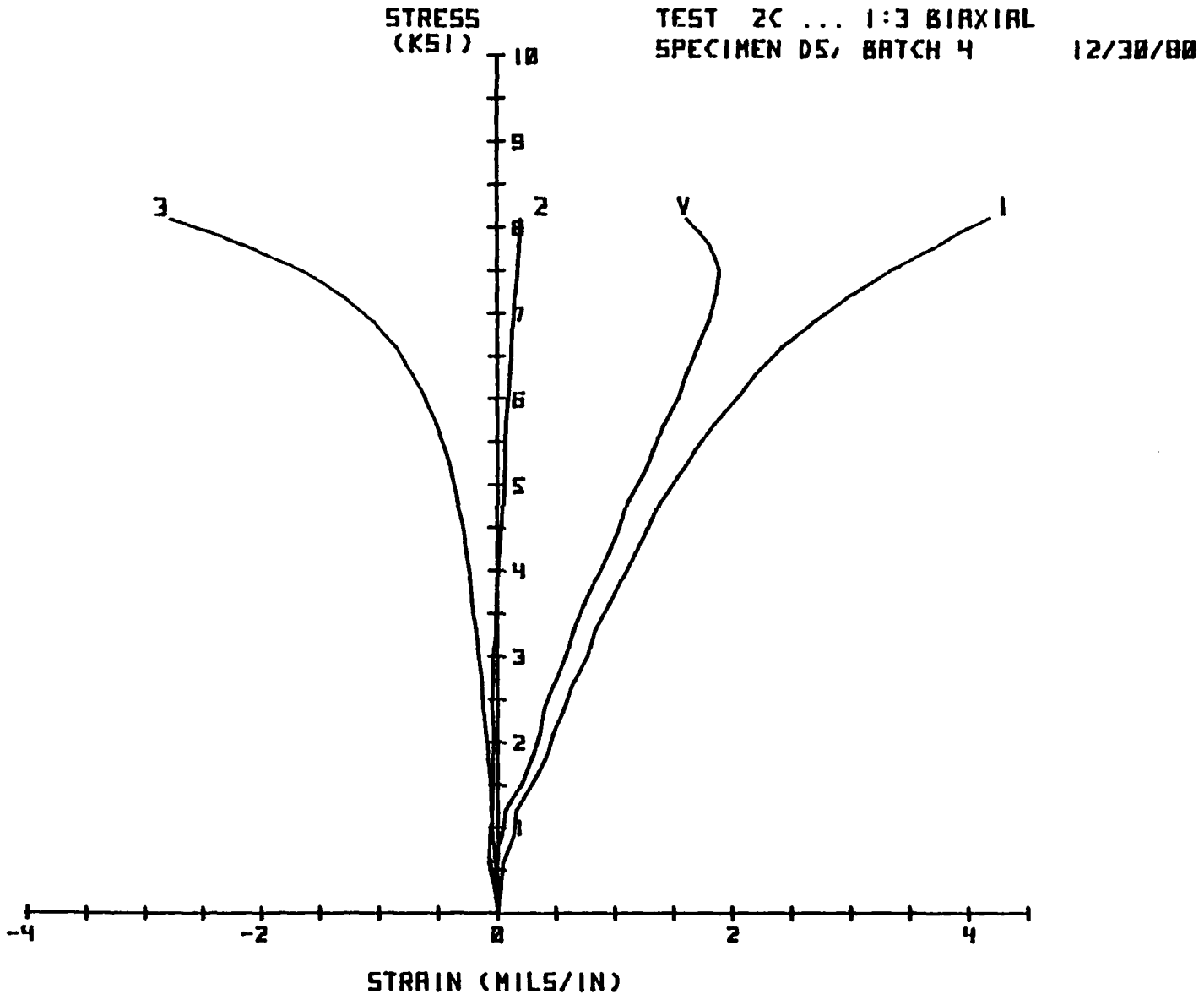
STRESS
(KSI)
TEST 2C ... 1:3 BIAXIAL
SPECIMEN D5/ BATCH 4
12/30/80
10
9
8
7
6
5
4
3
2
1
3
2
V
1
-4
-2
0
2
4
STRAIN (MILS/IN)

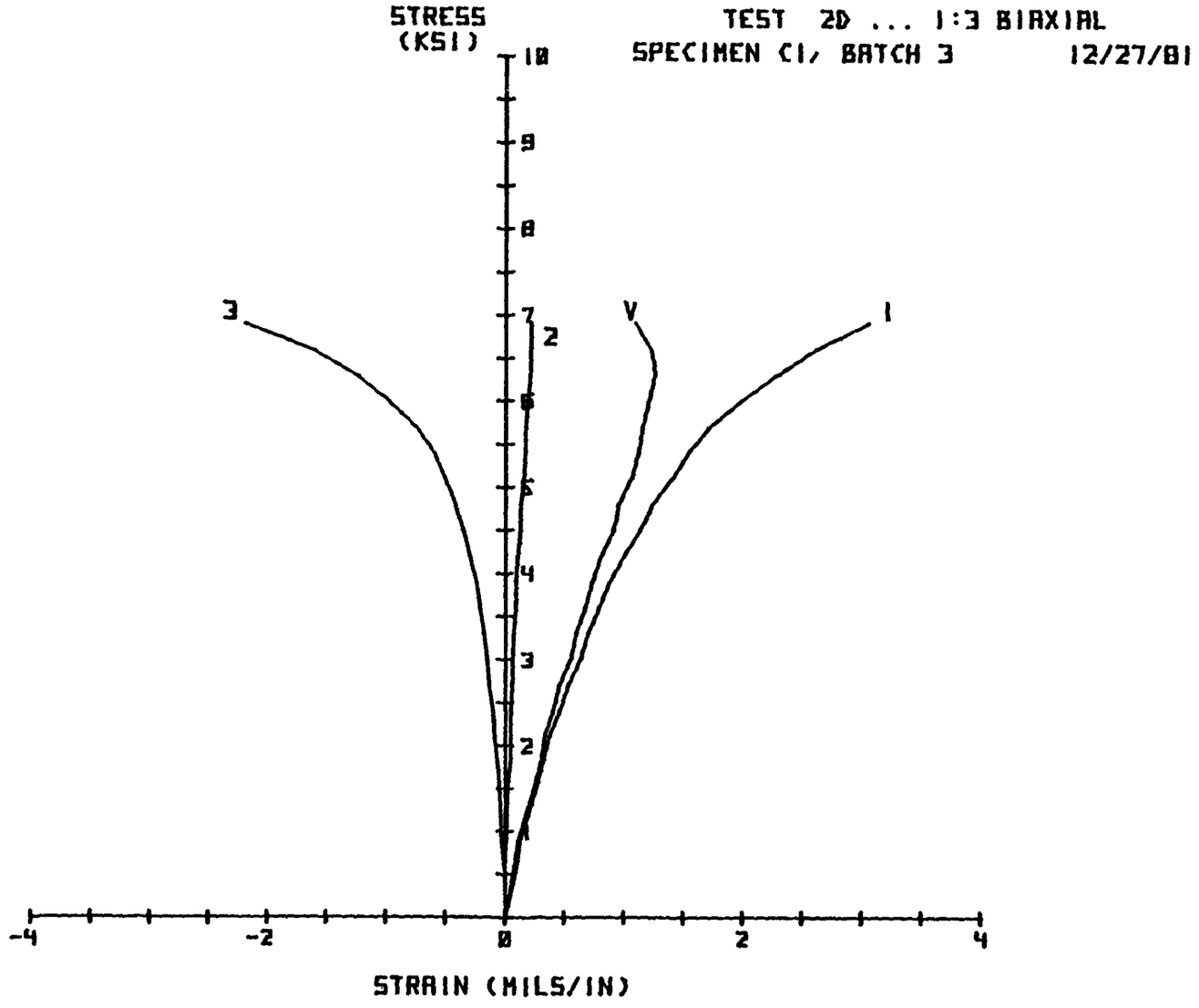
STRESS
(KSI)
TEST 2D ... 1:3 BIAXIAL
SPECIMEN C1, BATCH 3
12/27/81
10
9
8
7
6
5
4
3
2
1
3
V
1
-4
-2
0
2
4
STRAIN (MILS/IN)

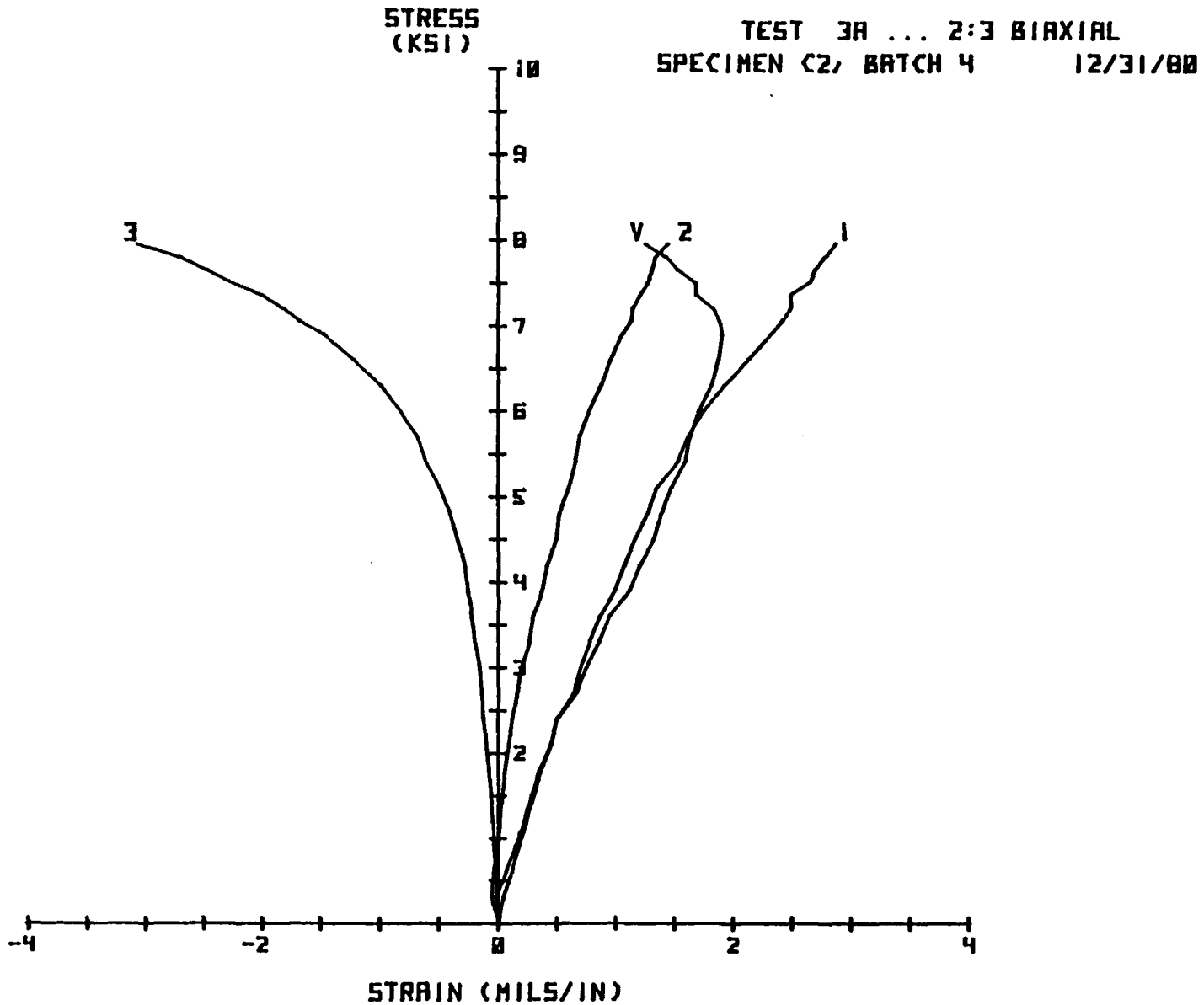
STRESS
(KSI)
TEST 3A ... 2:3 BIAXIAL
SPECIMEN (2) BATCH 4 12/31/80
10
9
8
7
6
5
4
3
2
1
3
V
2
1
-4
-2
0
2
4
STRAIN (MILS/IN)

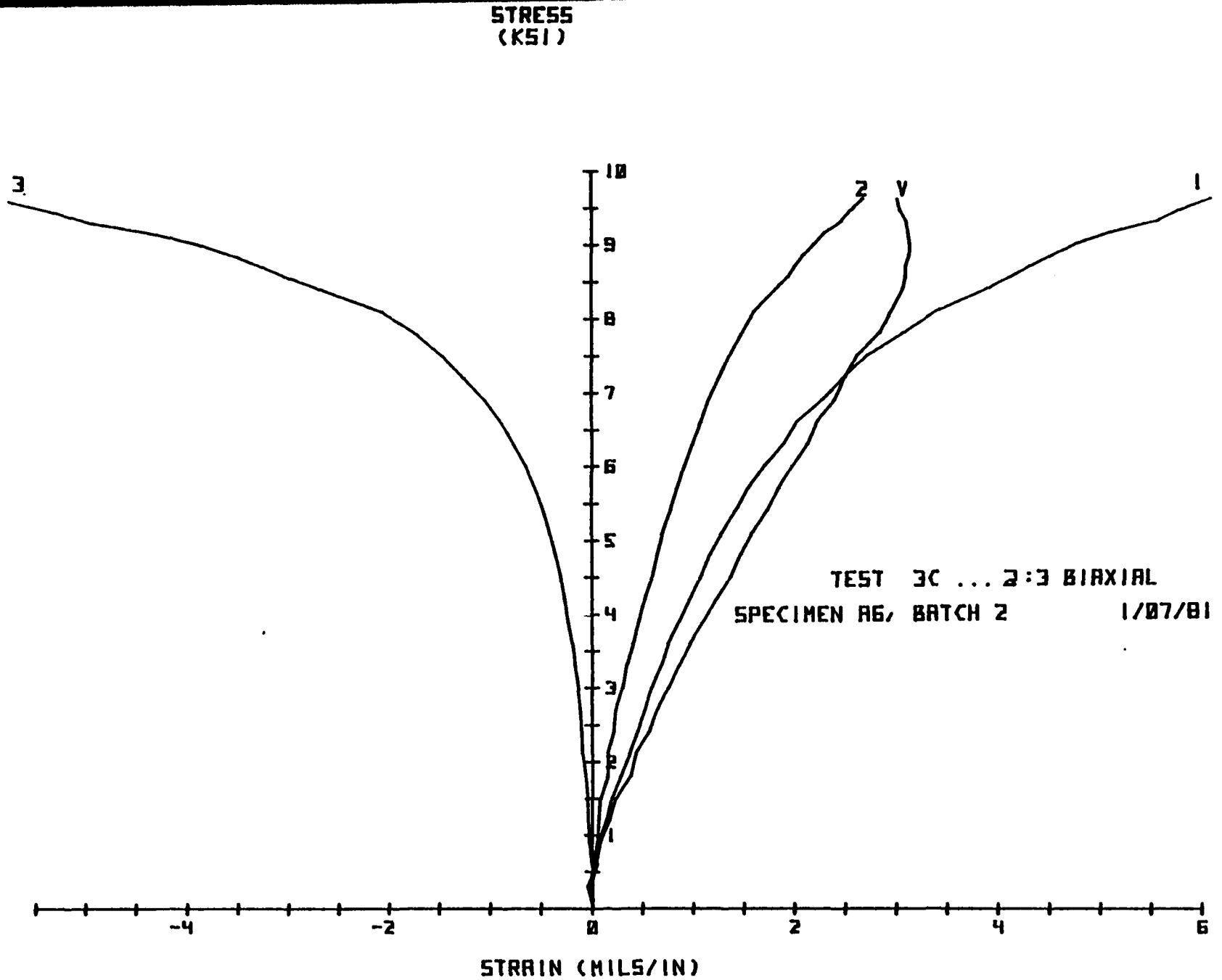
STRESS
(KSI)
10
9
8
7
6
5
4
3
2
1
3
2
V
1
TEST 3C ... 2:3 BIAXIAL
SPECIMEN A6, BATCH 2 1/07/81
-4
-2
0
2
4
6
STRAIN (MILS/IN)

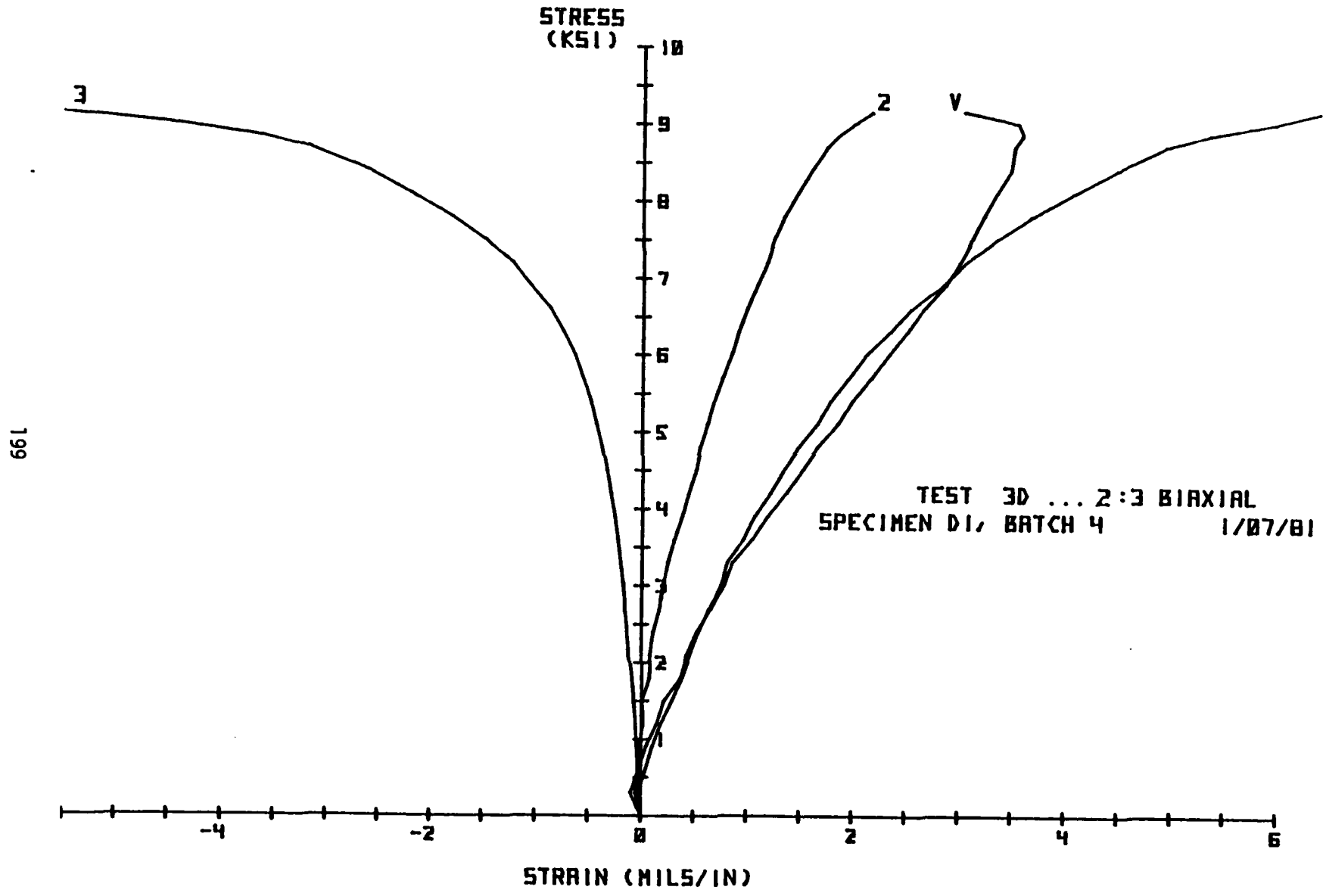
STRESS
(KSI)
10
9
8
7
6
5
4
3
2
1
3
2
V
TEST 3D ... 2:3 BIAXIAL
SPECIMEN D1, BATCH 4
1/07/81
-4
-2
0
2
4
6
STRAIN (MILS/IN)
199

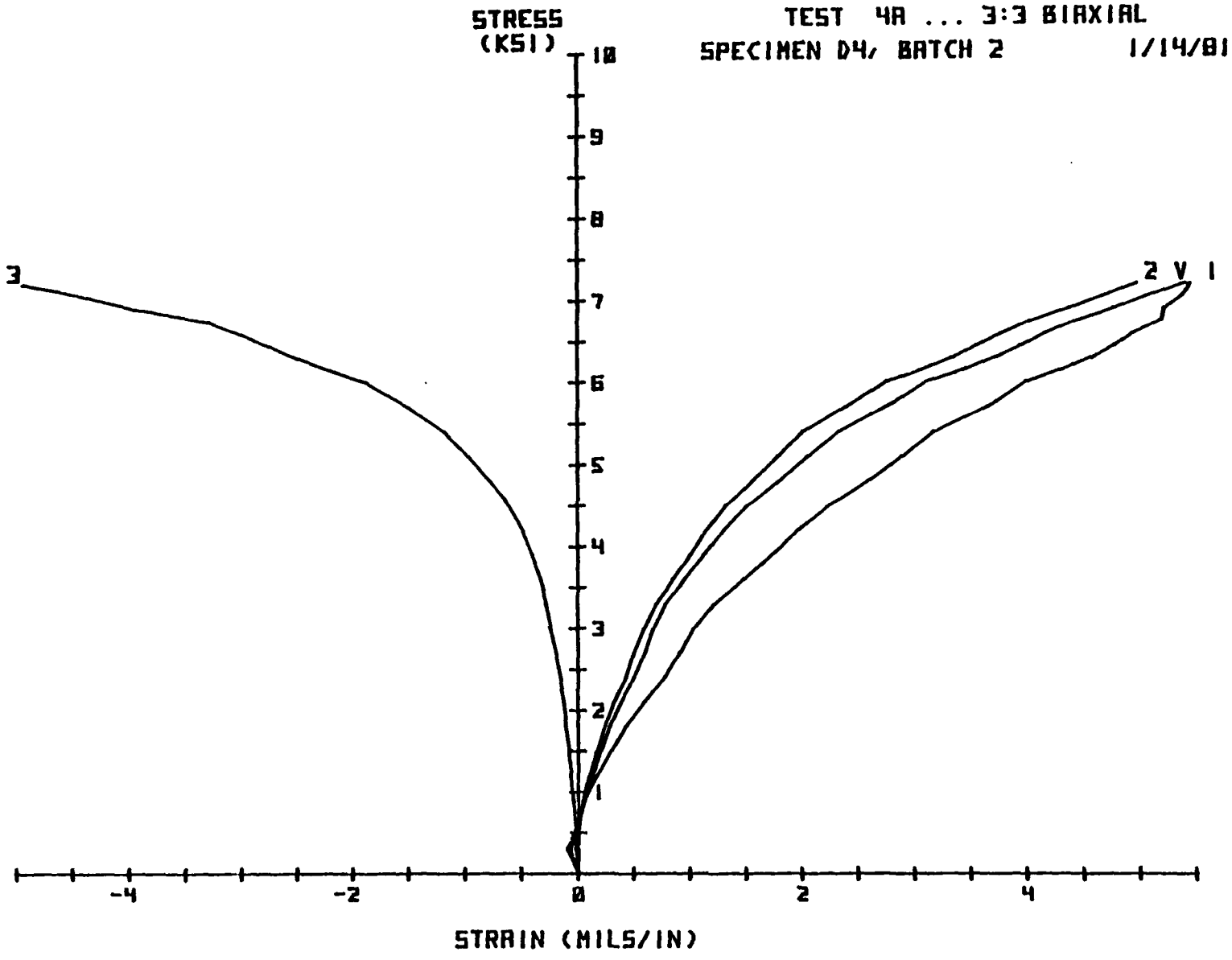
STRESS
(KSI)
TEST 4A ... 3:3 BIAXIAL
SPECIMEN D4/ BATCH 2
1/14/81
10
9
8
7
6
5
4
3
2
1
3
2 V 1
-4
-2
0
2
4
STRAIN (MILS/IN)

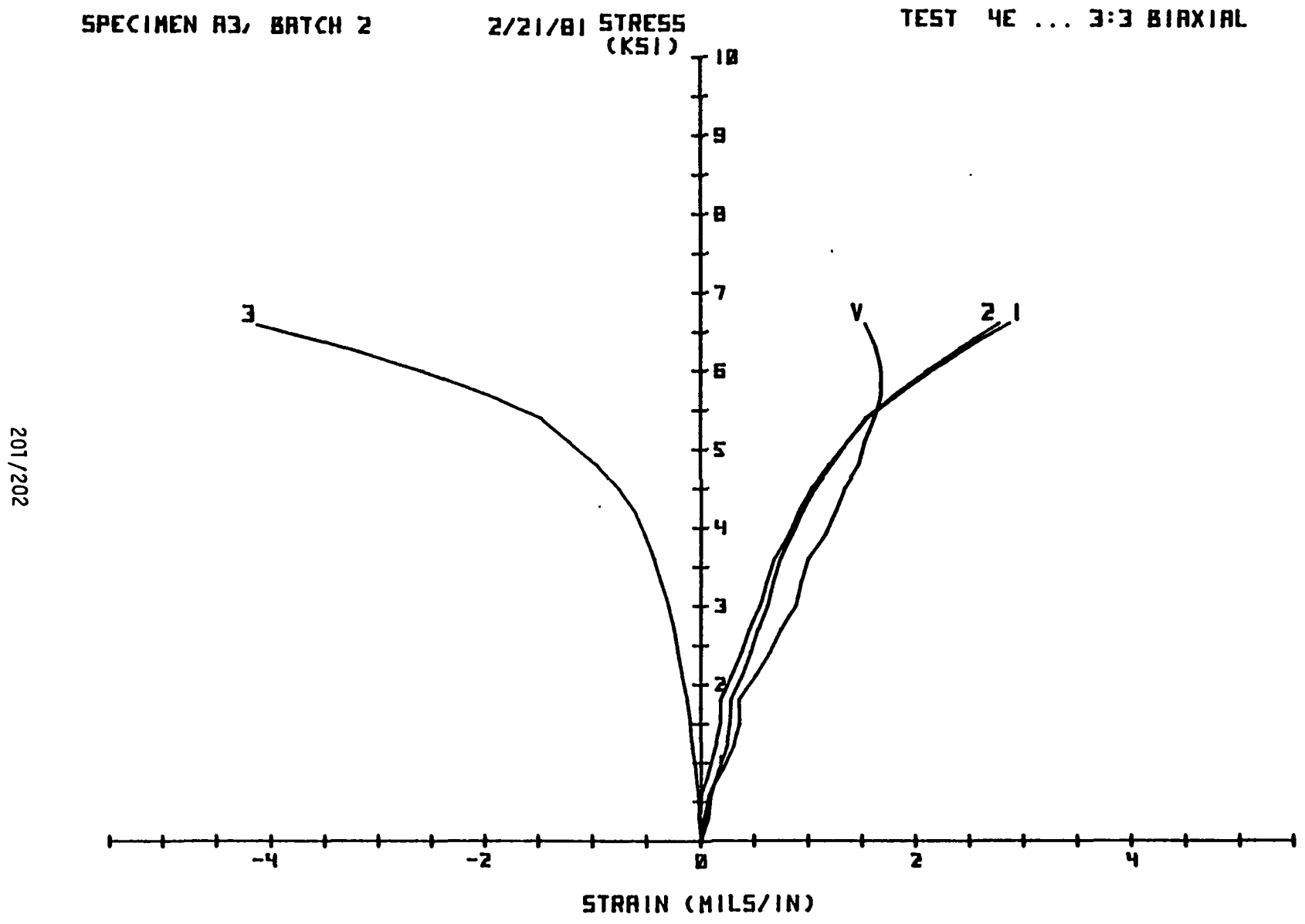
SPECIMEN A3, BATCH 2
2/21/81 STRESS (KSI)
TEST 4E ... 3:3 BIAXIAL
10
9
8
7
6
5
4
3
2
3
V
2
1
-4
-2
0
2
4
STRAIN (MILS/IN)

APPENDIX C

PLAIN CONCRETE PRISM TESTING

DR. G. KRISHNAMOORTHY

SUBMITTED BY
SAN DIEGO STATE UNIVERSITY
SAN DIEGO, CALIFORNIA
TO
NEW MEXICO ENGINEERING RESEARCH INSTITUTE
UNIVERSITY OF NEW MEXICO
ALBUQUERQUE, NEW MEXICO

Presented to: Dr. Golden E. Lane

June 8, 1981

Note: This appendix is a self-contained document, provided for the reader's information, with its own figures, tables, and appendixes.

Note:

The San Diego State work consisted of testing twenty-four 152- by 305-mm plain concrete cylinders under displacement control. The testing was conducted in a modified Riehle testing machine with a 1.33-MN capacity. This machine can accommodate up to 3-m specimens. The Riehle machine has a 300K MTS load cell and electronic instrumentation for imposing a specified rate of deformation and for automatic data logging, including a facility for X-Y recording along with digital readout for direct monitoring of tests.

The concrete cylinders were tested by imposing a deformation rate of 0.51 mm/min. Four linear variable-differential transformers (LVDT) were mounted in a circle around the specimen, 90 deg apart, to measure the deformations. The signals from the diametrically opposite LVDT's were combined and averaged to eliminate rotation of the loading platten. Signals from the MTS load cell were obtained to measure the load. These signals were fed into signal conditioners and amplifiers to obtain the load-deformation plots. To obtain the initial slopes of the plots accurately, extremely sensitive Hewlett-Packard X-Y recorders were used.

BATCH NO.	SPECIMEN NO.	TYPE OF LOADING	STRENGTH PSI	INITIAL MODULUS 10^{+6} LB/IN^2
1	2	MONOTONIC	5036	2.92
	3	"	4902	2.68
	4	"	4775	3.08
	5	"	5185	2.82
	6	"	4746	2.80
	MEAN		4929	2.86
	ST. DEV.		184	0.15
2	1	MONOTONIC	4909	2.52
	2	"	5482	2.66
	3	"	5199	2.66
	4	CYCLIC	5256	2.62
	5	"	5227	2.64
	6	"	5341	2.72
	MEAN		5236	2.64
	ST. DEV.		190	.07
3	1	MONOTONIC	5447	2.58
	2	CYCLIC	5567	2.64
	3	"	5220	2.90
	4	MONOTONIC	5624	2.80
	5	"	5022	2.42
	6	CYCLIC	5227	2.66
	MEAN		5351	2.67
	ST. DEV.		233	0.17
4	1	MONOTONIC	4782	2.60
	2	"	5160	2.66
	3	CYCLIC	5447	3.50
	4	"	4761	3.42
	5	MONOTONIC	4952	3.66
	6	CYCLIC	5079	3.14
	MEAN		5030	3.16
	ST. DEV.		258	0.45

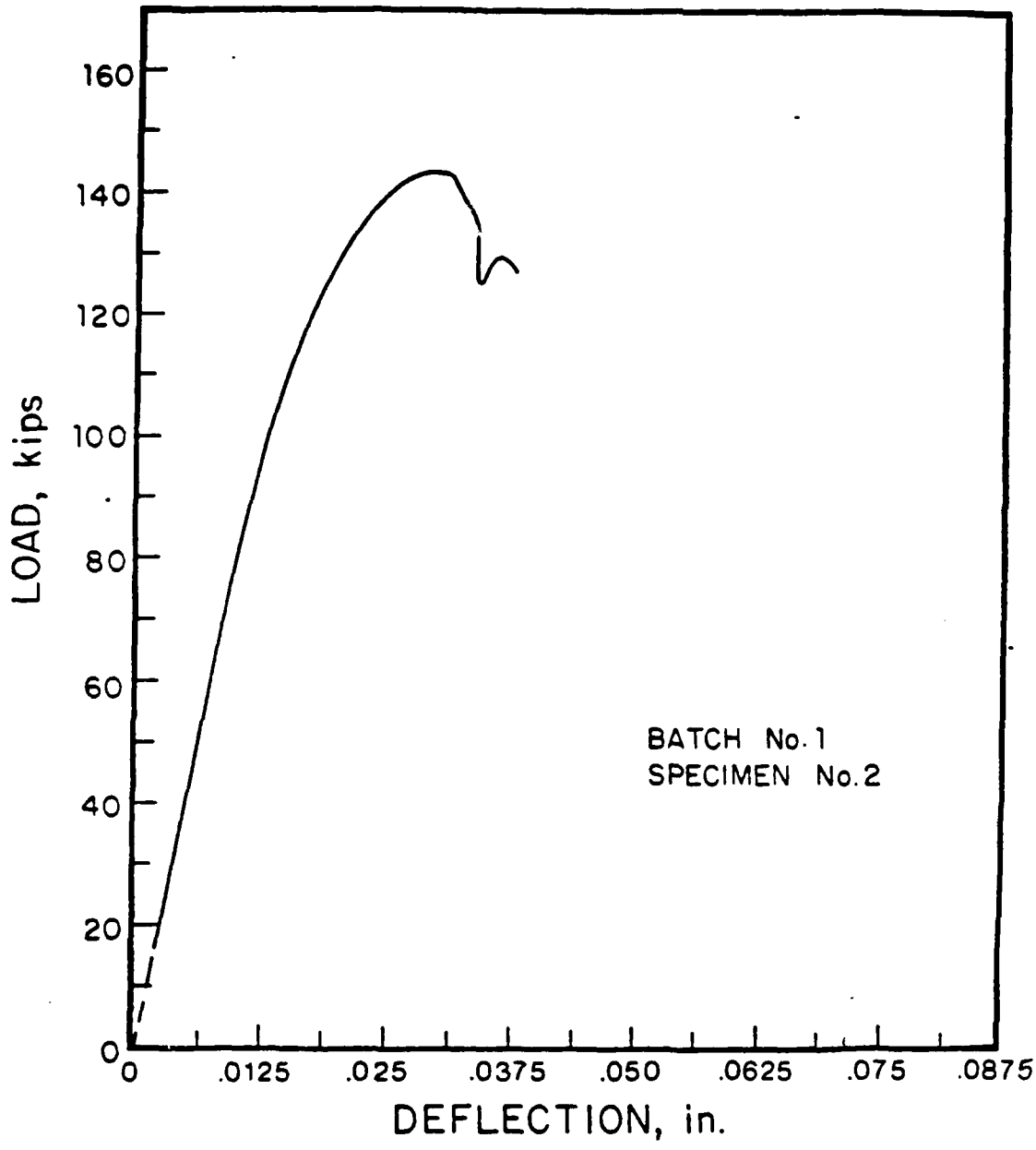
160
140
120
100
80
60
40
20
0
LOAD, kips
0
.0125
.025
.0375
.050
.0625
.075
.0875
DEFLECTION, in.
BATCH No. 1
SPECIMEN No. 2

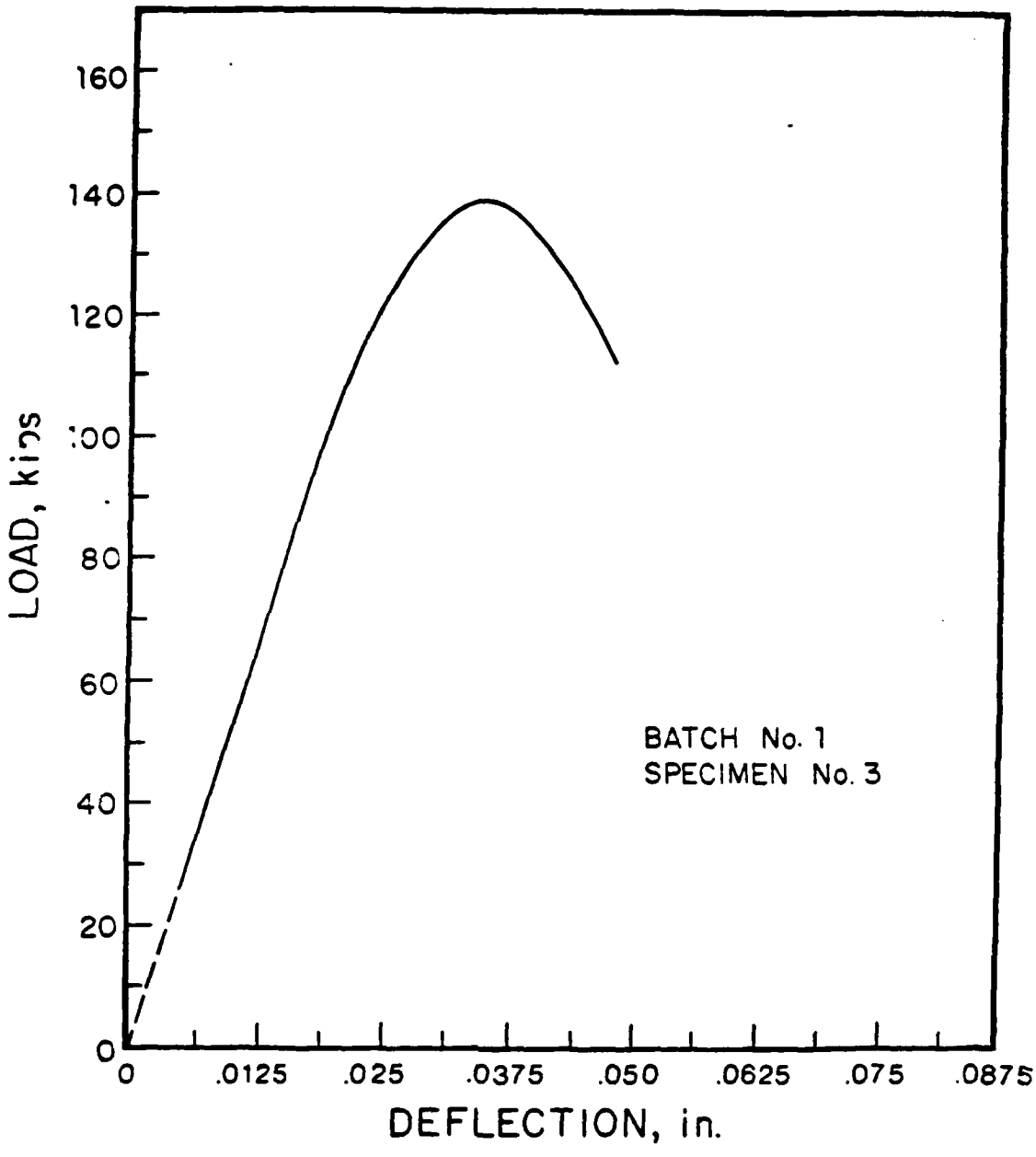
160
140
120
100
80
60
40
20
0
LOAD, kips
0
.0125
.025
.0375
.050
.0625
.075
.0875
DEFLECTION, in.
BATCH No. 1
SPECIMEN No. 3

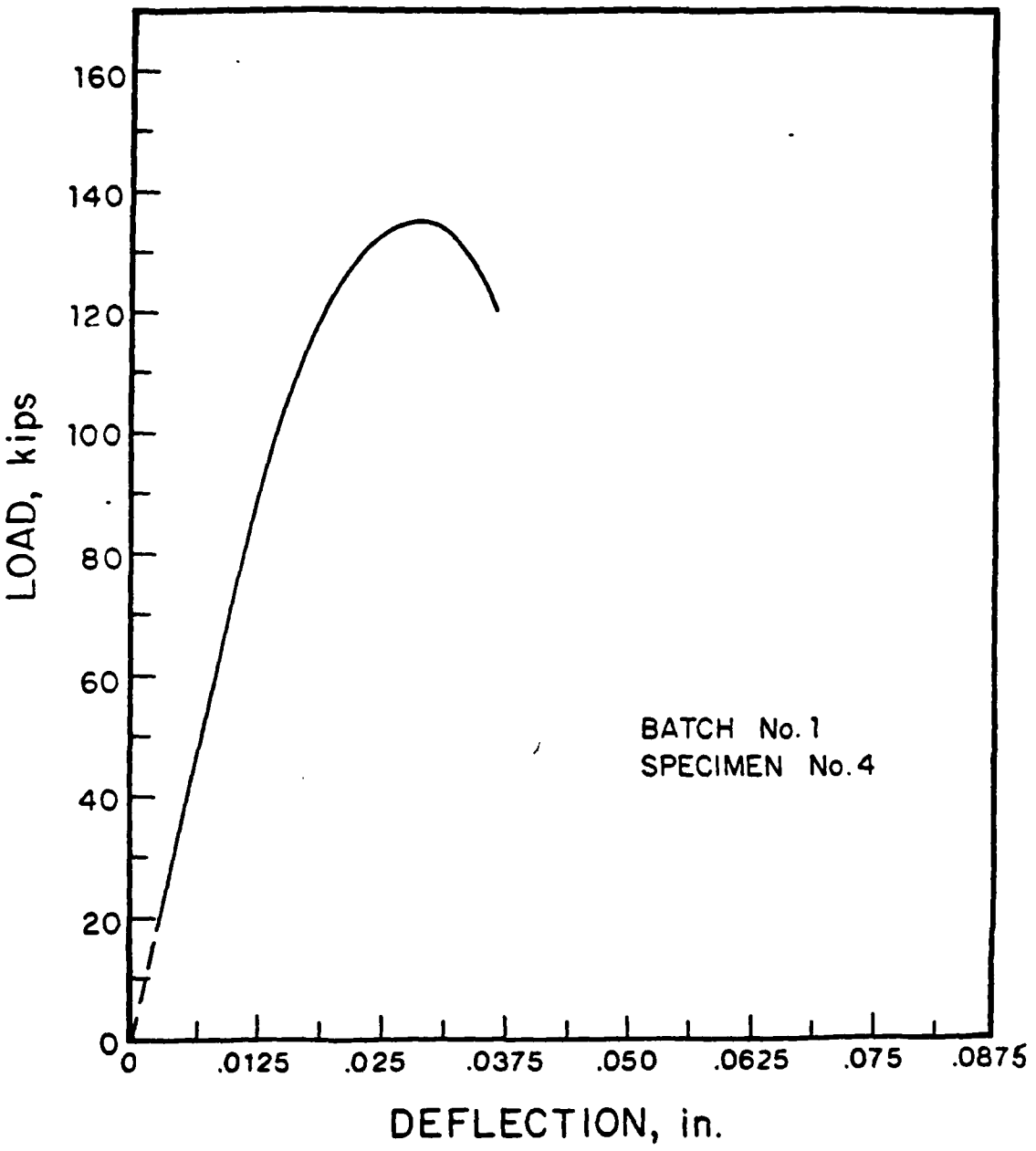
160
140
120
100
80
60
40
20
0
LOAD, kips
0
.0125
.025
.0375
.050
.0625
.075
.0875
DEFLECTION, in.
BATCH No. 1
SPECIMEN No. 4

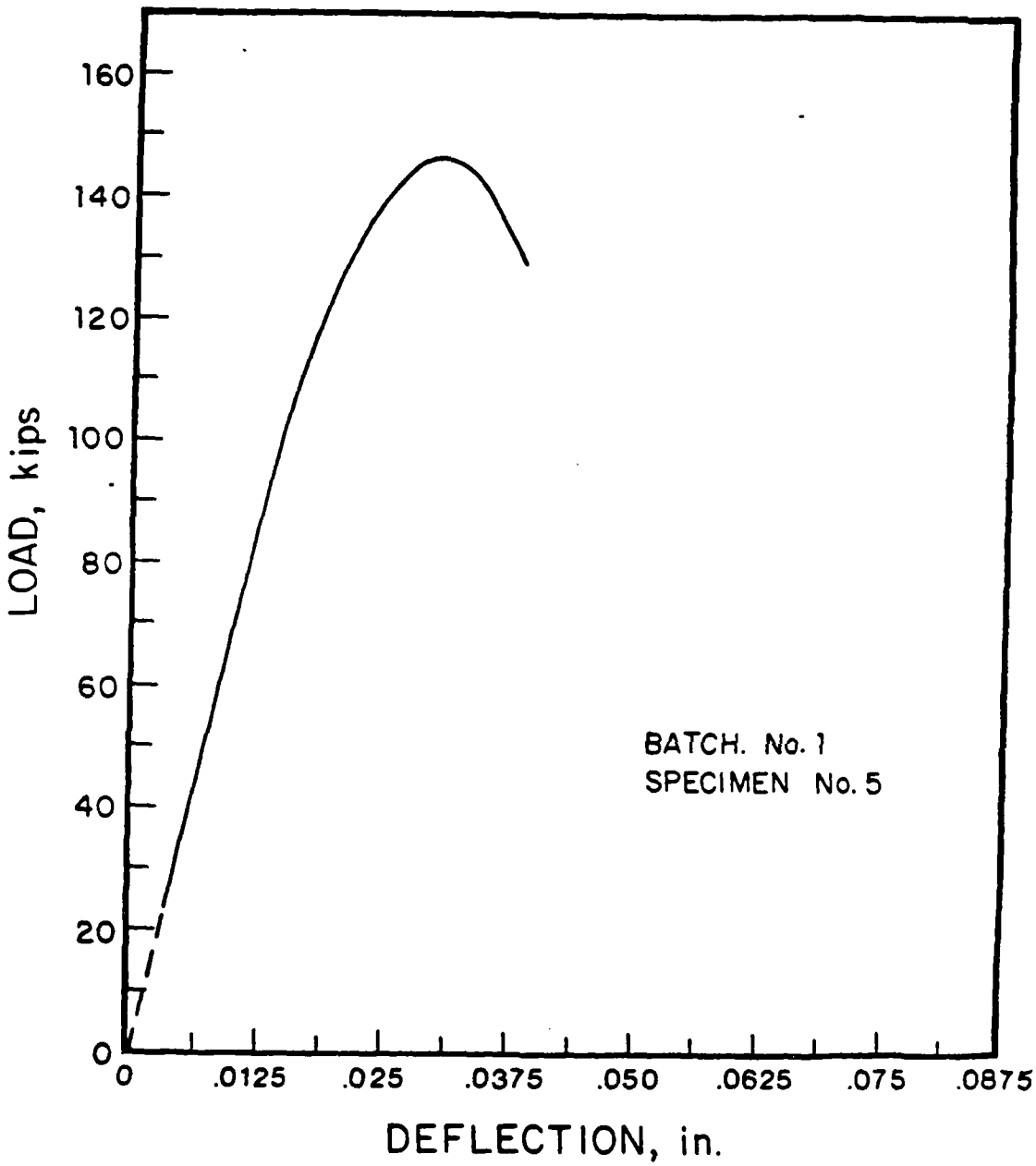
160
140
120
100
80
60
40
20
0
LOAD, kips
0
.0125
.025
.0375
.050
.0625
.075
.0875
DEFLECTION, in.
BATCH. No. 1
SPECIMEN No. 5

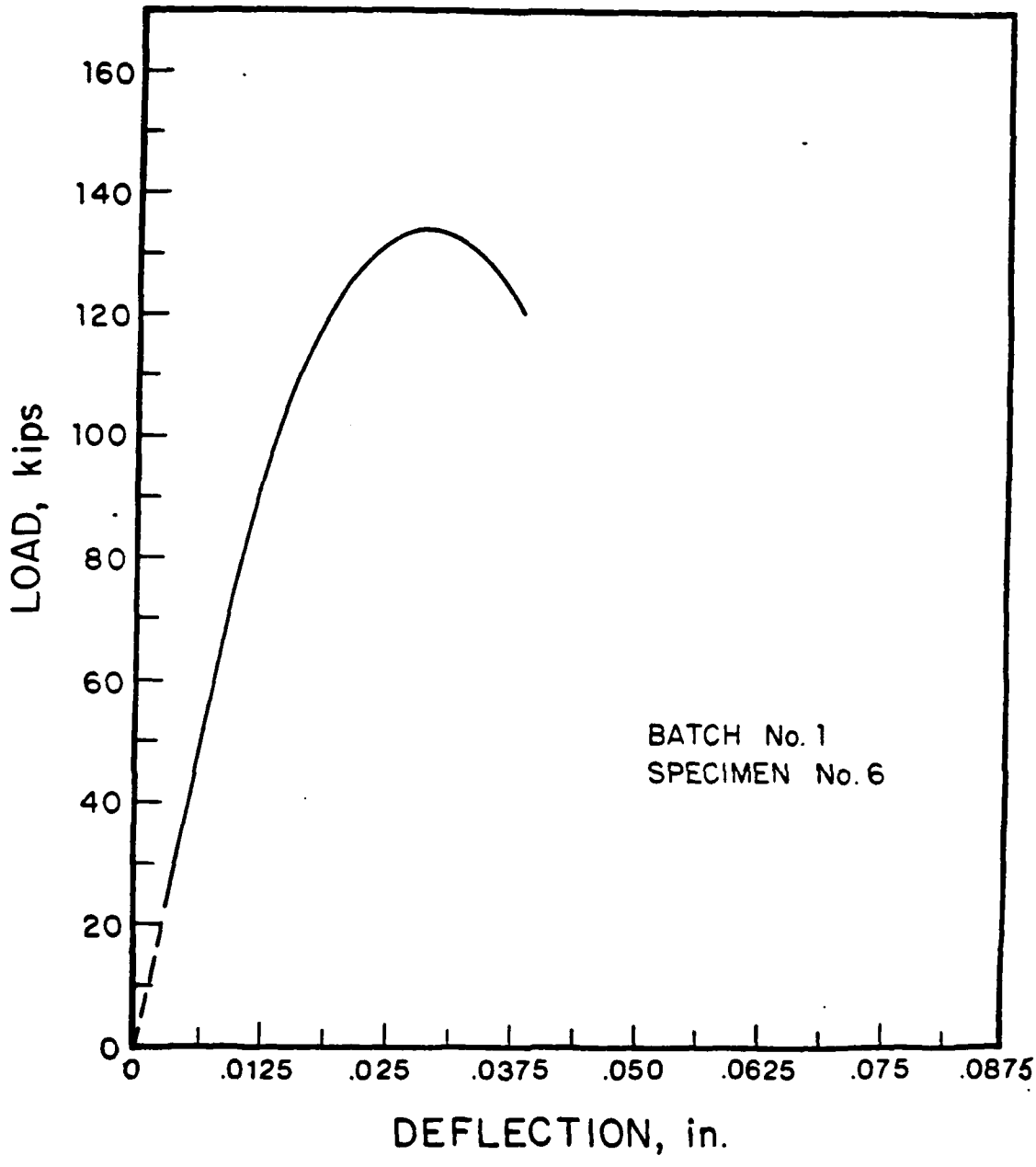
160
140
120
100
80
60
40
20
0
LOAD, kips
0
.0125
.025
.0375
.050
.0625
.075
.0875
DEFLECTION, in.
BATCH No. 1
SPECIMEN No. 6

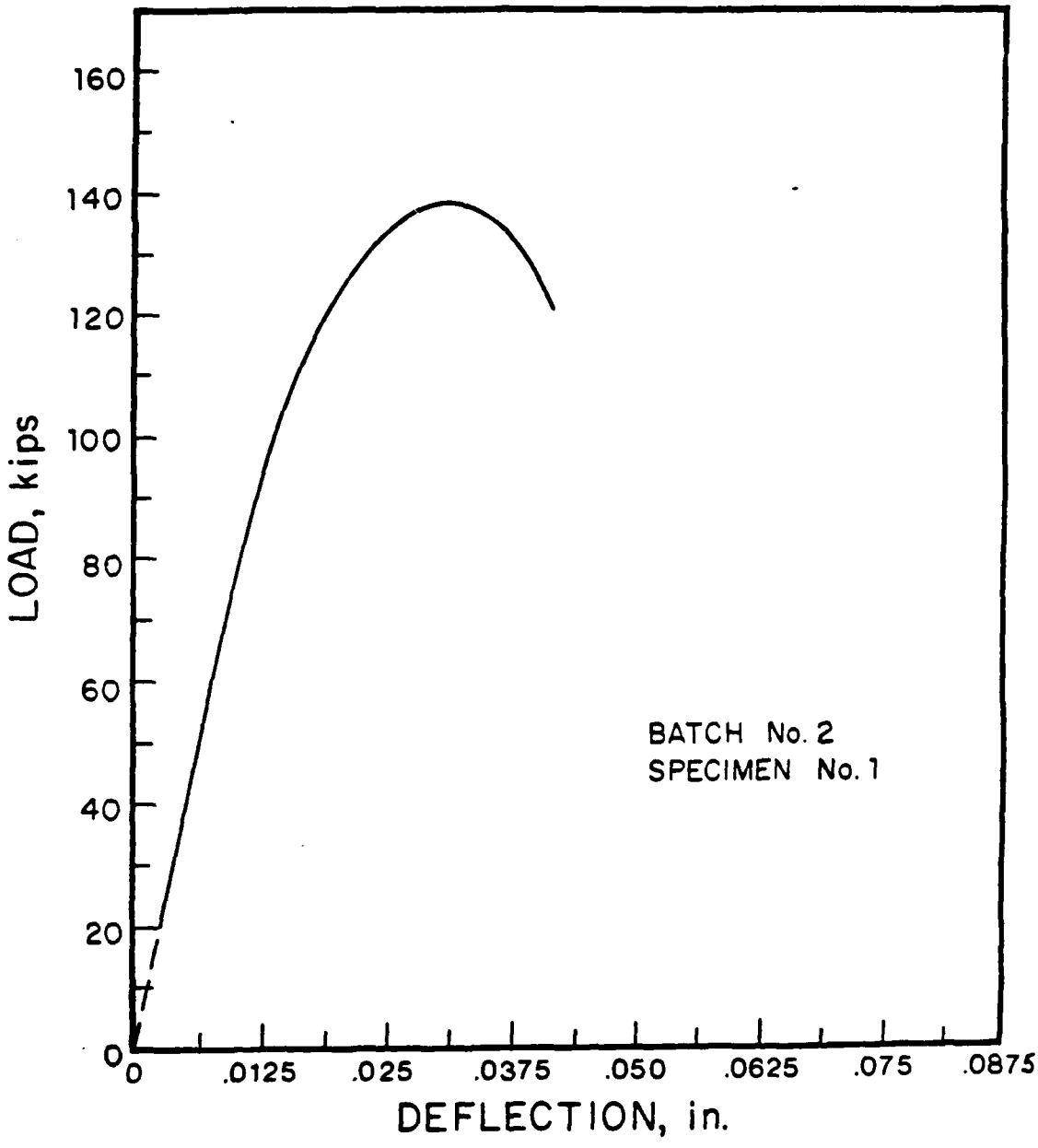
160
140
120
100
80
60
40
20
0
LOAD, kips
0
.0125
.025
.0375
.050
.0625
.075
.0875
DEFLECTION, in.
BATCH No. 2
SPECIMEN No. 1

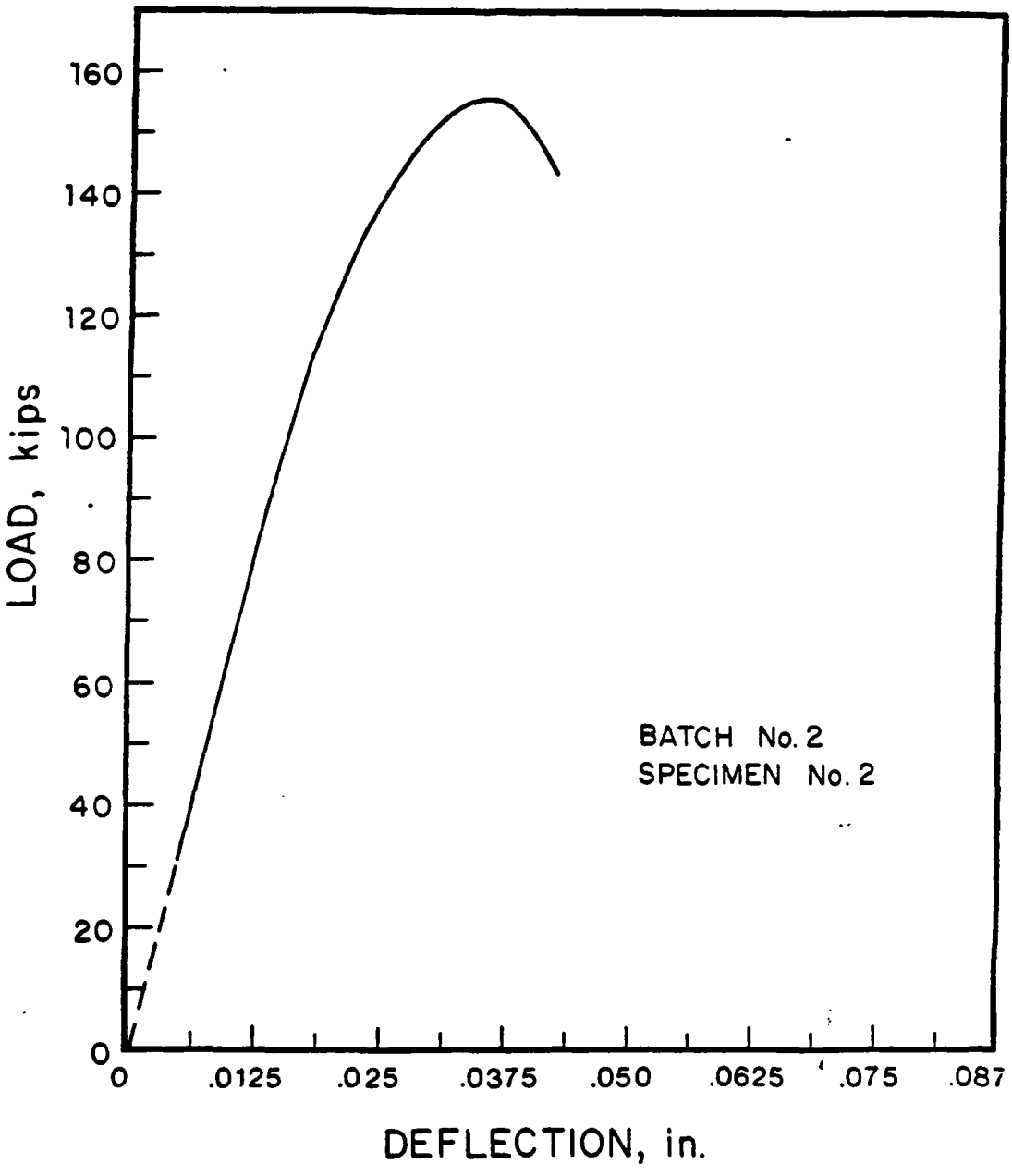
160
140
120
100
80
60
40
20
0
LOAD, kips
0
.0125
.025
.0375
.050
.0625
.075
.087
DEFLECTION, in.
BATCH No. 2
SPECIMEN No. 2

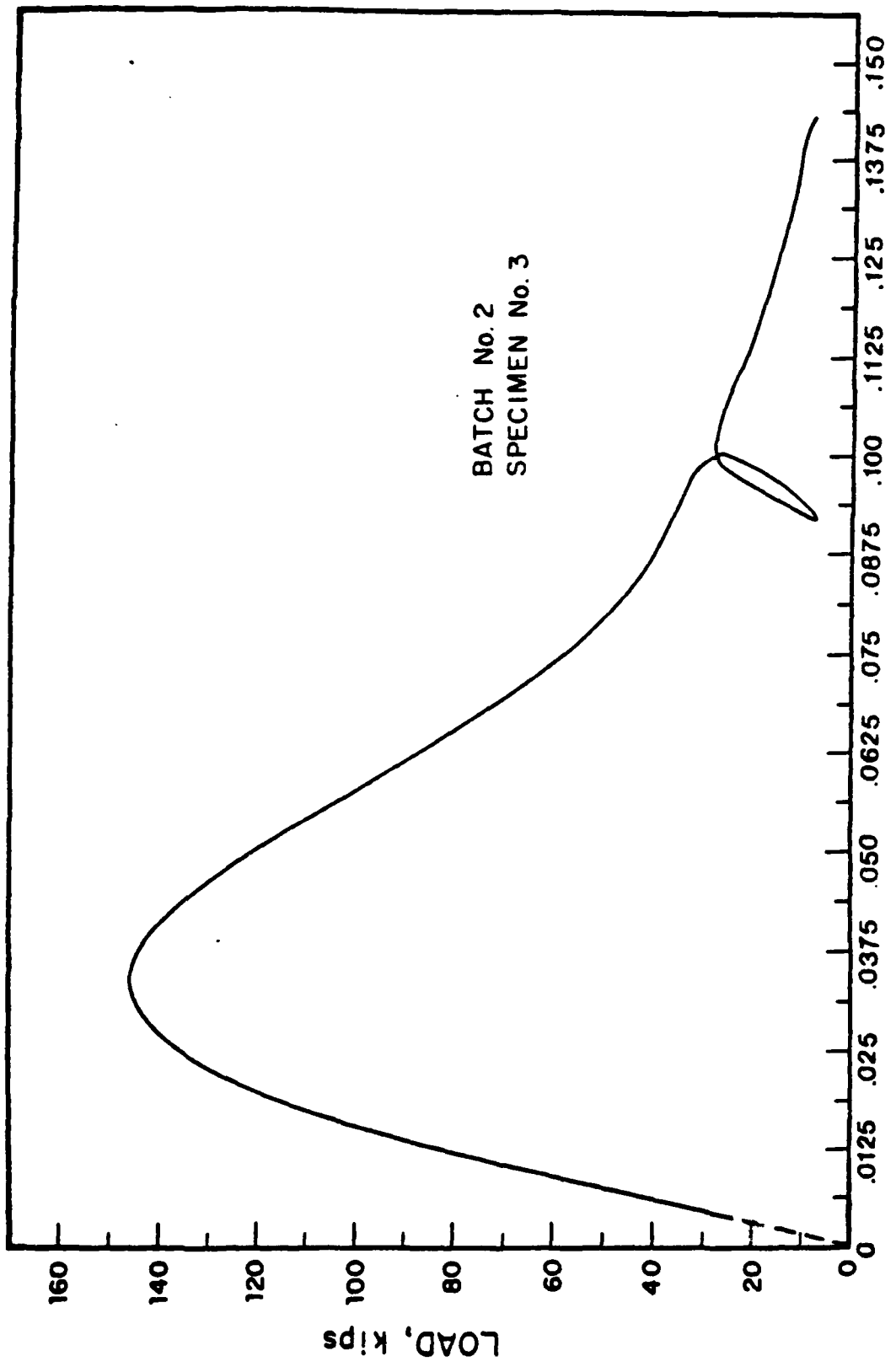
BATCH No. 2
SPECIMEN No. 3
LOAD, kips
160
140
120
100
80
60
40
20
0
0
.0125
.025
.0375
.050
.0625
.075
.0875
.100
.1125
.125
.1375
.150
DEFLECTION, in.

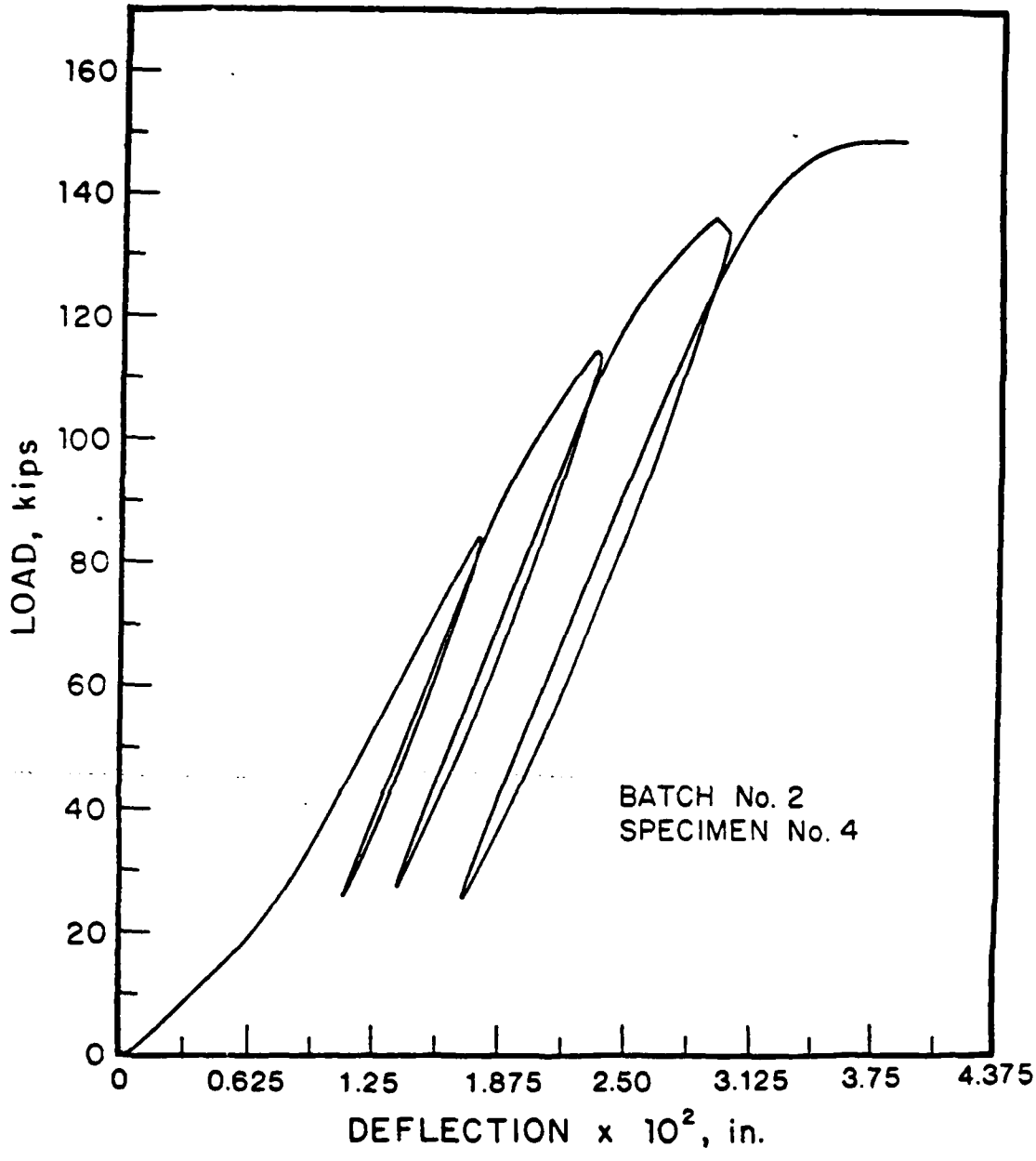
160
140
120
100
80
60
40
20
0
LOAD, kips
0
0.625
1.25
1.875
2.50
3.125
3.75
4.375
DEFLECTION x 10², in.
BATCH No. 2
SPECIMEN No. 4

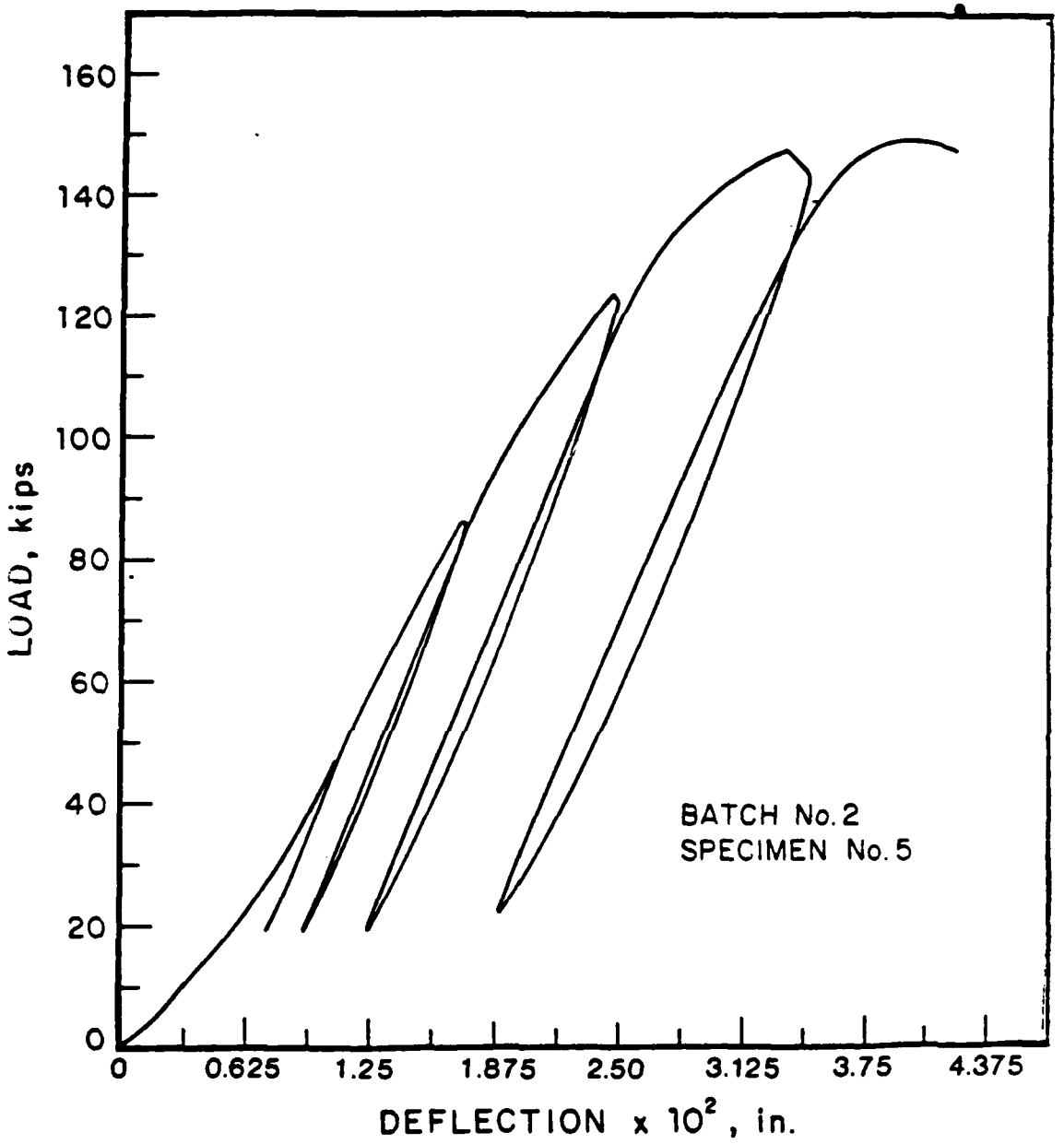
160
140
120
100
80
60
40
20
0
LOAD, kips
0
0.625
1.25
1.875
2.50
3.125
3.75
4.375
DEFLECTION x 10², in.
BATCH No.2
SPECIMEN No.5

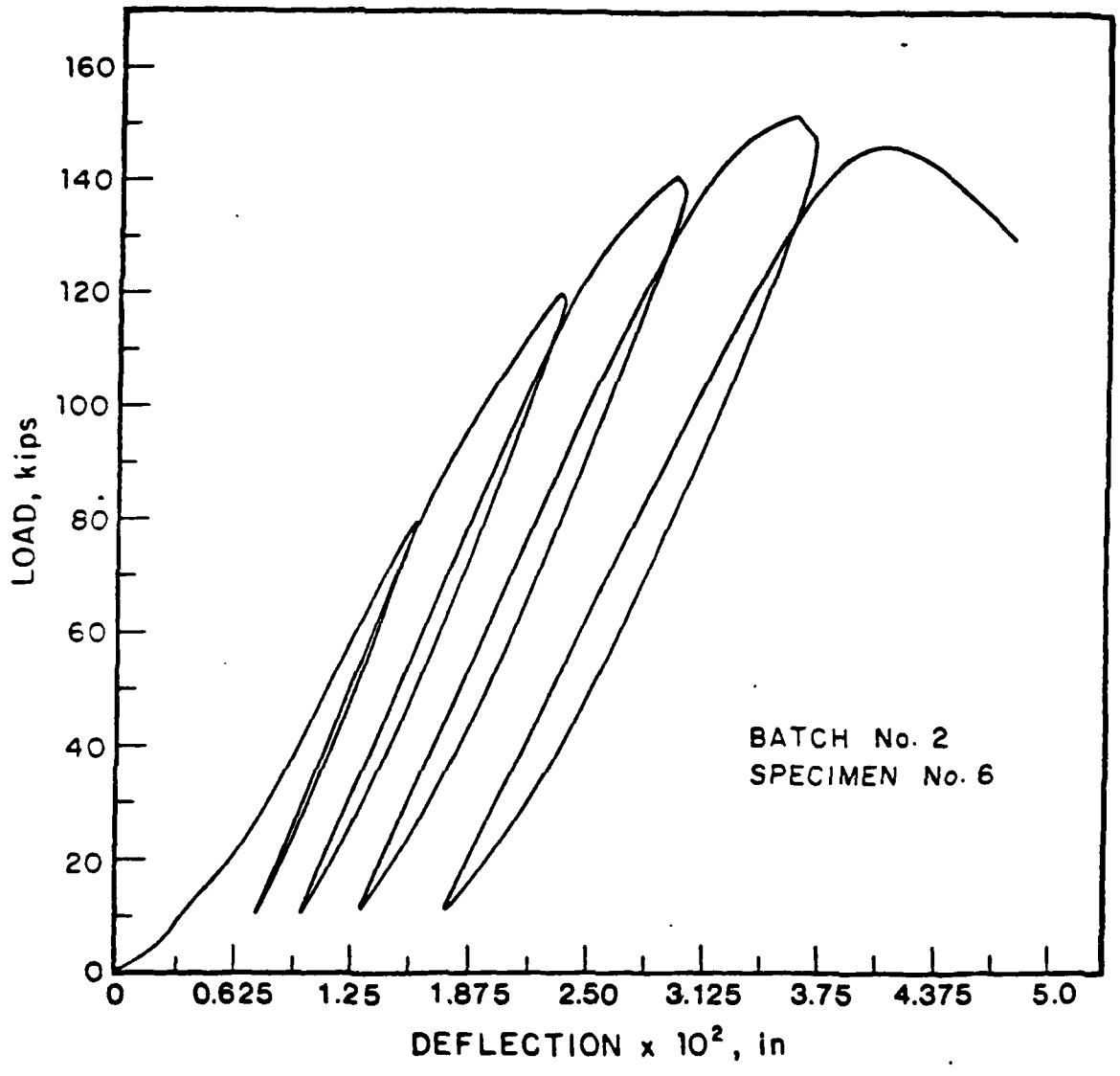
160
140
120
100
80
60
40
20
0
LOAD, kips
0
0.625
1.25
1.875
2.50
3.125
3.75
4.375
5.0
DEFLECTION x 10^2, in
BATCH No. 2
SPECIMEN No. 6

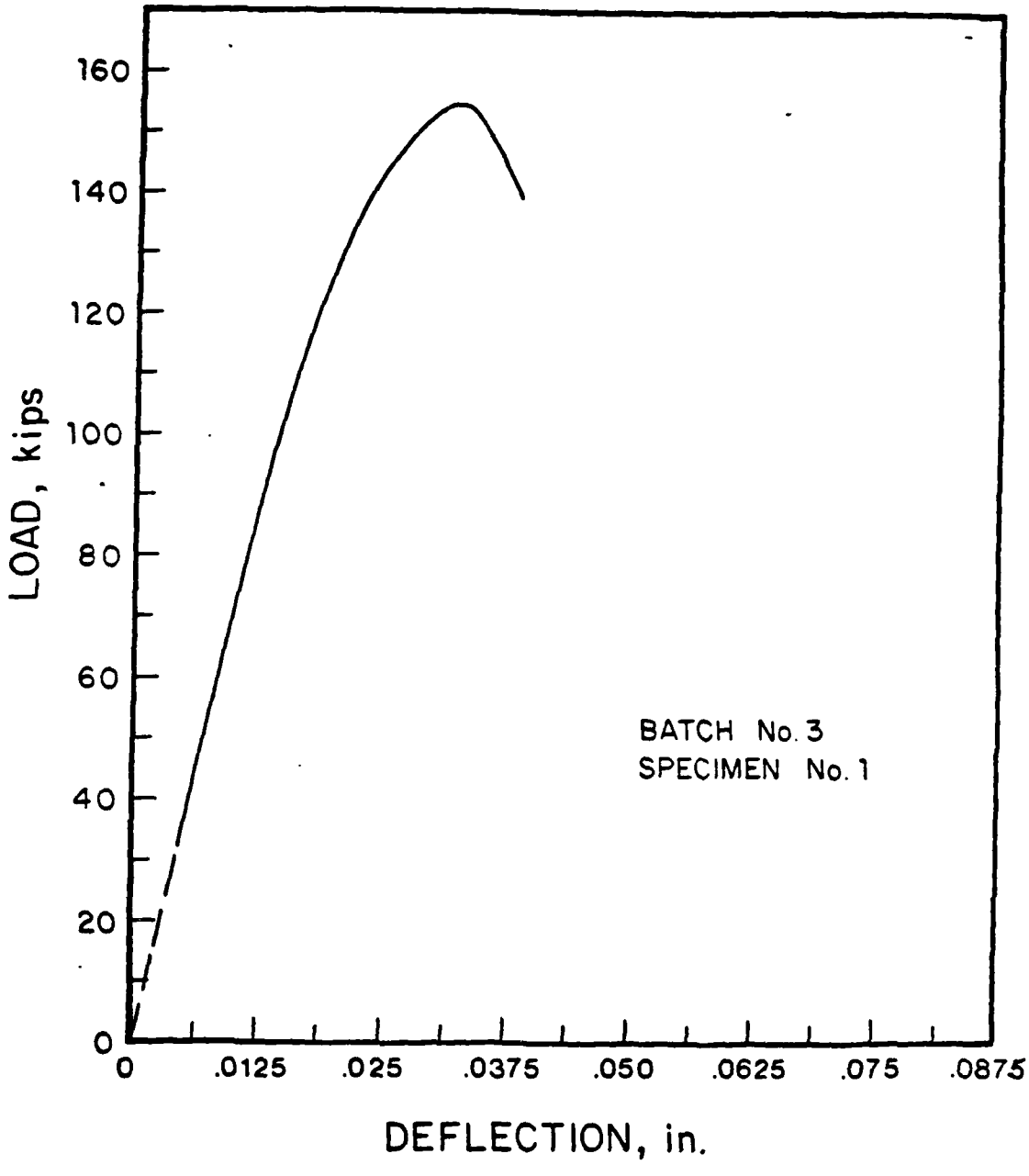
160
140
120
100
80
60
40
20
0
LOAD, kips
0
.0125
.025
.0375
.050
.0625
.075
.0875
DEFLECTION, in.
BATCH No. 3
SPECIMEN No. 1

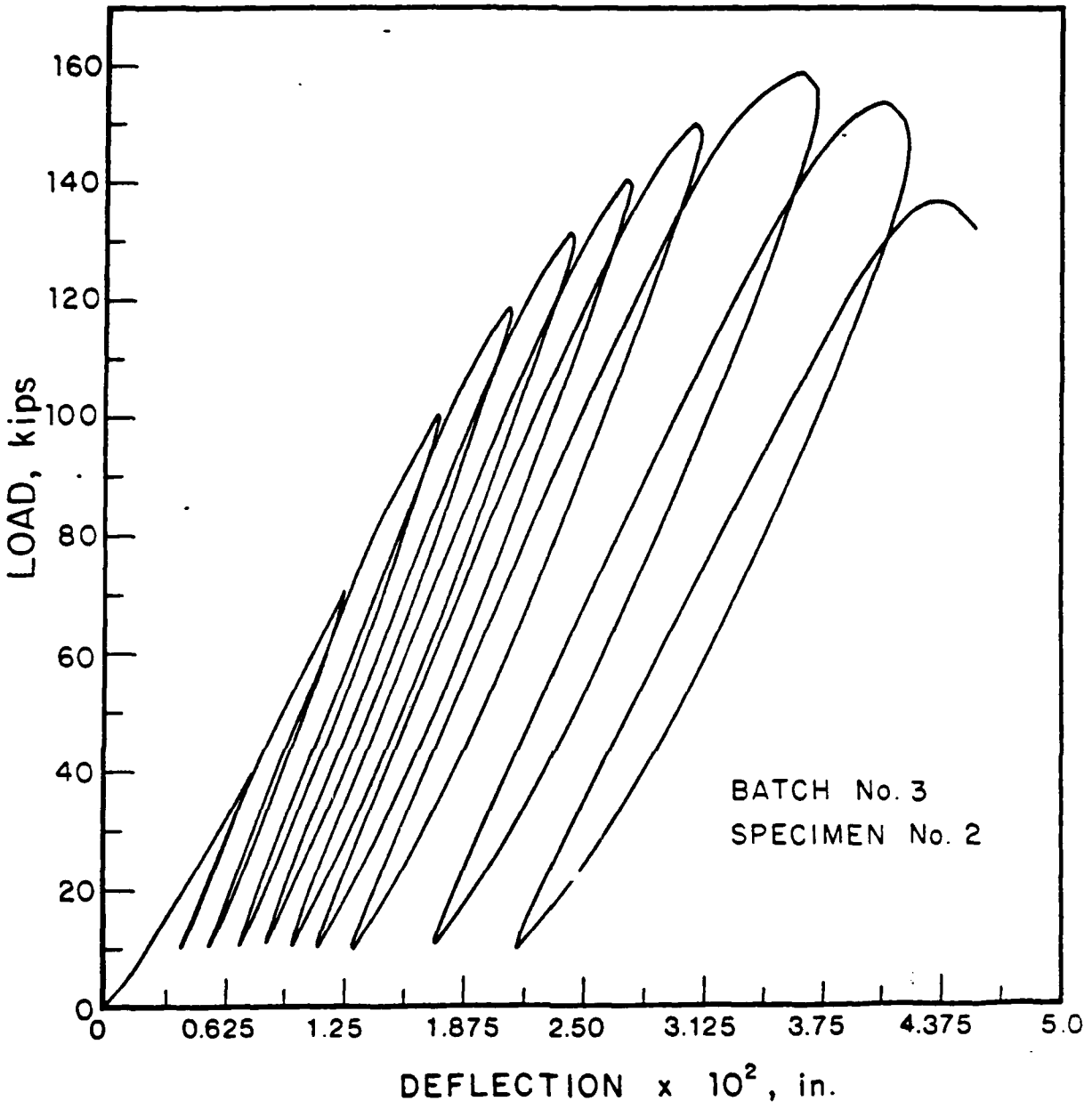
160
140
120
100
80
60
40
20
0
LOAD, kips
0
0.625
1.25
1.875
2.50
3.125
3.75
4.375
5.0
DEFLECTION x 10², in.
BATCH No. 3
SPECIMEN No. 2

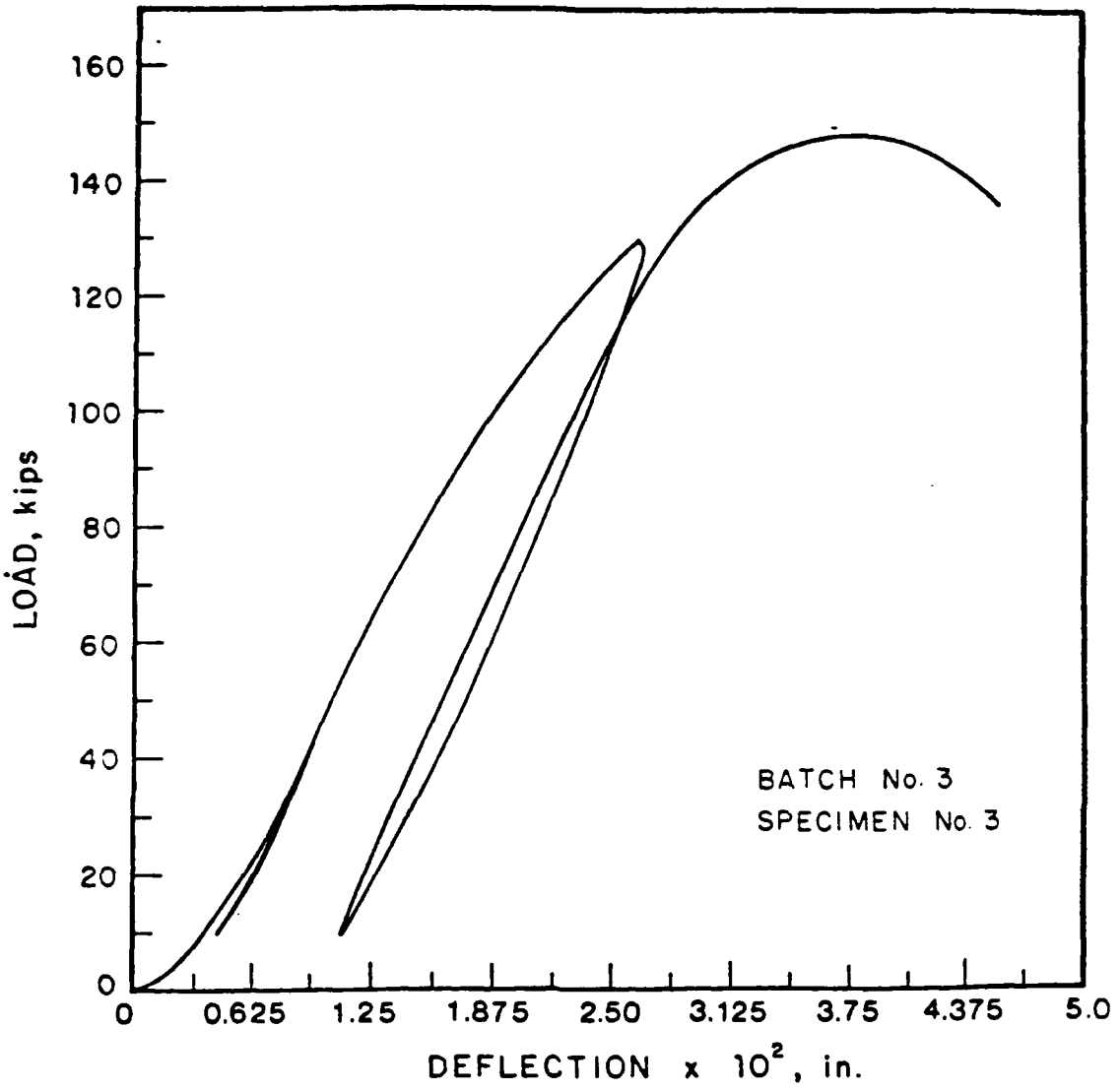
160
140
120
100
80
60
40
20
0
LOAD, kips
0
0.625
1.25
1.875
2.50
3.125
3.75
4.375
5.0
DEFLECTION x 10², in.
BATCH No. 3
SPECIMEN No. 3

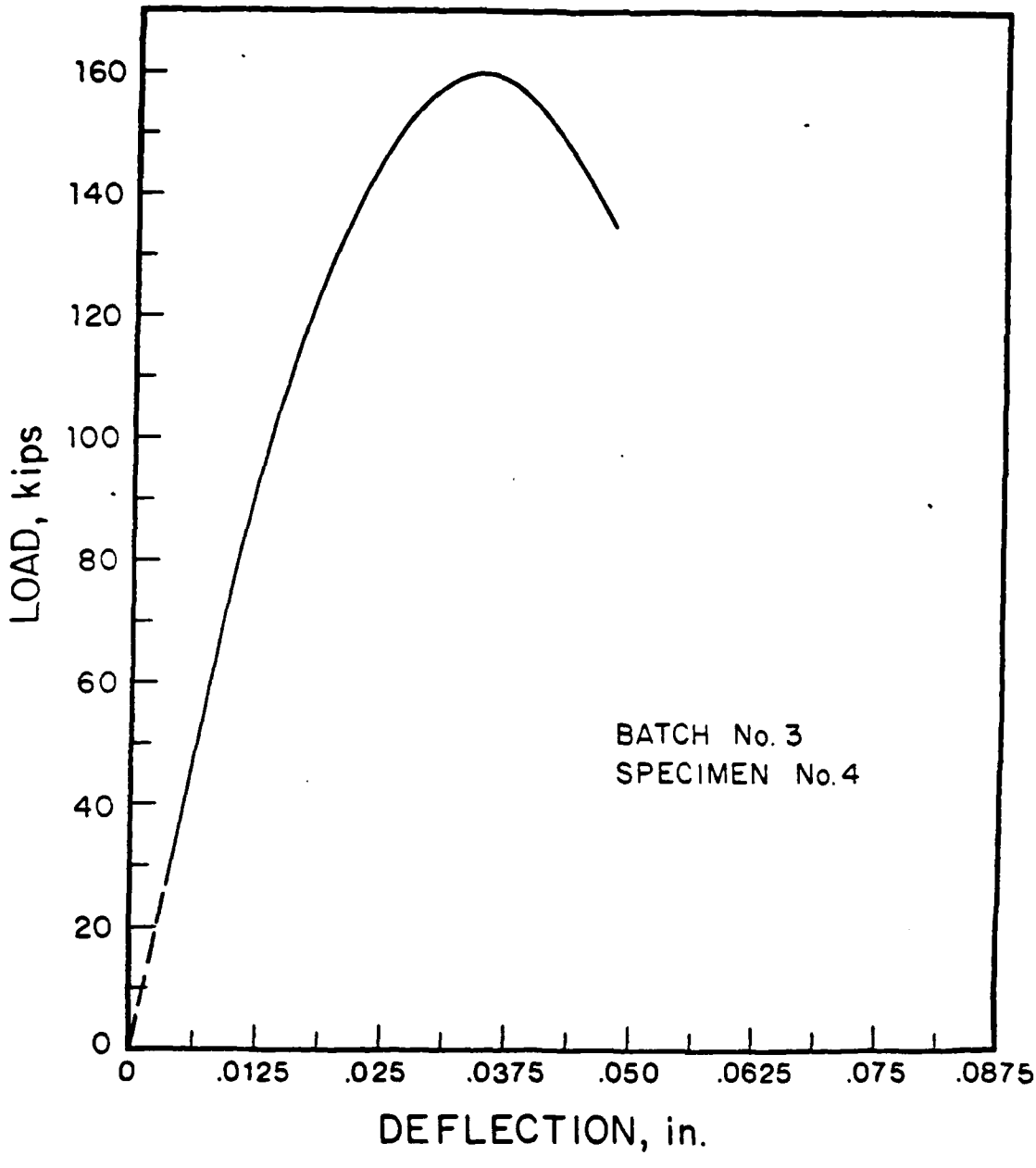
160
140
120
100
80
60
40
20
0
LOAD, kips
0
.0125
.025
.0375
.050
.0625
.075
.0875
DEFLECTION, in.
BATCH No. 3
SPECIMEN No. 4

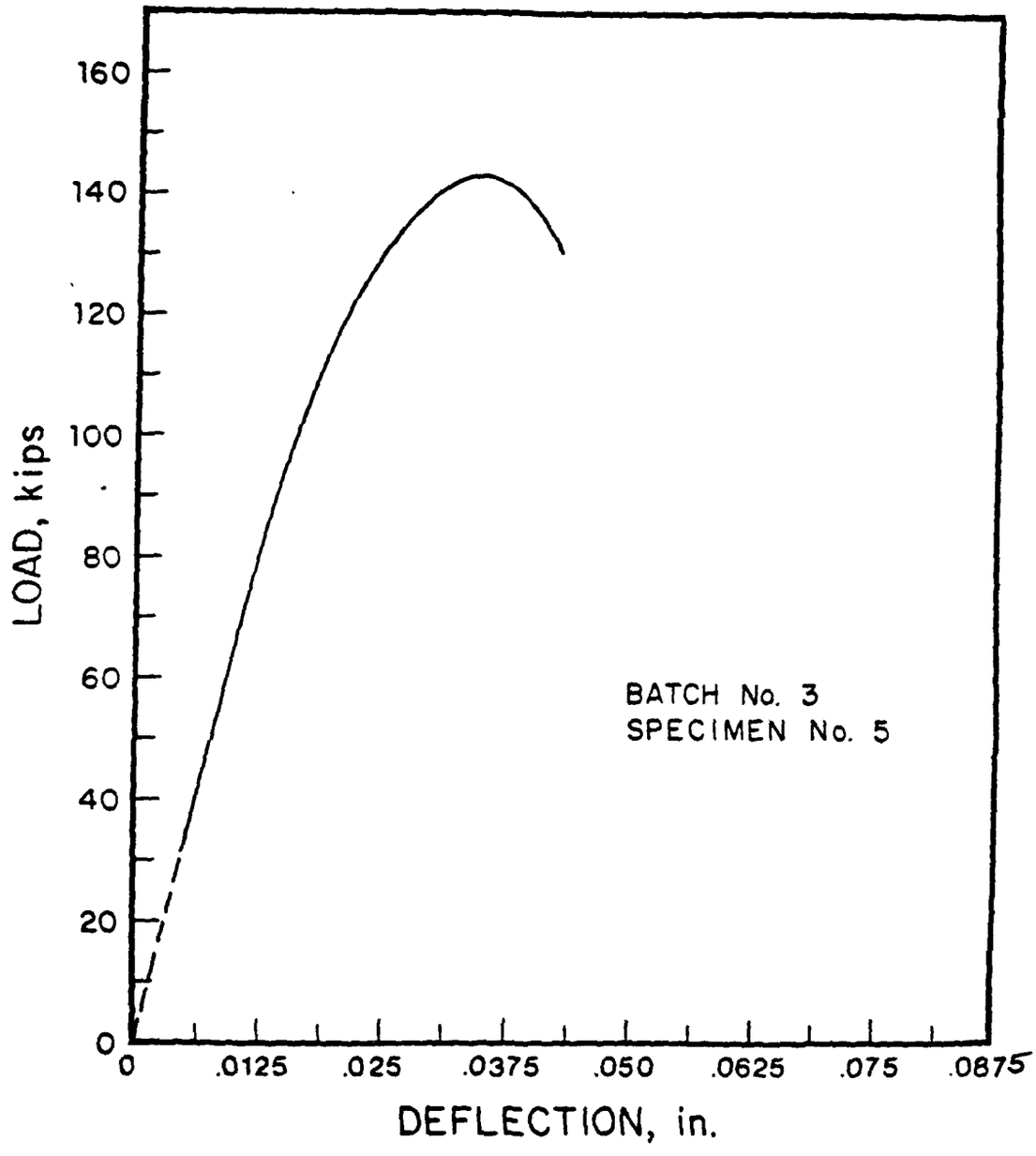
160
140
120
100
80
60
40
20
0
LOAD, kips
0
.0125
.025
.0375
.050
.0625
.075
.0875
DEFLECTION, in.
BATCH No. 3
SPECIMEN No. 5

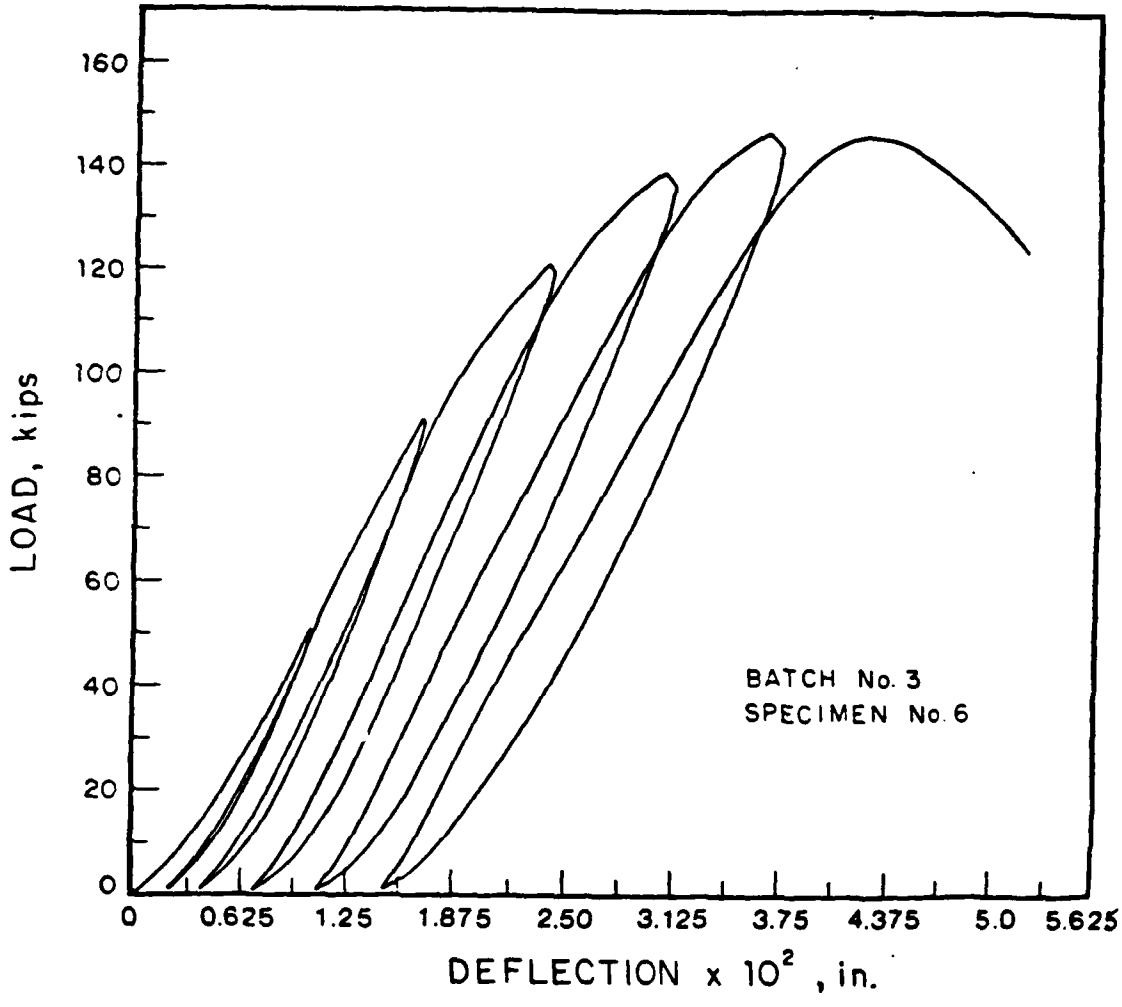
160
140
120
100
80
60
40
20
0
LOAD, kips
BATCH No. 3
SPECIMEN No. 6
0
0.625
1.25
1.875
2.50
3.125
3.75
4.375
5.0
5.625
DEFLECTION x 10² , in.

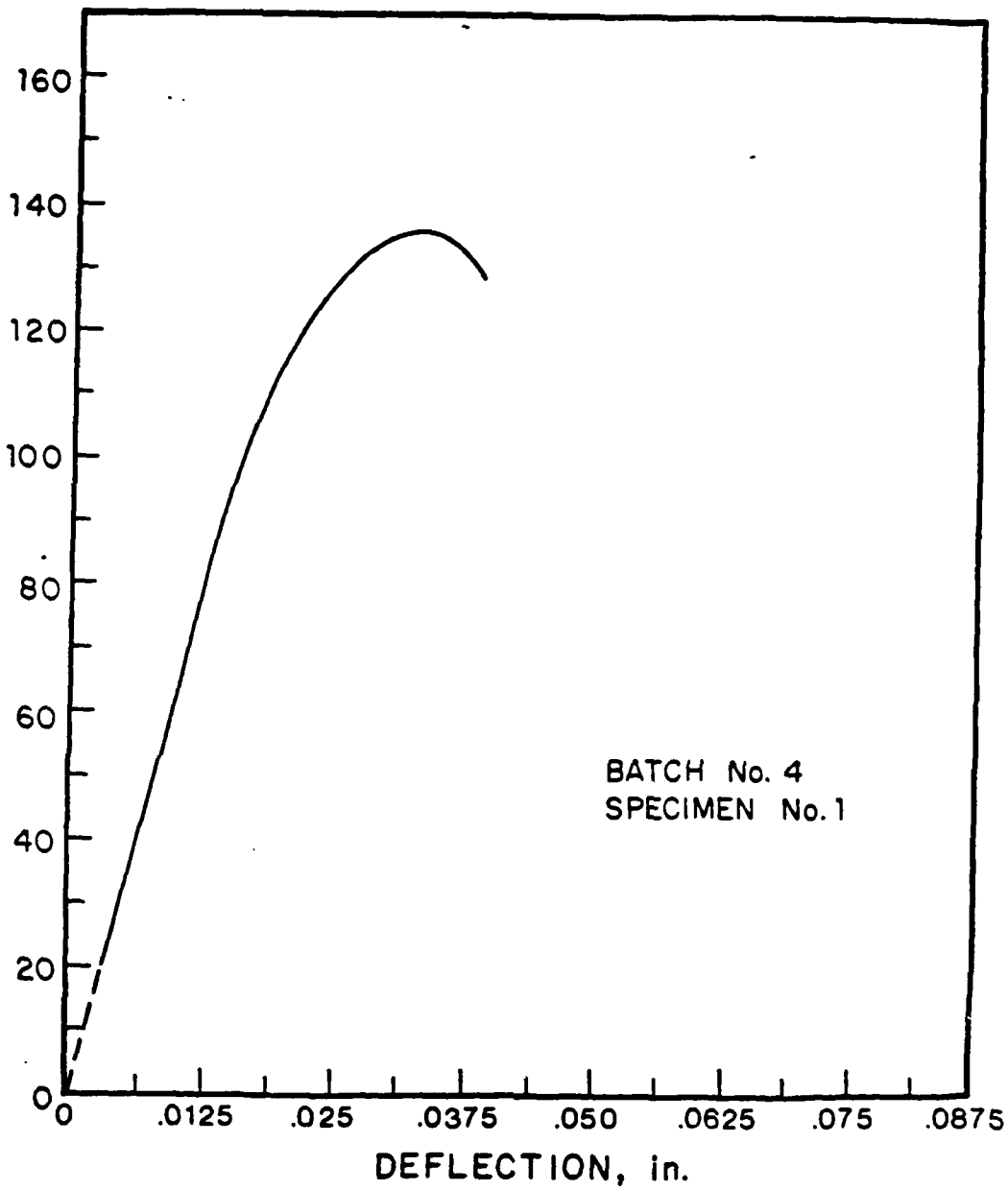
160
140
120
100
80
60
40
20
0
0
.0125
.025
.0375
.050
.0625
.075
.0875
DEFLECTION, in.
BATCH No. 4
SPECIMEN No. 1

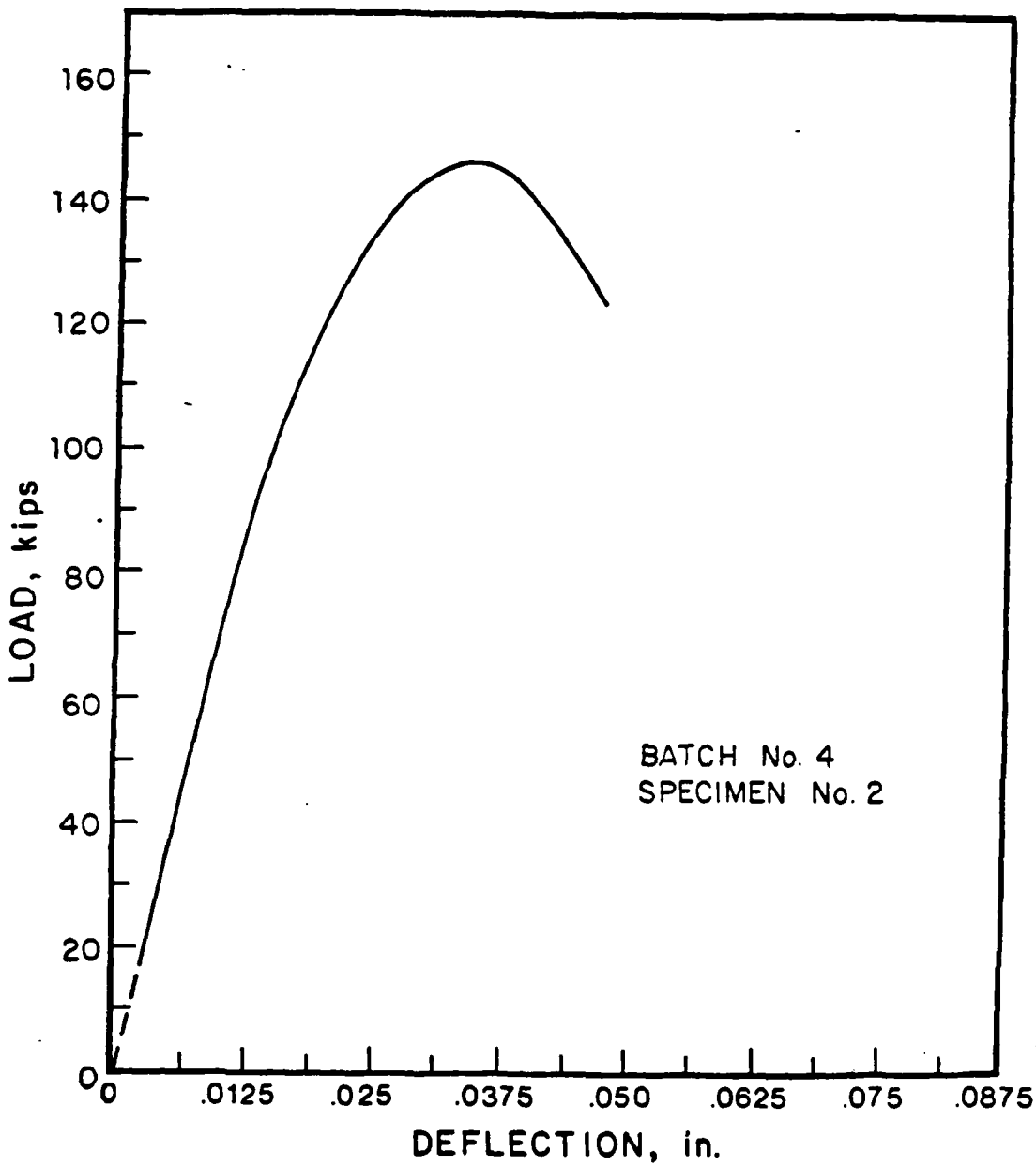
160
140
120
100
80
60
40
20
0
LOAD, kips
0
.0125
.025
.0375
.050
.0625
.075
.0875
DEFLECTION, in.
BATCH No. 4
SPECIMEN No. 2

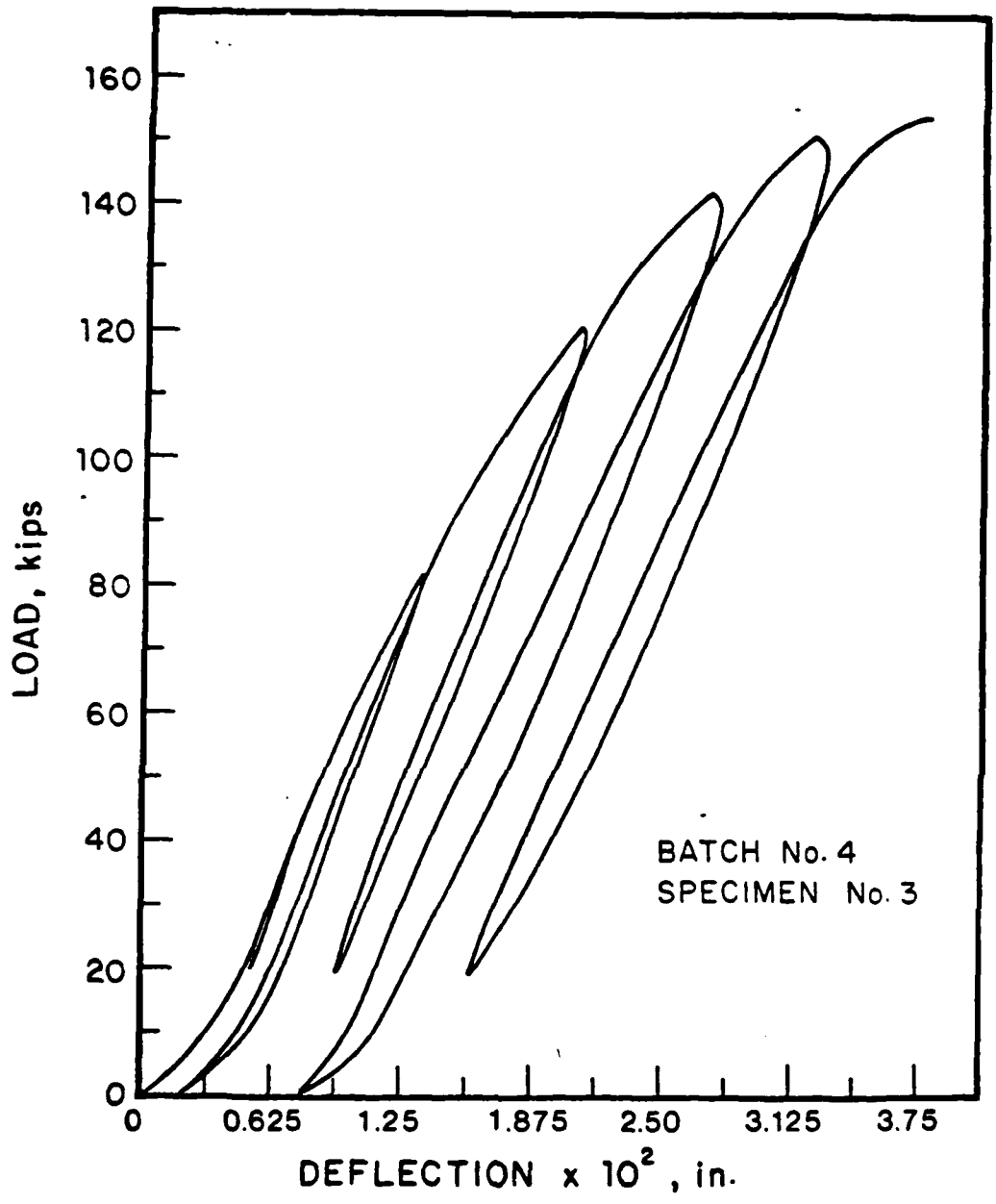
160
140
120
100
80
60
40
20
0
LOAD, kips
0
0.625
1.25
1.875
2.50
3.125
3.75
DEFLECTION x 10^2, in.
BATCH No. 4
SPECIMEN No. 3

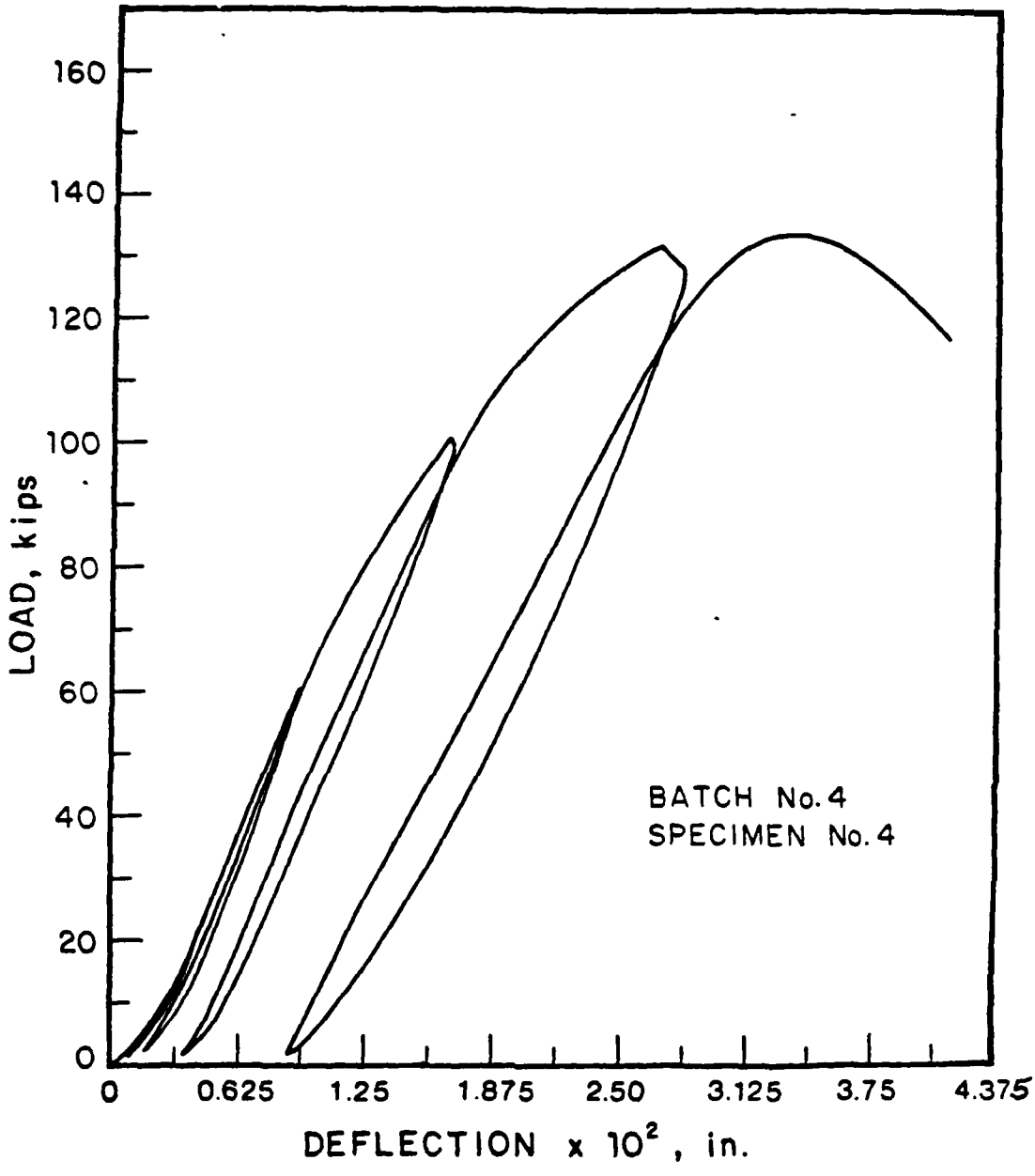
160
140
120
100
80
60
40
20
0
LOAD, kips
0
0.625
1.25
1.875
2.50
3.125
3.75
4.375
DEFLECTION x 10², in.
BATCH No. 4
SPECIMEN No. 4

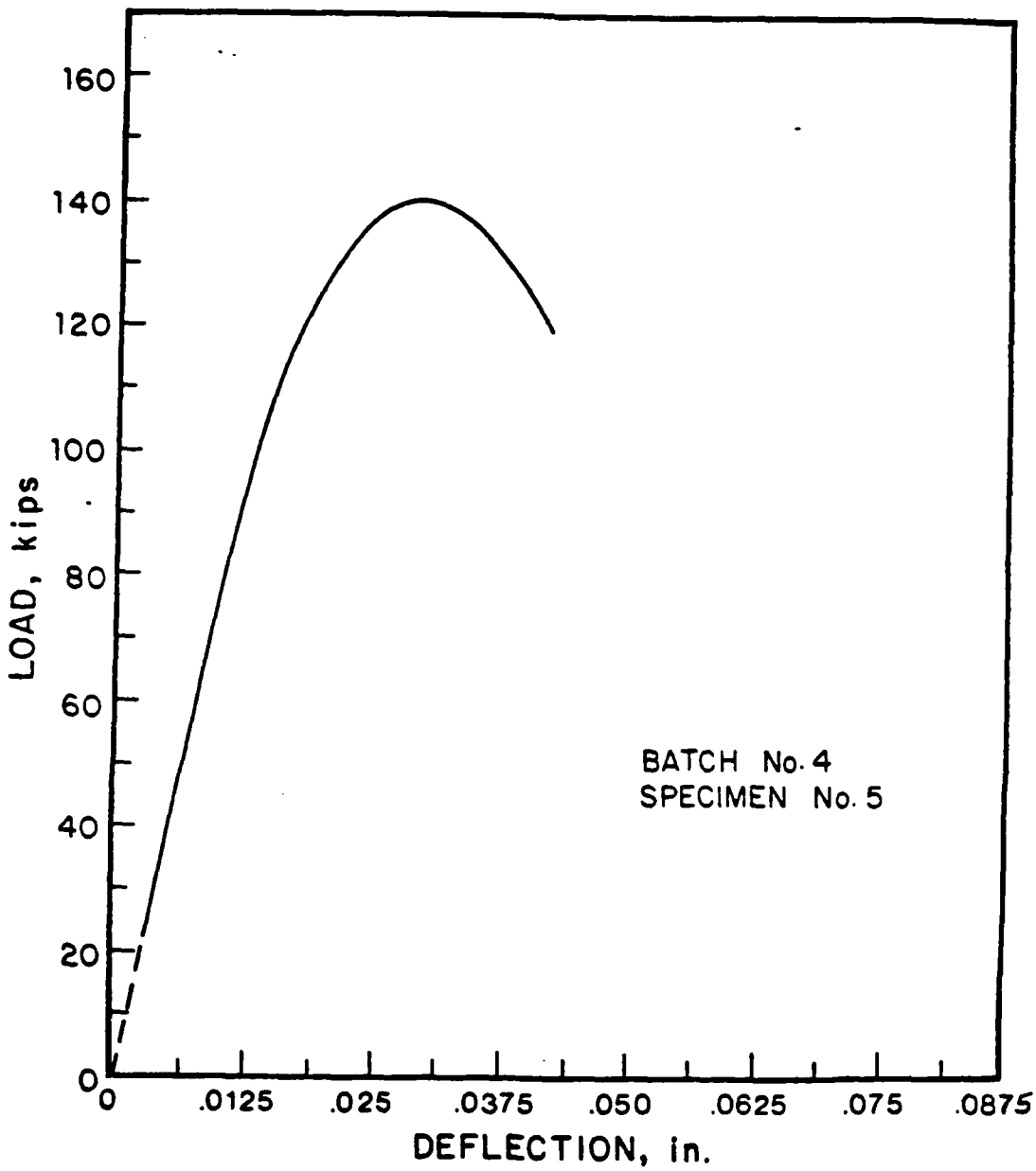
160
140
120
100
80
60
40
20
0
LOAD, kips
0
.0125
.025
.0375
.050
.0625
.075
.0875
DEFLECTION, in.
BATCH No. 4
SPECIMEN No. 5

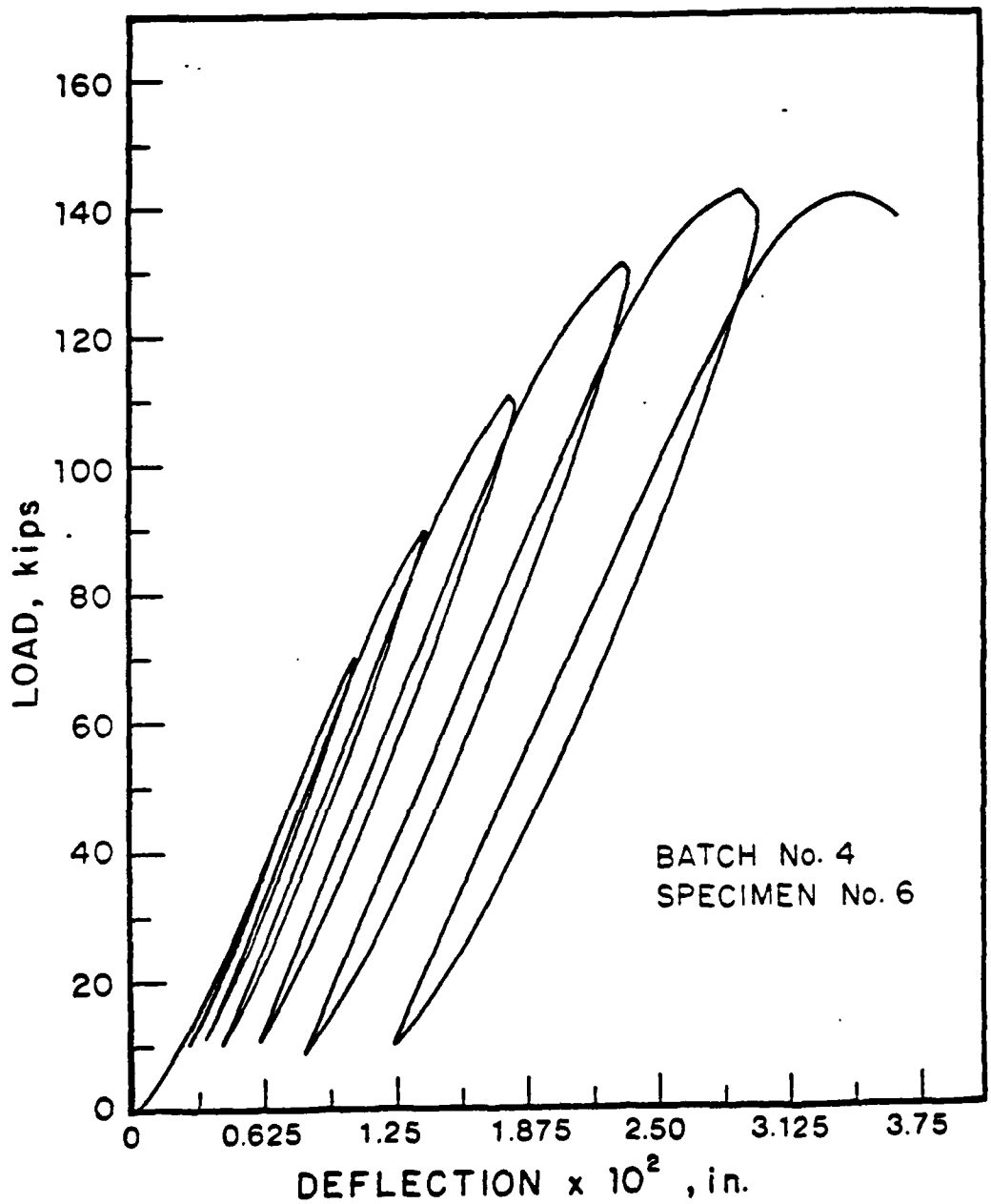
160
140
120
100
80
60
40
20
0
LOAD, kips
0
0.625
1.25
1.875
2.50
3.125
3.75
DEFLECTION x 10² , in.
BATCH No. 4
SPECIMEN No. 6